CAPITAL UNIVERSITY OF SCIENCE AND TECHNOLOGY, ISLAMABAD

Single Phase Analysis of MHD Convective Heat Transport in Nanofluids Using Finite Difference Method

by

Abid Kamran

A thesis submitted in partial fulfillment for the degree of Doctor of Philosophy

in the

Faculty of Computing
Department of Mathematics

2020

Single Phase Analysis of MHD Convective Heat Transport in Nanofluids Using Finite Difference Method

By

Abid Kamran

(DMT143003)

Dr. Bengisen Pekmen, Geridönmez,

TED University, Kolej Çankaya, Ankara, Turkey.

Dr. Chaudry Masood Khalique,

North-West University, South Africa.

Dr. Shafqat Hussain

(Thesis Supervisor)

Dr. Muhammad Sagheer

(Head, Department of Mathematics)

Dr. Muhammad Abdul Qadir

(Dean, Faculty of Computing)

DEPARTMENT OF MATHEMATICS

CAPITAL UNIVERSITY OF SCIENCE AND TECHNOLOGY

ISLAMABAD

2020

Dedicated to my parents, wife and in memory of my late brother-in-law Adeel Khan

CAPITAL UNIVERSITY OF SCIENCE & TECHNOLOGY
ISLAMABAD

Expressway, Kahuta Road, Zone-V, Islamabad
Phone:+92-51-111-555-666 Fax: +92-51-4486705
Email: info@cust.edu.pk Website: https://www.cust.edu.pk

CERTIFICATE OF APPROVAL

This is to certify that the research work presented in the thesis, entitled "**Single Phase Analysis of MHD Convective Heat Transport in Nanofluid using Finite Difference Method**" was conducted under the supervision of **Dr. Shafqat Hussain**. No part of this thesis has been submitted anywhere else for any other degree. This thesis is submitted to the **Department of Mathematics, Capital University of Science and Technology** in partial fulfillment of the requirements for the degree of Doctor in Philosophy in the field of **Mathematics**. The open defence of the thesis was conducted on **July 08, 2020**.

Student Name : Mr. Abid Kamran (DMT143003)

The Examining Committee unanimously agrees to award PhD degree in the mentioned field.

Examination Committee :

(a) External Examiner 1: Dr. Abdullah Shah
Associate Professor
COMSATS University, Islamabad

(b) External Examiner 2: Dr. Rashid Mahmood
Associate Professor
Air University, Islamabad

(c) Internal Examiner : Dr. Rashid Ali
Associate Professor
CUST, Islamabad

Supervisor Name : Dr. Shafqat Hussain
Associate Professor
CUST, Islamabad

Name of HoD : Dr. Muhammad Sagheer
Professor
CUST, Islamabad

Name of Dean : Dr. Muhammad Abdul Qadir
Professor
CUST, Islamabad

AUTHOR'S DECLARATION

I, **Mr. Abid Kamran (Registration No. DMT-143003)**, hereby state that my PhD thesis titled, '**Single Phase Analysis of MHD Convective Heat Transport in Nanofluid using Finite Difference Method**' is my own work and has not been submitted previously by me for taking any degree from Capital University of Science and Technology, Islamabad or anywhere else in the country/ world.

At any time, if my statement is found to be incorrect even after my graduation, the University has the right to withdraw my PhD Degree.

(Mr. Abid Kamran)

Dated: 08 July, 2020

Registration No : DMT-143003

PLAGIARISM UNDERTAKING

I solemnly declare that research work presented in the thesis titled "**Single Phase Analysis of MHD Convective Heat Transport in Nanofluid using Finite Difference Method**" is solely my research work with no significant contribution from any other person. Small contribution/ help wherever taken has been duly acknowledged and that complete thesis has been written by me.

I understand the zero tolerance policy of the HEC and Capital University of Science and Technology towards plagiarism. Therefore, I as an author of the above titled thesis declare that no portion of my thesis has been plagiarized and any material used as reference is properly referred/ cited.

I undertake that if I am found guilty of any formal plagiarism in the above titled thesis even after award of PhD Degree, the University reserves the right to withdraw/ revoke my PhD degree and that HEC and the University have the right to publish my name on the HEC/ University Website on which names of students are placed who submitted plagiarized thesis.

(Mr. Abid Kamran)

Dated: 08 July, 2020

Registration No : DMT-143003

List of Publications

It is certified that following publication(s) have been made out of the research work that has been carried out for this thesis:-

1. **A. Kamran**, S. Hussain, M. Sagheer and N. Akmal, "A numerical study of magnetohydrodynamics flow in Casson nanofluid combined with Joule heating and slip boundary conditions," *Results in Physics*, vol. 7, pp. 3037-3048, 2017.

2. **A. Kamran**, S. Hussain and M. Sagheer. "Impact of induced magnetic field on free convective flow of kerosene/water based single and multiwalled carbon nanotubes," *AIP Advances*, vol. 8, p. 105130, 2018.

3. **A. Kamran**, S. Hussain and M. Sagheer. "Transport phenomena in Marangoni driven alumina-Dihydrogen oxide nanofluid with thermal inertia," *Journal of Nanofluids*, vol. 8, pp. 1023-1032, 2019.

Abid Kamran
(DMT143003)

Acknowledgements

All praise is for the Almighty **ALLAH** (Subhana watalah) who created this universe and all that is in it. Countless thanks to him for creating us among the humans and giving us birth in the house of muslims. Peace and blessing be upon **HAZRAT MUHAMMAD** (SAW) for enlightening our souls with the message of the Almighty. Who taught us to strive for knowledge from the cradle to the grave and directed us on the path to success in this life and the hereafter.

I extend my gratitude and acknowledgment to my learned supervisor **Dr. Shafqat Hussain** for his keen involvement in my pursuit of Ph.D degree. His valuable suggestions, guidance and motivation has paved the way to bring my research to this point successfully. I also appreciate the painstaking attitude of **Dr. Muhammad Sagheer**, Head of Mathematics Department, for his worthy involvement in improving the quality of research articles. He has used his expertise in English language and article presentation which enhanced the chances of its publication in highly reputed International Journals. Besides this, his understanding and grip in the subject of numerical methods helped us to code the technique of Keller box on Matlab.

I am grateful to my parents for their prayers and special thanks to my father, **Mr. Gul Jang** for not giving up on me and backed me in hard times during my studies. I would like to appreciate the tireless support of my wife throughout my Ph.D studies.

I would like to thank Higher Education Commission of Pakistan for providing me with the funding to complete my Ph.D studies. In the last but not least I would like to show my gratitude to all my Ph.D fellows who showed great support and were source of inspiration for me, specially, **Mr. Naveed Akmal**. With out his support, it would have been almost impossible for me to complete my studies.

Abstract

The present dissertation is an effort to explore the heat and mass transfer in Newtonian and non-Newtonian nanofluids flowing in various physical domains. The non-Newtonian nanofluid models of Casson and micropolar fluids are utilized to highlight the thermal transport in such fluids. Homogeneous single model and Buongiorno nanofluid models are used in the study to analyze the fluid flow and heat transfer in nanofluids. Water and kerosene oil are used as the base fluids in homogeneous single phase model and the nanoparticles used are alumina, single and multiwalled carbon nanotubes. Impact of magnetic field on the fluid flow and heat transfer is observed. The application of magnetic field is responsible for the heat dissipation in fluid for which the Joule heating effect is made a part of the mathematical modeling of the problems. The mathematical modeling is carried out using the continuity, linear momentum, energy and the concentration equations. The impact of microrotating structures has been made a part of the study. For the micropolar nanofluid model an additional angular momentum equation is used to observe the effect of microstructures present within the fluid. These microstructures can move independently and rotate irrespective of the motion of the fluid. Microstructures give rise to an additional viscosity factor called the rotation viscosity. They are also responsible for the stress tensor to be antisymmetric, the impact of which can be observed in the momentum equation. To account for the induced magnetic field effects the Maxwell equations of electromagnetism are included. Other aspects of the study involves the impact of the shape effects of the nanoparticles, velocity slip and convective boundary conditions. The mathematical models are transformed into ordinary differential equations (ODEs). The system of ODEs are solved by an efficient finite difference scheme of Keller box. The validity of Matlab code for Keller box method is acclaimed by its comparison with the already published work. The numerical results are analyzed by variation in the pertinent physical parameters appearing in the nondimentionalized ODEs using graphs and table of values.

Symbols

$\mathbf{N}$	angular velocity
$\mathbf{b}$	body force
κ_B	Boltzmann constant
N_B	Brownian motion parameter
Br	Brinkman number
Bi	Biot number
$\boldsymbol{b_F}$	body force due to free convection
D_B	Brownian diffusion coefficient
L	characteristic length
S_0'''	characteristic entropy generation
$\frac{\partial u}{\partial y}$	deformation rate
β	dynamic plastic viscosity parameter
μ	dynamic viscosity
Ng	dimensionless entropy generation
Ec	Eckert number
σ_{el}	electric conductivity
J	electric current density
$\mathbf{E}$	electrical strength vector
λ	effective thermal diffusivity
T	fluid temperature
T_∞	free stream temperature
ρ	fluid density
g_e	gravitational acceleration

q_w	heat flux at the wall
$\mathbf{q}$	heat flux across any surface
Ha	Hartmann number
$\mathbf{I}$	identity tensor
ν	kinematic viscosity
$\boldsymbol{b_M}$	Lorentz forces
Le	Lewis number
μ_e	magnetic permeability
$\mathbf{B}$	magnetic strength vector
q_m	mass flux
D_m	mass diffusion coefficient
j	micro-inertia per unit mass
K	material parameter
M	magnetic number
Pm	magnetic Prandtl number
∇	Nabla operator
Nu	Nusselt number
$f^{'}$	nondimensional velocities
θ	nondimensional temperature
g	nondimensional angular velocity
B_x	nondimensional induced magnetic field
η	nondimensional length
α	opening angle of channel
μ_B	plastic dynamic viscosity
Pr	Prandtl number
d_p	particle's diameter
$\mathbf{A}$	Revlin-Ericksen tensor
Re	Reynolds number
κ^*	rotation viscosity
π_p	ratio of circumference to diameter of the particle
R	Real gas constant

τ	shear stress
v_0	suction velocity
γ	spin gradient viscosity
σ	surface tension
ϕ	solid volume fraction
C_p	specific heat
Sc	Schmidt number
C_f	skin friction coefficient
V_0	suction parameter
Sh	Sherwood number
τ_w	shear stress at the surface
D_T	thermal diffusion coefficient
κ	thermal conductivity
β_T	thermal expansion coefficient
h_T	thermal slip parameter
$\alpha^{'}$	thermal diffusivity
ω_T	thermal boundary layer thickness
λ_E	thermal relaxation time
N_T	thermophoresis
κ_p	thermal conductivity of nanoparticle
γ_0	velocity slip parameter
ω	velocity boundary layer thickness
$\mathbf{V}$	velocity vector
u	x-component of velocity field
p_y	yield stress
v	y-component of velocity field
w	z-component of velocity field

Contents

List of Figures

List of Tables

Abbreviations

KBM	Keller box method
MHD	magnetohydrodynamics
PDEs	partial differential equations
ODEs	ordinary differential equations
BVP	boundary value problem
SWCNT	single-walled Carbon nanotubes
MWCNT	multi-walled Carbon nanotubes
EG	ethylene glycol
NaDDBS	sodium dodecylbenzene sulfonate

Chapter 1

Introduction

This chapter is structured in a manner to explain the motivation, objectives and approach adopted to carry the present study. The importance of heat transfer in many industrial and commercial areas is hidden to no researcher working in the field. Recently, an urge to improve the heat transfer process in such systems has greatly increased. Different approaches have been used to find ways to enhance the heat transfer rate in heat transport processes. Of the different ways, one way to increase the conductivity of the system is by increasing the surface area of the assembly carrying the fluid to provide greater contact of the fluid with the surface but this approach is not feasible in systems which have size constraints. Another approach developed recently is engineering of fluid containing nanomaterials. This approach has gathered immense attention in recent times. Both experimental and numerical aspect have been adopted to study its contribution to thermal heat transfer. Based on this theme, the details are given in the subsequent sections.

1.1 Motivation

With the development of the industrial era, a primary concern of diverse industrial processes is to devise ways of increasing heat dissipation through the surface so as to cool down the entire system. The conventional methods such as increasing the

area available comes with a drawback that an undesirable increase in the surface area of the system is required. Therefore, new and improved ways are the need of the hour to serve the purpose. In the search of finding ways to achieve the target, a revolutionary material engineered is the "nanofluids"-heat transfer fluid containing suspensions of the nanoparticles. The advent of the nanofluids has had a revolutionary impact on the heat transfer processes as a minute amount of the nanoparticles added to the conventional fluids improve the system's heat transfer ability significantly. Nanofluids are receiving monumental attention as it is being used in many applications of heat transfer processes such as heat exchangers, solar collectors, automotive industry, nuclear reactors etc [1, 2].

1.2 Nanofluid Engineering

Nanofluids are a modification in the conventional fluids by the addition of a very small proportion of nanosized particles with size in the range 1-100 nm. Nanofluids have attracted immense attention because of great heat transfer capabilities. For instance, small amount of the nanoparticles such as copper Cu or carbon nanotubes (CNT) to the conventionally poor thermal conducting fluids such as ethylene glycol (EG) improved the thermal conductivity by 40% to 150% [3]. Two methods have been adopted for the preparation of nanofluids [3]. A two step process, in which production of powdered nanoparticles is carried out by inert gas condensation or by chemical vapors deposition. Then, as a second step, dispersal of that dry powder in working fluid by ultrasonic agitation or by the addition of surfactants. In single step process, the vaporization of nanofluid material containing dispersed nanoparticles in vacuum conditions is carried out. The advantage of this method is that the chances of nanoparticles agglomeration are minimum. Among the base fluids used for the preparation of nanofluids, water is reported the most commonly used base fluid [2]. The other frequently used working fluids are ethylene glycol and also the combination of water and ethylene glycol. Among the nanoparticles aluminum oxide Al_2O_3 is the most commonly used nanoparticles [2]. Also, carbon nanotubes (CNTs) have also been used frequently. Other famous nanoparticles

used are ferrous oxide Fe_3O_4, copper Cu, silver Ag, titanium oxide TiO_2, silicon dioxide SiO_2 etc. Studies have shown that the multiwalled carbon nanotubes (MWCNTs) are the most effective in increasing the thermal conductivity of the conventional fluid [2].

1.3 Mathematical Approach

Theoretically, various mathematical models have been proposed by many researchers on the basis of experimental results. Among these nanofluid models, two widely used are the single and two phase models [4] . Generically, a nanofluid is a two-phase fluid but by making use of suitable suppositions it can be presumed as a homogeneous composite because of the ultra-fine size of the solid additives dispersed easily in the fluid. Thermal balance is found between the nanoparticles and the host fluid with no slip mechanisms prevailing among them. In two phase models, classical theory of solid-liquid mixture is applied. The nanoparticles and base fluid are assumed to have different velocities and temperatures and the slip factors are made as source terms in the momentum and energy equations.

Making use of these models, many researchers have carried out numerous work which has many interesting findings. Choi and Eastman [5] wrote their breakthrough paper on nanofluid in 1995 in which they introduced a new family of fluids engineered by adding nanoparticles to the orthodox fluids. Nanoparticles used were of spherically shaped carbon element and the base fluid used was water. A measure of the fact that heat transfer capabilities of thermal processes enhanced for nanofluid as compared to the conventional fluids was established by You et al. [6] and Vassallo et al. [7]. They determined that even very small proportion of nanoparticles addition to the conventional fluid resulted in big improvement in the heat conduction of the fluid. Recently, Moldoveanu [8] conducted an experiment on an aqueous solution of two types of oxide nanomaterial to explore its thermal conductivity. The preparation of nanofluids was carried out using ultrasonic vibrations for one hour. Thermal conductivity augmented with the temperature

and nanoparticles concentration upgradations. In an another study, Loni et al. [9] investigated the thermal performance of three different types of working fluids, the alumina-oil, silica-oil and alumina-thermal oil, in cylindrical solar cavity receivers. The findings of the study mentioned that the cavity heat and thermal efficiency are comparable for both the alumina-oil and silica-oil based nanofluids. The average thermal efficiency of alumina-thermal oil was the highest amongst the other working fluids. Minea et al. [10] computationally studied the thermal conductivity in the shear thinning fluids using power-law model. On the basis of the numerical results, correlations were proposed in regard of heat transport rate dependent on the Reynolds number, Prandtl number and pipe location. Sheikholeslami et al. [11] pondered on the MHD convective heat transport in alumina-water nanofluid flow in a permeable medium. Different shaped alumina nanparticles were used in their study and the mathematical model was solved by finite element technique. The conclusion declared that the Nusselt number increased with the rise in Richardson and radiation numbers but decreased for an augmentation in Hartmann number. Further references are cited in [12–14] for reader's interest.

1.4 Non-Newtonian Base Fluids

As mentioned earlier, in a large number of studies, water or EG is used as the working fluid. Then, studies can be found in which the two base fluids water and EG are mixed together to work as a base fluid. Of course, all of this is done to somehow increase the conduction ability of the working fluid. These fluids behave like Newtonian fluids but there are instances where the working fluids may not exhibit properties pertaining to Newtonian fluid. Recently, there are instance seen in which such working fluid are used as base fluid. For example, Sodium alginate has been used as base fluid in many applications of science and engineering. It is derived from seaweed made up of blocks of mannuronic acid and guluronic acid. In food industry, sodium alginate is used as thickening, emulsifying and stabilizing agents [15]. Alginate modifications make it suitable for its use in drug delivery systems and biomedical devices [16]. Some other applications are cited in [17, 18].

Sodium alginate is treated as viscoplastic shear thinning fluid for which Casson model is used to study its heat transfer properties. Casson fluid is discussed under the class of non-Newtonian fluids. Shortcomings of the Bingham fluid model is countered by this model as it explains the nonlinear behaviour seen once the yield stress is achieved. Casson fluid model successfully explains the physical behaviour of many fluids used in science and industry. For instance, in chocolate manufacturing industry, the quality of chocolate products depend on the viscosity of the chocolate. Chocolate shows a shear thinning behaviour which is explained best by the Casson fluid model [19]. Blood when flowing at moderate shear stresses behaves like a Casson fluid [20]. It is observed experimentally that the drilling oils also behave like Casson fluid [21]. Similarly, toothpaste, tomato ketchups and many other examples can be given which behave like Casson fluid.

Then, there are instances where the working fluid may have microstructures which can rotate independently irrespective of the motion of base fluid. These fluids are classified as micropolar fluid. Such microstructure are found in liquid crystals, animal bloods, polymers etc [22]. The mathematical explanation of the presence of such structures require asymmetric definition of the coupled stress tensor and the inclusion of the angular momentum equation along with the mass, momentum and energy equations. The mathematical equations along with the boundary conditions of micropolar fluid flow were defined by Eringen [23]. Since then, the Eringen's theory has been extensively used by many authors while studying the properties of micropolar fluids. Tiwari and Das approach [24] which is basically single phase model with experimentally defined correlations, was used by Swalmeh et al. [25] in the study on the flow of CuO and Al_2O_3-water based nanofluid around a solid sphere. The numerical approach used by the authors was the Keller box method [26]. The obtained numerical results showed that CuO nanofluid had excellence over Al_2O_3 nanofluid in terms of heat transfer rate for growing values of the microrotating parameter. Izadi et al. [27] established the shooting method solutions for a biocovective flow of microrotating fluid past a sheet that is stretched. It was noted that a greater rotation viscosity tended to reduce the angular velocity.

1.5 Magnetic Field Impact on Nanofluids

Of the many ways of enhancing thermal conductivity in nanofluids, one useful method is by the influence of external magnetic field. A group of researchers, Crainic et al. [28], was the first one to successfully apply the magnetic field to obtain new nanocomposites mixtures. These mixtures were an amalgam of magnetic and nonmagnetic materials which contained the desired properties for the use in applications such as radars, magnetic levitation trains, electric engine motors and kinetic energy accumulators. Hong et al. [29] witnessed that when the external magnetic field is applied to 0.01-0.02% wt. of Fe_2O_3 nanoparticles in water improves its thermal conductivity. The physical reason was that in the presence of magnetic field, Fe_2O_3 nanoparticles formed connected networks which got oriented to some extent toward the field direction and the induction of more physical contacts led to an upgrade in the heat conduction. Wensel et al. [30] and Hong et al. [31] used sodium dodecylbenzene sulfonate (NaDDBS) which when added to a solution containing single walled carbon nanotubes (SWCNTs) made SWCNTs positively charged. Then, the negatively charged metal oxides were added to the solution mantained at a pH 7 which got aggregated with the positively charged SWCNTs. Results showed that in such scenario, thermal conductivity improved by 10% for the nanofluid with 0.017% wt. SWCNTs and MgO, 0.17% wt. NADDBS. Wensel et al. [30] showed that when external magnetic field was applied, the thermal conductivity increased by 35% to that in the absence of magnetic field. Shima et al. [32] inverted the polarity of the solvents containing magnetite nanoparticles to prepare stabilized nanofluids. It was reported that the existence of a controlled magnetic field significantly augmented the ratio of viscosity and thermal conductivity.

1.6 A Review of Convective Heat Transport

Convective heat transport is a fundamental phenomenon in diverse fields of engineering and science with widespread applications in geophysics, heat exchangers,

solar collectors, electronic cooling, nuclear engineering and many other [33]. A primary concern of such processes is to have efficient thermal dissipation system for the removal and transport of heat energy. Use of nanofluids has served this purpose for over two decades and still a lot of research is being carried out to even better the achievements that have been made till now. Experimental study on natural convective flows are few and far between due to the difficulty in preparation of nanofluids and handling of the parameters. Putra et al. [34] made an experimental work on natural convective flow of an Al_2O_3 and CuO nanofluid with water as a base fluid inside a cylinder which is heated and cooled form both ends. They found that nanomaterial concentration augmentation in nanofluid diminished the natural convective heat transport characterized by a decrease in Nusselt number.

Benos et al. [35] used the matched asymptotic expansions to observe the convective phenomenon in the nanofluid flowing in a shallow horizontal cavity taking into account the MHD and internal heat generation effects. Sithole et al. [36] numerically observed the entropy generation in a non-Newtonian fluid flowing over a convectively heated stretching sheet with nonlinear thermal radiation and viscous dissipation effects. Hashemi et al. [37] adopted the Galerkin finite element method to observe the thermal transport in water based CuO micropolar nanofluid using the KKL model. For further reading, see [12, 13, 38–40].

A free surface exists at the liquid-liquid and liquid-gas interface. This free surface contains energy of which surface tension is one of the contributing factor. The surface tension is often a function of temperature difference prevailing at the surface and a region with high temperature has a low surface tension. This makes the liquid to move from a point of low surface tension to the point of high surface tension. The resulting convection is named as Marangoni convection. Scientists knew of this convection for many years but the popularity of this phenomenon came to the surface in recent past as space technology has shown great progress where the thermo-capillary effect is a major cause of motion in nonuniformly heated fluids

[41]. The introduction of nanoparticles to the conventional fluids is a contributing factor which results in Marangoni convection. The phenomenon of Marangoni convection in nanofluids has been explored by many scientists and researchers these days. Homotopic solutions of the Cu-water nanofluid model subject to the Marangoni convection were established by Lin and Zheng [42]. Mahanthesh and Gireesha [43] investigated the suspension of dust particles in the magneto-Casson nanofluid. In the study, working fluid's surface tension was assumed a linear function of its temperature. They concluded that the presence of dust particles in the nanofluid were responsible for the enhancement in heat transfer rate.

1.7 Objectives of the Thesis

Focus of the thesis revolves around the mathematical exploration of heat transport in nanofluids. This phenomena has been investigated in the convective flow and heat transport in the fluid. Assumption is made that the working fluid is significantly electrically conductive so that the concept of magnetohydrodynamics can be utilized. Owing to the fact that many engineering applications sees most of the heat transfer near the surface, boundary layer theory has been adopted. Heat transfer rate is measured by calculating the Nusselt number at the boundary. Classical homogeneous single phase nanofluid model and Buongiorno nanofluid model have been utilized to achieve this objective for various configurations. Besides the measurement of heat transfer rate, skin friction coefficient has also been calculated. This helped in analyzing the drag force imposed by the nanofluids on the walls of the boundary abounding it. One subsidiary purpose was to examine numerically the nanoparticles and base fluids for their impact on heat transfer in channels and stretching sheet like geometry. Although such investigations can be found in abundance in literature but there is still the strive for improvement. Physical parameters arising in the nondimensional equations also influence the heat transfer. In the present study, the coupling impact of physical parameters has also been observed and deductions have been made on the basis of the obtained numerical results.

1.8 Structure of the Thesis

In the light of the brief discussion in the preceding paragraphs, the present thesis is further structured in the following manner.

Chapter 2 Terminologies and solution methodology

Chapter 2 contains details related to the terminologies and definitions that are necessary in the context of the work carried out in the next chapters. Single and Buongiorno nanofluid model alongwith the BL theory have been discussed in detail. Also, the governing laws and their mathematical equations are described in detail. The mathematical procedure of Keller box method is discussed via solving a fourth order BVP using the method. Numerical solution is compared to the exact solution to validate the KBM procedure.

Chapter 3 Convectively heated boundary impact on heat transfer in MHD Casson nanofluid

In this chapter, consideration is given to a magnetohydrodyanamical flow of Casson nanofluid over a sheet horizontally stretched. The stretching surface is convectively heated and slip takes place at the surface of the sheet. Joule heating effects are also considered and the energy dissipation is evaluated numerically by entropy generation taking place in the system. Buongiorno nanofluid model is considered which accounts the Brownian motion and thermophoresis effects. The nondimensionalized seventh order coupled system of nonlinear ODEs is solved by KBM. The numerical results are interpreted in the forms of graphs and tables. The contents of this chapter are published in "Results in Physics", vol. 7, pp. 3037-3048, 2017.

Chapter 4 Induced magnetic field effect on free convective flow and heat transfer in micropolar nanofluid

Chapter 4 presents a discussion on the affect of induced magnetic field on the buoyancy driven flow of micropolar nanofluid containing CNTs between two plates parallel to each other with upper plate nonconducting and lower plate conducting. The upper plate is provided a constant heating while heat flux is applied at the lower plate. Applying the assumptions on the governing equations of momentum, angular momentum, Maxwell's equation of induction and the energy equation lead to a linear coupled eight order system. The resulting system is computationally handled by KBM. Graphical results are used to gain an insight of the pertinent parameters' influence on the flow features that arise in the system of linear equations. This chapter's contents are published in"AIP Advances", vol. 8, pp. 105130, 2018.

Chapter 5 Marangoni convective flow and heat transfer in MHD micropolar alumina-water nanofluid

Boundary layer analysis of Marangoni convective flow of an Al_2O_3-water micropolar nanofluid influenced by external magnetic field is carried out in Chapter 5. In the study, Cattaneo-Christov heat flux model is utilized to account for the heat transfer in the nanofluid flow. Four different shaped nanoparticles sphere, tetrahedron, column and lamina are used to ponder upon the heat transport mechanism in the flow. The ninth order coupled system is managed numerically by KBM and the influential parameter effects are observed via graphs. This chapter's content are published in"Journal of Nanofluids" vol. 8, pp. 1133-1146, 2019.

Chapter 6 Jeffery-Hamel flow and heat transport in non- Newtonian nanofluid between nonparallel plates.

Chapter 6, is an exploration of the thermal and mass transfer characteristics of non-Newtonian channel flow of a nanofluid flowing between two deviating/converging walls. There exists a magnetic field across the walls for which the Joule heating effect is examined. The impact of the presence of microstructures inside the nanofluids is examined for the heat transport and flow characteristics of the nanofluid. Eringen's theory is used for the modeling of micropolar fluids along with the Navier-Stokes equations of fluid dynamics. Buongiorno's nanofluid model assumptions have been incorporated to mathematical model describing the nanofluids. A numerical solution to the model is achieved using the KBM.

Chapter 7 Conclusions

The summary of the work carried out in the thesis is given in the concluding Chapter 7.

Chapter 2

Terminologies and Solution Methodology

2.1 Fluid

Fluid is defined as a substance that continuously deforms when a tangential shear stress is applied to it, however small the stress may be, fluid will deform on contrary to solids which tend to resist the applied shear stress. The reason for this continuous deformation is the presence of greater inter-molecular distances between the molecules of liquids as compared to that of solids. Fluid is categorized as Newtonain/non-Newtonian depending on the deformation rate.

Deformation rate shows a linear behaviour to the applied shear stress in Newtonian fluids. Mathematically, Newtonian fluids are expressed as:

$$\tau_{xy} = \mu \frac{\partial u}{\partial y}. \tag{2.1}$$

The fluids in which relation (2.1) doesn't hold are called non-Newtonian fluids. Non-Newtonian fluids are further classified on the basis of the relation of shear stress and deformation rate. Some of the non-Newtonain fluids of interest are discussed here.

2.1.1 Casson Fluid

Casson fluid belongs to the class of non-Newtonian fluids. It comes under the class of fluids which manifest a shear thinning behaviour after a certain yield stress is achieved. At a zero stress rate, it has an infinite viscosity but the viscosity becomes zero when shear stress is raised to an infinite level. Casson fluid model is mathematically explained by the relation [44, 45]:

$$\tau_{ij} = \begin{cases} 2\left(\mu_B + \frac{p_y}{\sqrt{2\pi}}\right) e_{ij}, & \pi \geq \pi_c, \\ 2\left(\mu_B + \frac{p_y}{\sqrt{2\pi_c}}\right) e_{ij}, & \pi < \pi_c. \end{cases} \tag{2.2}$$

Here, e_{ij} is the $(i,j)th$ of the strain rate, π is the product of the deformation rate with itself i.e. $\pi = e_{ij}e_{ji}$ and the critical value of this product is π_c. Casson fluid model successfully explains the behaviour of many fluids used in science and industry. For instance, in chocolate manufacturing industry, the quality of chocolate products depends on the viscosity of the chocolate. Chocolate shows a shear thinning behaviour which is explained best by the Casson fluid model [19]. Blood when flowing at moderate shear stresses behaves like a Casson fluid [20].

2.1.2 Micropolar Fluid

Micropolar fluids are categorized as non-Newtonian fluids because in these fluids the Newton's law of viscosity does not hold. There is an additional factor of rotation viscosity along with the dynamic viscosity of the fluid. The feature of these microstructures that their motion is independent of the flow results in a unsymmetrical stress tensor. In such fluids, shear stress is related to deformation rate by the relation:

$$\tau_{xy} = (\mu + \kappa^*) \frac{\partial u}{\partial y}, \tag{2.3}$$

where κ^* represents the rotation viscosity, a term associated to the resistance of fluid due to the presence of micro-rotating particles present in the constituent

fluid. Some examples of micropolar fluids are liquid crystals and animal blood [22].

2.1.3 Nanofluids

Fluids containing nanosized particles with the size ranging from 1 nm-100 nm are called as nanofluids. Nanofluids are engineered to enhance the heat transfer ability of the conventional fluids used in heat transport processes. The nanoparticles are fine pulverable form of metals and their oxides, carbides, ceramics and ceramic oxides, which have high thermal conductivity. The commonly used base fluids are water, ethylene glycol, kerosene oil etc. To study the working mechanism of nanofluids, it is important to study the heat transfer phenomenon.

2.2 Heat Transfer

Heat is transferred in a medium via:

- conduction
- convection
- radiation

Conductive heat transport in a medium takes place by exchange of kinetic energy between the neighboring molecules. It usually takes place in solids where the molecules are closely packed together. In liquids, thermal transport by the convection is dominated over the conduction. In convection, the transfer of thermal energy is resultant due to molecules movement under the influence of temperature differences. Natural convection is resulted when temperature gradient is present with in the fluid while the forced convection takes place by the way of some external force generating the flow. In the mixed convection, both natural and forced

convections collectively transfer heat in the fluid. Then, there is Marangoni convection which takes place at the surface of liquid-liquid or liquid-gas interface. The surface at the interface has an energy due to the presence of surface tension gradients. Due to these gradients, fluid migrates from a higher surface tension potential to a lower surface tension potential. The surface tension gradients depend upon the temperature and concentration differences present with in the fluid. In heat transfer by thermal radiation, heat is transferred by the electromagnetic waves without the requirement of any medium.

2.3 Differential Operators in Cartesian Coordinate System

In the context of present study, some important operators are defined here.

"Nabla Operator":

The Nabla operator in index form is:

$$\nabla = \mathbf{i}\frac{\partial}{\partial x} + \mathbf{j}\frac{\partial}{\partial y} + \mathbf{k}\frac{\partial}{\partial z}.$$

"Gradient of a scalar field f":

$$\nabla f = \mathbf{i}\frac{\partial f}{\partial x} + \mathbf{j}\frac{\partial f}{\partial y} + \mathbf{k}\frac{\partial f}{\partial z}.$$

"Divergence of a vector field $\boldsymbol{V} = [u, v, w]$*"*:

$$\nabla \cdot \mathbf{V} = \frac{\partial u}{\partial x} + \frac{\partial v}{\partial y} + \frac{\partial w}{\partial z}.$$

"Curl of vector field":

$$\nabla \times \mathbf{V} = \mathbf{i}\left(\frac{\partial w}{\partial y} - \frac{\partial v}{\partial z}\right) + \mathbf{j}\left(\frac{\partial u}{\partial z} - \frac{\partial w}{\partial x}\right) + \mathbf{k}\left(\frac{\partial v}{\partial x} - \frac{\partial u}{\partial y}\right).$$

"Laplacian of a scalar field f":

$$\nabla^2 f = \frac{\partial^2 f}{\partial x^2} + \frac{\partial^2 f}{\partial y^2} + \frac{\partial^2 f}{\partial z^2}.$$

"Laplacian of a vector field":

$$\nabla^2 \mathbf{V} = \mathbf{i}\nabla^2 u + \mathbf{j}\nabla^2 v + \mathbf{k}\nabla^2 w.$$

‘‘Operator $\mathbf{V} \cdot \nabla$":

$$\mathbf{V} \cdot \nabla = u\frac{\partial}{\partial x} + v\frac{\partial}{\partial y} + w\frac{\partial}{\partial z}.$$

2.4 Differential Operators in Cylindrical Coordinate System

"Nabla Operator":

$$\nabla = \mathbf{e}_r \frac{\partial}{\partial r} + \mathbf{e}_\Theta \frac{1}{r}\frac{\partial}{\partial \Theta} + \mathbf{e}_z \frac{\partial}{\partial z}.$$

"Gradient of a scalar field f":

$$\nabla f = \mathbf{e}_r \frac{\partial f}{\partial r} + \mathbf{e}_\Theta \frac{1}{r}\frac{\partial f}{\partial \Theta} + \mathbf{e}_z \frac{\partial f}{\partial z}.$$

"Divergence of a vector field" :

$$\nabla \cdot \ \mathbf{V} = \frac{1}{r}\frac{\partial ru}{\partial r} + \frac{1}{r}\frac{\partial v}{\partial \Theta} + \frac{\partial w}{\partial z}.$$

"Curl of vector field" :

$$\nabla \times \mathbf{V} = \mathbf{e}_r \left(\frac{1}{r}\frac{\partial w}{\partial \Theta} - \frac{\partial v}{\partial z}\right) + \mathbf{e}_\Theta \left(\frac{\partial u}{\partial z} - \frac{\partial w}{\partial r}\right) + \mathbf{e}_z \left(\frac{1}{r}\frac{\partial rv}{\partial r} - \frac{1}{r}\frac{\partial u}{\partial \Theta}\right).$$

"Laplacian of a scalar field f":

$$\nabla^2 f = \frac{1}{r}\frac{\partial}{\partial r}\left(r\frac{\partial f}{\partial r}\right) + \frac{1}{r^2}\frac{\partial^2 f}{\partial \Theta^2} + \frac{\partial^2 f}{\partial z^2}.$$

"Laplacian of a vector field":

$$\nabla^2 \mathbf{V} = \mathbf{e}_r \nabla^2 u + \mathbf{e}_\Theta \nabla^2 v + \mathbf{e}_z \nabla^2 w.$$

"Operator $\boldsymbol{V} \cdot \nabla$*"*:

$$\mathbf{V} \cdot \nabla = u\frac{\partial}{\partial r} + \frac{v}{r}\frac{\partial}{\partial \Theta} + w\frac{\partial}{\partial z}.$$

2.5 The Substantial Derivative

In any physical process, which involve change in some physical property with respect to time and space, substantial derivative comes into play. The substantial derivative is represented by $\frac{D}{Dt}$ and is defined as:

$$\frac{D(*)}{Dt} = \frac{\partial(*)}{\partial t} + \mathbf{V} \cdot \nabla(*). \tag{2.4}$$

In Eq. (2.4), the term on the left hand side is called the total rate of change. On the right hand side, the first term represents the change with respect to time, also called as local rate of change. The second term gives the change of some property at a particular position in space, also called as the convective rate of change.

2.6 The Governing Equations

To analyze the heat transfer process in nanofluids mathematically, conservation equations of state are defined as follows:

Mass equation[46]:

Mass equation is also known as the continuity equation. "The mathematical form

of law of conservation of mass which states that the total rate of change in mass of a system equals zero" is given as:

$$\frac{\partial \rho}{\partial t} + \nabla \cdot \rho \mathbf{V} = 0. \tag{2.5}$$

Here, ρ is considered constant if the fluid is incompressible.

Momentum equation [46]:

Momentum equation is basically the mathematical form of "Newton's second law of motion". For fluid flow, the "Newton's second law of motion states that the rate of change of momentum within a fluid element equals the external forces acting on it". The external forces are divided into surface and body forces. The forces that act normally along tangential stresses constitutes the surface forces while the body forces act at every point of the fluid element. Magnetic field and bouyancy are some of the examples of body forces. Mathematically, momentum law is defined as:

$$\rho \frac{D\mathbf{V}}{Dt} = \nabla \cdot (-p\mathbf{I} + \mu \mathbf{A}) + \mathbf{B}, \tag{2.6}$$

where, $\mathbf{A} = \nabla \mathbf{V} + (\nabla \mathbf{V})^*$. In Eq. (2.6) , p represents the pressure forces,$\mathbf{A}$ gives the tensor form of the tangential forces and $\mathbf{B}$ are the body forces acting on the fluid element.

Energy equation [46]:

The balance of energy in a fluid element is represented mathematically by the energy equation. The underlying principle for energy conservation comes for the first law of thermodynamics that states "the rate of change of internal energy of a system equals the rate of heat addition plus the rate of work done ". Mathematically, we have:

$$\frac{DT}{Dt} = \alpha' \nabla^2 T + (\tau \cdot \nabla)\mathbf{V}, \tag{2.7}$$

where, $\alpha' = \frac{\kappa}{\rho C_p}$ is thermal diffusivity. On the right hand side of Eq. (2.7), the 1^st term is the heat source term which comes from Fourier's law [47]. The

mathematical form of the law is given by:

$$\mathbf{q} = -\kappa \nabla T.$$

$(\tau \cdot \nabla)\mathbf{V}$ represents the work done by the viscous force on the fluid element. In addition to the surface forces doing work on the fluid element, there are pressure forces acting at the surface and body forces like the magnetic field doing work on the body.

Concentration equation [48]:

Analogous to the conservation of energy, the conservation of mass law states "the rate of change of mass with in a system equals the rate of mass added to the system plus the mass generated inside the system". In the absence of mass consumption or production, the conservation of nanoparticles equation is given as :

$$\frac{DC}{Dt} = D_m \nabla^2 C. \tag{2.8}$$

2.7 Cattaneo-Christov Heat Flux Model

Fourier's concept of heat conduction remained valid for a century. A shortcoming of the Fourier's interpretation of heat transport was that a disturbance in the temperature gradient at the boundary is felt instantly through the medium which means that heat energy travels at an infinite speed which is not possible physically. This drawback of Fourier's law was addressed by Cattaneo [47]. Cattaneo's modification to the Fourier's law is given as:

$$\left(1 + \lambda_0 \frac{\partial}{\partial t}\right) \mathbf{q} = -\kappa \nabla T.$$

Here, λ_0 is termed as thermal relaxation time. It is the time lag involved in achieving the steady state solution once a temperature gradient is applied across a volume element.

Cattaneo's modification addressed the drawback of the Fourier's law but resulted

in a coupled system to be solved in order to get knowledge about the energy distribution in the system. Christov [47], further modified the Cattaneo's concept by considering a material Oldroyds' upper-convected derivative instead of the ordinary time derivative. With the help of this modification, a single energy equation was achieved. Hence, in terms of Christov's theory the heat conduction law is written as:

$$\mathbf{q} + \lambda_0 \left(\frac{\partial \mathbf{q}}{\partial t} + \mathbf{V} \cdot \nabla \mathbf{q} - \mathbf{q} \cdot \nabla \mathbf{V} + (\nabla \cdot \mathbf{V})\mathbf{q} \right) = -\kappa \nabla T. This model of heat transfer has been exten$$

2.8 Body Forces

Body forces are the forces that act on the whole volume of the fluid element. For example, mangetic force, bouyancy force etc. In fluid mechanics, body forces are added to the momentum equation as a source term. Such forces play a signifcant role as they affect the fluid characteristics pertaining to the flow.

2.8.1 Magnetohydrodynamics

A constant feature of the present thesis is the application of magnetic field on the flow of the fluid. As discussed in the introduction section, external magnetic field affects the heat conduction abilities of nanofluids. This feature makes it useful to discuss it in our heat transfer analysis. MHD [49] works on the notion "that electrical current is produced when an electrically conducting fluid passes through a magnetic field". Maxwell's electromagnetism equations when used to model the mathematical form of MHD, under certain assumptions reduce to Lorentz forces, added as body force in the momentum equation as:

$$\boldsymbol{b_m} = \mathbf{J} \times \mathbf{B}, \tag{2.9}$$

where

$$\mathbf{J} = (\sigma_{el})_f(\mathbf{E} + \nabla \times \mathbf{B}). \tag{2.10}$$

If the fluid has strong magnetic conductance or the fluid flow is at a high rate that is flow is highly inertial, then the induced magnetic field is generated thus magnetic induction equation comes into picture which is defined as:

$$\frac{\partial \mathbf{B}}{\partial t} = \nabla \times (\mathbf{V} \times \mathbf{B}) + \mu_e \nabla^2 \mathbf{B}. \tag{2.11}$$

2.8.2 Natural Convection

Natural convection occurs in the fluid where there exists temperature differences. The temperature differences affect the relative buoyancy of the fluid as the density of the fluid is disturbed due to the thermal imbalances inside it. In convective transport due to the buoyancy forces, free convection is taken as body force given mathematically as:

$$\boldsymbol{b_F} = \rho_f g_e \beta_T (T - T_0). \tag{2.12}$$

Here, $\boldsymbol{b_F}$ represents the Boussinesq approximation of the bouyancy force in which the density alone is a function of temperature. Density of the fluid varies linearly with temperature under this assumption.

2.9 Single Phase Nanofluid Models

Nanofluid inherently is a two-phase fluid but for numerical simulation some assumptions are made in a way that the nanofluid can be considered as a single phase model. Single phase models can be classified as homogeneous, dispersion and Buongiorno models.

2.9.1 Homogeneous Single Phase Model

In this thesis, a homogeneous single phase model approach [50] is adopted in Chapter 4 and 5. Throughout the thesis, fluid considered is steady that is the fluid properties don't change over time and incompressible which means that the fluid's density is constant. The particles are supposed to be ultrafine which are homogeneously dispersed inside the base fluid. Also, there is no relative velocity between the fluid particles and nanoparticles. The nanoparticles and the base fluids are in thermal equilibrium. The governing equations defined in (2.5)-(2.7) for incompressible fluid, the homogeneous single phase model takes the form:

$$\nabla \cdot \mathbf{V} = 0, \tag{2.13}$$

$$\rho_{nf} \frac{D\mathbf{V}}{Dt} = \nabla \cdot (-p\mathbf{I} + \mu_{nf}\mathbf{A}) + \mathbf{b}, \tag{2.14}$$

$$\frac{DT}{Dt} = \alpha'_{nf} \nabla^2 T + (\tau \cdot \nabla)\mathbf{V}. \tag{2.15}$$

Here, the physical quantities appearing in the above equations with subscript "nf", "f" and "p" representing the nanofluids, base fluids and nanoparticles respectively. The correlations between the physical properties of nanofluid and base fluids are defined as [14]:

$$\mu_{nf} = \frac{\mu_f}{(1-\phi)^{2.5}}, \tag{2.16}$$

$$\rho_{nf} = \rho_p \phi + (1-\phi)\rho_f, \tag{2.17}$$

$$(\rho C_p)_{nf} = (\rho C_p)_p \phi + (1-\phi)(\rho C_p)_f, \tag{2.18}$$

$$\frac{(\sigma_{el})_{nf}}{(\sigma_{el})_f} = 1 + \frac{3\left(\frac{(\sigma_{el})_p}{(\sigma_{el})_f} - 1\right)\phi}{\left(\frac{(\sigma_{el})_p}{(\sigma_{el})_f} + 2\right) - \left(\frac{(\sigma_{el})_p}{(\sigma_{el})_f} - 1\right)\phi}, \tag{2.19}$$

$$\alpha'_{nf} = \frac{\kappa_{nf}}{(\rho C_p)_{nf}},$$

$$\nu_{nf} = \frac{\mu_{nf}}{\rho_{nf}}.$$

Here, σ_{el} is the electrical conductivity and C_p is the specific heat per unit mass. Hamilton–Crosser model [51] is utilized to define the thermal conductivity κ_{nf} of nanofluids in the following manner:

$$\frac{\kappa_{nf}}{\kappa_f} = 1 + \frac{\kappa_p + (m-1)\left(\kappa_f - \phi(\kappa_f - \kappa_p)\right)}{\kappa_p + (m-1)\kappa_f + \phi(\kappa_f - \kappa_p)}. \tag{2.20}$$

The thermophysical properties of the base fluid and nanoparticles are given in Table 2.1.

Table 2.1: Thermophysical properties of the nanofluid.

	C_p(J/kg K)	ρ(kg/m^3)	κ(W/mK)	σ_{el}(C/m^3)
Al_2O_3	765	3970	40	10^{-12}
SWCNT	425	2600	6600	–
MWCNT	796	1600	3000	–
H_2O	4179	997.1	0.613	0.05
kerosene oil	2090	783	0.145	–

2.9.2 Buongiorno Single Phase Model

Buongiorno nanofluid model [52] is a combination of homogeneous and dispersion models. Of the various slip mechanisms, Buongiorno deduced that the Brownian and thermal diffusion affects are potent slip mechanisms in the nanofluids. The set of constitutive equations differ in the sense that in the energy and concentration equations the effects of Brownian motion and the thermophoresis are incorporated as :

$$\frac{DT}{Dt} = \alpha'_{nf}\nabla^2 T + \tau^*(D_B \nabla T \cdot \nabla C + \frac{D_T}{T_0}\nabla T \cdot \nabla T), \tag{2.21}$$

Here, $\tau^* = \dfrac{(\rho C_p)_p}{(\rho C_p)_f}$.

$$\frac{DC}{Dt} = D_B \nabla^2 T + \tau \frac{D_T}{T_0}\nabla^2 T. \tag{2.22}$$

Buongiorno nanofluid model approach is utilized in Chapter 3 and Chapter 6 of the present thesis.

2.10 Governing Equations of Micropolar Fluids

Making use of the Eringen theory, for the micropolar fluid, the momentum (2.6) and angular momentum equations take the form:

$$\rho_{nf}\frac{D\mathbf{V}}{Dt} = -\nabla p + (\mu_{nf} + \kappa^*)\nabla^2\mathbf{V} + \kappa^*(\nabla \times \mathbf{V}) + \mathbf{b}. \tag{2.23}$$

$$\rho_{nf} j\frac{D\mathbf{N}}{Dt} = \gamma_{nf}\nabla^2\mathbf{N} + \kappa^*(-2\mathbf{N} + \nabla \times \mathbf{V}), \tag{2.24}$$

where, $\mathbf{N} = [N_x, N_y, N_z]$ is angular velocity vector and $\gamma_{nf} = (\mu_{nf} + \frac{\kappa^*}{2})j$ is the rotation viscosity of the nanofluids.

2.11 Boundary Layer Flow

A viscous fluid flowing over a surface can be divided into two regions. The region where the viscosity effects can be neglected and flow is almost inviscid and the region of boundary layer where viscosity effects compete with the convective effects. Boundary layer is formed due to presence of no slip at the surface with which the fluid is in contact. Introduction to this concept was given by Ludwig Prandtl [53] in 1904. The distance from the surface to the point where the fluid has 99% of the free stream velocity is called boundary layer thickness. It is denoted by ω. Analogous to velocity boundary layer, thermal and concentration boundary layers can be defined [26].

Outside the boundary layer, the velocity gradient $\frac{\partial u}{\partial y}$ perpendicular to the wall is

of the order of $\frac{\partial u}{\partial x}$ but within the boundary layer, we have

$$\frac{\partial u}{\partial x} << \frac{\partial u}{\partial y},$$

and the boundary layer thickness ω, in growing x-direction satisfies

$$\frac{\omega}{L} << 1. \tag{2.25}$$

Here, L characterizes the flat surface's length. Similar analogy is applied to thermal and concentration boundary layers provided that the temperature and concentration gradients are significant. Consider a 2D, steady and incompressible laminar flow.The expanded form of mass and Navier Stokes equations are given as:

$$\frac{\partial u}{\partial x} + \frac{\partial v}{\partial y} = 0, \tag{2.26}$$

$$u\frac{\partial u}{\partial x} + v\frac{\partial u}{\partial y} = -\frac{1}{\rho}\frac{\partial p}{\partial x} + \nu\left(\frac{\partial^2 u}{\partial x^2} + \frac{\partial^2 u}{\partial y^2}\right), \tag{2.27}$$

$$u\frac{\partial v}{\partial x} + v\frac{\partial v}{\partial y} = -\frac{1}{\rho}\frac{\partial p}{\partial y} + \nu\left(\frac{\partial^2 v}{\partial x^2} + \frac{\partial^2 v}{\partial y^2}\right). \tag{2.28}$$

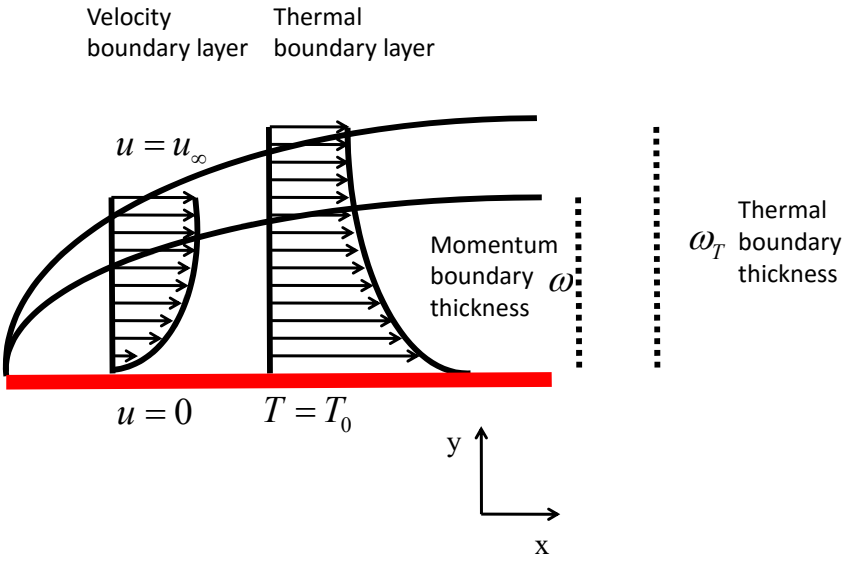

Figure 2.1: Boundary layer flow model

The proper nondimensional variables are:

$$x^* = \frac{x}{L}, \qquad y^* = \frac{y}{\omega}, \qquad u^* = \frac{u}{u_w}, \qquad v^* = \frac{v\sqrt{Re}}{u_w}, \qquad p^* = \frac{p}{\rho u_w^2}.$$

Using these nondimensional parameters in (2.26)-(2.28) lead to the following nondimensional equations:

$$\frac{\partial u^*}{\partial x^*} + \frac{\partial v^*}{\partial y^*} = 0, \tag{2.29}$$

$$u^*\frac{\partial u^*}{\partial x^*} + v^*\frac{\partial u^*}{\partial y^*} = -\frac{\partial p^*}{\partial x^*} + \nu\left(\frac{1}{Re}\frac{\partial^2 u^*}{\partial x^{*2}} + \frac{\partial^2 u^*}{\partial y^{*2}}\right), \tag{2.30}$$

$$\frac{1}{Re}\left(u^*\frac{\partial v^*}{\partial x^*} + v^*\frac{\partial v^*}{\partial y^*}\right) = -\frac{\partial p^*}{\partial y^*} + \nu\left(\frac{1}{Re^2}\frac{\partial^2 v^*}{\partial x^{*2}} + \frac{1}{Re}\frac{\partial^2 v^*}{\partial y^{*2}}\right). \tag{2.31}$$

The inequality (2.25) is satified only if $Re \to \infty$. After dropping "*", we have:

$$\frac{\partial u}{\partial x} + \frac{\partial v}{\partial y} = 0, \tag{2.32}$$

$$u\frac{\partial u}{\partial x} + v\frac{\partial u}{\partial y} = -\frac{\partial p}{\partial x} + \nu\frac{\partial^2 u}{\partial y^2}, \tag{2.33}$$

$$0 = -\frac{\partial p}{\partial y}. \tag{2.34}$$

2.12 Entropy

Entropy of a system is its inability to make use of the energy 100%. Greater is the entropy generation in a system, less is the usefulness of that system. The quality of a heat transfer system greatly depends upon the entropy generation in that system. Only in an ideal system where no energy is lost, the entropy of the system is zero. In our study, the considered factors contributing to the entropy of a system are fluid friction irreversibly, heat transfer irreversibly, mass transfer irreversibly and entropy generation due to Lorentz forces [54]:

$$S'''_{gen} = (S'''_{gen})_{FF} + (S'''_{gen})_{HT} + (S'''_{gen})_{MT} + (S'''_{gen})_{MF}.$$

For a two dimensional flow, the mathematical equation of local entropy generation is given as:

$$S'''_{gen} = \frac{\tau : \nabla V}{T} + \frac{\lambda}{T}(\nabla T)^2 + \frac{RD}{T}\left[(\nabla C)^2 + \nabla C \cdot \nabla T\right] + (\sigma)_{el}\frac{|\mathbf{V} \times \mathbf{B}|^2}{T}. \quad (2.35)$$

Here, ":" represents double dot product of τ and $\nabla \mathbf{V}$. The first term at the right hand side of the Eq. (2.35) is due to fluid friction, second term is due to heat transfer, third is due to mass transfer and the fourth is due to magnetic force.

2.13 Physical Quantities

In the heat transfer analysis in nanofluids, some important physical parameters appear in the mathematical equations. Here, some insight is provided about these numbers and their physical aspect in order to develop an understanding about their impact on the properties of the fluid in this study.

2.13.1 Hartmann Number

Hartmann number Ha, arises in the term involving Lorentz forces present in the momentum equation, when nondimensionalized. It is defined mathematically as:

$$Ha = \sqrt{\frac{\sigma_{el} B_0^2}{\mu}}.$$

"Hartmann number is a measure of the strength of resistance or assistance offered by the magnetic field when applied to the electrically conducting fluid flow". Sometimes, Hartmann number is defined in the form of magnetic number M which is defined as $M = Ha^2$..

2.13.2 Material Parameter

Material or the so called rotation viscosity parameter K, arises in the nondimensionalized linear and angular momentum equations due to the presence of microstructures in the constitutive fluids. This parameter is a measure of the resistance provided by the rotation viscosity of the nanofluid. Mathematically, it is defined as [23]:

$$K = \frac{\kappa^*}{\mu}.$$

2.13.3 Eckert Number

Eckert number Ec, is a dimensionless number which characterizes the relative heat dissipation taking place in a system by conduction and convection. Mathematically, it is given as [48]:

$$Ec = \frac{u^2}{C_p(T - T_w)}.$$

2.13.4 Reynolds Number

"Reynolds number Re, is the ratio of the inertial to viscous forces. When Reynolds number is small, the viscous forces are dominant and the velocity boundary layer is significant but as it increases, the boundary layer effects and boundary layer thickness diminishes". It is defined mathematically as [48]:

$$Re = \frac{uL}{\nu}.$$

2.13.5 Prandtl Number

The Prandtl number Pr characterizes the heat transfer mechanism in fluid. It tells whether the heat transport in fluid is dominated by heat conduction or by

convection. Prandtl number is analogous to Reynolds number [48].

$$Pr = \frac{\nu}{\alpha'}.$$

Prandtl number for liquid metals is less than 1, for gases, it is almost 1 and for liquids, it is greater than 1.

2.13.6 Schmidt Number

Schmidt number Sc characterizes the mass transfer phenomenon in fluids. It gives information whether the mass transport in fluid is dominated by diffusion or by convection [48]:

$$Sc = \frac{\nu}{D_m}.$$

2.13.7 Brownian Motion Parameter

"Brownian motion is the random motion of solid particles present inside the host fluid due to their collisions with the constitutive particles". In heat transfer applications, heat transport mechanism is significantly affected due to the presence of the nanoparticles in the nanofluid. The Brownian motion coefficient D_B is defined in the following manner as [55]:

$$D_B = \frac{\kappa_B T C}{3\pi_p \mu_f d_P}.$$

2.13.8 Thermophoresis Parameter

Thermophoresis force can be viewed as a symmetrical force to the Brownian motion imposed by the temperature gradient. In nanofluids, due to this force the nanoparticles travel under the influence of the thermal imbalances existing with

in the fluid. The thermophoresis coefficient D_T is defined as [55]:

$$D_T = 0.26\frac{\kappa_{nf}\nu_{nf}}{2\kappa_{nf} + \kappa_p}C.$$

2.13.9 Skin Friction Coefficient

"Skin friction coefficient C_f is the measure of friction between the surface and the fluid. The coefficient of skin friction is obtained by dividing the shear stress by the dynamic pressure of the free stream [48]":

$$C_f = \frac{\tau_w}{\frac{1}{2}\rho_f u_w^2}.$$

The viscosity of the fluid is responsible for this force and the presence of nanoparticles in the nanofluid add to the skin friction.

2.13.10 Nusselt Number

"Nusselt number Nu is a measure of the heat transfer rate at the surface of the fluid". It is important to study the heat transfer at the surface of the fluid in boundary layer flow. Its importance is more highlighted when most of the heat transfer takes place near the boundary. It is defined as [48]:

$$Nu = \kappa_{nf}\frac{\nabla T}{\kappa_f}.$$

2.13.11 Sherwood Number

"Sherwood number Sh, is a dimensionless number which is a measure of the mass transfer rate at the surface of the fluid". It is defined as [48]:

$$Sh = D_m \nabla C.$$

2.14 Keller Box Method

The numerical procedure used to solve the system of ODEs arising in the problems considered in the present study is the KBM. KBM is widely used to solve BVPs of complex nature. The details, accuracy and stability criteria of the scheme can be found in [26, 56]. The layout of the scheme is given as follows:

- First, we convert the BVPs into first order ODEs.
- The resulting ODEs are discretized by central differences for the derivative terms and average values for the functions at the $(\zeta - \frac{1}{2})$ nodes appearing in the equations as follows:

$$\begin{cases} *'_{\zeta-\frac{1}{2}} = \frac{*_\zeta - *_{\zeta-1}}{h}, \\ *_{\zeta-\frac{1}{2}} = \frac{*_\zeta + *_{\zeta-1}}{2}. \end{cases} \tag{2.36}$$

- Linearization of the resulting nonlinear difference equations is achieved by the Newton's method.

$$*_\zeta^{i+1} = *_\zeta^i + \varepsilon\, *_\zeta^i \,. \tag{2.37}$$

- The resulting linear system is written in the matrix form as:

$$\mathbf{W}\mathbf{x} = \mathbf{r}. \tag{2.38}$$

- The vector of unknowns $\mathbf{x}$ is obtained by solving the system (2.38) using the LU-decomposition method.
- Updation is made to the solution vector and the process is continued until the required accuracy is achieved. To explain KBM, two nonlinear ODEs are considered. The deliberation of each step of KBM is carried out in full description for a complete understanding of the method.

Example 2.1. *Consider the following* 4^{th} *order boundary value problem:*

$$f'''' - (1 - x^2)(f'')^2 + 5f^2 = 0, \tag{2.39}$$

subject to

$$f(0) = 1, \qquad f'(0) = 0, \qquad f''(1) = -2, \qquad f'''(1) = -3. \tag{2.40}$$

We convert (2.39) to four first order ODEs as:

$$f' = Y_1, \tag{2.41}$$
$$f'' = Y_1' = Y_2, \tag{2.42}$$
$$f''' = Y_2' = Y_3, \tag{2.43}$$
$$Y_3' - (1 - x^2)Y_2^2 + 5f^2 = 0, \tag{2.44}$$

and the boundary conditions in (2.45) become:

$$f(0) = 1, \qquad Y_1(0) = 0, \qquad Y_2(1) = -2, \qquad Y_3(1) = -3. \tag{2.45}$$

Next, making use of the relations defined in (2.36), the system in (2.41)-(2.44) is transformed as:

$$\frac{(f)_\zeta - (f)_{\zeta-1}}{h} = \frac{(Y_1)_\zeta + (Y_1)_{\zeta-1}}{2}, \tag{2.46}$$

$$\frac{(Y_1)_\zeta - (Y_1)_{\zeta-1}}{h} = \frac{(Y_2)_\zeta + (Y_2)_{\zeta-1}}{2}, \tag{2.47}$$
$$\frac{(Y_2)_\zeta - (Y_2)_{\zeta-1}}{h} = \frac{(Y_3)_\zeta + (Y_3)_{\zeta-1}}{2}, \tag{2.48}$$
$$\frac{(Y_3)_\zeta - (Y_3)_{\zeta-1}}{h} - (1 - x^2_{\zeta-\frac{1}{2}})\left[\frac{(Y_2)_\zeta + (Y_2)_{\zeta-1}}{2}\right]^2 + 5\left[\frac{(f)_\zeta + (f)_{\zeta-1}}{2}\right]^2 = 0. \tag{2.49}$$

After linearization, (2.46)-(2.49) take the form:

$$\varepsilon(f)_\zeta - \varepsilon(f)_{\zeta-1} - \frac{1}{2}h\big[\varepsilon(Y_1)_\zeta + \varepsilon(Y_1)_{\zeta-1}\big] = (r_1)_{\zeta-\frac{1}{2}}, \tag{2.50}$$

$$\varepsilon(Y_1)_\zeta - \varepsilon(Y_1)_{\zeta-1} - \frac{1}{2}h\big[\varepsilon(Y_2)_\zeta + \varepsilon(Y_2)_{\zeta-1}\big] = (r_2)_{\zeta-\frac{1}{2}}, \tag{2.51}$$

$$\varepsilon(Y_1)_\zeta - \varepsilon(Y_1)_{\zeta-1} - \frac{1}{2}h\big[\varepsilon(Y_2)_\zeta + \varepsilon(Y_2)_{\zeta-1}\big] = (r_3)_{\zeta-\frac{1}{2}}, \tag{2.52}$$

$$\begin{aligned}&(a_1)_\zeta\varepsilon(f)_\zeta + (a_2)_\zeta\varepsilon(f)_{\zeta-1} + (a_3)_\zeta\varepsilon(Y_1)_\zeta + (a_4)_\zeta\varepsilon(Y_1)_{\zeta-1} + (a_5)_\zeta\varepsilon(Y_2)_\zeta \\ &+ (a_6)_\zeta\varepsilon(Y_2)_{\zeta-1} + (a_7)_\zeta\varepsilon(Y_3)_\zeta + (a_8)_\zeta\varepsilon(Y_3)_{\zeta-1} = (r_4)_{\zeta-\frac{1}{2}}.\end{aligned} \tag{2.53}$$

Here,

$$(a_1)_\zeta = (a_2)_\zeta = 5Y_{\zeta-\frac{1}{2}},$$

$$(a_3)_\zeta = (a_4)_\zeta = 0,$$

$$(a_5)_\zeta = (a_6)_\zeta = -(1 - x^2_{\zeta-\frac{1}{2}})v_{\zeta-\frac{1}{2}},$$

$$(a_7)_\zeta = 1,$$

$$(a_8)_\zeta = -1,$$

$$(r_1)_{\zeta-\frac{1}{2}} = -(f)_\zeta + (f)_{\zeta-1} + \frac{1}{2}h\big[(Y_1)_\zeta + (Y_1)_{\zeta-1}\big],$$

$$(r_2)_{\zeta-\frac{1}{2}} = -(Y_1)_\zeta + (Y_1)_{\zeta-1} + \frac{1}{2}h\big[(Y_2)_\zeta + (Y_2)_{\zeta-1}\big],$$

$$(r_3)_{\zeta-\frac{1}{2}} = -(Y_2)_\zeta + (Y_2)_{\zeta-1} + \frac{1}{2}h\big[(Y_3)_\zeta + (Y_3)_{\zeta-1}\big],$$

$$(r_4)_{\zeta-\frac{1}{2}} = -\frac{(Y_3)_\zeta - (Y_3)_{\zeta-1}}{h} + (1 - x^2_{\zeta-\frac{1}{2}})\left[\frac{(Y_2)_\zeta - (Y_2)_{\zeta-1}}{2}\right]^2 - 5\left[\frac{(f)_\zeta - (f)_{\zeta-1}}{2}\right]^2.$$

The boundary conditions in (2.45) give rise to the following constraints:

$$\varepsilon(f)_0 = \varepsilon(Y_1)_0 = \varepsilon(Y_2)_J = \varepsilon(Y_3)_J = 0.$$

The vector of unknowns is defined using the above constriants as:

$$\varepsilon_\zeta = \begin{bmatrix}\varepsilon(Y_2)_{\zeta-1} \\ \varepsilon(Y_3)_{\zeta-1} \\ \varepsilon(f)_\zeta \\ \varepsilon(Y_1)_\zeta\end{bmatrix}, \qquad \zeta = 1, ..., J.$$

Making use of the above defined vector, the system is written as:

$$\mathbf{W}\mathbf{x} = \mathbf{r}. \tag{2.54}$$

where

$$\mathbf{W} = \begin{bmatrix} A_1 & C_1 & & & & \\ B_2 & A_2 & C_2 & & & \\ & \ddots & \ddots & \ddots & & \\ & & & B_{J-1} & A_{J-1} & C_{J-1} \\ & & & & B_J & A_J \end{bmatrix}, \quad \mathbf{x} = \begin{bmatrix} \varepsilon_1 \\ \varepsilon_2 \\ \vdots \\ \varepsilon_{J-1} \\ \varepsilon_J \end{bmatrix}, \quad \mathbf{r} = \begin{bmatrix} (r_1)_{\zeta-\frac{1}{2}} \\ (r_2)_{\zeta-\frac{1}{2}} \\ \vdots \\ (r_{J-1})_{J-\frac{1}{2}} \\ (r_J)_{J-\frac{1}{2}} \end{bmatrix}. \tag{2.55}$$

$$A_\zeta = \begin{bmatrix} 0 & 0 & 1 & \frac{-h}{2} \\ \frac{-h}{2} & 0 & 0 & 1 \\ -1 & \frac{-h}{2} & 0 & 0 \\ (a_6)_\zeta & (a_8)_\zeta & (a_1)_\zeta & (a_3)_\zeta \end{bmatrix}, \qquad \zeta = 1, 2, 3, ..., J,$$

$$B_\zeta = \begin{bmatrix} 0 & 0 & -1 & \frac{-h}{2} \\ 0 & 0 & 0 & -1 \\ 0 & 0 & 0 & 0 \\ 0 & 0 & (a_2)_\zeta & (a_4)_\zeta \end{bmatrix}, \qquad \zeta = 2, 3, ..., J,$$

$$C_\zeta = \begin{bmatrix} 0 & 0 & 0 & 0 \\ \frac{-h}{2} & 0 & 0 & 0 \\ 1 & \frac{-h}{2} & 0 & 0 \\ (a_5)_\zeta & (a_7)_\zeta & 0 & 0 \end{bmatrix}, \qquad \zeta = 1, 2, ..., J-1.$$

The system defined by (2.54) is solved using LU-block factorization method. The vector of unknowns is updated and the process is continued till the relative error calculated at each iteration becomes less than the required accuracy. The numerical results obtained by KBM for the present problem are demonstrated graphically in Figure 2.3.

Example 2.2. *Consider the following* 3^{rd} *order boundary value problem:*

$$f''' + ff'' - (f')^2 = 0, \tag{2.56}$$

subject to

$$f(0) = 0, \qquad f''(0) = -2, \qquad f'(\infty) = 0. \tag{2.57}$$

The exact solution to this problem is given by:

$$f(x) = (2)^{\frac{1}{3}}(1 - \exp(-(2)^{\frac{1}{3}}x)). \tag{2.58}$$

Following the KBM procedure as defined for Rxample 2.1, the numerical solution to the present example is achieved. A comparison of the exact solution (2.59) to the numerical solution is given in Figure 2.4.

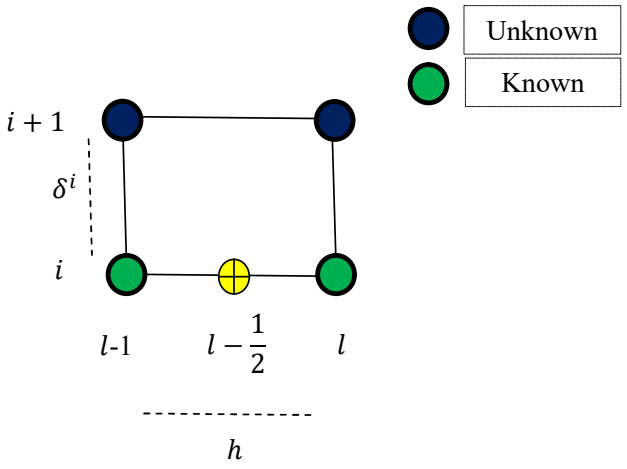

Figure 2.2: Stencil: KBM.

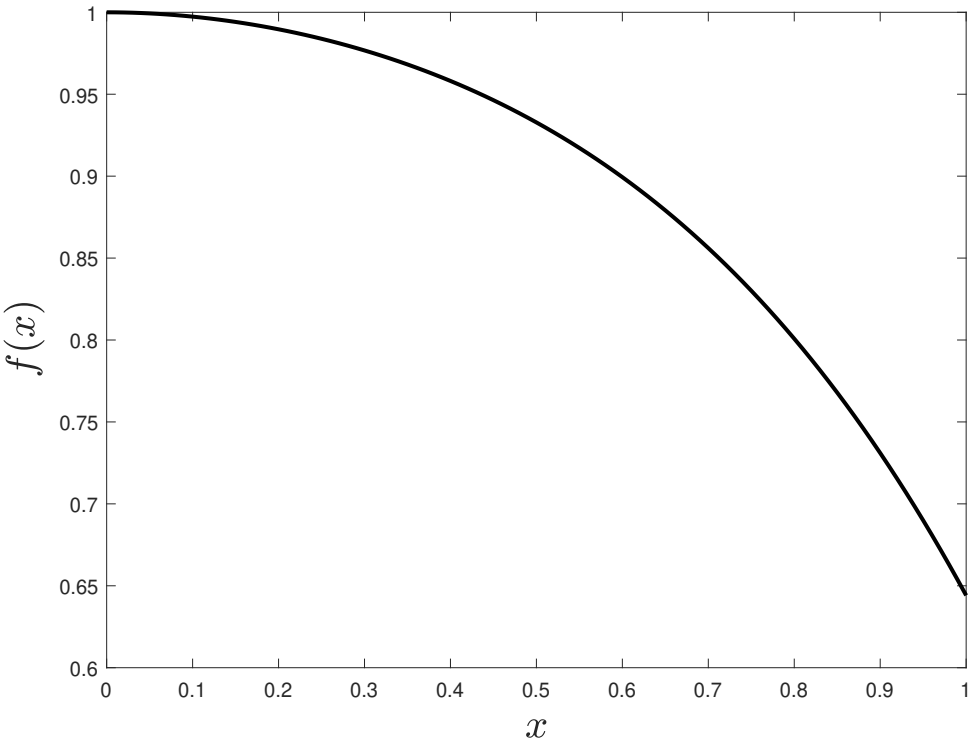

Figure 2.3: Graphical results of the Example 2.1.

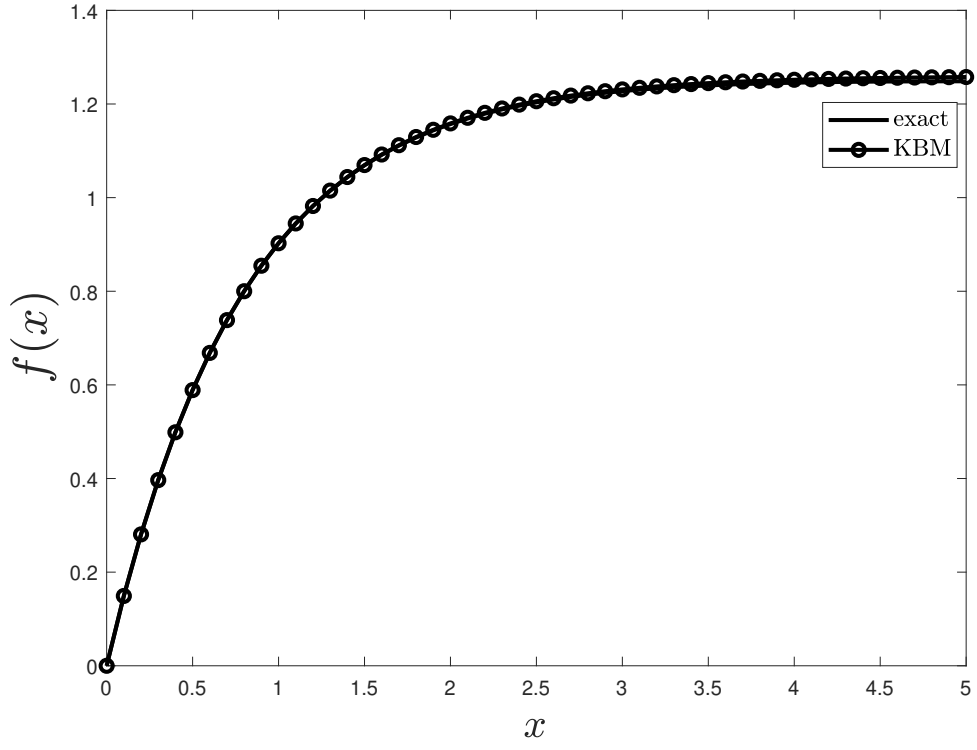

Figure 2.4: Graphical results of the Example 2.2.

Chapter 3

Convectively Heated Boundary Impact on Heat Transfer in MHD Casson Nanofluid

3.1 Introduction

Flows over flat plates has been seen with great interest in boundary layer flows for a very long time. Many phyiscal applications witnesses a flow which is generated by a sheet pulled in a certain direction. In the present chapter, Casson nanofluid flow over a flat surface horizontally stretched is analyzed mathematically with MHD effect. Boundary conditions at the surface are taken in the sense of slip and thermal convection. Mathematical modeling is carried out using the Boungiorno nanofluid model. Boundary layer approximations are applied to the model to observe the flow properties of Casson nanofluid near the surface. KBM solution is obtained to the nonlinear ODEs resultant after application of the similarity transformation to the nonlinear PDEs. Besides this the energy dissipation in the flow has been measured by the entropy generation number. Graphical representations are used to scrutinize the effect of effective parameters on the nanofluid properties.

3.2 Problem Statement and Mathematical Formulation

A $2D$ Casson nanofluidic flow over a stretching sheet is considered in the positive x-direction. Magnetic field B_0 is supposed to be acting perpendicularly to the flow. Joule heating effect is incorporated in the study to observe the heat dissipation. It is assumed that the fluid doesn't induces a magnetic field for the scenario presented. The surface of the sheet is assumed to be slippery so at $y = 0$, the slip boundary conditions are applied. A temperature gradient results in the use of convective BCs at the surface. The nanofluid mixture is assumed to be homogeneous so that the Boungiorno nanofluid model can be utilized in the study. The free stream temperature and concentration are taken as T_∞ and C_∞. Casson fluid is characterized by the relation given in Eq. (2.2). Using the Casson nanofluid shear stress tensor along with the above assumptions, the Buongiorno single phase nanofluid model is defined as:

$$\frac{\partial v}{\partial y} + \frac{\partial u}{\partial x} = 0, \tag{3.1}$$

$$u\frac{\partial u}{\partial x} + v\frac{\partial v}{\partial y} = \nu\left(1 + \frac{1}{\beta}\right)\frac{\partial^2 u}{\partial y^2} - \sigma_{el}\frac{{B_0}^2 u}{\rho}, \tag{3.2}$$

$$u\frac{\partial T}{\partial x} + v\frac{\partial T}{\partial y} = \alpha'\frac{\partial^2 T}{\partial y^2} + \tau D_B\frac{\partial C}{\partial y}\frac{\partial T}{\partial y} + \frac{\tau D_T}{T_\infty}\left(\frac{\partial T}{\partial y}\right)^2 + \sigma_{el}\frac{B_0^2 u^2}{\rho C_p}, \tag{3.3}$$

$$u\frac{\partial C}{\partial x} + v\frac{\partial C}{\partial y} = \frac{D_T}{T_\infty}\frac{\partial^2 T}{\partial y^2} + D_B\frac{\partial^2 C}{\partial y^2}. \tag{3.4}$$

The boundary conditions are given as [57]:

$$\begin{cases} u = u_w + \gamma_0\left(1 + \frac{1}{\beta}\right)\frac{\partial u}{\partial y}, v = 0, -\kappa\frac{\partial T}{\partial y} = h_T(T_w - T), C = C_w, & \text{at} \quad y = 0, \\ u \to 0, \quad v \to 0, \quad T \to T_\infty, \quad C \to C_\infty, & \text{as} \quad y \to \infty. \end{cases}$$

The dimensionless functions and similarity variables are as follows [58]:

$$u = u_w f'(\eta), \quad v = -\sqrt{\frac{\nu u_w}{x}}f(\eta), \quad \theta = \frac{T - T_w}{T_w - T_\infty}, \quad \phi = \frac{C - C_w}{C_w - C_\infty}, \quad \eta = \sqrt{\frac{u_w}{\nu x}}y.$$

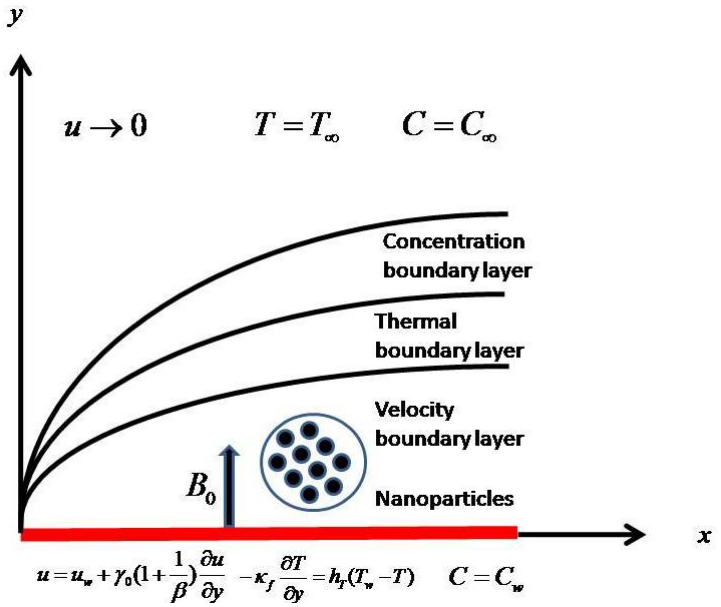

Figure 3.1: Schematic flow model diagram.

Using the similarity transforms, (3.1) is satisfied identically and (3.2)-(3.4) get the form:

$$f''' + \left(\frac{\beta}{1+\beta}\right)\left(ff'' - f'^2 - Mf'\right) = 0, \tag{3.5}$$

$$\frac{1}{Pr}\theta'' + f\theta' + N_B\ \theta'\phi' + N_T\ \theta'^2 + Ec\ Mf'^2 = 0, \tag{3.6}$$

$$\phi'' + Lef\phi' + \frac{N_T}{N_B}\theta'' = 0, \tag{3.7}$$

where $Pr = \dfrac{\nu}{\alpha'}$, $N_T = \dfrac{\tau D_T\,(T_w - T_\infty)}{\nu T_\infty}$, $N_B = \dfrac{\tau D_B\,(C_w - C_\infty)}{\nu}$, $Le = \dfrac{\nu}{D_B}$, $M = \dfrac{{B_0}^2\sigma_{el}}{\rho C_P}$ and $Ec = \dfrac{\mu u_w^2}{\alpha'\rho C_P(T_w - T_\infty)}$.

The dimensionless form of the boundary conditions becomes:

$$\begin{cases} f(0) = 0, f'(0) = 1 + \gamma_0\left(1 + \frac{1}{\beta}\right) f''(0), \theta'(0) = -Bi\,(1 - \theta(0)), \\ \phi(0) = 1, f'(\eta) \to 0, \theta(\eta) \to 0, \phi(\eta) \to 0, \quad \text{as} \quad \eta \to \infty. \end{cases} \tag{3.8}$$

Here $\gamma = \gamma_0\left(\frac{a}{\nu}\right)^{\frac{1}{2}}$ and $Bi = \frac{h_T}{\kappa}\left(\frac{\nu}{a}\right)^{\frac{1}{2}}$.

Here a is a positive constant representing the stretching rate of the sheet. The

physical quantities which govern the flow are the Nusselt number Nu_x^* and Sherwood number Sh_x^*, which are given by:

$$Nu_x^* = \frac{xq_w}{\kappa\left(T_w - T_\infty\right)}, \quad Sh_x^* = \frac{xq_m}{D_B\left(C_w - C_\infty\right)}, \tag{3.9}$$

where heat and mass flux at the surface are q_w and q_m respectively, defined as:

$$q_w = -\kappa\left(\frac{\partial T}{\partial y}\right)_{y=0}, \quad q_m = -D_B\left(\frac{\partial C}{\partial y}\right)_{y=0}. \tag{3.10}$$

Using the similarity transformations, we obtain:

$$Nu_x = \frac{Nu_x}{Re_x^{1/2}} = -\theta'(0), \quad Sh_x = \frac{Sh_x}{Re_x^{1/2}} = -\phi'(0). \tag{3.11}$$

According to [59, 60], the Casson nanofluid over the stretching surface has the volumetric rate of local entropy generation. After applying the boundary layer approximations, it can be described as:

$$\begin{aligned} S_{gen}''' = &\frac{\kappa}{T_\infty^2}\left(\frac{\partial T}{\partial y}\right)^2 + \frac{\mu}{T_\infty}\left(1+\frac{1}{\beta}\right)\left(\frac{\partial u}{\partial y}\right)^2 \\ &+ \frac{RD}{C_\infty}\left(\frac{\partial C}{\partial y}\right)^2 + \frac{RD}{T_\infty}\frac{\partial T}{\partial y}\frac{\partial C}{\partial y} + \sigma\frac{B_0^2u^2}{T_\infty}, \end{aligned} \tag{3.12}$$

The above equation represents the actual entropy which is produced in the system when some work is done. In Eq. (3.12), R is the ideal gas constant and D is the molecular diffusion coefficient. The ratio of the actual entropy produced in the system to the characteristic function $S_0''' = \frac{\kappa(\triangle T)^2}{L^2T_\infty^2}$ defines the entropy generation number given by:

$$\begin{aligned} Ng = Re&\left\{\theta'^2 + \left(1+\frac{1}{\beta}\right)\frac{Br}{\Omega}f''^2 + \lambda_1\left(\frac{\chi}{\Omega}\right)^2\phi'^2\right\} \\ &+ Re\left\{\lambda_1\left(\frac{\chi}{\Omega}\right)\theta'\phi' + \frac{\lambda}{\Omega}BrMf'^2\right\}, \end{aligned} \tag{3.13}$$

where

$$Re = \frac{u_wL^2}{\nu x}, \quad Br = \frac{\mu u_w^2}{\kappa(T-T_\infty)^2}, \quad \Omega = \frac{T-T_\infty}{T_\infty}, \quad \chi = \frac{C-C_\infty}{C_\infty}.$$

3.3 Keller Box Formulation

The details of Keller box method for the present problem are given below.

- Conversion of BVP (3.5)-(3.7) to seven first order ODEs given by (3.14)-(3.20):

$$f = Y_1,$$

$$Y_1^{'} = Y_2, \tag{3.14}$$

$$Y_2^{'} = Y_3, \tag{3.15}$$

$$\theta = Y_4,$$

$$Y_4^{'} = Y_5, \tag{3.16}$$

$$\phi = Y_6,$$

$$Y_6^{'} = Y_7, \tag{3.17}$$

$$Y_3' + \left(\frac{\beta}{1+\beta}\right)\left(M\ Y_2 + Y_1\ Y_3 - Y_2^2\right) = 0, \tag{3.18}$$

$$\frac{1}{Pr}Y_5' + Y_1\ Y_5 + N_B\ Y_5\ Y_7 + N_T\ Y_5^2 + Ec\ M\ Y_2^2 = 0, \tag{3.19}$$

$$\frac{1}{Le}\left(Y_7' + \frac{N_T}{N_B}\ Y_5'\right) + Y_1\ Y_7 = 0. \tag{3.20}$$

- The boundary conditions in (3.8) become:

$$\begin{cases} Y_1(0) = 0, Y_2(0) = 1 + \gamma\left(1 + \frac{1}{\beta}\right) Y_3(0), Y_5(0) = -Bi(1 - Y_4(0)), \\ Y_6(0) = 1, Y_2(\eta) \to 0,\ Y_4(\eta) \to 0,\ Y_6(\eta) \to 0,\ \text{as } \eta \to \infty. \end{cases} \tag{3.21}$$

- As defined in section 2.14, derivatives and functions are discretized accordingly. As a result, (3.14)-(3.20) become:

$$(Y_1)_\zeta - (Y_1)_{\zeta-1} - \frac{h}{2}\left((Y_2)_\zeta + (Y_2)_{\zeta-1}\right) = 0, \tag{3.22}$$

$$(Y_2)_\zeta - (Y_2)_{\zeta-1} - \frac{h}{2}\left((Y_3)_\zeta + (Y_3)_{\zeta-1}\right) = 0, \tag{3.23}$$

$$(Y_4)_\zeta - (Y_4)_{\zeta-1} - \frac{h}{2}\left((Y_5)_\zeta + (Y_5)_{\zeta-1}\right) = 0, \tag{3.24}$$

$$(Y_6)_\zeta - (Y_6)_{\zeta-1} - \frac{h}{2}\left((Y_7)_\zeta + (Y_7)_{\zeta-1}\right) = 0, \tag{3.25}$$

$$\frac{(Y_3)_\zeta - (Y_3)_{\zeta-1}}{h} + \left(\frac{\beta}{1+\beta}\right)\Big[M((Y_2)_{\zeta-\frac{1}{2}}) + ((Y_1)_{\zeta-\frac{1}{2}})((Y_3)_{\zeta-\frac{1}{2}}) - ((Y_2)_{\zeta-\frac{1}{2}})^2\Big] = 0, \tag{3.26}$$

$$\frac{1}{Pr}\frac{(Y_5)_\zeta - (Y_5)_{\zeta-1}}{h} + ((Y_1)_{\zeta-\frac{1}{2}})((Y_5)_{\zeta-\frac{1}{2}}) + N_B((Y_5)_{\zeta-\frac{1}{2}})((Y_7)_{\zeta-\frac{1}{2}}) + N_T((Y_5)_{\zeta-\frac{1}{2}})^2 + Ec\ M((Y_2)_{\zeta-\frac{1}{2}})^2 = 0, \tag{3.27}$$

$$\frac{1}{Le}\left(\frac{(Y_7)_\zeta - (Y_7)_{\zeta-1}}{h} + \frac{N_T}{N_B}\frac{(Y_5)_\zeta - (Y_5)_{\zeta-1}}{h}\right) + ((Y_1)_{\zeta-\frac{1}{2}})\ ((Y_7)_{\zeta-\frac{1}{2}}) = 0, \tag{3.28}$$

- Recalling section 2.14, the Newton's method is utilized and (3.22)-(3.28) are converted to a linear tridiagonal system by ignorng the quadratic and higher terms of $\varepsilon(*)_\zeta^i$ as follows:

$$\varepsilon(Y_1)_\zeta - \varepsilon(Y_1)_{\zeta-1} - \frac{1}{2}h(\varepsilon(Y_2)_\zeta + \varepsilon(Y_2)_{\zeta-1}) = (r_1)_{\zeta-\frac{1}{2}}, \tag{3.29}$$

$$\varepsilon(Y_2)_\zeta - \varepsilon(Y_2)_{\zeta-1} - \frac{1}{2}h(\varepsilon(Y_3)_\zeta + \varepsilon(Y_3)_{\zeta-1}) = (r_2)_{\zeta-\frac{1}{2}}, \tag{3.30}$$

$$\varepsilon(Y_4)_\zeta - \varepsilon(Y_4)_{\zeta-1} - \frac{1}{2}h(\varepsilon(Y_5)_\zeta + \varepsilon(Y_5)_{\zeta-1}) = (r_3)_{\zeta-\frac{1}{2}}, \tag{3.31}$$

$$\varepsilon(Y_6)_\zeta - \varepsilon(Y_6)_{\zeta-1} - \frac{1}{2}h(\varepsilon(Y_7)_\zeta + \varepsilon(Y_7)_{\zeta-1}) = (r_4)_{\zeta-\frac{1}{2}}, \tag{3.32}$$

$$\begin{cases} (a_1)_\zeta\varepsilon(Y_1)_\zeta + (a_2)_\zeta\varepsilon(Y_1)_{\zeta-1} + (a_3)_\zeta\varepsilon(Y_2)_\zeta + (a_4)_\zeta\varepsilon(Y_2)_{\zeta-1} + \\ (a_5)_\zeta\varepsilon(Y_3)_\zeta + (a_6)_\zeta\varepsilon(Y_3)_{\zeta-1} + (a_7)_\zeta\varepsilon(Y_4)_\zeta + (a_8)_\zeta\varepsilon(Y_4)_{\zeta-1} + \\ (a_9)_\zeta\varepsilon(Y_5)_\zeta + (a_{10})_\zeta\varepsilon(Y_5)_{\zeta-1} + (a_{11})_\zeta\varepsilon(Y_6)_\zeta + (a_{12})_\zeta\varepsilon(Y_6)_{\zeta-1} + \\ (a_{13})_\zeta\varepsilon(Y_7)_\zeta + (a_{14})_\zeta\varepsilon(Y_7)_{\zeta-1} = (r_5)_{\zeta-\frac{1}{2}}, \end{cases} \tag{3.33}$$

$$\begin{cases} (b_1)_\zeta\varepsilon(Y_1)_\zeta + (b_2)_\zeta\varepsilon(Y_1)_{\zeta-1} + (b_3)_\zeta\varepsilon(Y_2)_\zeta + (b_4)_\zeta\varepsilon(Y_2)_{\zeta-1} + \\ (b_5)_\zeta\varepsilon(Y_3)_\zeta + (b_6)_\zeta\varepsilon(Y_3)_{\zeta-1} + (b_7)_\zeta\varepsilon(Y_4)_\zeta + (b_8)_\zeta\varepsilon(Y_4)_{\zeta-1} + \\ (b_9)_\zeta\varepsilon(Y_5)_\zeta + (b_{10})_\zeta\varepsilon(Y_5)_{\zeta-1} + (b_{11})_\zeta\varepsilon(Y_6)_\zeta + (b_{12})_\zeta\varepsilon(Y_6)_{\zeta-1} + \\ (b_{13})_\zeta\varepsilon(Y_7)_\zeta + (b_{14})_\zeta\varepsilon(Y_7)_{\zeta-1} = (r_5)_{\zeta-\frac{1}{2}}, \end{cases} \tag{3.34}$$

$$\begin{cases} (c_1)_\zeta \varepsilon(Y_1)_\zeta + (c_2)_\zeta \varepsilon(Y_1)_{\zeta-1} + (c_3)_\zeta \varepsilon(Y_2)_\zeta + (c_4)_\zeta \varepsilon(Y_2)_{\zeta-1} + \\ (c_5)_\zeta \varepsilon(Y_3)_\zeta + (c_6)_\zeta \varepsilon(Y_3)_{\zeta-1} + (c_7)_\zeta \varepsilon(Y_4)_\zeta + (c_8)_\zeta \varepsilon(Y_4)_{\zeta-1} + \\ (c_9)_\zeta \varepsilon(Y_5)_\zeta + (c_{10})_\zeta \varepsilon(Y_5)_{\zeta-1} + (c_{11})_\zeta \varepsilon(Y_6)_\zeta + (c_{12})_\zeta \varepsilon(Y_6)_{\zeta-1} + \\ (c_{13})_\zeta \varepsilon(Y_7)_\zeta + (c_{14})_\zeta \varepsilon(Y_7)_{\zeta-1} = (r_5)_{\zeta-\frac{1}{2}}, \end{cases} \tag{3.35}$$

$$(r_1)_{\zeta-\frac{1}{2}} = -(Y_1)_\zeta + (Y_1)_{\zeta-1} + \frac{h}{2}((Y_2)_\zeta + (Y_2)_{\zeta-1}), \tag{3.36}$$

$$(r_2)_{\zeta-\frac{1}{2}} = -(Y_2)_\zeta + (Y_2)_{\zeta-1} + \frac{h}{2}((Y_3)_\zeta + (Y_3)_{\zeta-1}), \tag{3.37}$$

$$(r_3)_{\zeta-\frac{1}{2}} = -(Y_4)_\zeta + (Y_4)_{\zeta-1} + \frac{h}{2}((Y_5)_\zeta + (Y_5)_{\zeta-1}), \tag{3.38}$$

$$(r_4)_{\zeta-\frac{1}{2}} = -(Y_6)_\zeta + (Y_6)_{\zeta-1} + \frac{h}{2}((Y_7)_\zeta + (Y_7)_{\zeta-1}), \tag{3.39}$$

$$\begin{aligned}(r_5)_{\zeta-\frac{1}{2}} = -h\Bigg[\left(1+\frac{1}{\beta}\right) \frac{(Y_3)_\zeta - (Y_3)_{\zeta-1}}{h} + \frac{1}{4}((Y_1)_\zeta (Y_3)_\zeta + (Y_1)_\zeta (Y_3)_{\zeta-1} \\ + (Y_1)_{\zeta-1}(Y_3)_\zeta + (Y_1)_{\zeta-1}(Y_3)_{\zeta-1}) - \frac{1}{2}((Y_2)_{\zeta-\frac{1}{2}})^2 \Bigg],\end{aligned} \tag{3.40}$$

$$\begin{aligned}(r_6)_{\zeta-\frac{1}{2}} = -(Y_5)_\zeta + (Y_5)_{\zeta-1} + hPr\Bigg[(Y_1)_{\zeta-\frac{1}{2}} (Y_5)_{\zeta-\frac{1}{2}} \\ + N_B (Y_5)_{\zeta-\frac{1}{2}} (Y_7)_{\zeta-\frac{1}{2}} + N_T \left((Y_5)_{\zeta-\frac{1}{2}}\right)^2 \Bigg],\end{aligned} \tag{3.41}$$

$$\begin{aligned}(r_7)_{\zeta-\frac{1}{2}} = -(Y_7)_\zeta + (Y_7)_{\zeta-1} + hLe\Bigg[(Y_1)_{\zeta-\frac{1}{2}} (Y_7)_{\zeta-\frac{1}{2}} \Bigg] \\ - \frac{N_T}{N_B}((Y_5)_\zeta - (Y_5)_{\zeta-1}),\end{aligned} \tag{3.42}$$

subject to the boundary conditions:

$$\varepsilon(Y_1)_0 = \varepsilon(Y_2)_0 = \varepsilon(Y_5)_0 = \varepsilon(Y_7)_0 = \varepsilon(Y_2)_J = \varepsilon(Y_4)_J = \varepsilon(Y_6)_J = 0. \tag{3.43}$$

The system of linear (3.29)-(3.35) can be written in matrix form as defined in (2.54)-(2.55). Here, $\mathbf{W}$ is $J \times J$ block tridiagonal matrix with each block of size 7×7.

To claim the validity of our Matlab code, we compute reduced Nusselt number and Sherwood number for the Newtonian case when $\beta \to \infty$ for various values of some physical parameters and compare these with those already published in

the literature. Tables 3.1 and 3.2 reflect a very convincing comparison of these numbers.

Pr	[57]	[61]	[62]	[63]	[64]	Present
0.20	0.1691	0.1691	0.1691	0.1691	0.1691	0.1691
0.70	0.4539	0.4539	0.4539	0.4539	0.4539	0.4539
2.00	0.9114	0.9114	0.9114	0.9114	0.9114	0.9114
7.00	1.8954	1.8954	1.8954	1.8954	1.8954	1.8954

Table 3.1: The reduced Nusselt number for different Pr when $N_B = 0, N_T = 0, \gamma = 0$, $Bi = 0$ and $\beta \to \infty$.

Pr	[57]		[64]		Present	
	Nu_x	Sh_x	Nu_x	Sh_x	Nu_x	Sh_x
1	0.0789	1.5477	0.0789	1.5477	0.0789	1.5477
2	0.0806	1.5554	0.0806	1.5554	0.0806	1.5554
5	0.0735	1.5983	0.0735	1.5983	0.0734	1.5984

Table 3.2: The reduced Nusselt number and the reduced Sherwood number for varying Pr when $N_T = N_B = 0.5, Le = 5, \gamma = 0, Bi = 0.1$ and $\beta \to \infty$.

3.4 Numerical Results and Discussion

The impact of different physical parameters on the reduced Nusselt number and reduced Sherwood number are described in Table 3.3. The CPU time for the computations with grid spacing $h = 0.01$, $\eta_\infty = 20$ and $\epsilon_a < 10^{-5}$ on an INTEL core i5 processor with 4 GB ram on Windows 10 operating system is carried out. The reduced Nusselt number is the relative heat transfer by conduction or convection in fluid at the boundary whereas the reduced Sherwood number represents convective mass transfer fraction to the rate of diffusive mass transfer. The value of the reduced Nusselt number increases for more turbulent flow. More viscous fluids have a low Reynolds number value, thus less heat transfer results which in return should reduce Nusselt number. This fact is evident from Table 3.3 as we

see that an increase in Casson fluid parameter decreases the Nusselt number. A similar behaviour is seen in Table 3.3 in the case of comparison between reduced Sherwood number and Casson fluid parameter β. The impact of Lewis number is also observed on Nusselt number and Sherwood number. It is seen that increase in Le raises the mass transfer rate but diminishes the heat transfer rate. Nusselt number and Sherwood numbers reduce but with rise in thermophoresis parameter N_T. Larger Brownian motion parameter N_B accounts for greater Sherwood number but smaller Nusselt number. A higher value of Prandtl number means more thermal heat transfer thus more heat is transferred through the surface which can be observed from the Table 3.3. A similar behaviour is observed in the case of Sherwood number. An increase in Biot number means conductive heat transport dominates the convective heat transport at the surface thus increasing the heat transfer rate at the surface but at the same time it decreases the mass transfer rate. Thus, a rise in Biot number results in decrease in Sherwood number but increase in the Nusselt number. A greater slip parameter is an indication that lesser resistivity is awarded by the sheet thus a smaller friction which results in smaller heat dissipation. An increase in velocity slip parameter decreases both Nusselt number and Sherwood number. Eckert number is the ratio of heat dissipation by conduction to convection. Greater values of Ec means heat transfer by conduction dominates the convection heat transfer. Higher values of Ec results in decrease in the Nusselt number but augments Sherwood number. Greater values of the magnetic parameter implies that the fluid is repelled away from the surface which in return has a negative impact on the heat and mass transfer rates as both decrease.

The impact of some of the physical parameters on the nanofluid properties is discussed in the form of graphs. The parameter values set as a standard are $\beta = 1, Le = 1, M = 0.5, Ec = 0.5, Bi = 0.2, \gamma = 0.3, N_B = 0.1, N_T = 0.1, Pr = 0.71, Re = 5, Br = 20$. Shear thinning behaviour of the Casson fluid and the reduction in yield stress are characterized by the growing values of Casson parameter β. These factors have a diminishing impact on the fluid velocity as it decreases with an increase in β as depicted in Figure 3.2. In Figure 3.3, an elevation in the

values of β results in the rise in temperature of the fluid due to frictional factor caused by the applied stress on the flow of the fluid. It can be seen in Figure 3.4 that a more viscous fluid flow upsurges the concentration boundary layer. The entropy of the system against β is analyzed in Figure 3.5. Noteworthy is the fact that the entropy of the system is reduced by a greater shear thinning and lesser

β	Le	N_T	N_B	Pr	Bi	γ	Ec	M	Sh_x	Nu_x	CPU Time (sec)
1	1	0.1	0.1	0.71	0.2	0.3	0.5	0.5	0.4324	0.1141	3.8560
3									0.4259	0.1128	4.2998
5									0.4131	0.1119	5.1298
7									0.4028	0.1113	5.5737
	1.5								0.5900	0.1138	2.3222
	2								0.7218	0.1136	2.2417
	3								0.9409	0.1134	2.4030
		0.3							0.3134	0.1130	3.9667
		0.5							0.1989	0.1119	4.0846
		0.9							-0.0166	0.1096	5.2746
			0.3						0.4748	0.1097	3.8817
			0.5						0.4833	0.1052	4.2858
			0.9						0.4890	0.0956	6.1376
				2.0					0.4257	0.1307	3.8984
				5.0					0.4332	0.1344	3.9260
				8.0					0.4432	0.1328	4.0103
					0.0				0.5045	0.0	4.0257
					0.1				0.4607	0.0692	3.9124
					0.3				0.4126	0.1455	11.3798
						0.1			0.5055	0.1146	3.4845
						0.4			0.4060	0.1135	7.7850
						0.5			0.3837	0.1127	18.7855
							0.1		0.4154	0.1269	4.3833
							0.3		0.4239	0.1205	4.1547
							0.7		0.4409	0.1077	3.8593
								0.2	0.4562	0.1262	3.9532
								0.7	0.4177	0.1071	4.5132
								1.0	0.3976	0.0979	5.3500

Table 3.3: Sherwood and Nusselt numbers for different values of the parameters β, Le, N_T, N_B, Pr, Bi and γ.

yield stress in the fluid as β grows.

Where there is slip, velocity is not zero at the surface of the sheet or the flow velocity adjacent to the sheet surface is not equal to the stretching sheet velocity. Figure 3.6 reveals that when γ increases, the fluid velocity as well as the entropy decreases in the boundary layer as displayed in Figure 3.7. $Bi > 0.1$ means that the heat convection through the surface is much faster than the heat conduction inside the body and temperature gradients are significant inside the body. Thus the temperature changes within the fluid by increasing the values of Biot number. Figure 3.8 shows that the temperature of the fluid rises as we increase the values of Bi as well as the entropy of the system by increasing values of Bi as it can be seen from Figure 3.9.

Brownian motion is observed in the fluid due to the very small size of nanofluid particles. This makes a contribution toward the heat transfer in the fluid. This effect is taken into account in Figure 3.10. In the figure, it is observed that rise in the values of Brownian motion parameter N_B increases the temperature of the fluid as well as the boundary layer thickness. In Figure 3.11, it is observed that the concentration boundary layer decreases by increasing the values of N_B. Figures 3.12–3.13 display the effect of N_T on the thermal distribution in nanofluid and nanoparticle concentration. It is noted that the temperature of the fluid rises as well as the nanoparticles concentration by increasing N_T. The entropy of the system tends to increase with increase in N_B but decreases with higher N_T as it can be seen in Figures 3.14–3.15.

When Prandtl number Pr is increased, conductive heat transfer dominates the convective heat transfer. The thermal energy of the system is increased and the temperature of the fluid rises. This phenomenon is noticed in Figure 3.16 that the temperature in the boundary layer of the fluid falls with a rise in Pr. In Figure 3.17, it is noticed that the concentration of the fluid increases near the wall with the increase in the Prandtl number. Greater Prandtl number account for greater

convection near the wall where the temperature difference is large as compared to that away from the wall. Due to more convection near the wall, the concentration of the nanoparticles near the wall rises. As we move away from the wall these convective currents decreases so for a material with higher convective transport the concentration falls. Greater Prandtl number plays a role in enhances the entropy of the system as it can be observed in Figure 3.18.

Analogous to the Prandtl number, Lewis number Le depicts the pattern in which the mass is transfer in fluid. Larger Lewis number indicates that the mass transfer by diffusion is large as compared to the convective mass tranport. Diffusive mass transport is usually much smaller as compared to convective mass transfer thus the concentration of the nanoparticles in the boundary region reduces. This fact can be seen in Figure 3.19. Figure 3.20 reveals a sharp rise with postive variation in Ec in the temperature of the fluid near the surface of the sheet but the effects are less prominent away from the sheet. In Figure 3.21, it is seen that the entropy of the system increases with the rise in Eckert number.

Figures 3.22-3.23 portray the effect of magnetic number on flow and thermal disturbance of the nanofluid respectively. The results show that increasing the magnetic number decreases the velocity of the fluid in the boundary layer but increases the thermal boundary layer thickness. The reason behind such a behavior is that increasing the value of magnetic number amplifies the Lorentz forces which resists the fluid motion and due to this resistance an increase in temperature distribution is observed. The impact of the magnetic number on the entropy of the system is looked in Figure 3.24. Greater magnetic number increases the entropy of the system. Higher Reynolds number results in turbulent flow and greater fluid friction. Consequently entropy of the system tends to increase. Figure 3.25 depicts this fact quiet clearly. Brinkman number Br is the relative measure of heat dissipation to the heat conduction inside the fluid. Greater Br means heat dissipates at faster rate as compared to the heat conducted by the fluid. The dissipation of energy causes the entropy of the system to increase as is evident from Figure 3.26.

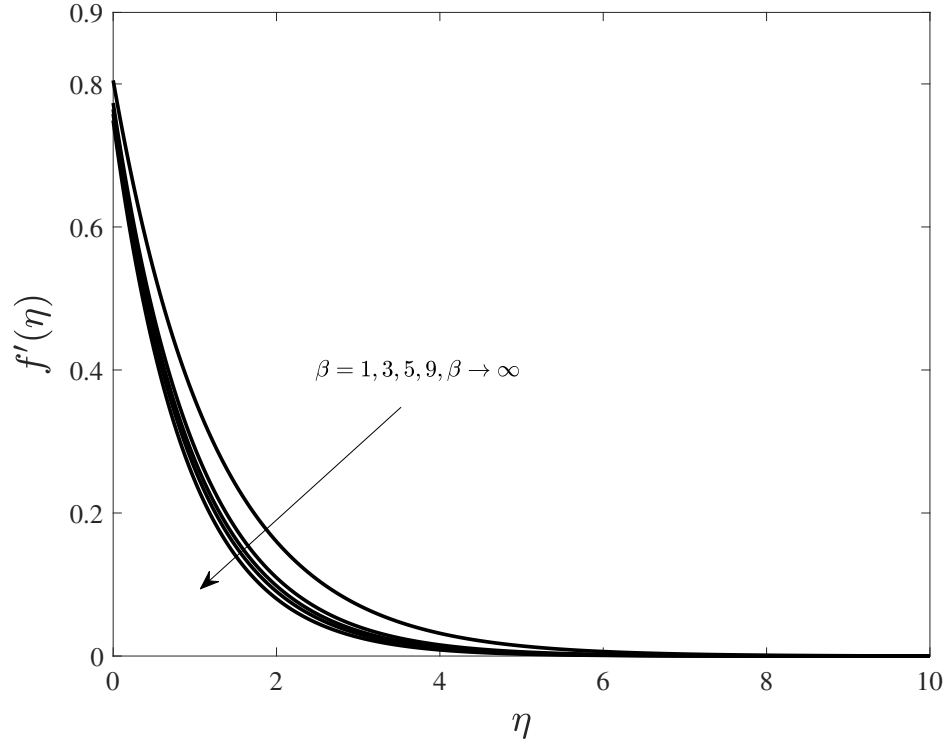

Figure 3.2: Impact of β on the velocity profile.

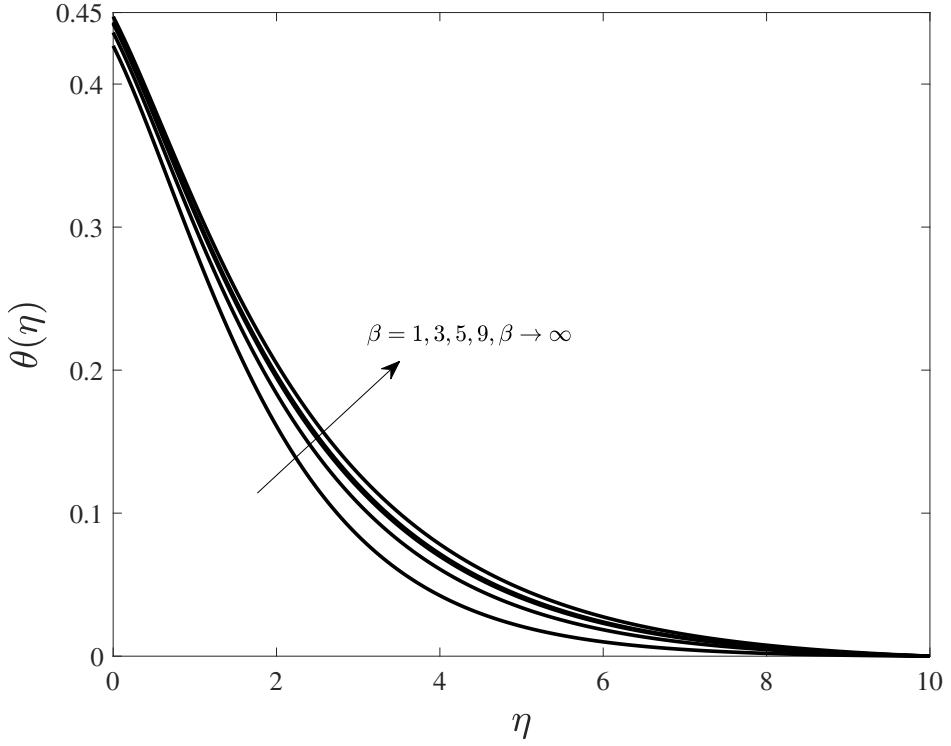

Figure 3.3: Impact of β on the temperature profile.

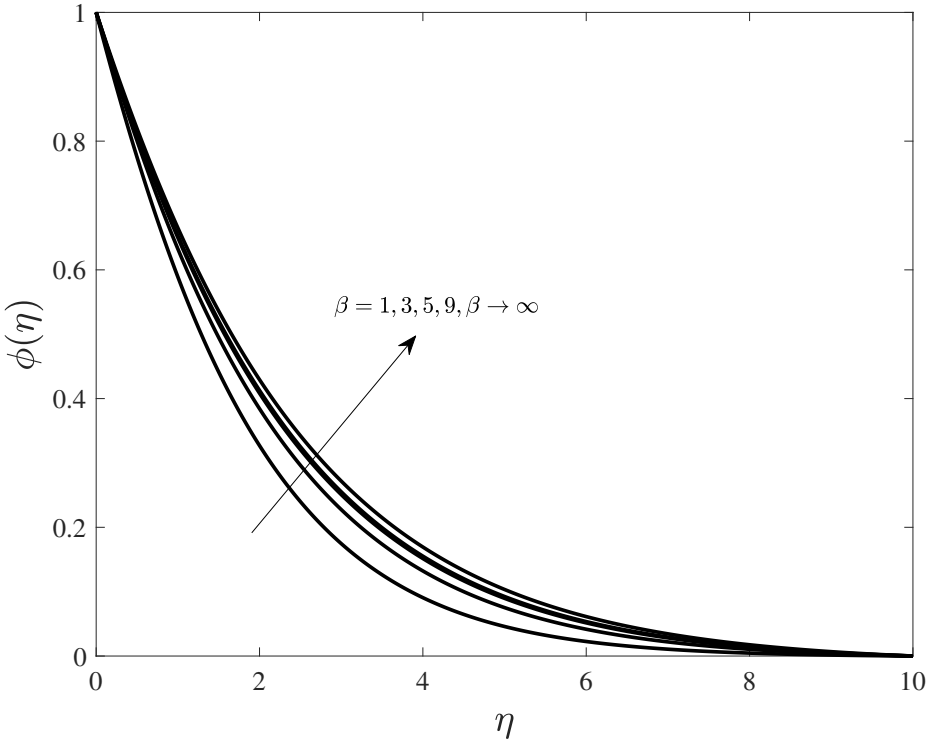

Figure 3.4: Impact of β on the concentration profile.

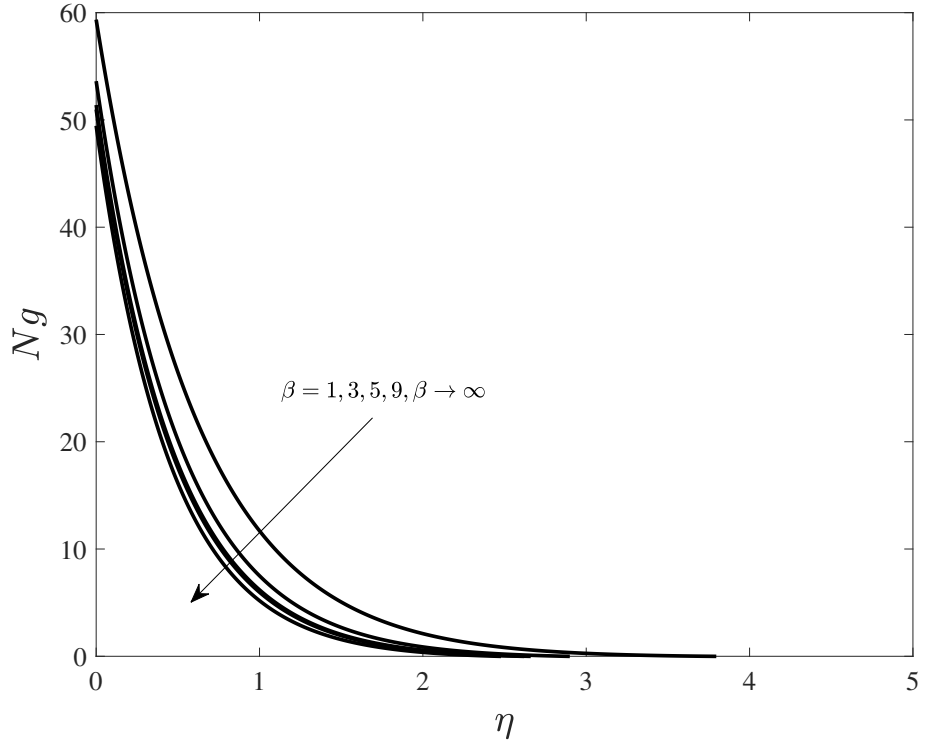

Figure 3.5: Impact of β on the entropy.

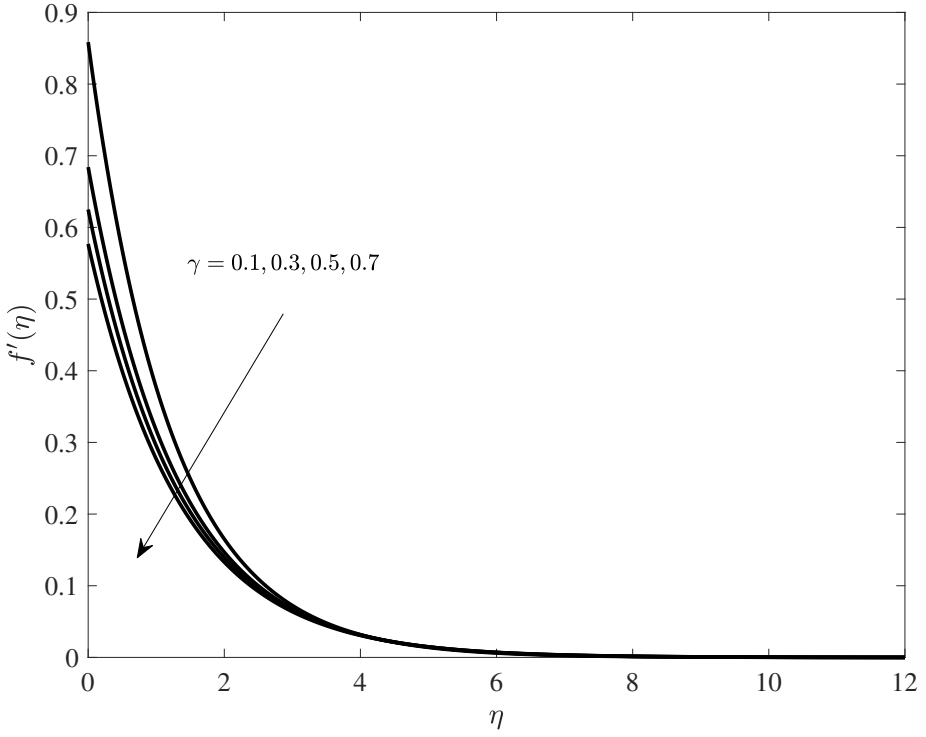

Figure 3.6: Impact of γ on the velocity profile.

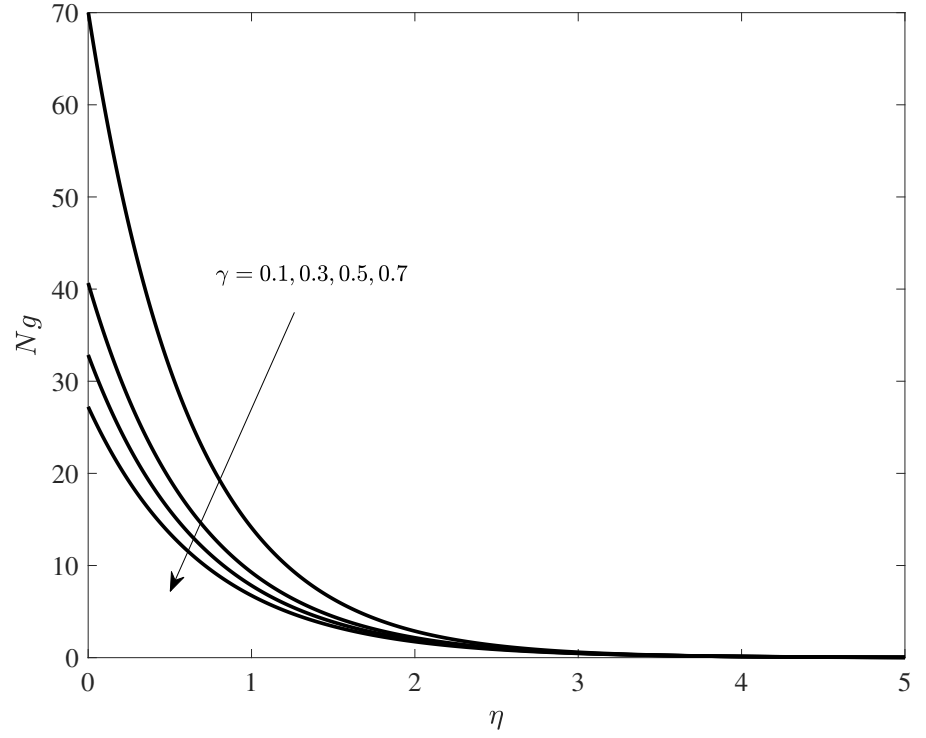

Figure 3.7: Impact of γ on the entropy.

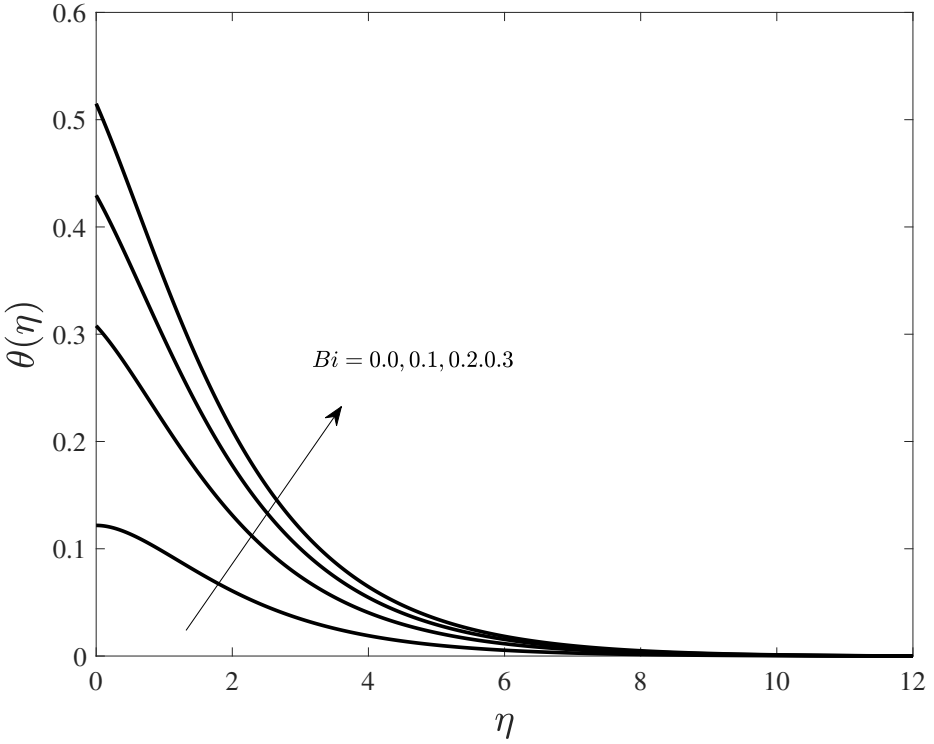

Figure 3.8: Impact of Bi on the temperature profile.

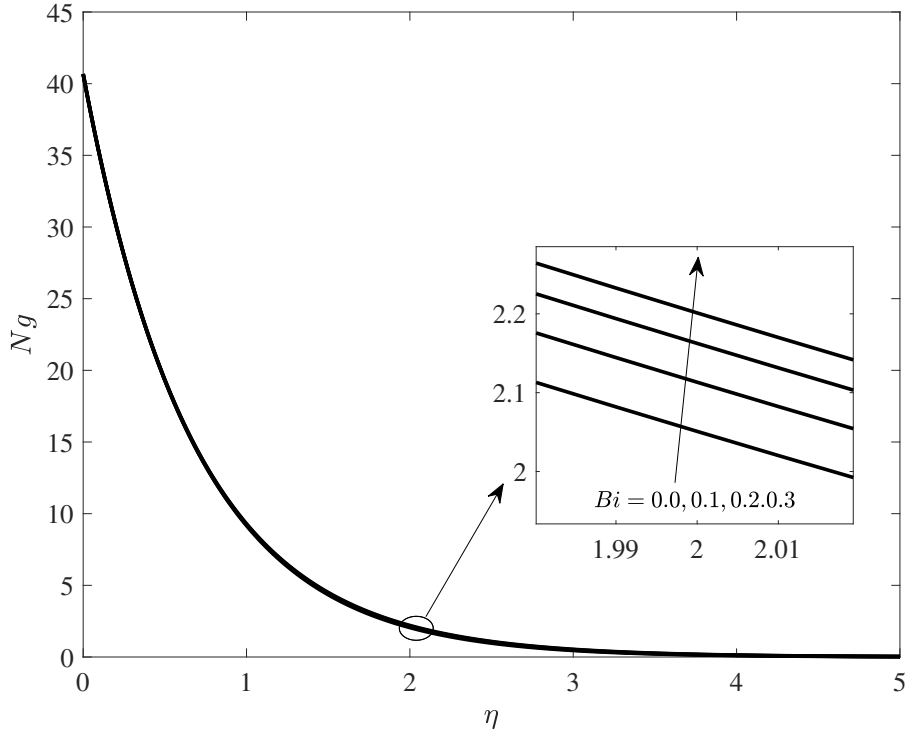

Figure 3.9: Impact of Bi on the entropy.

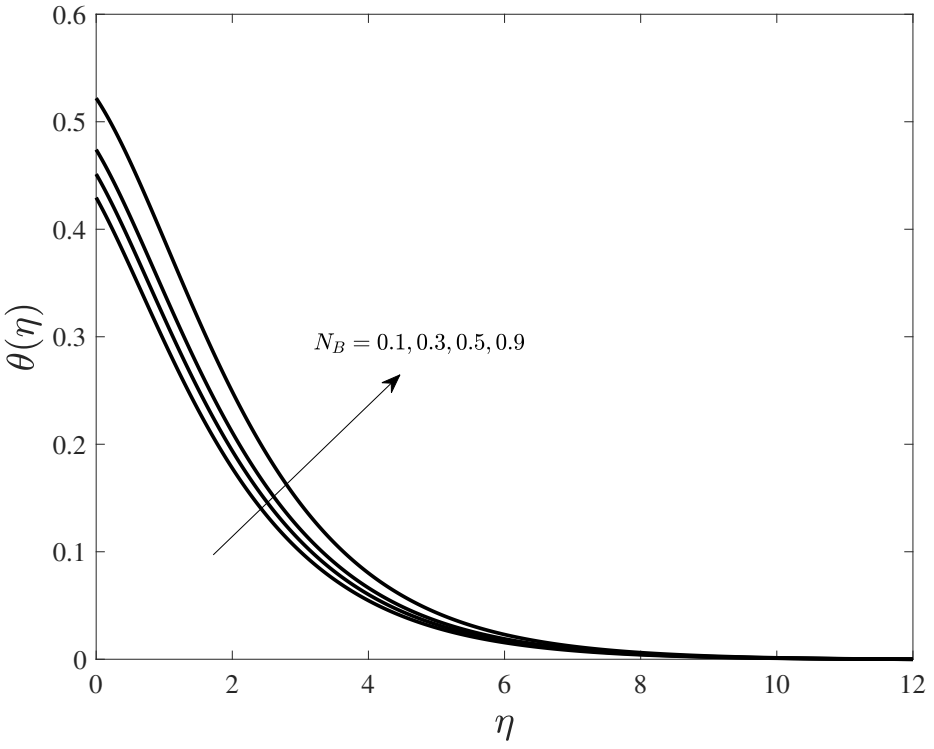

Figure 3.10: Impact of N_B on the temperature profile.

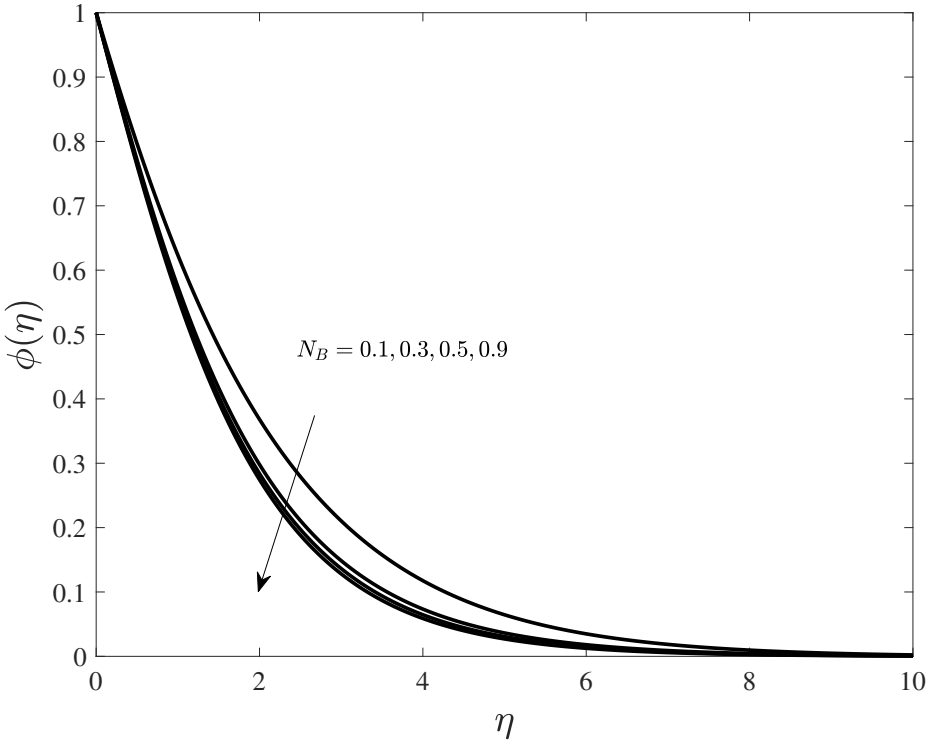

Figure 3.11: Impact of N_B on the concentration profile.

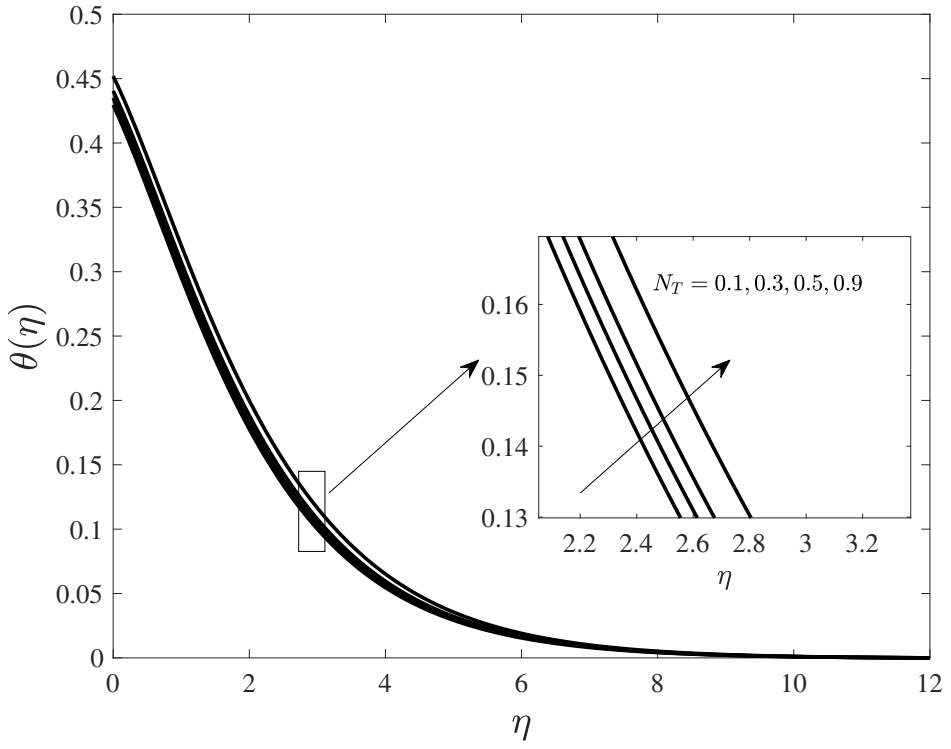

Figure 3.12: Impact of N_T on the temperature profile.

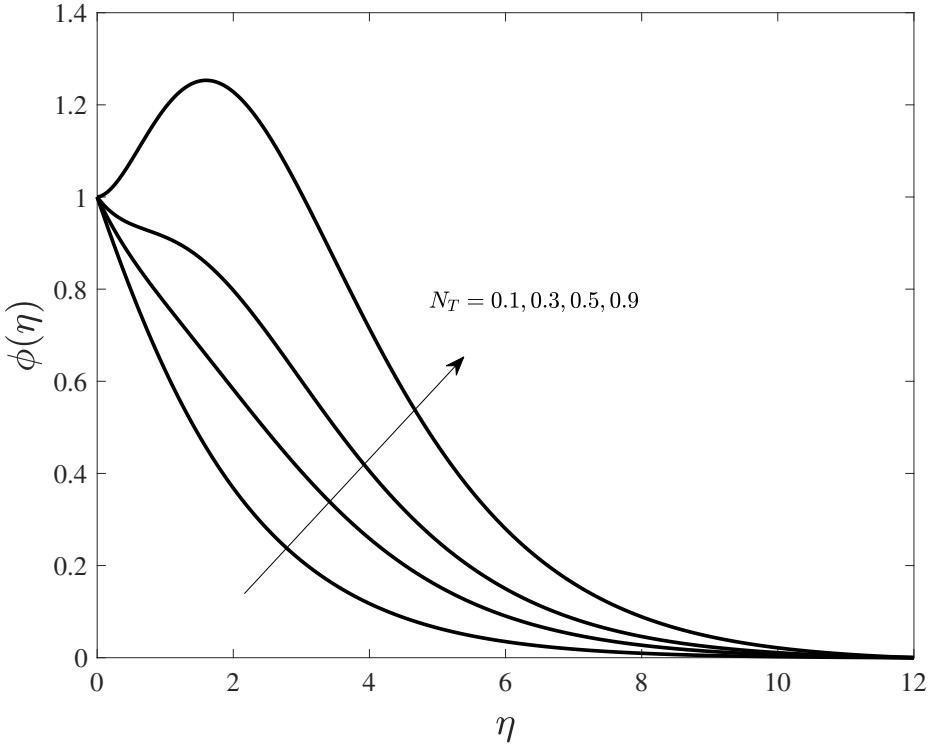

Figure 3.13: Impact of N_T on the concentration profile.

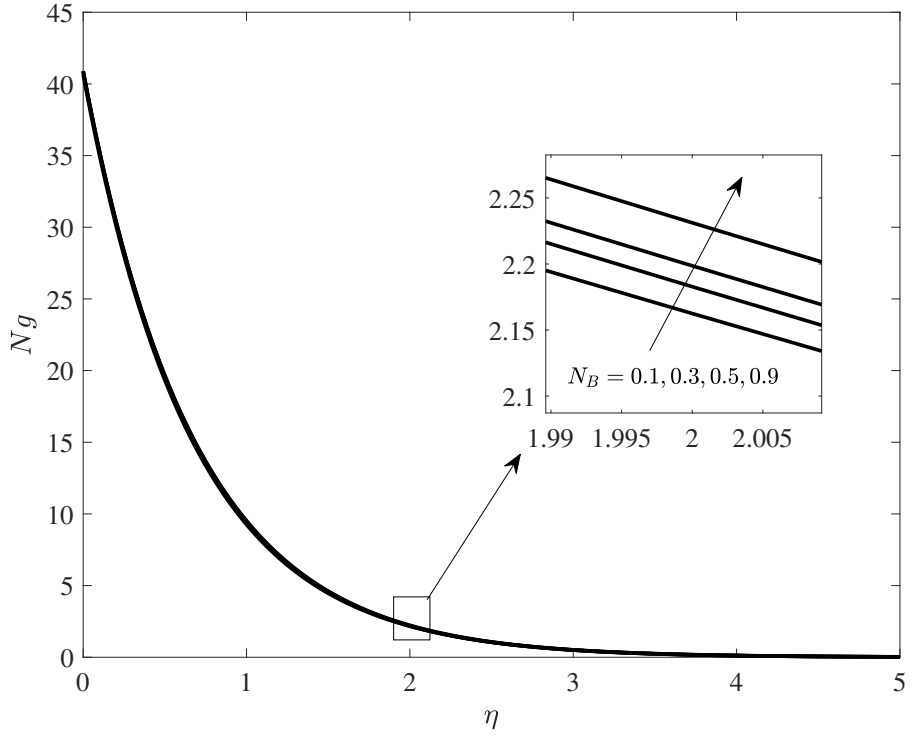

Figure 3.14: Impact of N_B on the entropy.

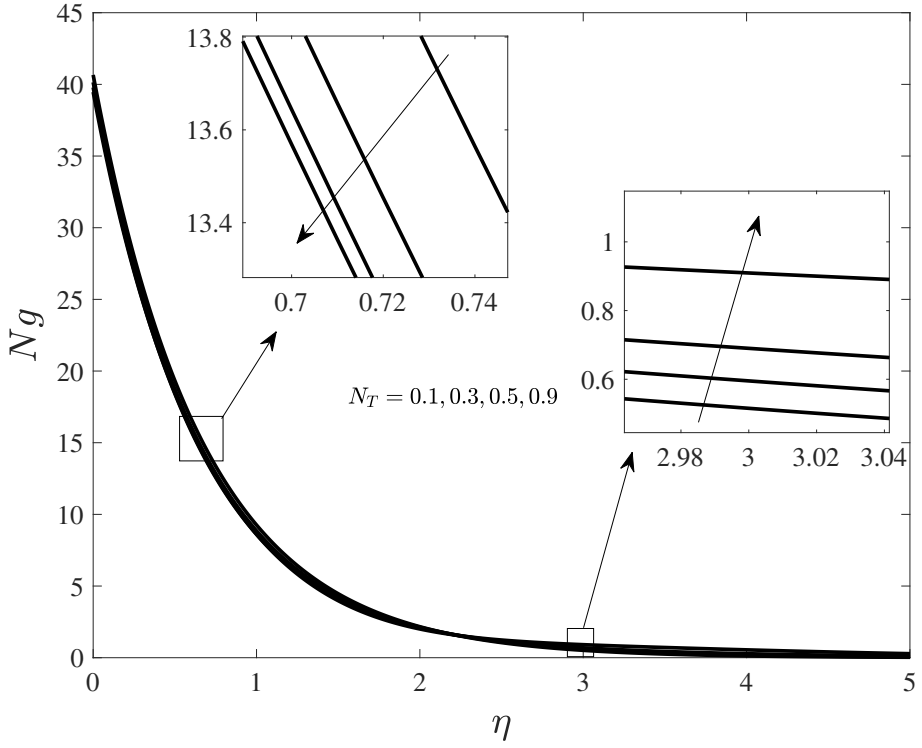

Figure 3.15: Impact of N_T on the entropy.

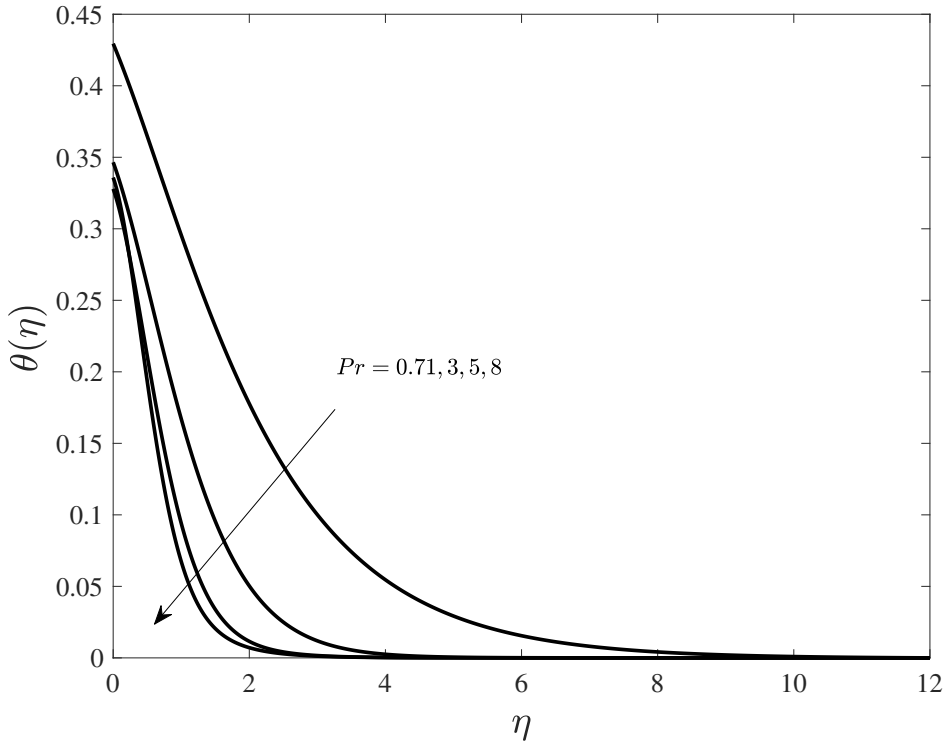

Figure 3.16: Impact of Pr on the temperature profile.

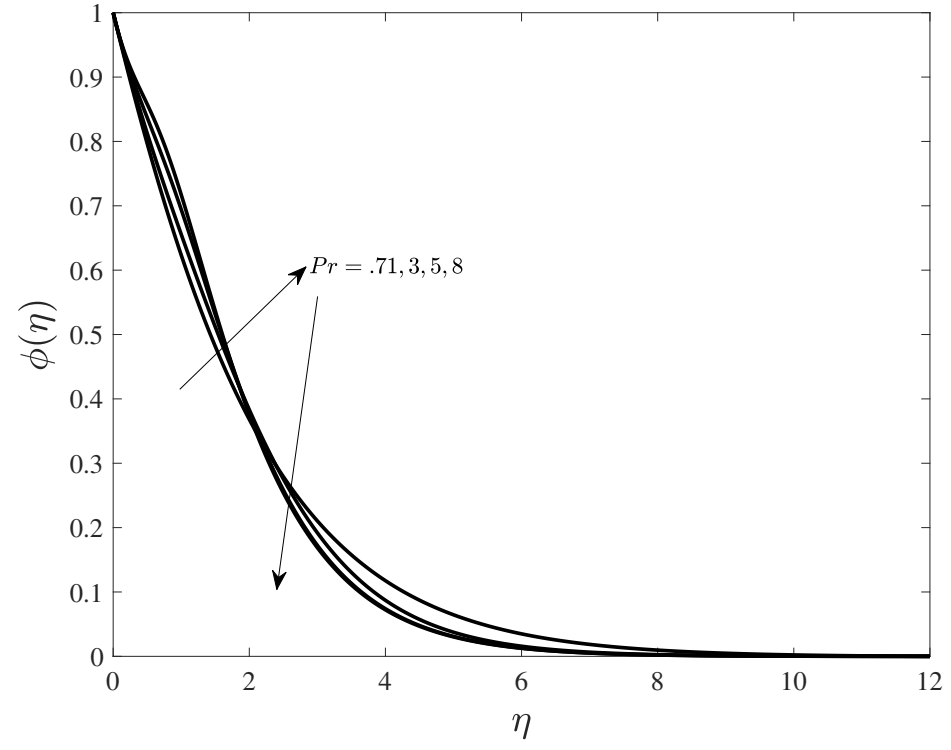

Figure 3.17: Impact of Pr on the concentration profile.

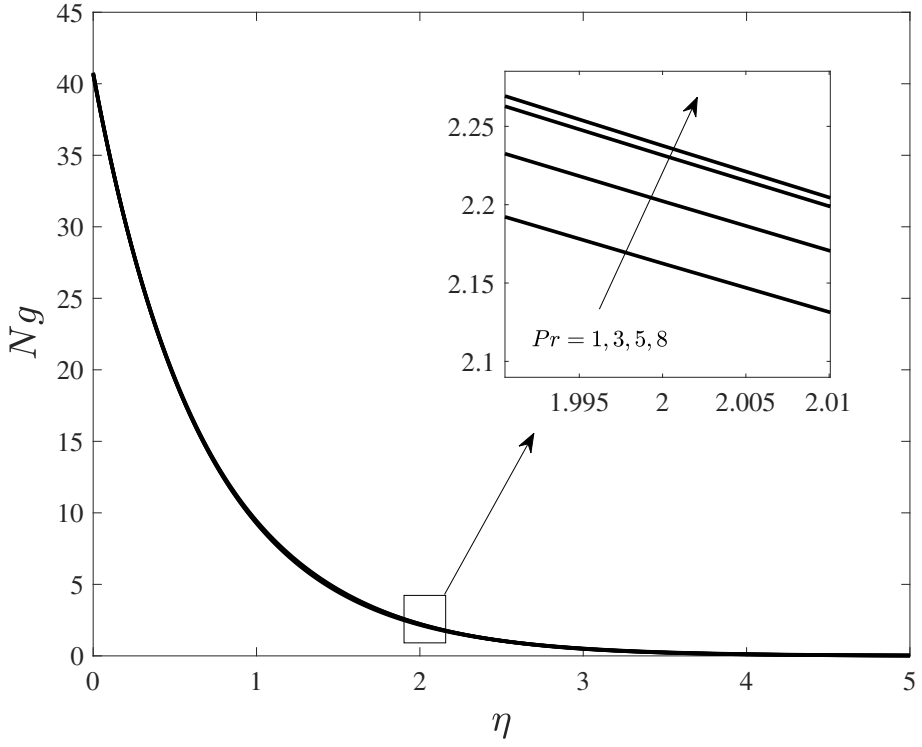

Figure 3.18: Impact of Pr on the entropy.

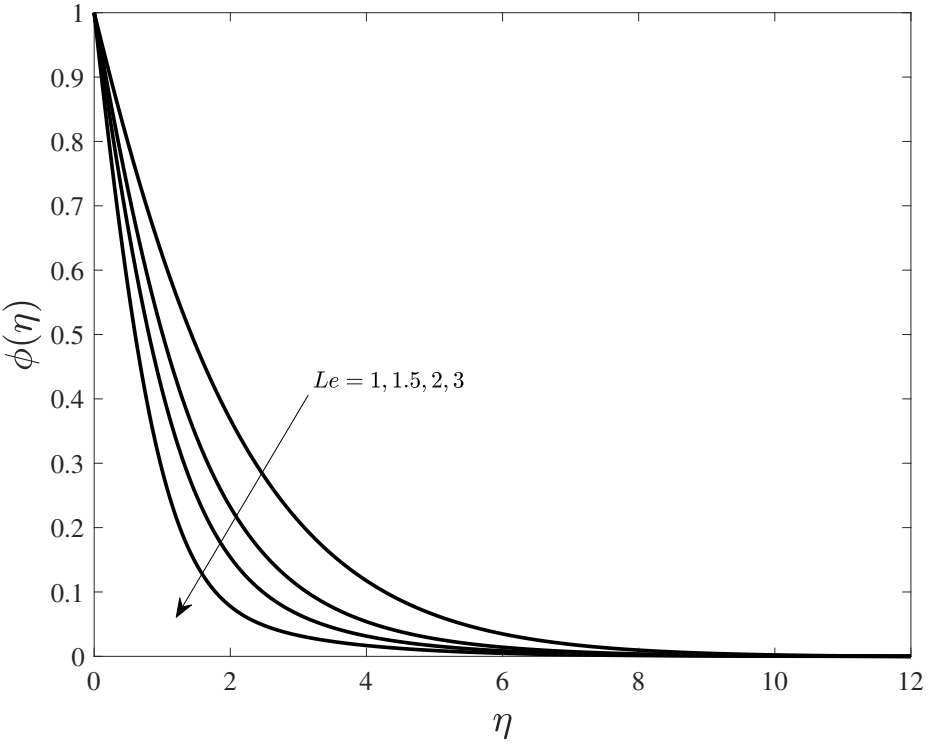

Figure 3.19: Impact of Le on the concentration profile.

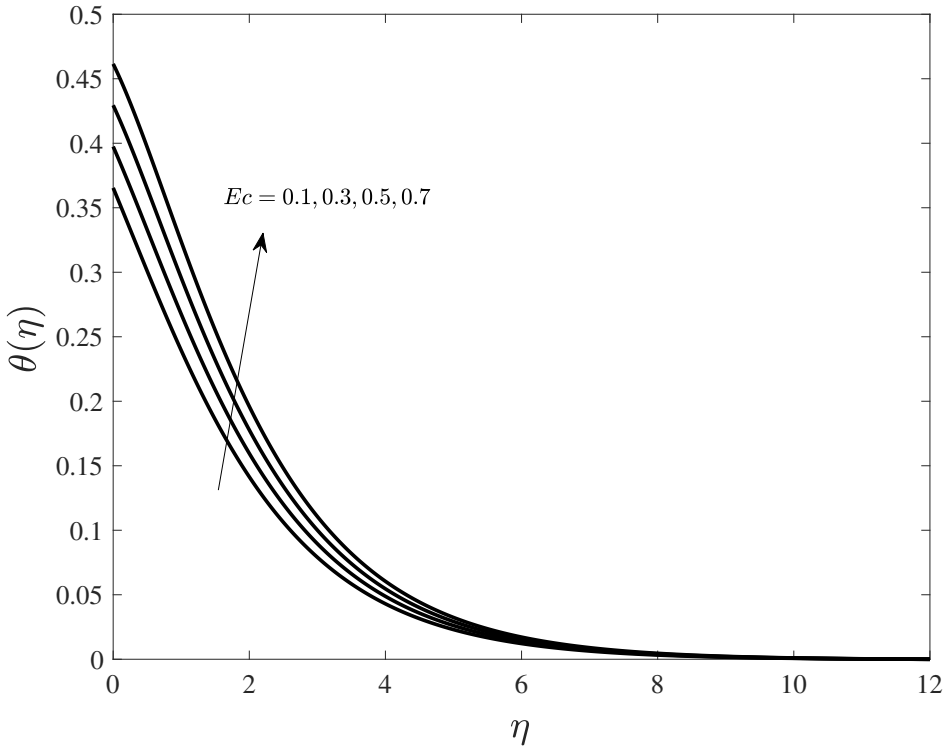

Figure 3.20: Impact of Ec on the temperature profile.

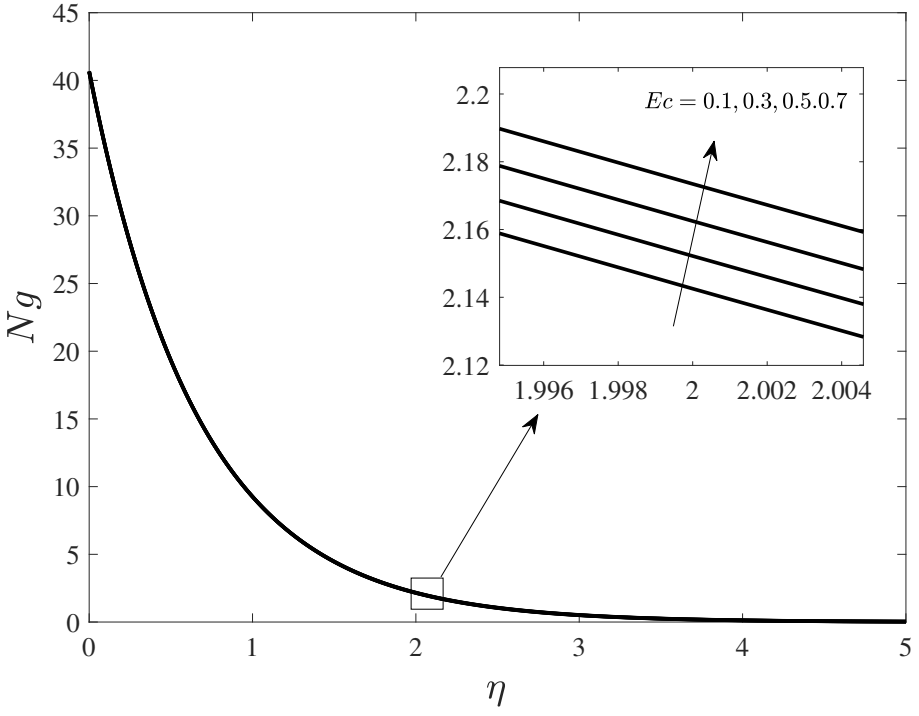

Figure 3.21: Impact of Ec on the entropy.

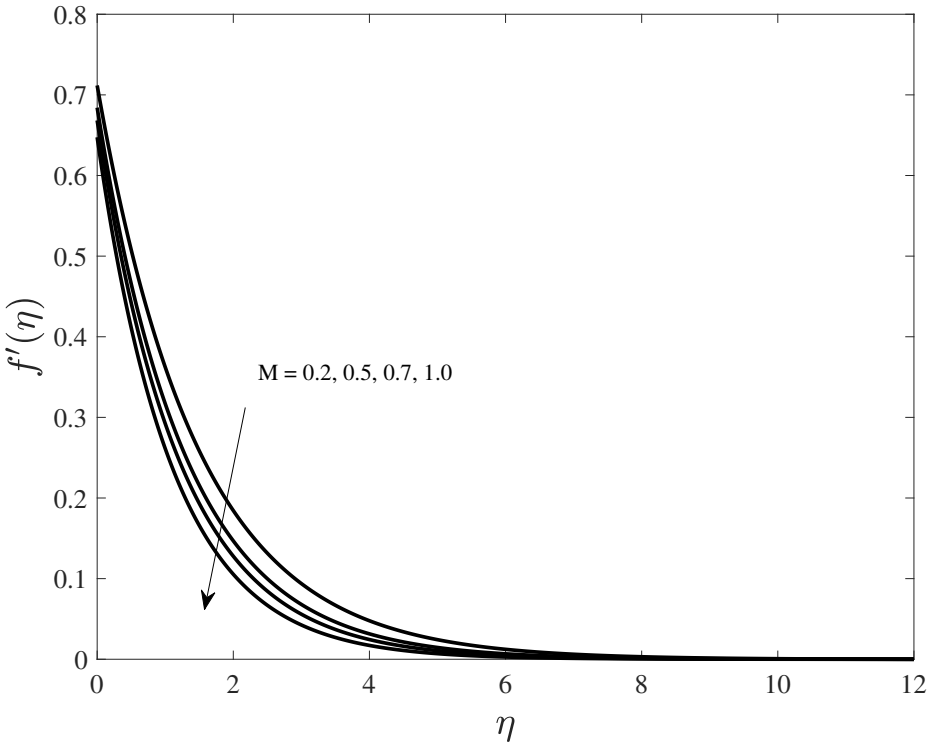

Figure 3.22: Impact of M on the velocity profile.

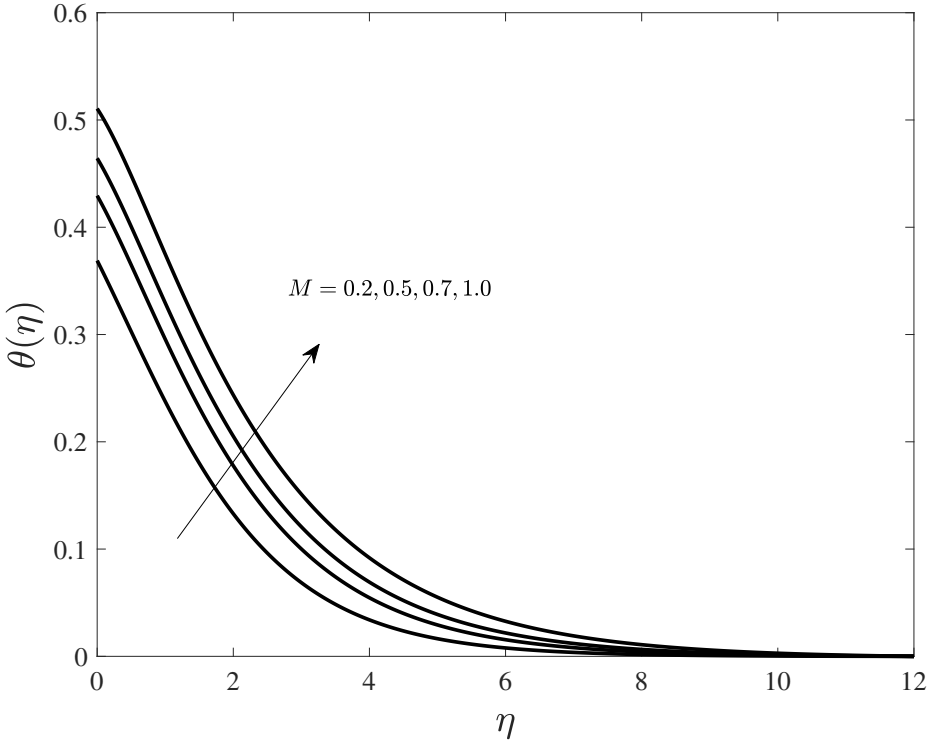

Figure 3.23: Impact of M on the temperature profile.

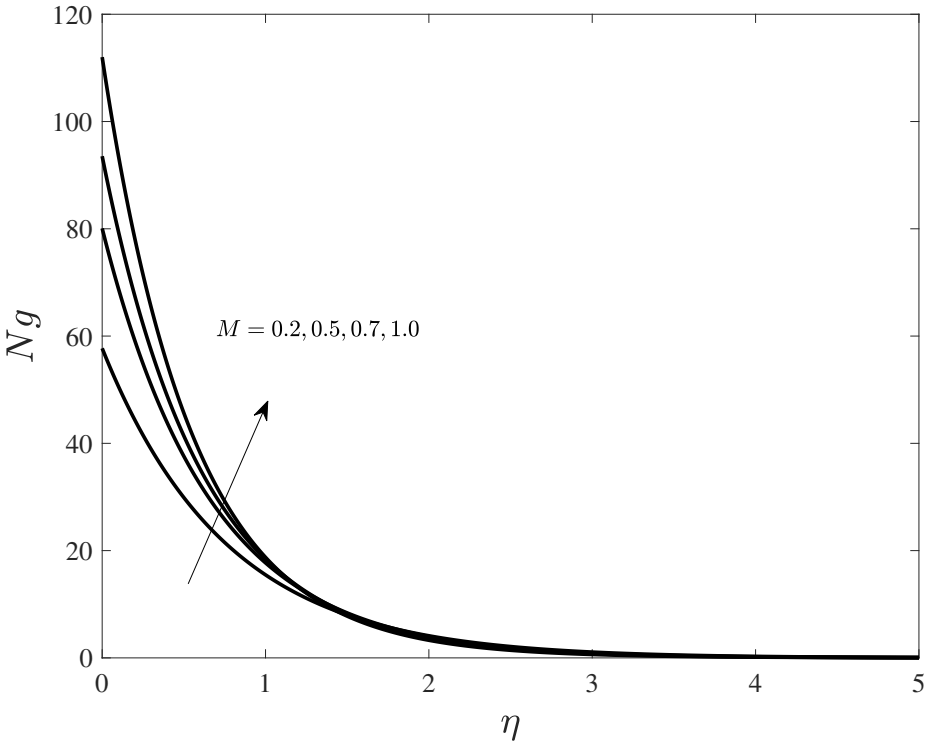

Figure 3.24: Impact of M on the entropy.

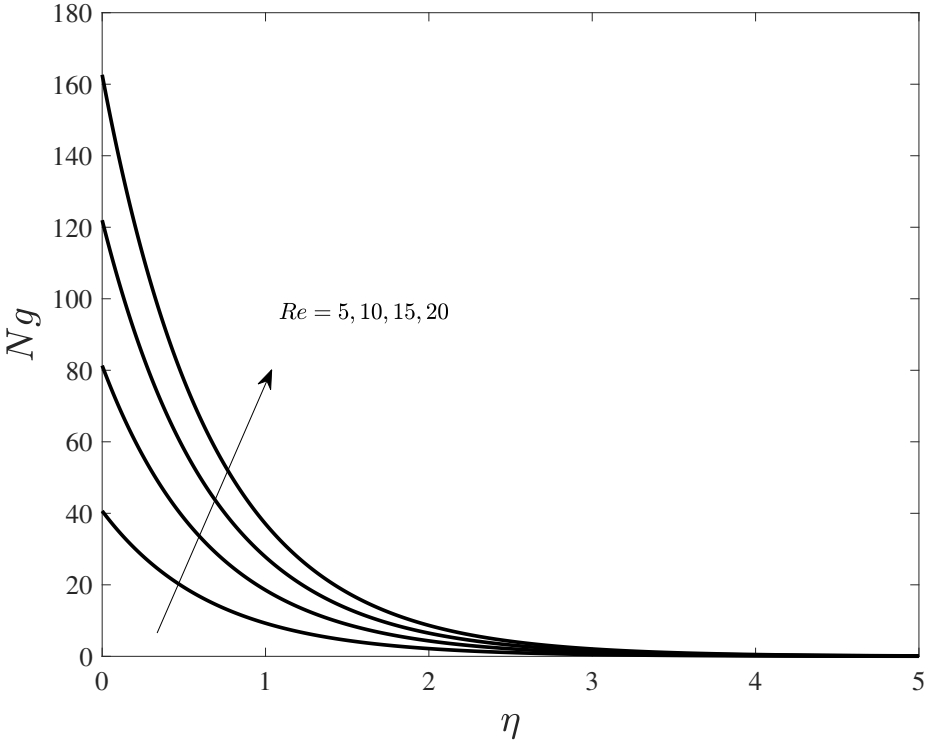

Figure 3.25: Impact of Re on the entropy.

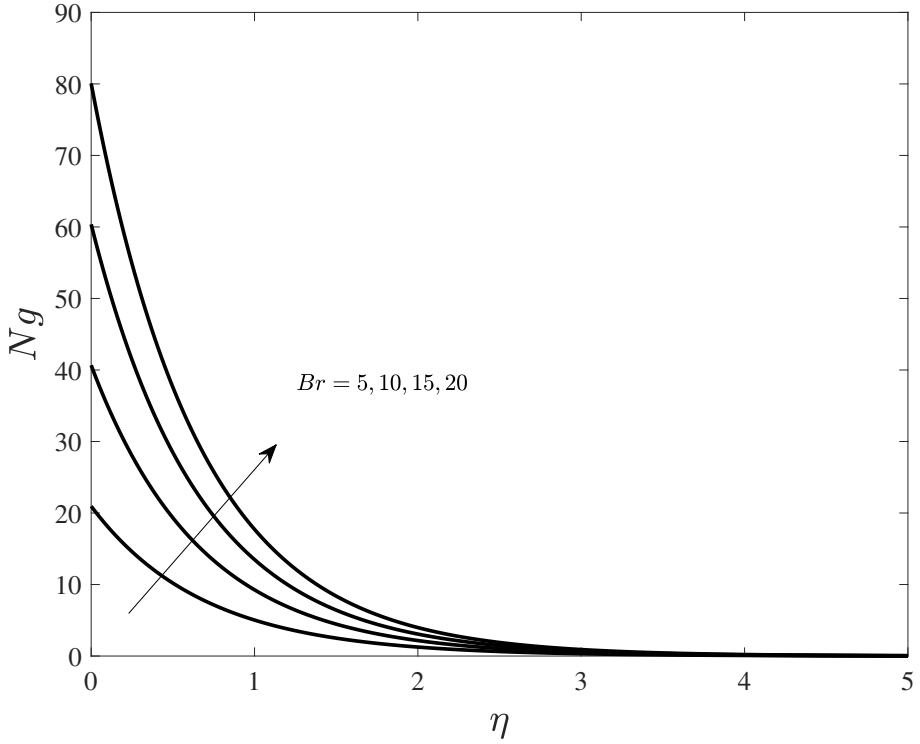

Figure 3.26: Impact of Br on the entropy.

3.5 Chapter Summary

Entropy analysis of Casson nanofluid over a stretching sheet with convective and slip boundary conditions subject to magnetic field and Joule heating was studied in the present chapter. The transformed ordinary differential equations were solved using an efficient Keller box finite difference scheme. The effects of some important physical parameters on the flow and heat transport characteristics were analyzed in the form of tables and graphs. Nusselt and Sherwood numbers were also calculated to observe the heat and mass transfer phenomena for the present model. Some of the important findings in the study can be summarized in the following points.

- Velocity decreases with the increase in the values of slip parameter γ, magnetic number M and non-Newtonian Casson fluid parameter β.
- Temperature in the boundary layer flow rises with rise in Casson fluid parameter β, Eckert number Ec, Brownian motion parameter N_B, thermophoresis

parameter N_T, Biot number Bi, magnetic number M but falls with the increase in Prandtl number Pr.

- Concentration profile witnesses an increase with greater values of Prandtl number Pr, Casson fluid parameter β and thermophoresis parameter N_T whereas decreases with greater values of Brownian motion parameter N_B and Lewis number Le.

- Entropy of the system jumps with the greater Reynolds number Re, magnetic number M, Brownian motion parameter N_B and Brinkman number Br but falls for larger Prandtl number Pr, thermophoresis parameter N_T, slip parameter γ, Casson fluid parameter β, Biot number Bi and Eckert number Ec.

Chapter 4

Induced Magnetic Field Effect on Free Convective Flow and Heat Transfer in CNT Micropolar Nanofluid

4.1 Introduction

Heat transfer in flows between parallel plates is observed in many physical applications. Parallel plates heat exchangers is on such example in which the heat exchanges between the working fluid and the walls of the exchanger. In this chapter, mathematical analysis of buoyancy driven micropolar fluid subjected to a strong magnetic field with induced magnetic field effects has been carried out. The base fluids considered are water and kerosene oil and the nanoparticles utilzied are single walled and multiwalled carbon nanotubes (SWCNTs and MWCNTs). Eriegen formulation is applied for the construction of the micropolar fluid model. The effect of rotation viscosity is pondered on the heat transfer rate of nanofluids. Numerical approach of KBM is implied to solve the dimensionless constitutive equations of fluid flow along with magnetic induction equation.

4.2 Problem Statement and Mathematical Formulation

Steady and incompressible SWCNT/MWCNT-water/kerosene oil micropolar nanofluid has been considered between two parallel plates with lower plate at $y^{'} = 0$ and upper plate at $y^{'} = h$. The plates are porous with a constant suction velocity v_0 in the y-direction. The fluid velocity vector is given as $\mathbf{V} = \left[u^{'}, v_0, 0\right]$. A constant magnetic field B_0 is applied perpendicular to the nanofluid. It is assumed that the magnetic Prandtl number for the present case is close to "1" so the induced magnetic field is developed due to electromotive forces generated by the motion of free electrons present with the nanofluid. The upper plate is assumed to be electrically conducting while the lower plate is non-conducting. The fluid is supposed to have sufficient electrical conductivity σ_{el} and induces a magnetic field of strength $B_x^{'}$ in the x-direction. The magnetic field vector is given by $\mathbf{B} = \left[B_x^{'}, B_0, 0\right]$ (See Figure 6.1). The homogeneous single phase model is considered with carbon nanotubes as nanoparticles with water and kerosene oil as the base fluids with constant thermophysical properties. The momentum and the

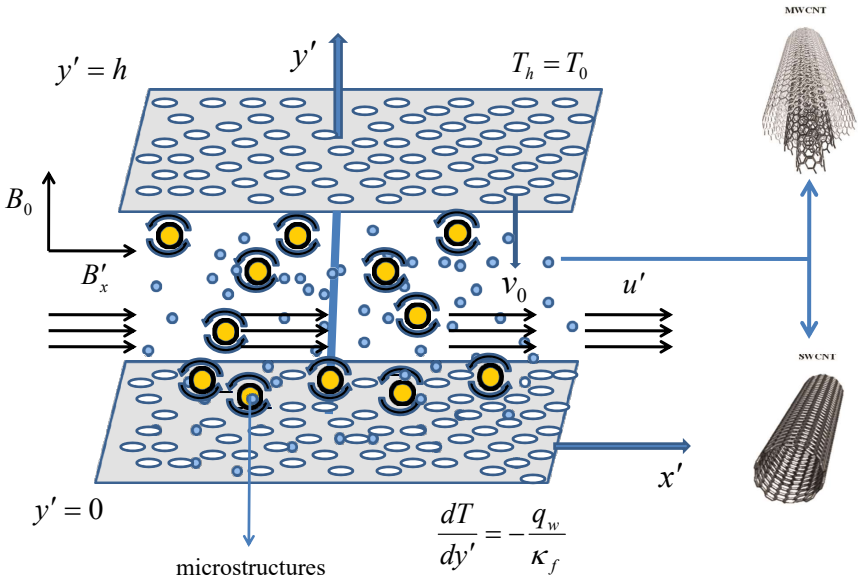

Figure 4.1: Schematic diagram of the flow model

induced magnetic field equation for Buongiorno model are given as [65]:

$$\left(\nu_{nf}+\frac{\kappa^*}{\rho_{nf}}\right)\frac{d^2u^{'}}{dy^{'2}}+\frac{\kappa^*}{\rho_{nf}}\frac{dN}{dy^{'}}+v_0\frac{du^{'}}{dy^{'}}+\frac{\mu_e B_0}{\rho_{nf}}\frac{dB_x^{'}}{dy^{'}}+g_e\beta(T-T_0)=0, \tag{4.1}$$

$$\frac{1}{\mu_e\sigma_f}\frac{d^2B_x^{'}}{dy^{'2}}+B_0\frac{du^{'}}{dy^{'}}+v_0\frac{dB_x^{'}}{dy^{'}}=0. \tag{4.2}$$

The angular momentum equation accounting for the microrotation is defined as [66] :

$$\left(\nu_{nf}+\frac{\kappa^*}{2\rho_{nf}}\right)j\frac{d^2N}{dy^{'2}}-\frac{\kappa^*}{\rho_{nf}}\left(2N+\frac{du^{'}}{dy^{'}}\right)+jv_0\frac{dN}{dy^{'}}=0. \tag{4.3}$$

Since, there is a constant heat flux applied at the lower plate, the energy equation is defined as [67]:

$$\alpha_{nf}^{'}\frac{d^2T}{dy^{'2}}+v_0\frac{dT}{dy^{'}}=0. \tag{4.4}$$

The physical quantities of viscosity μ_{nf}, density ρ_{nf} and heat capacity are defined in Eqs. (2.19)-(2.18) whereas the thermal conductivity κ_{nf} of the nanofluid for the present problem is defined as [68]:

$$\frac{\kappa_{nf}}{\kappa_f}=\frac{(1-\phi)+2\phi\frac{\kappa_{CNT}}{\kappa_{CNT}-\kappa_f}\ln\left[\frac{\kappa_{CNT}+\kappa_f}{\kappa_f}\right]}{(1-\phi)+2\phi\frac{\kappa_f}{\kappa_{CNT}-\kappa_f}\ln\left[\frac{\kappa_{CNT}+\kappa_f}{\kappa_f}\right]}.$$

The thermophysical properties of the nanofluid are mentioned in Table 2.1. The boundary conditions have been considered as follows [65, 66]:

$$u^{'}=0,\quad N=0,\quad B_x^{'}=0,\quad \frac{dT}{dy^{'}}=-\frac{q_w}{\kappa_f},\quad \text{at}\quad y^{'}=0, \tag{4.5}$$

$$u^{'}=0,\quad N=0,\quad \frac{dB_x^{'}}{dy^{'}}=0,\quad T=T_0,\quad \text{at}\quad y^{'}=h. \tag{4.6}$$

The nondimensional form of (4.1)-(4.4) by using the following transformations [65]

$$y=\frac{y^{'}}{h},\quad u=\frac{\mu_f u^{'}}{\rho_f g_e\beta_T h^2\Delta T},\quad g=\frac{\mu_f N}{\rho_f g_e\beta_T h^2\Delta T},\quad B_x=\sqrt{\frac{\mu_e}{\rho_f}}\frac{B_x^{'}\mu_f}{g_e\beta_T h^2\Delta T}$$

$$\theta=\frac{T-T_0}{\Delta T},\quad \Delta T=\frac{hq}{\kappa_f},$$

is obtained as

$$(A_3 + K)\frac{d^2u}{dy^2} + A_1V_0\frac{du}{dy} + M\frac{dB_x}{dy} + K\frac{dg}{dy} + A_1\theta = 0, \tag{4.7}$$

$$\left(A_3 + \frac{K}{2}\right)\frac{d^2g}{dy^2} + A_1V_0\frac{dg}{dy} - K\left[2g + \frac{du}{dy}\right] = 0, \tag{4.8}$$

$$\frac{d^2B_x}{dy^2} + Pm\left[V_0\frac{dB_x}{dy} + M\frac{du}{dy}\right] = 0, \tag{4.9}$$

$$\frac{d^2\ \theta}{dy^2} + V_0Pr\frac{A_2}{A_4}\frac{d\theta}{dy} = 0. \tag{4.10}$$

The dimensionless form of the boundary conditions become

$$\begin{cases} u(0) = 0, \quad g(0) = 0, \quad B_x(0) = 0, \quad \left.\dfrac{d\theta}{dy}\right|_{y=0} = -1, \\ u(1) = 0, \quad g(1) = 0, \quad \theta(1) = 0, \quad \left.\dfrac{dB_x}{dy}\right|_{y=1} = 0. \end{cases} \tag{4.11}$$

Here,

$$Pr = \frac{C_p\mu_f}{k_f}, \quad Pm = \frac{\mu_f}{\rho_f}\mu_e\sigma_f, \quad M = \frac{B_0h}{\nu_f}\sqrt{\frac{\mu_e}{\rho_f}}, \quad V_0 = \frac{v_0h}{\nu_f}, \quad K = \frac{\kappa^*}{\mu_f},$$
$$A_1 = \frac{\rho_{nf}}{\rho_f}, \quad A_2 = \frac{(\rho C_p)_{nf}}{(\rho C_p)_f}, \quad A_3 = \frac{\mu_{nf}}{\mu_f}, \quad A_4 = \frac{\kappa_{nf}}{\kappa_f}.$$

The nondimensional form of the Nusselt number and skin friction are obtained as follows:

$$Nu_x = \frac{1}{\theta(0)},$$

$$\tau = (1 + K)u'(0) + Kg(0).$$

In the next section, a detailed procedure of the Keller box method is presented to solve the linear boundary value problem (4.7)-(4.11). Although the Keller box method has been applied successfully to nonlinear boundary value problems [26, 56], in the present study it has been successfully applied to a linear two point boundary value problem without any procedural changes required.

4.3 Keller Box Formulation

As a first step, the linear coupled system of ODEs in (4.7)-(4.10) is converted to eight first order ODEs as given in (4.12)-(4.20):

$$u = Y_1,$$
$$\frac{dY_1}{dy} = Y_2, \tag{4.12}$$
$$g = Y_3,$$
$$\frac{dY_3}{dy} = Y_4, \tag{4.13}$$
$$B_x = Y_5,$$
$$\frac{dY_5}{dy} = Y_6, \tag{4.14}$$
$$\theta = Y_7, \tag{4.15}$$
$$\frac{dY_7}{dy} = Y_8, \tag{4.16}$$
$$(A_3 + K)\frac{dY_2}{dy} + A_1 V_0 Y_2 + MY_6 + KY_4 + A_1 Y_7 = 0, \tag{4.17}$$
$$\left(A_3 + \frac{K}{2}\right)\frac{dY_4}{dy} + A_1 V_0 Y_4 - A_1 K\left[2Y_3 + Y_2\right] = 0, \tag{4.18}$$
$$\frac{dY_6}{dy} + Pm\left[V_0 Y_6 + MY_2\right] = 0, \tag{4.19}$$
$$\frac{dY_8}{dy} + V_0 Pr\frac{A_2}{A_4}Y_8 = 0. \tag{4.20}$$

Next, the derivative terms and the functions values in (4.12)-(4.20) are discretized following (2.36) as:

$$\frac{(Y_1)_\zeta - (Y_1)_{\zeta-1}}{h} = (Y_2)_{\zeta-\frac{1}{2}}, \tag{4.21}$$
$$\frac{(Y_3)_\zeta - (Y_3)_{\zeta-1}}{h} = (Y_4)_{\zeta-\frac{1}{2}}, \tag{4.22}$$
$$\frac{(Y_5)_\zeta - (Y_5)_{\zeta-1}}{h} = (Y_6)_{\zeta-\frac{1}{2}}, \tag{4.23}$$
$$\frac{(Y_7)_\zeta - (Y_7)_{\zeta-1}}{h} = (Y_8)_{\zeta-\frac{1}{2}}, \tag{4.24}$$
$$(A_3 + K)\left(\frac{(Y_2)_\zeta - (Y_2)_{\zeta-1}}{h}\right) + A_1\left[V_0(Y_2)_{\zeta-\frac{1}{2}} + (Y_7)_{\zeta-\frac{1}{2}}\right] + M(Y_6)_{\zeta-\frac{1}{2}}$$

$$+ K(Y_4)_{\zeta-\frac{1}{2}} = 0, \tag{4.25}$$

$$\left(A_3 + \frac{K}{2}\right)\left(\frac{(Y_4)_\zeta - (Y_4)_{\zeta-1}}{h}\right) + A_1 V_0 (Y_4)_{\zeta-\frac{1}{2}} - A_1 K\left[2(Y_3)_{\zeta-\frac{1}{2}} + (Y_2)_{\zeta-\frac{1}{2}}\right] = 0, \tag{4.26}$$

$$\left(\frac{(Y_6)_\zeta - (Y_6)_{\zeta-1}}{h}\right) + Pm\left[V_0 (Y_6)_{\zeta-\frac{1}{2}} + M(Y_2)_{\zeta-\frac{1}{2}}\right] = 0, \tag{4.27}$$

$$\left(\frac{(Y_8)_\zeta - (Y_8)_{\zeta-1}}{h}\right) + V_0 Pr \frac{A_2}{A_4}(Y_8)_{\zeta-\frac{1}{2}} = 0. \tag{4.28}$$

Next, consistent to the linearization procedure of Keller box method defined in (2.37), (4.21)-(4.28) takes the form:

$$\frac{\varepsilon(Y_1)_\zeta - \varepsilon(Y_1)_{\zeta-1}}{h} - \frac{\varepsilon(Y_2)_\zeta + \varepsilon(Y_2)_{\zeta-1}}{2} = (r_1)_{\zeta-\frac{1}{2}}, \tag{4.29}$$

$$\frac{\varepsilon(Y_3)_\zeta - \varepsilon(Y_3)_{\zeta-1}}{h} - \frac{\varepsilon(Y_4)_\zeta + \varepsilon(Y_4)_{\zeta-1}}{2} = (r_2)_{\zeta-\frac{1}{2}}, \tag{4.30}$$

$$\frac{\varepsilon(Y_5)_\zeta - \varepsilon(Y_5)_{\zeta-1}}{h} - \frac{\varepsilon(Y_2)_\zeta + \varepsilon(Y_6)_{\zeta-1}}{2} = (r_3)_{\zeta-\frac{1}{2}}, \tag{4.31}$$

$$\frac{\varepsilon(Y_7)_\zeta - \varepsilon(Y_7)_{\zeta-1}}{h} - \frac{\varepsilon(Y_8)_\zeta + \varepsilon(Y_2)_{\zeta-1}}{2} = (r_4)_{\zeta-\frac{1}{2}}, \tag{4.32}$$

$$\begin{cases} (\xi_1)_\zeta \varepsilon(Y_1)_\zeta + (\xi_2)_\zeta \varepsilon(Y_1)_{\zeta-1} + (\xi_3)_\zeta \varepsilon(Y_2)_\zeta + (\xi_4)_\zeta \varepsilon(Y_2)_{\zeta-1} + (\xi_5)_\zeta \\ \varepsilon(Y_3)_\zeta + (\xi_6)_\zeta \varepsilon(Y_3)_{\zeta-1} + (\xi_7)_\zeta \varepsilon(Y_4)_\zeta + (\xi_8)_\zeta \varepsilon(Y_4)_{\zeta-1} + (\xi_9)_\zeta \varepsilon(Y_5)_\zeta \\ +(\xi_{10})_\zeta \varepsilon(Y_5)_{\zeta-1} + (\xi_{11})_\zeta \varepsilon(Y_6)_\zeta + (\xi_{12})_\zeta \varepsilon(Y_6)_{\zeta-1} + (\xi_{13})_\zeta \varepsilon(Y_7)_\zeta \\ +(\xi_{14})_\zeta \varepsilon(Y_7)_{\zeta-1} + (\xi_{15})_\zeta \varepsilon(Y_8)_\zeta + (\xi_{16})_\zeta \varepsilon(Y_8)_{\zeta-1} = (r_5)_{\zeta-\frac{1}{2}}, \end{cases} \tag{4.33}$$

$$\begin{cases} (\chi_1)_\zeta \varepsilon(Y_1)_\zeta + (\chi_2)_\zeta \varepsilon(Y_1)_{\zeta-1} + (\chi_3)_\zeta \varepsilon(Y_2)_\zeta + (\chi_4)_\zeta \varepsilon(Y_2)_{\zeta-1} + (\chi_5)_\zeta \\ \varepsilon(Y_3)_\zeta + (\chi_6)_\zeta \varepsilon(Y_3)_{\zeta-1} + (\chi_7)_\zeta \varepsilon(Y_4)_\zeta + (\chi_8)_\zeta \varepsilon(Y_4)_{\zeta-1} + (\chi_9)_\zeta \varepsilon(Y_5)_\zeta \\ +(\chi_{10})_\zeta \varepsilon(Y_5)_{\zeta-1} + (\chi_{11})_\zeta \varepsilon(Y_6)_\zeta + (\chi_{12})_\zeta \varepsilon(Y_6)_{\zeta-1} + (\chi_{13})_\zeta \varepsilon(Y_7)_\zeta \\ +(\chi_{14})_\zeta \varepsilon(Y_7)_{\zeta-1} + (\chi_{15})_\zeta \varepsilon(Y_8)_\zeta + (\chi_{16})_\zeta \varepsilon(Y_8)_{\zeta-1} = (r_6)_{\zeta-\frac{1}{2}}, \end{cases} \tag{4.34}$$

$$\begin{cases} (\gamma_1)_\zeta \varepsilon(Y_1)_\zeta + (\gamma_2)_\zeta \varepsilon(Y_1)_{\zeta-1} + (\gamma_3)_\zeta \varepsilon(Y_2)_\zeta + (\gamma_4)_\zeta \varepsilon(Y_2)_{\zeta-1} + (\gamma_5)_\zeta \\ \varepsilon(Y_3)_\zeta + (\gamma_6)_\zeta \varepsilon(Y_3)_{\zeta-1} + (\gamma_7)_\zeta \varepsilon(Y_4)_\zeta + (\gamma_8)_\zeta \varepsilon(Y_4)_{\zeta-1} + (\gamma_9)_\zeta \varepsilon(Y_5)_\zeta \\ +(\gamma_{10})_\zeta \varepsilon(Y_5)_{\zeta-1} + (\gamma_{11})_\zeta \varepsilon(Y_6)_\zeta + (\gamma_{12})_\zeta \varepsilon(Y_6)_{\zeta-1} + (\gamma_{13})_\zeta \varepsilon(Y_7)_\zeta \\ +(\gamma_{14})_\zeta \varepsilon(Y_7)_{\zeta-1} + (\gamma_{15})_\zeta \varepsilon(Y_8)_\zeta + (\gamma_{16})_\zeta \varepsilon(Y_8)_{\zeta-1} = (r_7)_{\zeta-\frac{1}{2}}, \end{cases} \tag{4.35}$$

$$\begin{cases} (\lambda_1)_\zeta \varepsilon(Y_1)_\zeta + (\lambda_2)_\zeta \varepsilon(Y_1)_{\zeta-1} + (\lambda_3)_\zeta \varepsilon(Y_2)_\zeta + (\lambda_4)_\zeta \varepsilon(Y_2)_{\zeta-1} + (\lambda_5)_\zeta \\ \varepsilon(Y_3)_\zeta + (\lambda_6)_\zeta \varepsilon(Y_3)_{\zeta-1} + (\lambda_7)_\zeta \varepsilon(Y_4)_\zeta + (\lambda_8)_\zeta \varepsilon(Y_4)_{\zeta-1} + (\lambda_9)_\zeta \varepsilon(Y_5)_\zeta \\ +(\lambda_{10})_\zeta \varepsilon(Y_5)_{\zeta-1} + (\lambda_{11})_\zeta \varepsilon(Y_6)_\zeta + (\lambda_{12})_\zeta \varepsilon(Y_6)_{\zeta-1} + (\lambda_{13})_\zeta \varepsilon(Y_7)_\zeta \\ +(\lambda_{14})_\zeta \varepsilon(Y_7)_{\zeta-1} + (\lambda_{15})_\zeta \varepsilon(Y_8)_\zeta + (\lambda_{16})_\zeta \varepsilon(Y_8)_{\zeta-1} = (r_8)_{\zeta-\frac{1}{2}}. \end{cases} \tag{4.36}$$

Here, $\xi(l), \chi(l), \gamma(l), \lambda(l), \zeta = 1, ..., 16$ are constants. The linear system is written in the matrix form as given in (2.54)-(2.55). Making use of the boundary conditions defined in (4.11), we have:

$$\mathrm{x}_1 = \begin{bmatrix} \varepsilon(Y_2)_0 \\ \varepsilon(Y_4)_0 \\ \varepsilon(Y_6)_0 \\ \varepsilon(Y_7)_0 \\ \varepsilon(Y_2)_1 \\ \varepsilon(Y_4)_1 \\ \varepsilon(Y_5)_1 \\ \varepsilon(Y_8)_1 \end{bmatrix}, \quad \mathrm{x}_\zeta = \begin{bmatrix} \varepsilon(Y_1)_{\zeta-1} \\ \varepsilon(Y_3)_{\zeta-1} \\ \varepsilon(Y_6)_{\zeta-1} \\ \varepsilon(Y_7)_{\zeta-1} \\ \varepsilon(Y_2)_\zeta \\ \varepsilon(Y_4)_\zeta \\ \varepsilon(Y_5)_\zeta \\ \varepsilon(Y_8)_\zeta \end{bmatrix}, \qquad \zeta = 2, 3, ..., J, \tag{4.37}$$

$$A_1 = \begin{bmatrix} -0.5h & 0 & 0 & 0 & -0.5h & 0 & 0 & 0 \\ 0 & -0.5h & 0 & 0 & 0 & -0.5h & 0 & 0 \\ 0 & 0 & -0.5h & 0 & 0 & 0 & -0.5h & 0 \\ 0 & 0 & 0 & -1 & 0 & 0 & 0 & -0.5h \\ (\xi_4)_1 & (\xi_8)_1 & (\xi_{12})_1 & (\xi_{14})_1 & (\xi_3)_1 & (\xi_7)_1 & (\xi_9)_1 & (\xi_{15})_1 \\ (\chi_4)_1 & (\chi_8)_1 & (\chi_{12})_1 & (\chi_{14})_1 & (\chi_3)_1 & (\chi_7)_1 & (\chi_9)_1 & (\chi_{15})_1 \\ (\gamma_4)_1 & (\gamma_8)_1 & (\gamma_{12})_1 & (\gamma_{14})_1 & (\gamma_3)_1 & (\gamma_7)_1 & (\gamma_9)_1 & (\gamma_{15})_1 \\ (\lambda_4)_1 & (\lambda_8)_1 & (\lambda_{12})_1 & (\lambda_{14})_1 & (\lambda_3)_1 & (\lambda_7)_1 & (\lambda_9)_1 & (\lambda_{15})_1 \end{bmatrix},$$

$$A_\zeta = \begin{bmatrix} -1 & 0 & 0 & 0 & -0.5h & 0 & 0 & 0 \\ 0 & -1 & 0 & 0 & 0 & -0.5h & 0 & 0 \\ 0 & 0 & -0.5h & 0 & 0 & 0 & 1 & 0 \\ 0 & 0 & 0 & -1 & 0 & 0 & 0 & -0.5h \\ (\xi_2)_\zeta & (\xi_6)_\zeta & (\xi_{12})_\zeta & (\xi_{14})_\zeta & (\xi_3)_\zeta & (\xi_7)_\zeta & (\xi_9)_\zeta & (\xi_{15})_\zeta \\ (\chi_2)_\zeta & (\chi_6)_\zeta & (\chi_{12})_\zeta & (\chi_{14})_\zeta & (\chi_3)_\zeta & (\chi_7)_\zeta & (\chi_9)_\zeta & (\chi_{15})_\zeta \\ (\gamma_2)_\zeta & (\gamma_6)_\zeta & (\gamma_{12})_\zeta & (\gamma_{14})_\zeta & (\gamma_3)_\zeta & (\gamma_7)_\zeta & (\gamma_9)_\zeta & (\gamma_{15})_\zeta \\ (\lambda_2)_\zeta & (\lambda_6)_\zeta & (\lambda_{12})_\zeta & (\lambda_{14})_\zeta & (\lambda_3)_\zeta & (\lambda_7)_\zeta & (\lambda_9)_\zeta & (\lambda_{15})_\zeta \end{bmatrix}, \qquad \zeta = 2, 3, ..., J,$$

$$B_\zeta = \begin{bmatrix} 0 & 0 & 0 & 0 & -0.5h & 0 & 0 & 0 \\ 0 & 0 & 0 & 0 & 0 & -0.5h & 0 & 0 \\ 0 & 0 & 0 & 0 & 0 & 0 & -1 & 0 \\ 0 & 0 & 0 & 0 & 0 & 0 & 0 & -0.5h \\ 0 & 0 & 0 & 0 & (\xi_4)_\zeta & (\xi_8)_\zeta & (\xi_{10})_\zeta & (\xi_{16})_\zeta \\ 0 & 0 & 0 & 0 & (\chi_4)_\zeta & (\chi_8)_\zeta & (\chi_{10})_\zeta & (\chi_{16})_\zeta \\ 0 & 0 & 0 & 0 & (\gamma_4)_\zeta & (\gamma_8)_\zeta & (\gamma_{10})_\zeta & (\gamma_{16})_\zeta \\ 0 & 0 & 0 & 0 & (\lambda_4)_\zeta & (\lambda_8)_\zeta & (\lambda_{10})_\zeta & (\lambda_{16})_\zeta \end{bmatrix}, \qquad \zeta = 2, 3, ..., J,$$

$$C_\zeta = \begin{bmatrix} 1 & 0 & 0 & 0 & 0 & 0 & 0 & 0 \\ 0 & 1 & 0 & 0 & 0 & 0 & 0 & 0 \\ 0 & 0 & -0.5h & 0 & 0 & 0 & 0 & 0 \\ 0 & 0 & 0 & 1 & 0 & 0 & 0 & 0 \\ (\xi_1)_\zeta & (\xi_5)_\zeta & (\xi_{11})_\zeta & (\xi_{13})_\zeta & 0 & 0 & 0 & 0 \\ (\chi_1)_\zeta & (\chi_5)_\zeta & (\chi_{11})_\zeta & (\chi_{13})_\zeta & 0 & 0 & 0 & 0 \\ (\gamma_1)_\zeta & (\gamma_5)_\zeta & (\gamma_{11})_\zeta & (\gamma_{13})_\zeta & 0 & 0 & 0 & 0 \\ (\lambda_1)_\zeta & (\lambda_5)_\zeta & (\lambda_{11})_\zeta & (\lambda_{13})_\zeta & 0 & 0 & 0 & 0 \end{bmatrix}, \qquad \zeta = 1, 2, ..., J.$$

In the next step, the arising linear system is solved by block LU-factorization. The coding of the whole procedure was carried in Matlab. To validate the Keller box Matlab program developed for the present problem, the results are compared with a built-in Matlab routine of bvp4c. A good agreement is found amongst the results as evident from the Table 4.1.

V_0	τ	
	bvp4c	KBM
0.2	0.135173	0.135173
0.4	0.090768	0.090768
0.6	0.063248	0.063248
0.8	0.045697	0.045697
1	0.034158	0.034158

Table 4.1: Comparison table of Keller box and bvp4c solutions for τ with $M = 5, Pm = 1, K = 1, \phi = 0.04, Pr = 6.2$.

4.4 Numerical Results and Discussion

The present section provides a discussion on the impact of the sundry parameters affecting the flow and heat transfer properties. The results in Figures 4.2 and 4.3 show that the velocity and the angular velocity, both are decreasing functions of the magnetic parameter due to the resistance provided by the magnetic field. A stronger impact is seen in the case of kerosene oil-based SWCNT and MWCNT nanofluid as compared to water-based SWCNT and MWCNT nanofluid. The induced magnetic field is also seen declining for higher values of the magnetic parameter in

Figure 4.4. In Figures 4.5 and 4.6, it is seen that both the velocity and the angular velocity shrink with an increase in Pm. Figure 4.7 reveals that the induced magnetic field decreases with an increase in the values of Pm because of the increase in the momentum diffusion as compared to magnetic diffusion.

The velocity decreases with an increase in the material parameter K (see Figure 4.8) which is an indication that the couple stresses tend to reduce the velocity. An augmentation in the angular velocity is observed in Figure 4.9 as K augments. The induced magnetic field also grows with the rising values of the material parameter K as it is evident from Figure 4.10. The angular velocity profile is enhanced by increasing the nanoparticle volume fraction for all cases but particularly in the case of the SWCNT-water nanofluid (see Figure 4.11), the velocity is increased most rapidly. In Figure 4.12, the induced magnetic field is noticed as a decreasing function of the volume fraction when plotted for variation in the ϕ. The temperature profile when plotted against the values of volume fraction in Figure 4.13 shows that it increases when the amount of nanoparticles is increased. However the temperature profile grows most for the SWCNT-water and least for MWNCT-kerosene oil.

Figure 4.14 reveals that the angular velocity decreases for the greater values of the suction parameter. Furthermore near the lower plate, the profile is concave up while the concavity changes as we move towards the upper plate. The suction parameter V_0 enhances the induced magnetic field of the nanofluid as observed in Figure 4.15. Greater suction velocity is responsible for increasing the linear velocity of the fluid which in return increases the electromotive current due to the increased free electrons motion thus induced magnetic field is enhanced. The temperature profile shows a decline with the rising values of the suction parameter as it decreases the temperature gradient applied at the surface (see Figure 4.16). A comparison of the SWCNT and MWCNT nanoparticles with base fluid as water in Figure 4.18 indicates that the Nusselt number increases with the increase in the suction parameter V_0 but it is greater in SWCNT-water nanofluid. In Figure 4.20, the heat transfer rate increases appreciably when kerosene oil is used as the base fluid. The MWCNT-kerosene oil nanofluid is the most effective in heat transfer among the nanofluids used in the present study. Bar graphs have been utilized to evaluate the impact of various parameters on skin friction. In Figure 4.21, the magnetic parameter is seen reducing the skin friction of nanofluid because it repels the fluid away from the plate surface. A similar observation can be seen in the case of variation in the magnetic Prandtl number Pm (see Figure 4.22). Figure 4.23 reveals that the material parameter K, when increased, rises the skin friction of the nanofluids, particularly, the SWCNT-water nanofluid. Greater volume fraction of the nanoparticles increase the skin friction of the nanofluids as witnessed in Figure 4.24. From Figure 4.25, we observe that the skin friction of the nanofluids decreases with the increment in the suction parameter.

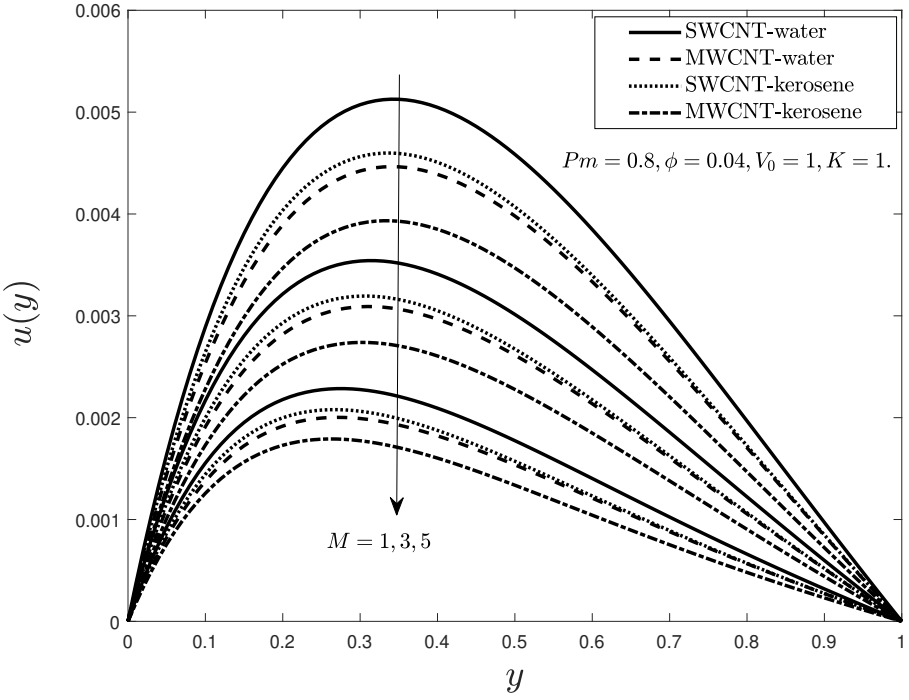

Figure 4.2: Effect of the magnetic parameter M on velocity.

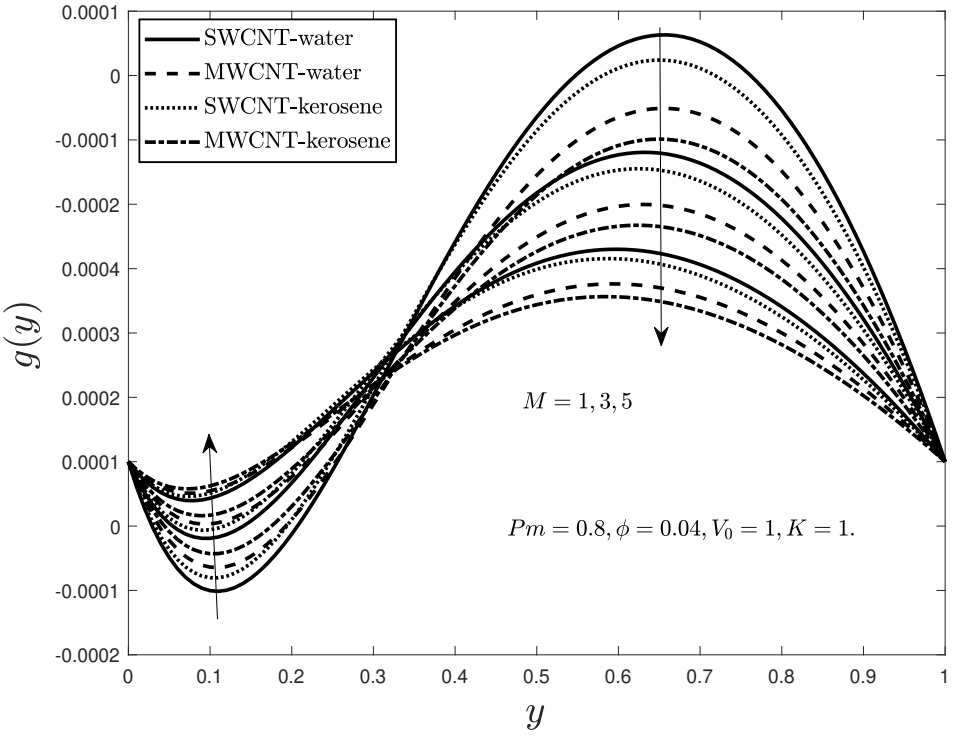

Figure 4.3: Effect of the magnetic parameter M on angular velocity.

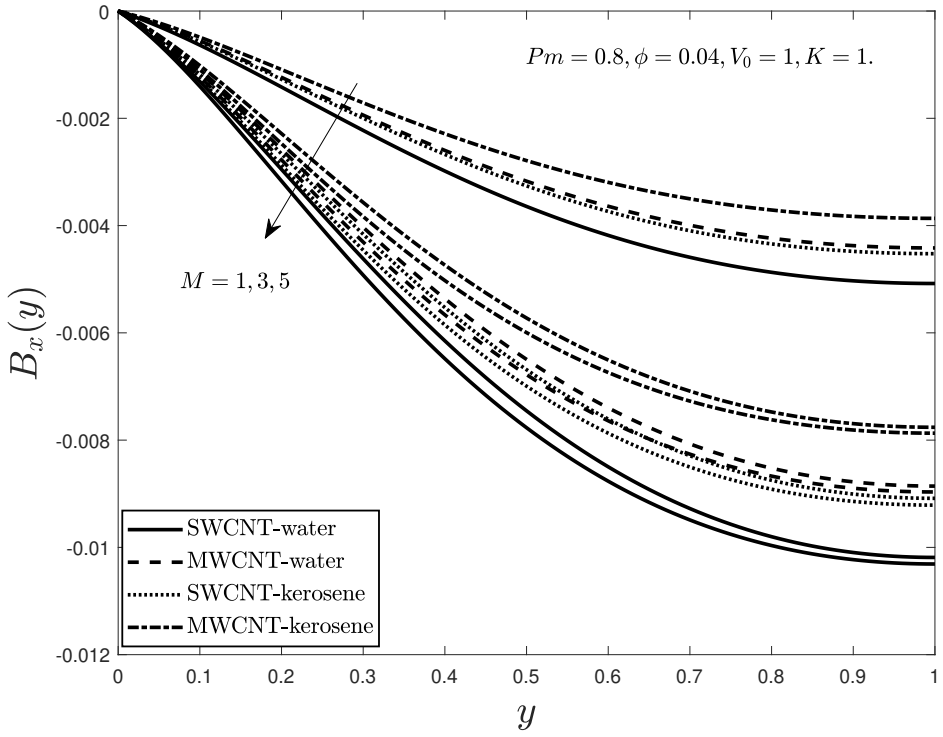

Figure 4.4: Effect of the magnetic parameter M on induced magnetic field.

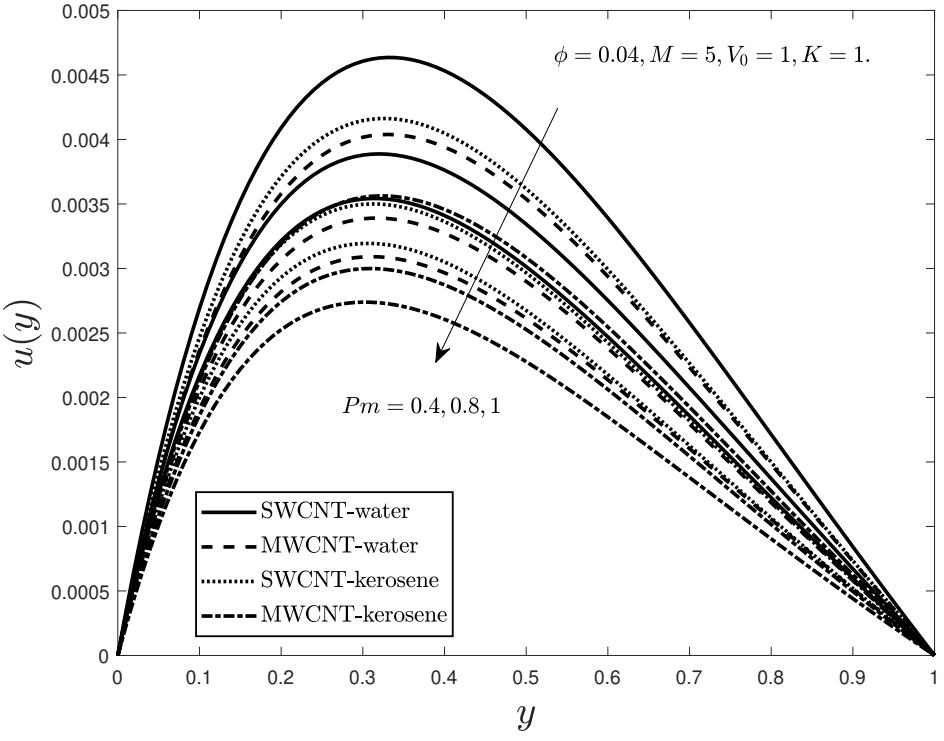

Figure 4.5: Impact of magnetic Prandtl number Pm on velocity.

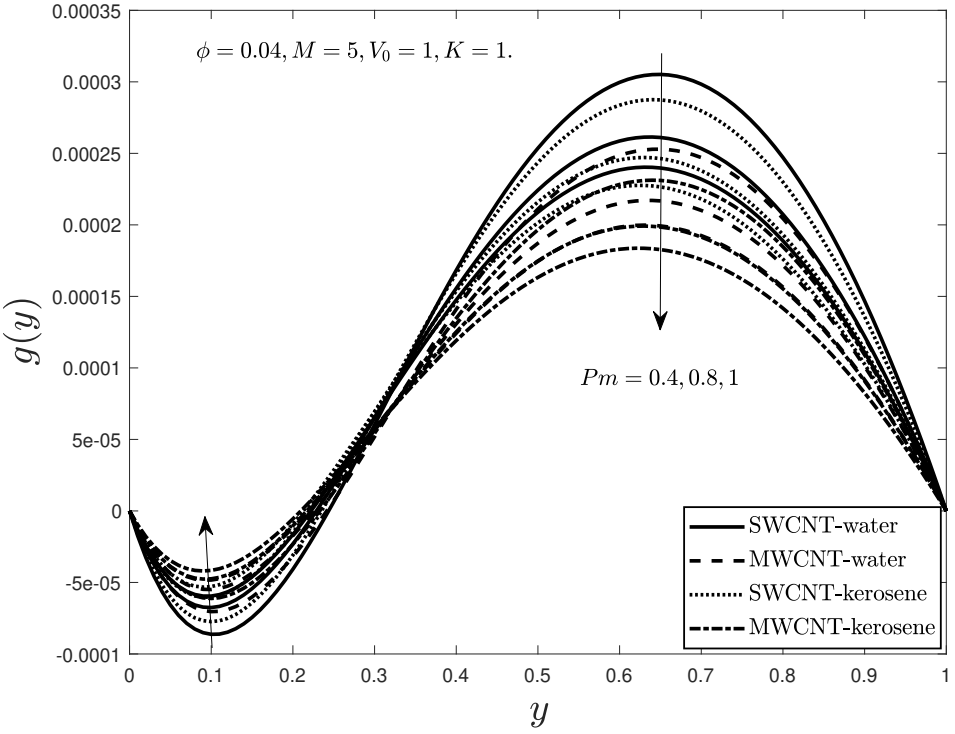

Figure 4.6: Impact of magnetic Prandtl number Pm on angular velocity.

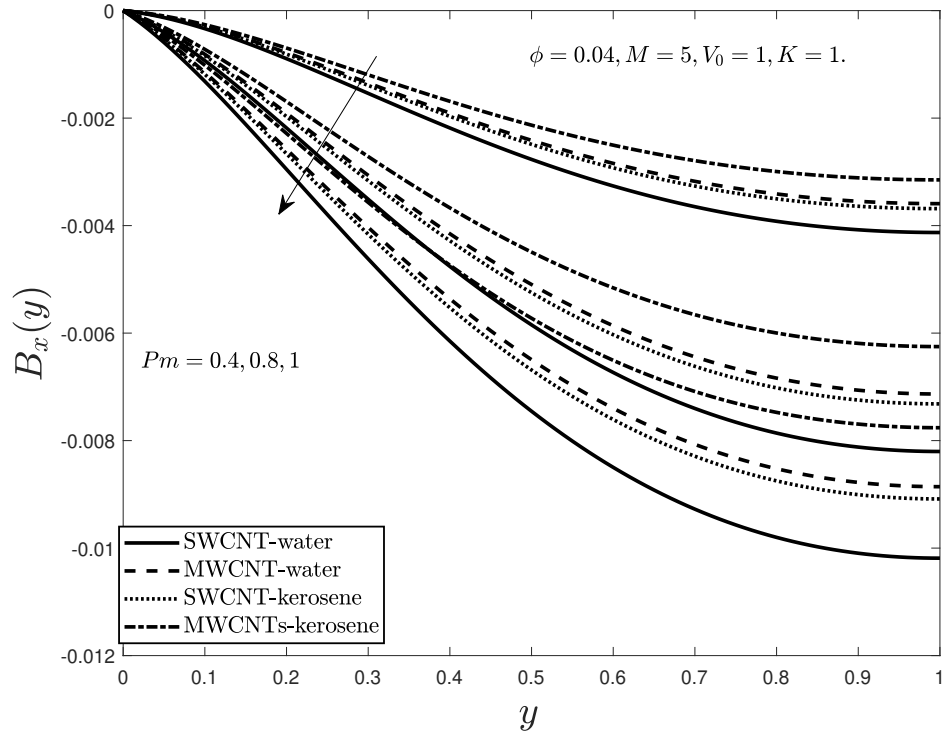

Figure 4.7: Impact of magnetic Prandtl number Pm on induced magnetic field.

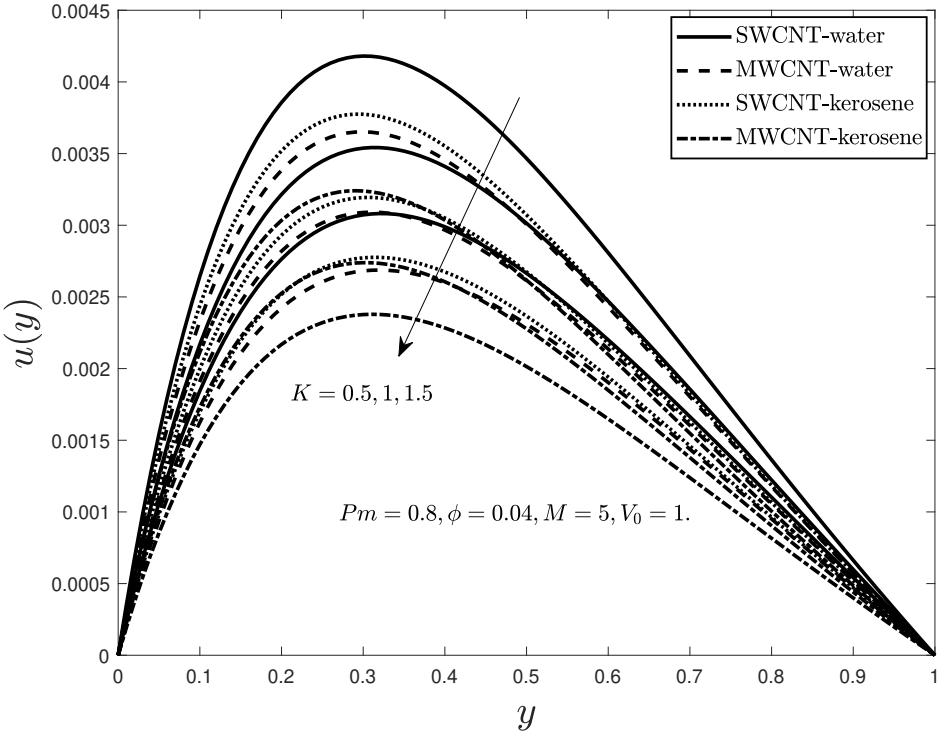

Figure 4.8: Impact of material parameter K on velocity.

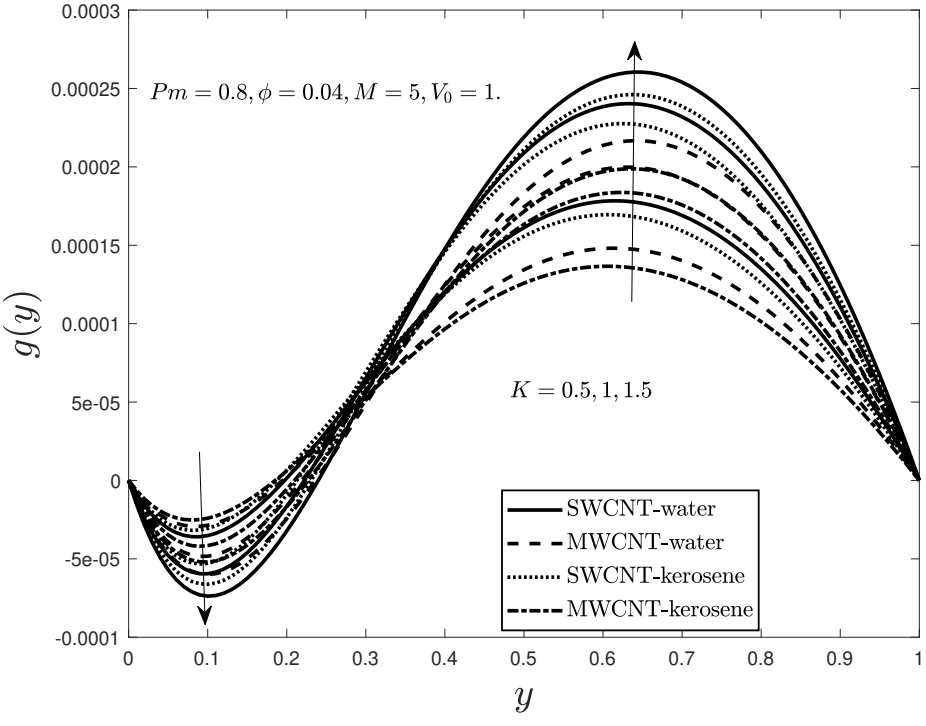

Figure 4.9: Impact of material parameter K on angular velocity.

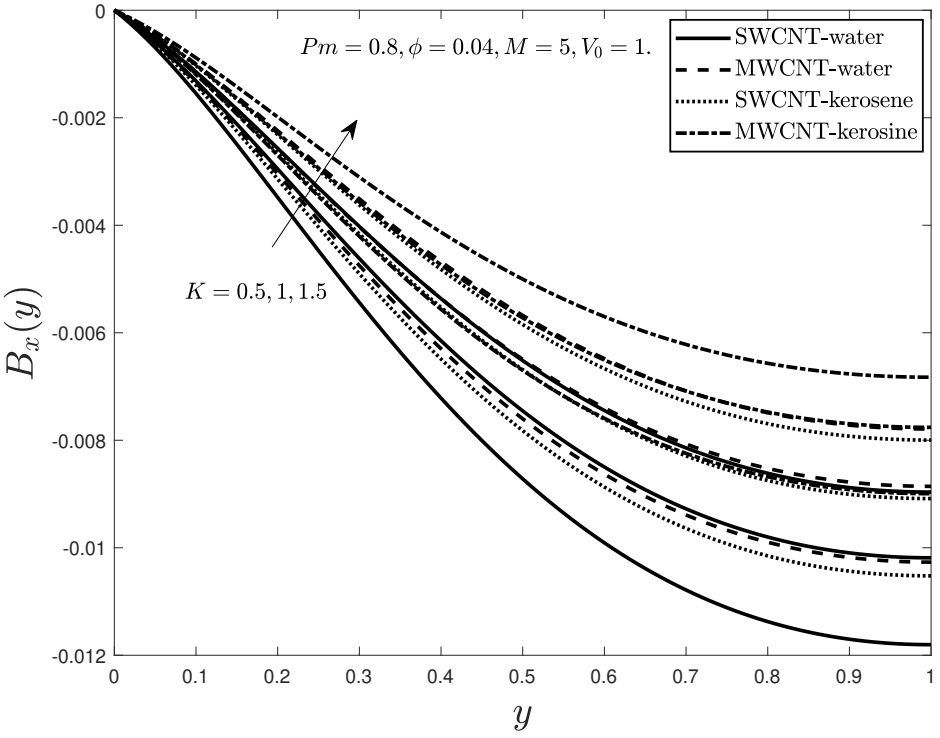

Figure 4.10: Impact of material parameter K on induced magnetic field.

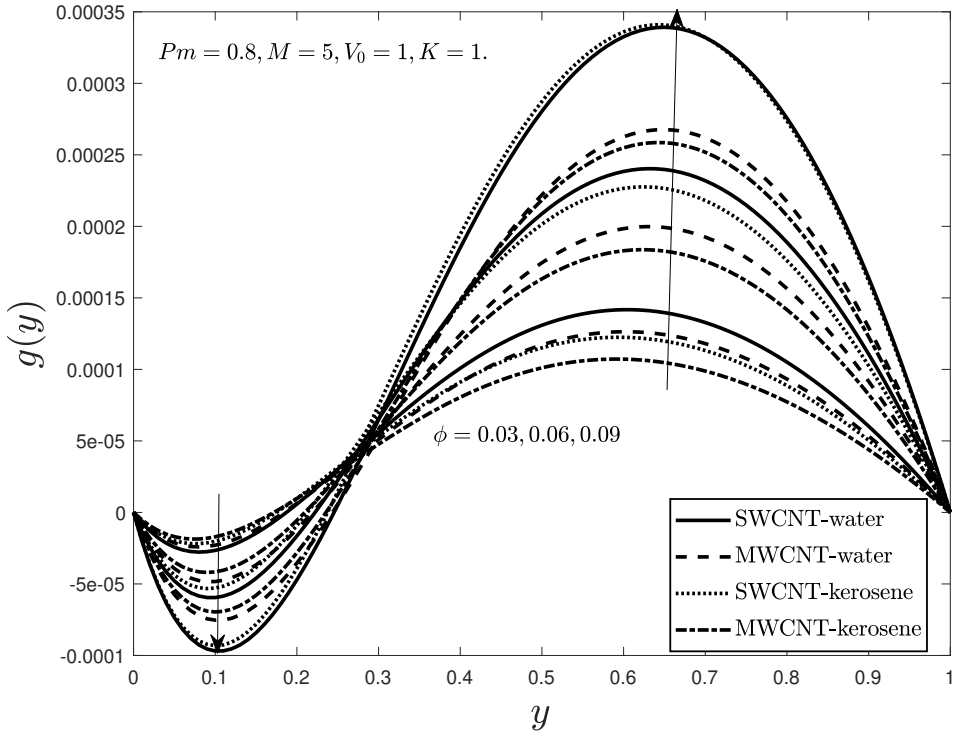

Figure 4.11: Impact of volume fraction ϕ on the angular velocity.

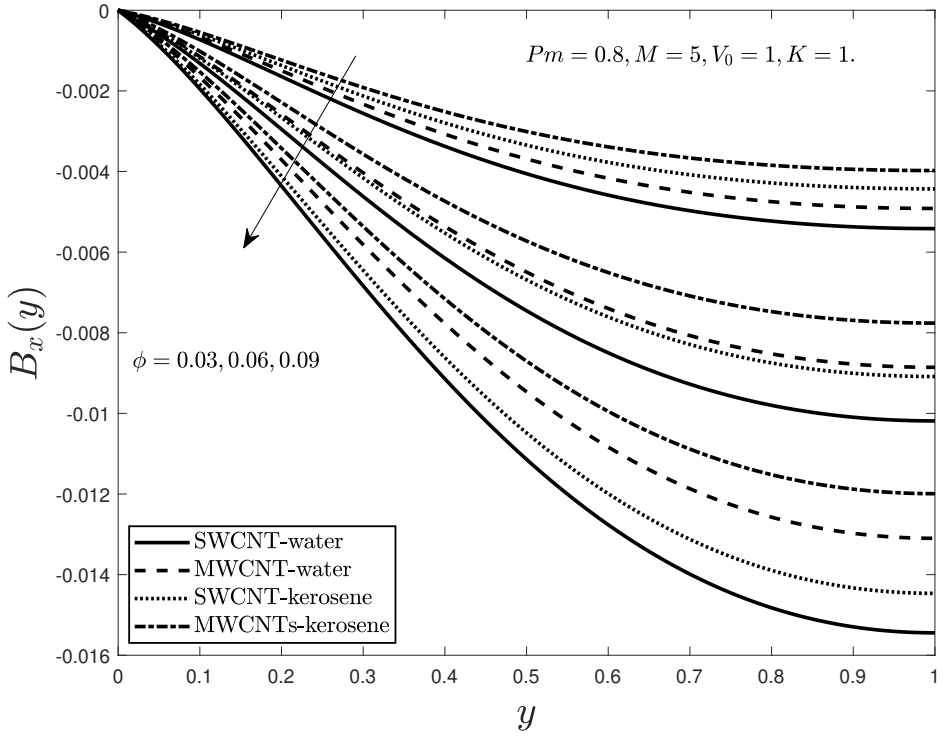

Figure 4.12: Impact of volume fraction ϕ on the induced magnetic field.

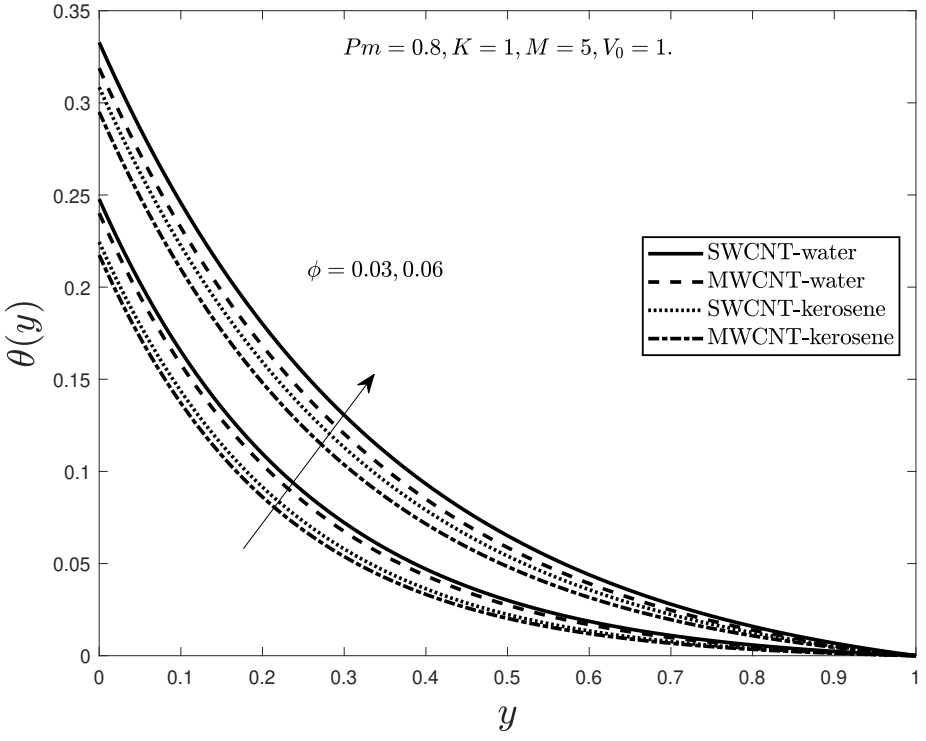

Figure 4.13: Impact of volume fraction ϕ on temperature.

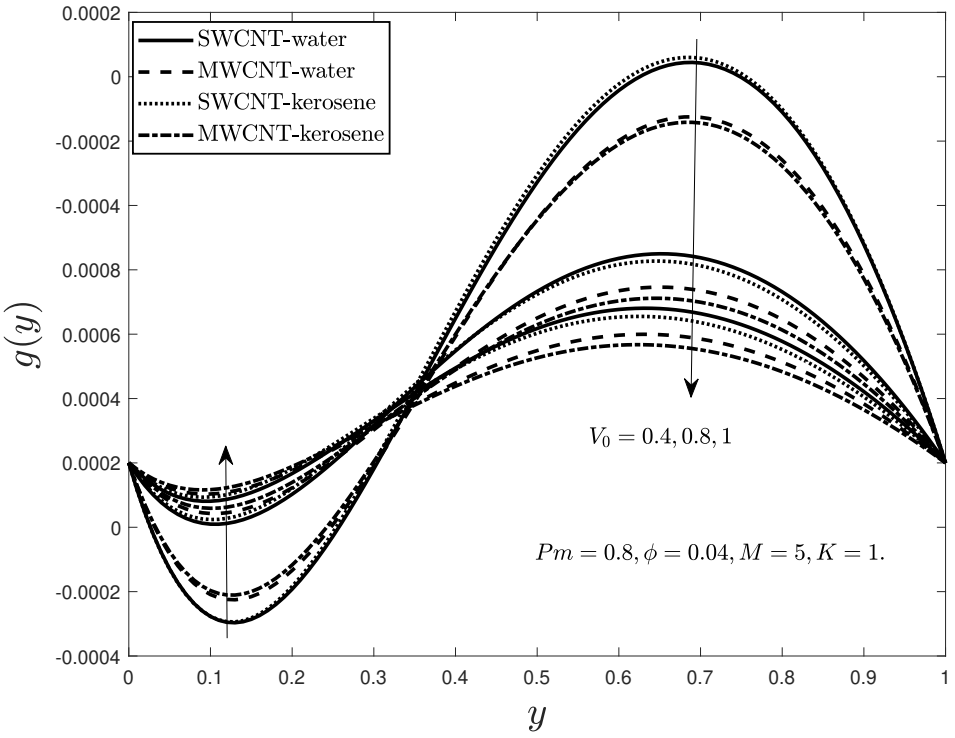

Figure 4.14: Impact of suction parameter V_0 on the angular velocity.

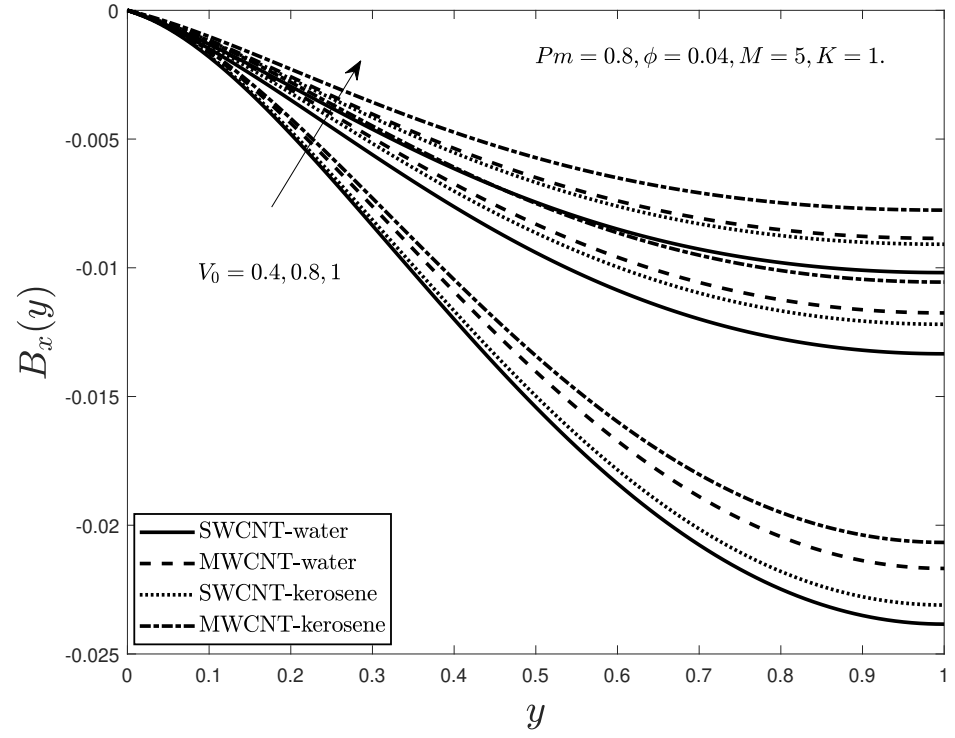

Figure 4.15: Impact of suction parameter V_0 on induced magnetic field.

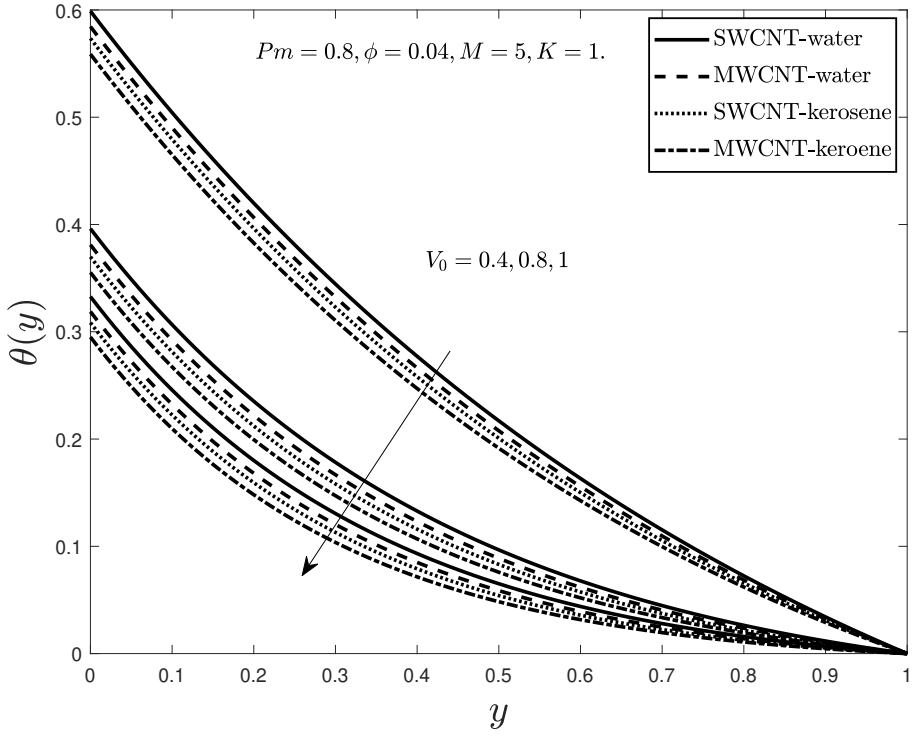

Figure 4.16: Impact of suction parameter V_0 on temperature.

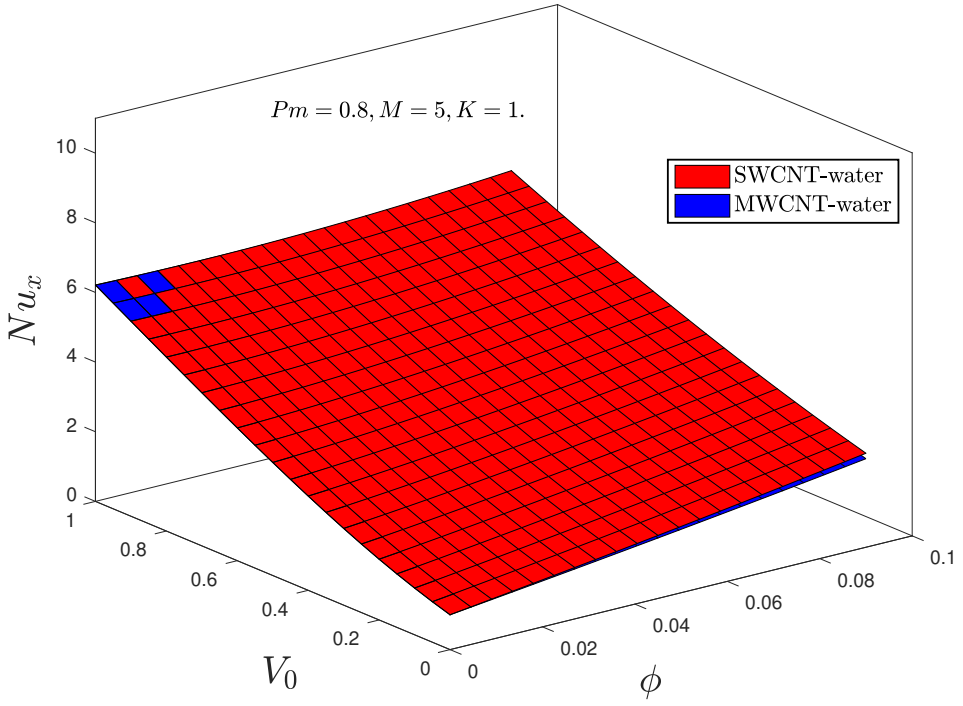

Figure 4.17: Impact of suction parameter V_0 and ϕ on the Nusselt number with water as base fluid.(3D)

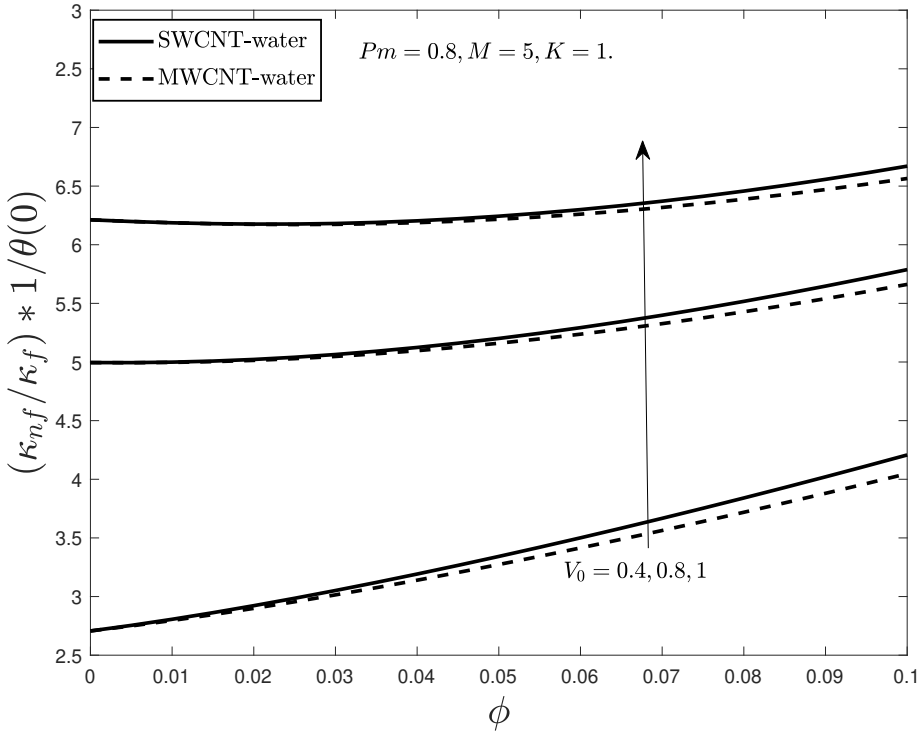

Figure 4.18: Impact of changing suction parameter V_0 and ϕ on the Nusselt number with water as base fluid. (2D)

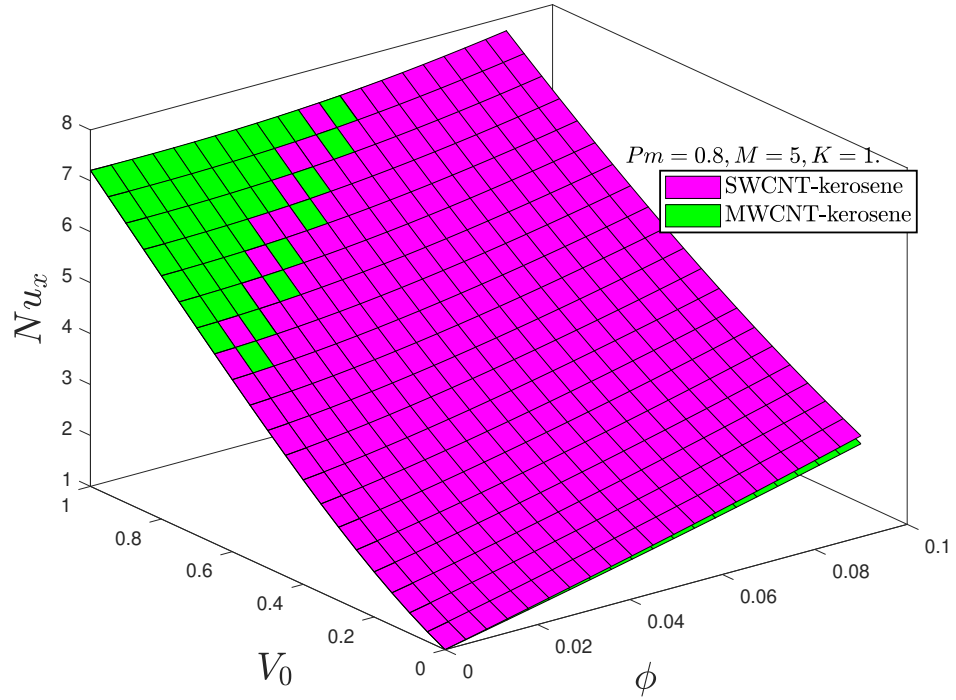

Figure 4.19: Impact of suction parameter V_0 and ϕ on the Nusselt number with kerosene oil as base fluid.

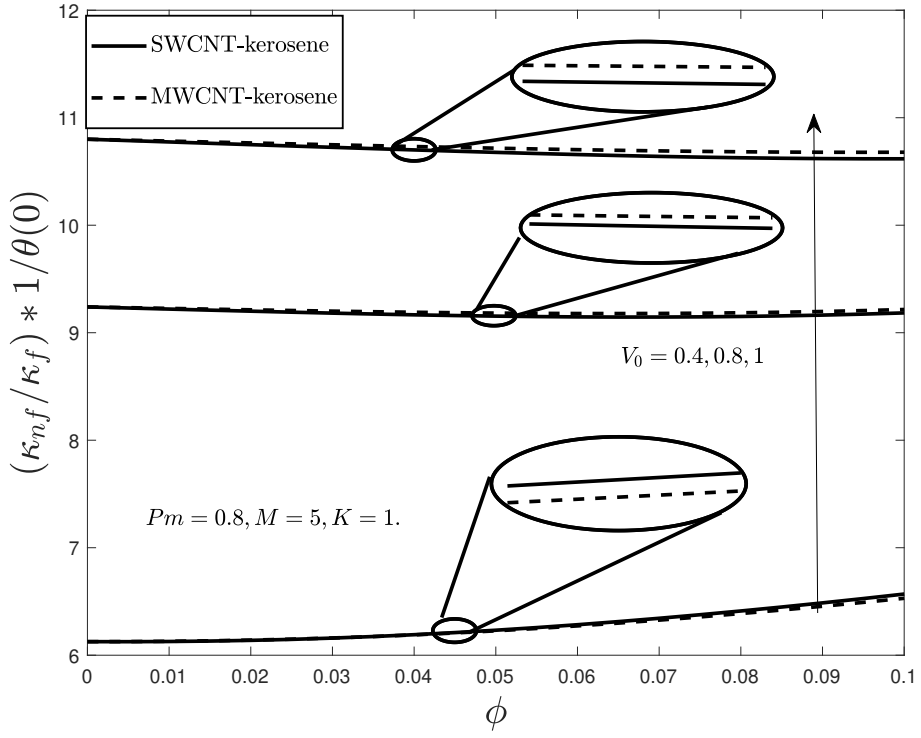

Figure 4.20: Impact of suction parameter V_0 and ϕ on the Nusselt number with kerosene oil as base fluid.

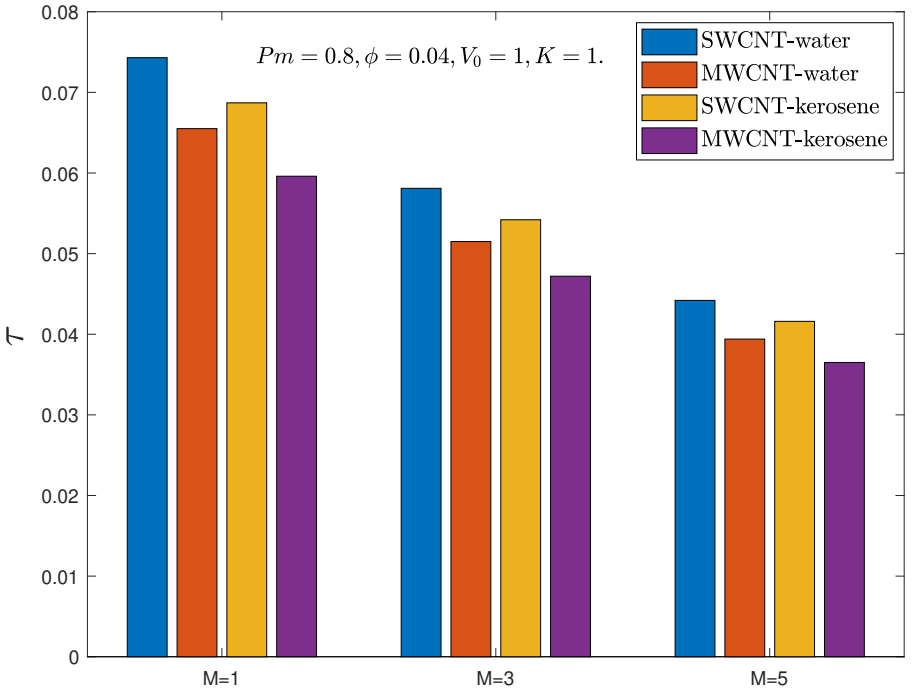

Figure 4.21: Impact of magnetic number M on the skin friction.

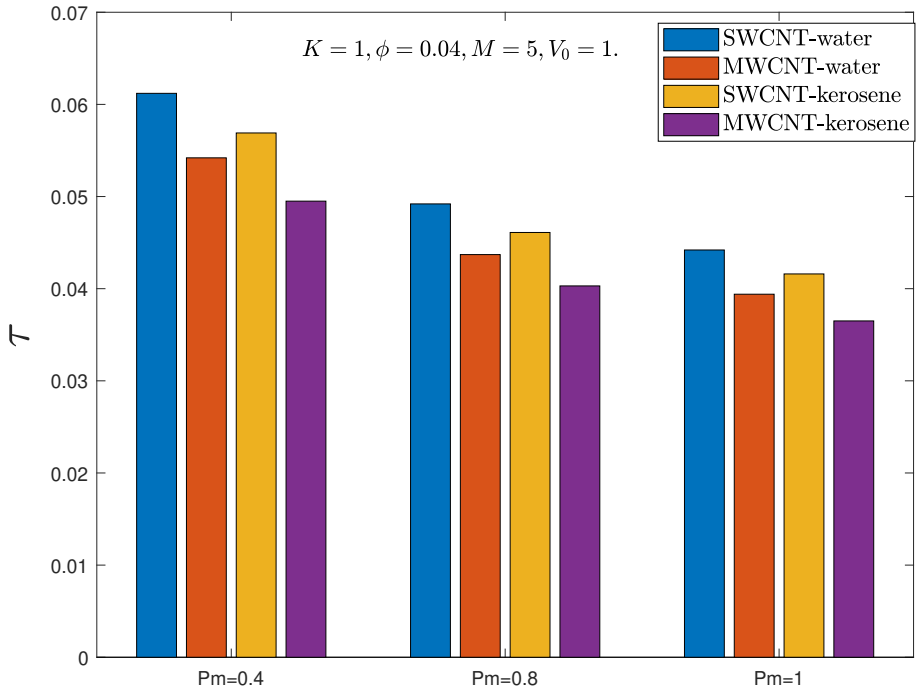

Figure 4.22: Impact of magnetic Prandtl number Pm on the skin friction.

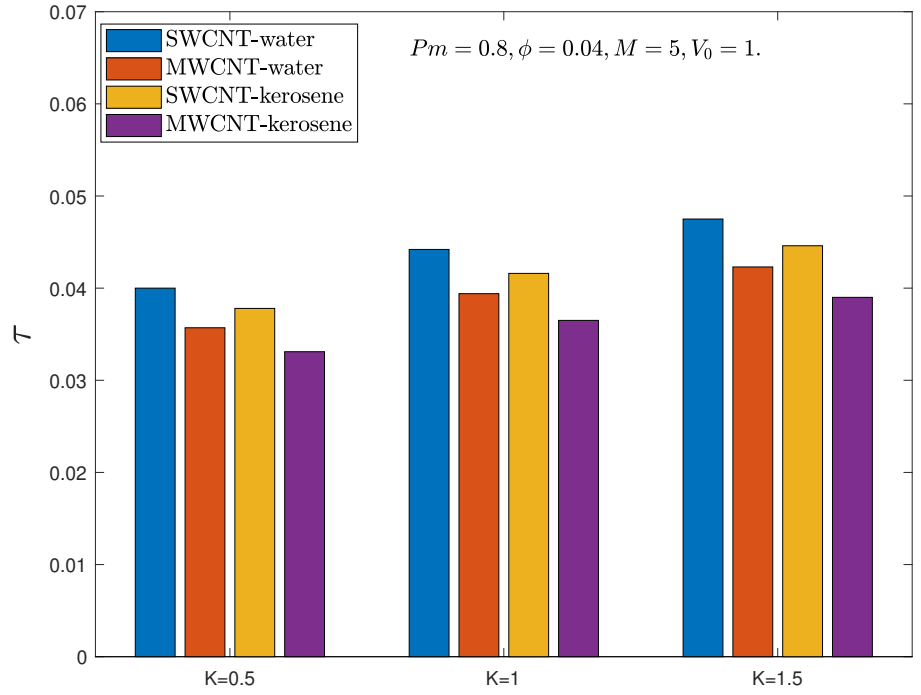

Figure 4.23: Impact of material parameter K on the skin friction.

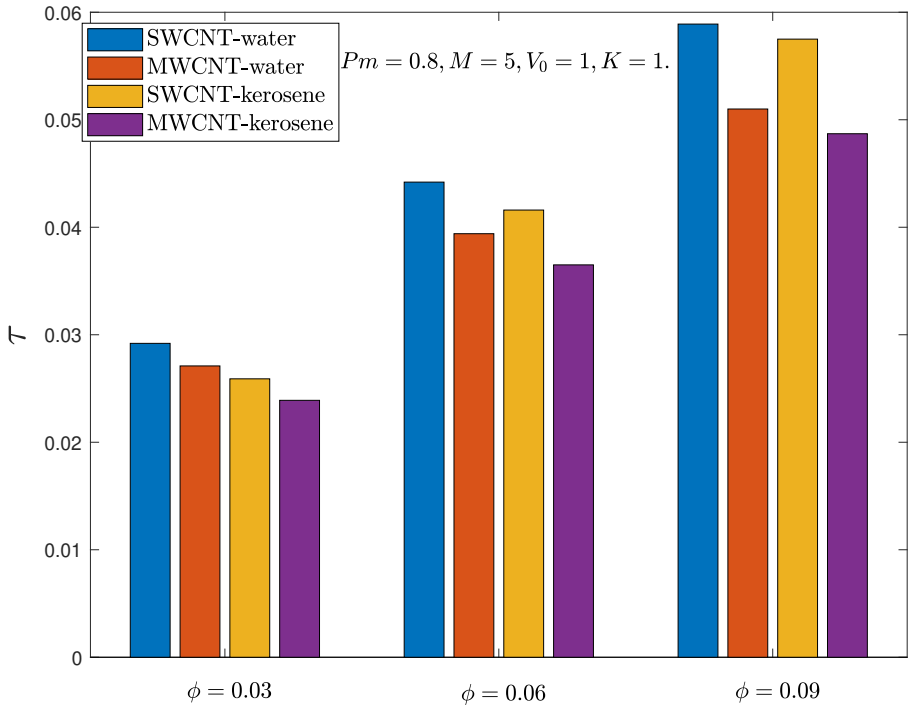

Figure 4.24: Impact of volume fraction ϕ on the skin friction.

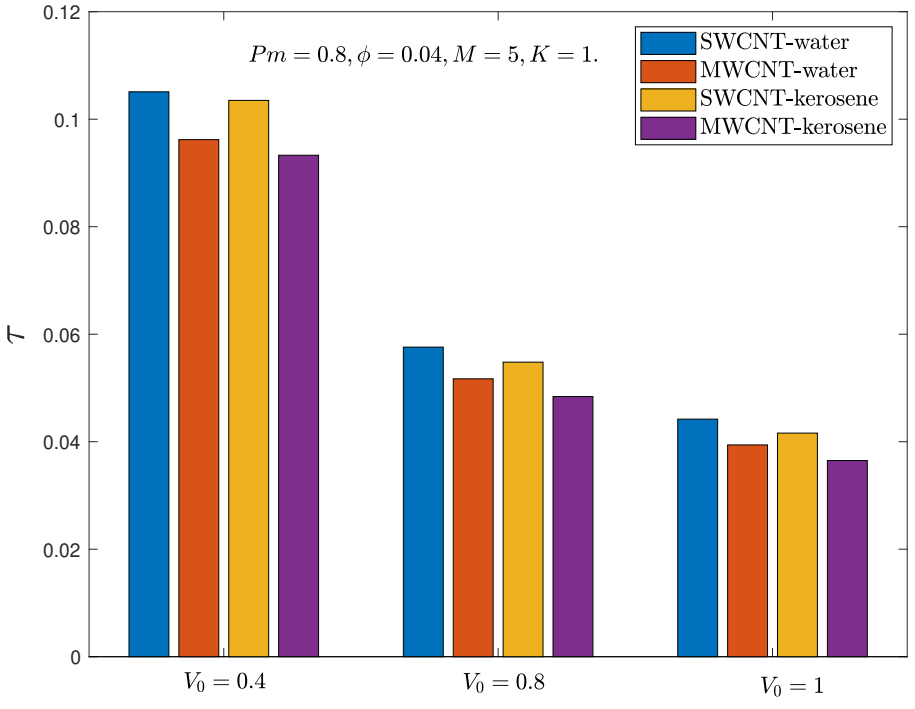

Figure 4.25: Impact of suction velocity V_0 on the skin friction.

4.5 Chapter Summary

On the basis of graphical results, the findings of the study can be summarized as follows:

- A greater decline in the fluid velocity and angular velocity with the growing values of magnetic number, is seen in the case of kerosene oil-based SWCNT and MWCNT nanofluid as compared to water-based SWCNT and MWCNT nanofluid.
- It is noted that induced magnetic field declines for greater values of volume fraction in all cases. The result indicates that the increase in the number of nanoparticles tend to reduce the effects of induced magnetic field in the SWCNT/MWCNT-water as well as SWCNT/MWCNT-kerosene oil nanofluids.
- Observing the comparison of the Nusselt number for SWCNT/MWCNT-kerosene oil nanofluid, it is noted that for smaller values of volume fraction ϕ the MWNCT-kerosene is more effective but for greater values of ϕ, MWCNT-kerosene oil is better suited in enhancement of heat transfer rate.
- The Suction parameter V_0 when coupled with the volume fraction ϕ and SWCNT-kerosene oil can bring about greatest heat transfer.

Chapter 5

Marangoni Convective Flow and Heat Transfer in MHD Micropolar Alumina-water Nanofluid

5.1 Introduction

The present chapter is aimed at the thermal transport analysis in alumina-water micropolar nanofluid spotlighted by the Cattaneo-Christov heat flux model. Fluid flow in the situations where either fluid is superbly heated or flowing in the region having microgravity such as space is accumulated to observe the effects of surface tension gradients on the thermal transport in nanofluids. This phenomena is seldomly discussed mathematically as very few researches can found on this topic. Here, Marangoni convection in alumina/water nanofluid is considered. Four different shaped nanoparticles are used to analyze the heat transfer in the nanofluid. The fluid flow is deemed with the application of a uniform magnetic field applied in way to control the flow of the fluid. The mathematical modeling is based on the coupled Naiver-Stokes equations of fluid dynamics and the energy equation with the thermal time relaxation factor. Model equations after applying the boundary layer approximations and similarity transformations are ODEs which are solved by the KBM. The results for fluid flow, temperature profile and Nusselt number are plotted and analyzed.

5.2 Problem Statement and Mathematical Formulation

Consider a steady, two dimensional and incompressible flow of alumina-water micropolar nanofluid. Flow of the nanofluid is due to the surface tension gradients prevailing at the interface as a result of the temperature imbalances in the fluid. Magnetic field is applied perpendicular to the fluid motion to optimize the flow (see Figure 5.1). The Joule heating effects and the electric currents produced in the nanofluid are supposed to be very small so these are ignored in the study. Fluid is supposed to contain microstrutures with in its composition so the angular momentum equation is added to the set of governing equations. Contrary to the study carried out in the previous chapter, the nanofluid is assumed to contain microstructures at the surface, the Impact on which is added to the boundary conditions at the surface. Also, microstructures are assumed not to contribute towards heat dissipation caused inside the nanofluid. Homogeneous single phase model is considered with Al_2O_3 as nanoparticles and water as the base fluid with constant thermophysical properties. The primary purpose of the study is to ponder on the heat transfer rate in the boundary layer formed close at the interface. The fluid is assumed to isotropic that is the viscosity of the fluid is constant and the value of magnetic Prandtl number Pr is close to "1". Implementation of the boundary layer approximation to the governing equations give the set of equations by following [69]:

$$\frac{\partial u}{\partial x}+\frac{\partial v}{\partial y}=0, \tag{5.1}$$

$$u\frac{\partial u}{\partial x}+v\frac{\partial u}{\partial y}=\left(\nu_{nf}+\frac{\kappa^*}{\rho_{nf}}\right)\frac{\partial^2 u}{\partial y^2}+\frac{\kappa^*}{\rho_{nf}}\frac{\partial N}{\partial y}-\left(\sigma_{el}\right)_{nf}\frac{{B_0}^2 u}{\rho_{nf}}, \tag{5.2}$$

$$j\left(u\frac{\partial N}{\partial x}+v\frac{\partial N}{\partial y}\right)=\left(\nu_{nf}+\frac{\kappa^*}{2\rho_{nf}}\right)j\frac{\partial^2 N}{\partial y^2}-\kappa^*\left(2N+\frac{\partial u}{\partial y}\right), \tag{5.3}$$

$$\begin{cases} u\frac{\partial T}{\partial x}+v\frac{\partial T}{\partial y}+\lambda_0\Big[u\frac{\partial u}{\partial x}\frac{\partial T}{\partial x}+v\frac{\partial v}{\partial y}\frac{\partial T}{\partial y}+u^2\frac{\partial^2 T}{\partial x^2}+v^2\frac{\partial^2 T}{\partial y^2}+2uv\frac{\partial^2 T}{\partial x\partial y}+u\frac{\partial v}{\partial x}\frac{\partial T}{\partial y} \\ +v\frac{\partial u}{\partial y}\frac{\partial T}{\partial x}\Big]=\alpha'_{nf}\frac{\partial^2 T}{\partial y^2}. \end{cases} \tag{5.4}$$

The physical quantities of viscosity μ_{nf}, density ρ_{nf}, heat capacity $(\rho C_p)_{nf}$ and electrical conductivity $(\sigma_{el})_{nf}$ of the nanofluid are defined in Eqs. (2.19)-(2.20). The shape factor m for different shaped nanoparticles is defined in Table 5.1 [70], whereas the thermophysical properties of the nanofluid in Table 2.1.

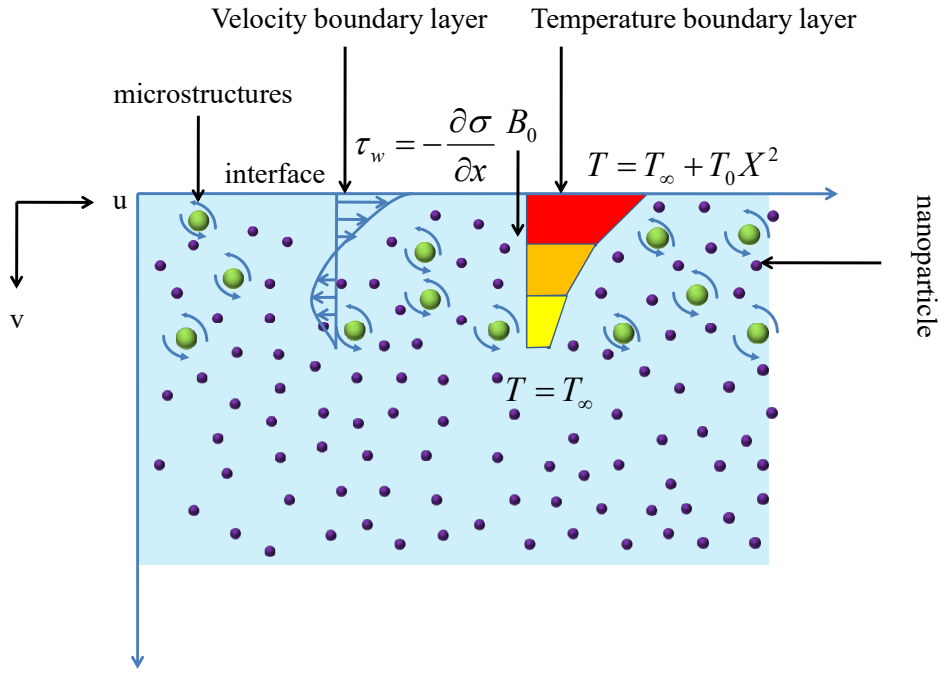

Figure 5.1: Schematic diagram of the flow model.

Shape	Sphere	Tetrahedron	Column	Lamina
m	3	4.0613	6.3598	16.1576

Table 5.1: Empirical shape factor values defining various shapes of the nanoparticles.

The surface tension σ is assumed to be a linear function of temperature and is defined as [69]:

$$\sigma = \sigma_0 \left[1 - \gamma_T \left(T - T_\infty\right)\right],$$

where $\gamma_T = -\frac{1}{\sigma_0} \frac{\partial \sigma}{\partial T}\Big|_T$.

The shear stress is related to the temperature gradient at the boundary surface as:

$$\frac{\partial \sigma}{\partial X} = \frac{\partial \sigma}{\partial T} \frac{\partial T}{\partial X},$$

where $X = \frac{x}{L}$.

The boundary conditions have been considered as follows [69]:

$$(\mu_{nf}+\kappa^{*})\left.\frac{\partial u}{\partial y}\right|_{y=0}=-\left.\frac{\partial \sigma}{\partial x}\right|_{y=0}=\sigma_0\gamma_T\left.\frac{\partial T}{\partial x}\right|_{y=0}, v\,(x,0)=0,\ N(x,0)=-n\left.\frac{\partial u}{\partial y}\right|_{y=0},$$

$$T\,(x,0)=T_\infty+T_0X^2, \tag{5.5}$$

$$u\to 0, v\to 0, N\to 0, T\to T_\infty \quad \text{as} \quad y\to\infty. \tag{5.6}$$

Here, n is a constant ranging between '0' and '1'. For the case $n=0$, the microstructures are unable to rotate in the boundary layer. The weak concentration corresponds to the case when $n=0.5$ for which the anti-symmetrical part of the stress tensor vanishes. $n=1$ give rise to turbulent flows where the couple stress effects are present. In the present analysis, the cases when $n=0$ and $n=0.5$ are considered. The self similar form of Eqs. (5.1)-(5.4) is obtained by using the following similarity variables

$$\begin{aligned}
&\Psi\,(x,y)=\nu_f X f\,(\eta)\,, \quad \eta=\frac{y}{L},\\
&u=\frac{\partial\Psi}{\partial y}, \quad v=-\frac{\partial\Psi}{\partial x},\\
&N\,(x,y)=\frac{\nu_f}{L^2}Xg(\eta),\\
&T\,(x,y)=T_0X^2\theta\,(\eta)+T_\infty.
\end{aligned}$$

Using the similarity transforms, Eq. (5.1) is satisfied identically and Eqs. (5.2)-(5.4) take the form:

$$\left(\frac{A_3+K}{A_1}\right)f'''+ff''-f'^2-\frac{A_5}{A_1}M\ f'+\frac{K}{A_1}g'=0, \tag{5.7}$$

$$\theta''-\frac{A_2\ A_3}{A_1\ A_4}Pr\left[2f'\theta-f\theta'+\lambda_E\left(4\ f'^2\ \theta-3\ f\ f'\ \theta'+f^2\ \theta''-2\ f\ f''\ \theta\right)\right]=0, \tag{5.8}$$

$$\left(\frac{A_3}{A_1}+\frac{K}{2A_1}\right)g''-\frac{K}{A_1}\left(2g+f''\right)-gf'+fg'=0, \tag{5.9}$$

where

$$Pr=\frac{\nu_f}{\alpha_f}, \lambda_E=\frac{\lambda_0\nu_f}{L^2}, M=\frac{B_0^2(\sigma_{el})_fL^2}{\rho_f\nu_f}, K=\frac{\kappa}{\mu_f}, A_1=\frac{\rho_{nf}}{\rho_f}, A_2=\frac{(\rho C_p)_{nf}}{(\rho C_p)_f},$$
$$A_3=\frac{\mu_{nf}}{\mu_f}, A_4=\frac{\kappa_{nf}}{\kappa_f}, A_5=\frac{(\sigma_{el})_{nf}}{(\sigma_{el})_f}, L=-\frac{\mu_f\nu_f}{\sigma_0\gamma_TT_0}.$$

The material parameter K correctly predicts the flow behavior in the limiting case when there is zero spin. In that case, spin N turns to angular flow velocity or fluid vorticity. The dimensionless

form of the boundary conditions become:

$$f(0) = 0,\ (A_3 + K)f''(0) = -2,\ g\,(0) = -nf''(0),\ \theta\,(0) = 1, \tag{5.10}$$

$$f'(\eta) \to 0,\ g(\eta) \to 0,\ \theta(\eta) \to 0,\ \text{as} \quad \eta \to \infty. \tag{5.11}$$

The heat flux at the interface is q_w, which is defined as:

$$q_w = -\kappa_{nf}\left(\frac{\partial T}{\partial y}\right)_{y=0}. \tag{5.12}$$

The strength of the heat transfer is given by the Nusselt number Nu_x, which is expressed as

$$Nu_x = x\frac{q_w}{\kappa_f(T - T_\infty)}.$$

Using the non-dimensional transformations, we obtain:

$$\frac{Nu_x\kappa_f}{X\kappa_{nf}} = -\theta'(0).$$

5.3 Keller Box Formulation

- BVP (5.7) - (5.11) is transformed to seven first order ODEs.

$$f = Y_1, \tag{5.13}$$

$$Y_1^{'} = Y_2, \tag{5.14}$$

$$Y_2^{'} = Y_3, \tag{5.15}$$

$$\theta = Y_4, \tag{5.16}$$

$$Y_4^{'} = Y_5, \tag{5.17}$$

$$g = Y_6, \tag{5.18}$$

$$Y_6^{'} = Y_7, \tag{5.19}$$

$$\left(\frac{A_3 + K}{A_1}\right)Y_3^{'} + Y_1Y_3 - Y_2^2 - \frac{A_5}{A_1}M\ Y_2 + \frac{K}{A_1}Y_7 = 0, \tag{5.20}$$

$$\begin{cases} Y_5^{'} - \frac{A_2}{A_1}\frac{A_3}{A_4}Pr\ \Big[2Y_2Y_4 - Y_1Y_5 + \lambda_E\Big(4\ Y_2^2\ Y_4 - 3\ Y_1\ Y_2\ Y_5 \\ +Y_1^2\ Y_5' - 2\ Y_1\ Y_3\ Y_4\Big)\Big] = 0, \end{cases} \tag{5.21}$$

$$\left(\frac{A_3}{A_1} + \frac{K}{2A_1}\right)Y_7^{'} - \frac{K}{A_1}\left(2Y_6 + Y_3\right) - Y_6Y_2 + Y_1Y_7 = 0. \tag{5.22}$$

- The set of discretized equations are given as:

$$\frac{(Y_1)_\zeta - (Y_1)_{\zeta-1}}{h} = (Y_2)_{\zeta-\frac{1}{2}}, \tag{5.23}$$

$$\frac{(Y_2)_\zeta - (Y_2)_{\zeta-1}}{h} = (Y_3)_{\zeta-\frac{1}{2}}, \tag{5.24}$$

$$\frac{(Y_4)_\zeta - (Y_4)_{\zeta-1}}{h} = (Y_5)_{\zeta-\frac{1}{2}}, \tag{5.25}$$

$$\frac{(Y_6)_\zeta - (Y_6)_{\zeta-1}}{h} = (Y_7)_{\zeta-\frac{1}{2}}, \tag{5.26}$$

$$\begin{cases} \left(\frac{A_3+K}{A_1}\right)\frac{(Y_3)_\zeta-(Y_3)_{\zeta-1}}{h} + (Y_1)_{\zeta-\frac{1}{2}}(Y_3)_{\zeta-\frac{1}{2}} - (Y_2)^2_{\zeta-\frac{1}{2}} \\ -\frac{A_5}{A_1}M\ (Y_2)_{\zeta-\frac{1}{2}} + \frac{K}{A_1}(Y_7)_{\zeta-\frac{1}{2}} = 0, \end{cases} \tag{5.27}$$

$$\begin{cases} \frac{(Y_5)_\zeta-(Y_5)_{\zeta-1}}{h} - \frac{A_2}{A_1}\frac{A_3}{A_4}Pr\ \Big[2(Y_2)_{\zeta-\frac{1}{2}}(Y_4)_{\zeta-\frac{1}{2}} - (Y_1)_{\zeta-\frac{1}{2}}(Y_5)_{\zeta-\frac{1}{2}} \\ +\lambda_E\Big(4\ (Y_2)^2_{\zeta-\frac{1}{2}}\ (Y_4)_{\zeta-\frac{1}{2}} - 3\ (Y_1)_{\zeta-\frac{1}{2}}\ (Y_2)_{\zeta-\frac{1}{2}}\ (Y_5)_{\zeta-\frac{1}{2}} \\ +(Y_1)^2_{\zeta-\frac{1}{2}}\ \frac{(Y_5)_\zeta-(Y_5)_{\zeta-1}}{h} - 2\ (Y_1)_{\zeta-\frac{1}{2}}\ (Y_3)_{\zeta-\frac{1}{2}}\ (Y_4)_{\zeta-\frac{1}{2}}\Big)\Big] = 0, \end{cases} \tag{5.28}$$

$$\begin{cases} \left(\frac{A_3}{A_1}+\frac{K}{2A_1}\right)\frac{(Y_7)_\zeta-(Y_7)_{\zeta-1}}{h} - \frac{K}{A_1}\Big(2(Y_6)_{\zeta-\frac{1}{2}} + (Y_3)_{\zeta-\frac{1}{2}}\Big) \\ -(Y_6)_{\zeta-\frac{1}{2}}(Y_2)_{\zeta-\frac{1}{2}} + (Y_1)_{\zeta-\frac{1}{2}}(Y_7)_{\zeta-\frac{1}{2}} = 0. \end{cases} \tag{5.29}$$

- Following section 2.14, the nonlinear difference equations are linearized as:

$$\frac{\varepsilon(Y_1)_\zeta - \varepsilon(Y_1)_{\zeta-1}}{h} - \frac{\varepsilon(Y_2)_\zeta + \varepsilon(Y_2)_{\zeta-1}}{2} = (r_1)_{\zeta-\frac{1}{2}}, \tag{5.30}$$

$$\frac{\varepsilon(Y_2)_\zeta - \varepsilon(Y_2)_{\zeta-1}}{h} - \frac{\varepsilon(Y_3)_\zeta + \varepsilon(Y_3)_{\zeta-1}}{2} = (r_2)_{\zeta-\frac{1}{2}}, \tag{5.31}$$

$$\frac{\varepsilon(Y_4)_\zeta - \varepsilon(Y_4)_{\zeta-1}}{h} - \frac{\varepsilon(Y_5)_\zeta + \varepsilon(Y_5)_{\zeta-1}}{2} = (r_3)_{\zeta-\frac{1}{2}}, \tag{5.32}$$

$$\frac{\varepsilon(Y_6)_\zeta - \varepsilon(Y_6)_{\zeta-1}}{h} - \frac{\varepsilon(Y_7)_\zeta + \varepsilon(Y_7)_{\zeta-1}}{2} = (r_4)_{\zeta-\frac{1}{2}}, \tag{5.33}$$

$$\begin{cases} (\xi_1)_\zeta\varepsilon(Y_1)_\zeta + (\xi_2)_\zeta\varepsilon(Y_1)_{\zeta-1} + (\xi_3)_\zeta\varepsilon(Y_2)_\zeta + (\xi_4)_\zeta\varepsilon(Y_2)_{\zeta-1} \\ +(\xi_5)_\zeta\varepsilon(Y_3)_\zeta + (\xi_6)_\zeta\varepsilon(Y_3)_{\zeta-1} + (\xi_7)_\zeta\varepsilon(Y_4)_\zeta + (\xi_8)_\zeta\varepsilon(Y_4)_{\zeta-1} \\ +(\xi_9)_\zeta\varepsilon(Y_5)_\zeta + (\xi_{10})_\zeta\varepsilon(Y_5)_{\zeta-1} + (\xi_{11})_\zeta\varepsilon(Y_6)_\zeta + (\xi_{12})_\zeta\varepsilon(Y_6)_{\zeta-1} \\ +(\xi_{13})_\zeta\varepsilon(Y_7)_\zeta + (\xi_{14})_\zeta\varepsilon(Y_7)_{\zeta-1} = (r_5)_{\zeta-\frac{1}{2}}, \end{cases} \tag{5.34}$$

$$\begin{cases} (\chi_1)_\zeta\varepsilon(Y_1)_\zeta + (\chi_2)_\zeta\varepsilon(Y_1)_{\zeta-1} + (\chi_3)_\zeta\varepsilon(Y_2)_\zeta + (\chi_4)_\zeta\varepsilon(Y_2)_{\zeta-1} \\ +(\chi_5)_\zeta\varepsilon(Y_3)_\zeta + (\chi_6)_\zeta\varepsilon(Y_3)_{\zeta-1} + (\chi_7)_\zeta\varepsilon(Y_4)_\zeta + (\chi_8)_\zeta\varepsilon(Y_4)_{\zeta-1} \\ +(\chi_9)_\zeta\varepsilon(Y_5)_\zeta + (\chi_{10})_\zeta\varepsilon(Y_5)_{\zeta-1} + (\chi_{11})_\zeta\varepsilon(Y_6)_\zeta \\ +(\chi_{12})_\zeta\varepsilon(Y_6)_{\zeta-1} + (\chi_{13})_\zeta\varepsilon(Y_7)_\zeta + (\chi_{14})_\zeta\varepsilon(Y_7)_{\zeta-1} = (r_6)_{\zeta-\frac{1}{2}}, \end{cases} \tag{5.35}$$

$$\begin{cases} (\gamma_1)_\zeta \varepsilon(Y_1)_\zeta + (\gamma_2)_\zeta \varepsilon(Y_1)_{\zeta-1} + (\gamma_3)_\zeta \varepsilon(Y_2)_\zeta + (\gamma_4)_\zeta \varepsilon(Y_2)_{\zeta-1} \\ +(\gamma_5)_\zeta \varepsilon(Y_3)_\zeta + (\gamma_6)_\zeta \varepsilon(Y_3)_{\zeta-1} + (\gamma_7)_\zeta \varepsilon(Y_4)_\zeta + (\gamma_8)_\zeta \varepsilon(Y_4)_{\zeta-1} \\ +(\gamma_9)_\zeta \varepsilon(Y_5)_\zeta + (\gamma_{10})_\zeta \varepsilon(Y_5)_{\zeta-1} + (\gamma_{11})_\zeta \varepsilon(Y_6)_\zeta \\ +(\gamma_{12})_\zeta \varepsilon(Y_6)_{\zeta-1} + (\gamma_{13})_\zeta \varepsilon(Y_7)_\zeta + (\gamma_{14})_\zeta \varepsilon(Y_7)_{\zeta-1} = (r_7)_{\zeta-\frac{1}{2}}. \end{cases} \tag{5.36}$$

- The resulting linear system is written in the matrix form as defined in (2.54)-(2.55). Where,

$$\mathrm{x}_1 = \begin{bmatrix} \varepsilon(Y_2)_0 \\ \varepsilon(Y_5)_0 \\ \varepsilon(Y_7)_0 \\ \varepsilon(Y_1)_1 \\ \varepsilon(Y_3)_1 \\ \varepsilon(Y_5)_1 \\ \varepsilon(Y_7)_1 \end{bmatrix}, \quad \mathrm{x}_\zeta = \begin{bmatrix} \varepsilon(Y_2)_{\zeta-1} \\ \varepsilon(Y_4)_{\zeta-1} \\ \varepsilon(Y_6)_{\zeta-1} \\ \varepsilon(Y_1)_\zeta \\ \varepsilon(Y_3)_\zeta \\ \varepsilon(Y_5)_\zeta \\ \varepsilon(Y_7)_\zeta \end{bmatrix}, \qquad \zeta = 2, 3, ..., J, \tag{5.37}$$

$$A_1 = \begin{bmatrix} \frac{-h}{2} & 0 & 0 & 1 & 0 & 0 & 0 \\ -1 & 0 & 0 & 0 & \frac{-h}{2} & 0 & 0 \\ 0 & \frac{-h}{2} & 0 & 0 & 0 & \frac{-h}{2} & 0 \\ 0 & 0 & \frac{-h}{2} & 0 & 0 & 0 & \frac{-h}{2} \\ (\xi_4)_1 & (\xi_{10})_1 & (\xi_{14})_1 & (\xi_1)_1 & (\xi_5)_1 & (\xi_9)_1 & (\xi_{13})_1 \\ (\chi_4)_1 & (\chi_{10})_1 & (\chi_{14})_1 & (\chi_1)_1 & (\chi_5)_1 & (\chi_9)_1 & (\chi_{13})_1 \\ (\gamma_4)_1 & (\gamma_{10})_1 & (\gamma_{14})_1 & (\gamma_1)_1 & (\gamma_5)_1 & (\gamma_9)_1 & (\gamma_{13})_1 \end{bmatrix},$$

$$A_\zeta = \begin{bmatrix} \frac{-h}{2} & 0 & 0 & -1 & 0 & 0 & 0 \\ -1 & 0 & 0 & 0 & \frac{-h}{2} & 0 & 0 \\ 0 & -1 & 0 & 0 & 0 & \frac{-h}{2} & 0 \\ 0 & 0 & -1 & 0 & 0 & 0 & \frac{-h}{2} \\ (\xi_4)_\zeta & (\xi_8)_\zeta & (\xi_{12})_\zeta & (\xi_1)_\zeta & (\xi_5)_\zeta & (\xi_9)_1 & (\xi_{13})_\zeta \\ (\chi_4)_\zeta & (\chi_8)_\zeta & (\chi_{12})_\zeta & (\chi_1)_\zeta & (\chi_5)_\zeta & (\chi_9)_\zeta & (\chi_{13})_\zeta \\ (\gamma_4)_\zeta & (\gamma_8)_\zeta & (\gamma_{12})_\zeta & (\gamma_\zeta)_\zeta & (\gamma_5)_\zeta & (\gamma_9)_\zeta & (\gamma_{13})_\zeta \end{bmatrix}, \qquad \zeta = 2, 3, ..., J,$$

$$B_\zeta = \begin{bmatrix} 0 & 0 & 0 & -1 & 0 & 0 & 0 \\ 0 & 0 & 0 & 0 & \frac{-h}{2} & 0 & 0 \\ 0 & 0 & 0 & 0 & 0 & \frac{-h}{2} & 0 \\ 0 & 0 & 0 & 0 & 0 & 0 & \frac{-h}{2} \\ 0 & 0 & 0 & (\xi_2)_\zeta & (\xi_6)_\zeta & (\xi_{10})_\zeta & (\xi_{14})_\zeta \\ 0 & 0 & 0 & (\chi_2)_\zeta & (\chi_6)_\zeta & (\chi_{10})_\zeta & (\chi_{14})_\zeta \\ 0 & 0 & 0 & (\gamma_2)_\zeta & (\gamma_6)_\zeta & (\gamma_{10})_\zeta & (\gamma_{14})_\zeta \end{bmatrix}, \qquad \zeta = 2, 3, ..., J,$$

$$C_\zeta = \begin{bmatrix} \frac{-h}{2} & 0 & 0 & 0 & 0 & 0 & 0 \\ 1 & 0 & 0 & 0 & 0 & 0 & 0 \\ 0 & 1 & 0 & 0 & 0 & 0 & 0 \\ 0 & 0 & 1 & 0 & 0 & 0 & 0 \\ (\xi_3)_\zeta & (\xi_7)_\zeta & (\xi_{11})_\zeta & 0 & 0 & 0 & 0 \\ (\chi_3)_\zeta & (\chi_7)_\zeta & (\chi_{11})_\zeta & 0 & 0 & 0 & 0 \\ (\gamma_3)_\zeta & (\gamma_7)_\zeta & (\gamma_{11})_\zeta & 0 & 0 & 0 & 0 \end{bmatrix}, \qquad \zeta = 1, 2, ..., J.$$

- The vector of unknowns $\mathbf{x}$ is obtained by solving the system $\mathbf{Wx} = \mathbf{r}$ by using LU-decomposition method.
- Updation is made to the solution vector and the process is continued until a required accuracy of 10^{-5} is achieved. For the present problem mesh spacing is taken as 0.01.
- Matlab code validation of the KBM used for the solution of the BVP (5.7)-(5.11) is achieved by a comparison of the present results to the already available results in Table 5.2. The results verifies the technique's effectiveness in solving BVPs of present nature. To have an estimate of the computational time required to produce results for the present problem, CPU time is calculated in Table 5.3.

		Ariffin et al. [71]			Present results		
n	S	$f^{'}(0)$	$g^{'}(0)$	$-\theta^{'}(0)$	$f^{'}(0)$	$g^{'}(0)$	$-\theta^{'}(0)$
0	-2	2.69002	0.46534	1.39916	2.69002	0.46535	1.39916
	-1	2.36794	0.52726	1.54924	2.36794	0.52727	1.54924
	0	2.02929	0.57939	1.74535	2.02929	0.57940	1.74535
	1	1.68896	0.52726	2.01542	1.68896	0.60499	2.01541
	2	1.37409	0.59299	2.39309	1.37409	0.59299	2.39309
0.5	-2	2.52510	-0.79204	1.32235	2.52510	-0.79204	1.32235
	-1	2.17998	-0.91743	1.44696	2.17997	-0.91743	1.44695
	0	1.81712	-1.10064	1.61252	1.81712	-1.10064	1.61252
	1	1.45616	-1.37347	1.85711	1.45616	-1.37347	1.85711
	2	1.13472	-1.76253	2.23294	1.13472	-1.76253	2.23294

Table 5.2: Values of $f^{'}(0)$, $g^{'}(0)$ and $-\theta^{'}(0)$ for varying S when $K = 1$ and $Pr = 0.78$.

K	$f^{'}(0)$	CPU time (sec)
0.5	1.5476	3.104
1	1.5726	3.520
1.5	1.5995	14.436

Table 5.3: Values of $f^{'}(0)$ for varying K when $\lambda_E = 0.5$, $M = 5$, $n = 0$ and $Pr = 6.2$.

5.4 Numerical Results and Discussion

A discussion based on the results obtained for the fluid properties in the form of graphs has been presented in the present section. Homogeneous single phase model with nanoparticles of Al_2O_3 are used along side water as the base fluid. The effectiveness of the nanoparticles shapes has also been pondered upon the graphs.

An increase in the material parameter values decreases the linear velocity of the fluid in the boundary layer in the case of weak concentration of the microstructures but the opposite behavior is observed in the absence of microstructures. This suggests that a greater rotation viscosity tends to resist the flow of the fluid which results in a decrease in the linear velocity as evident from Figure 5.2. A similar Impact on the material parameter can be found on the spin velocity as observed in Figure 5.3. The figure reveals that the inclination in the K results in the reduction of the angular velocity thus stabilizing the flow. It is observed in Figure 5.4 that the temperature in the boundary layer increases as the value of K is increased and the effect is more pronounced in the case of $n = 0.5$. Figures 5.5-5.6 reveal that the heat transfer rate decreases with an augmentation in the material parameter. The heat transfer drops at a greater rate when there is a weak concentration of the microstructures.

Figure 5.7 shows that the rising values of magnetic number imply an increase in the Lorentz forces which in return declines the linear velocity of the fluid. The spin velocity declines with an increase in the magnetic number which shows that the stronger magnetic field also impacts negatively on the spin velocity of the fluid (see Figure 5.8). In Figure 5.9, the temperature of the fluid rises for the growing values of magnetic number which suggests that more heat is dissipated in the case of a stronger magnetic field. A greater heat dissipation causes a decline in the heat transfer rate which is evident from Figures 5.10 and 5.11 as greater values of magnetic number decrease the heat transfer rate in the nanofluid. The loss of heat transfer is found greater in the case of weak concentration.

The Impact on the different shapes of the nanoparticles on the temperature profile has been pondered upon in Figure 5.12. The results show that the temperature in the boundary layer is maximum in the case of laminar particles but least in the case of the spherical particles. This is an indication that spherical particles tend to take more heat away from the boundary layer as compared to the other particles used in the present study. For the lamina nanoparticles, the heat transfer rate either in the case of the absence of microstructures or in the presence of microstructures is maximum (see Figure 5.13-5.14).

The effect of the nanoparticles concentration on the velocity and temperature profiles is discussed

in Figures 5.15–5.16. The linear velocity seems to be growing with a higher concentration of the nanoparticles (see Figure5.15). The physical reason for this is the random motion of the nanoparticles as well as their motion in the presence of temperature gradient prevalent in the regime which give rise to drift velocity, a greater number of nanoparticles will enhance the velocity of the fluid in the boundary layer. Similarly, the temperature of the fluid also increases with an increase in the nanoparticles concentration as it can be observed in Figure 5.16.

The thermal relaxation time is a measure of the resistance of the system in the change of its thermal state. This implies that a greater value of the thermal relaxation time parameter will lead to more delay in the system to change its thermal state thus lowering the temperature of the fluid in the boundary layer. Figure 5.17 shows that the growing values of the relaxation time parameter lead to a smaller temperature in the boundary layer. Physically due greater thermal inertia, the system opposes more to a temperature change with greater thermal relaxation time. Figures 5.18-5.19 gives an account of the effect of the thermal time relaxation on the heat transfer rate. It is observed that the greater values of λ_E lead to an enhancement in the Nusselt number.

Streamlines provides information about the flow pattern. The streamlines in the cases of zero spin concentration of the microstructures have been plotted in Figure 5.20.

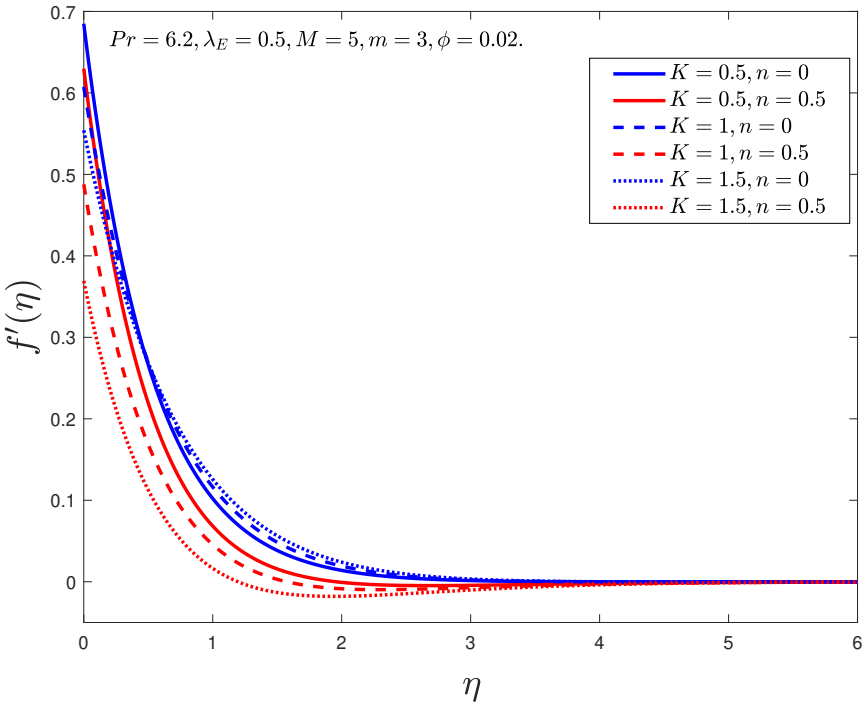

.

Figure 5.2: Impact on linear velocity for varying material parameter K.

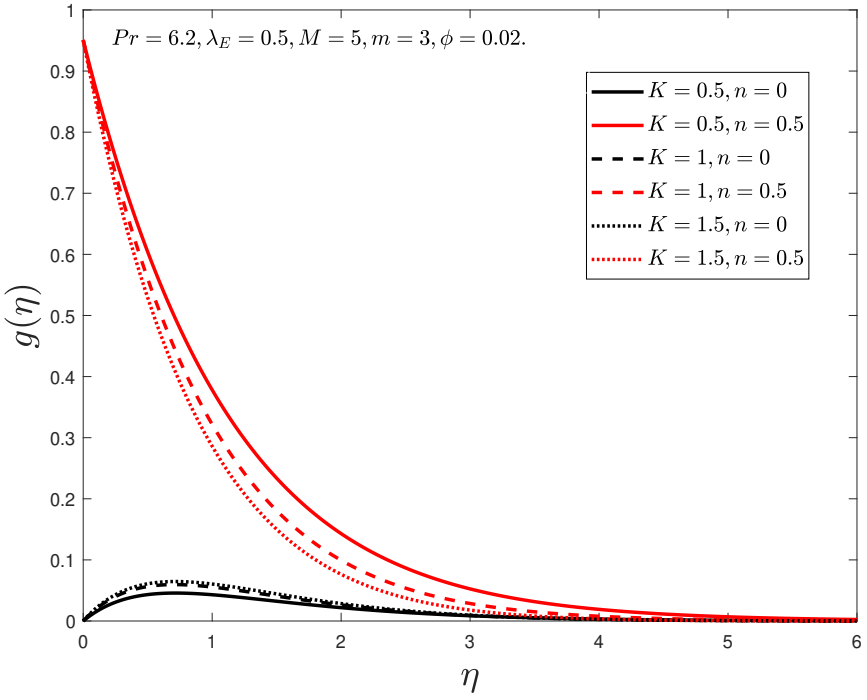

Figure 5.3: Impact on angular velocity for varying material parameter K.

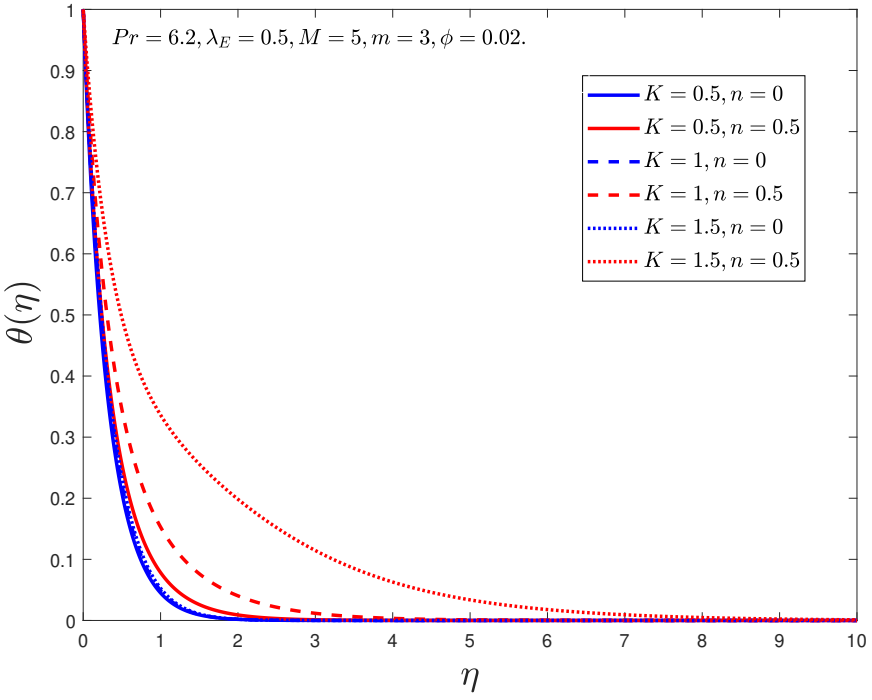

Figure 5.4: Impact on temperature for varying material parameter K.

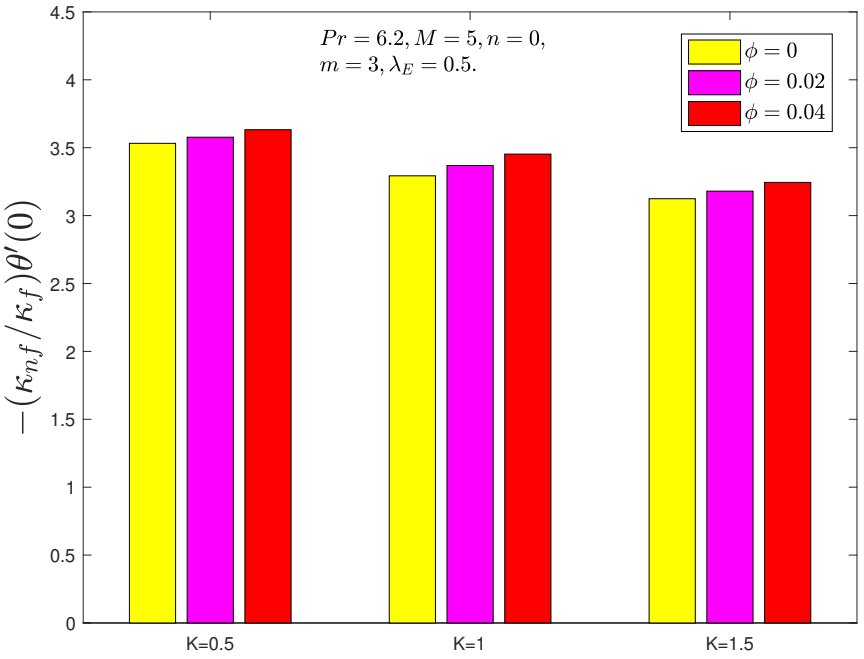

Figure 5.5: Impact on Nusselt number in the presence of microstructures.

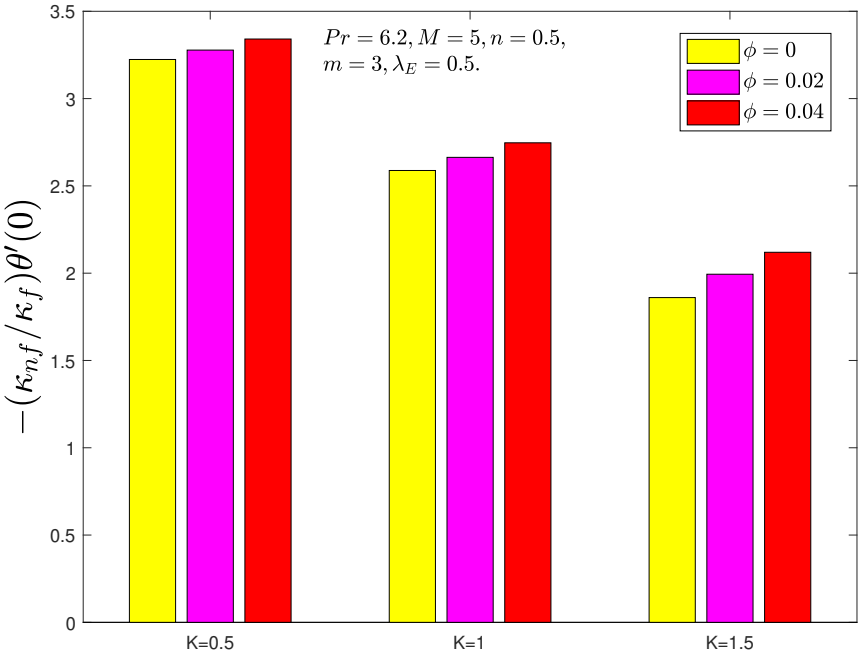

Figure 5.6: Impact on Nusselt number in the absence of microstructures for varying material parameter K.

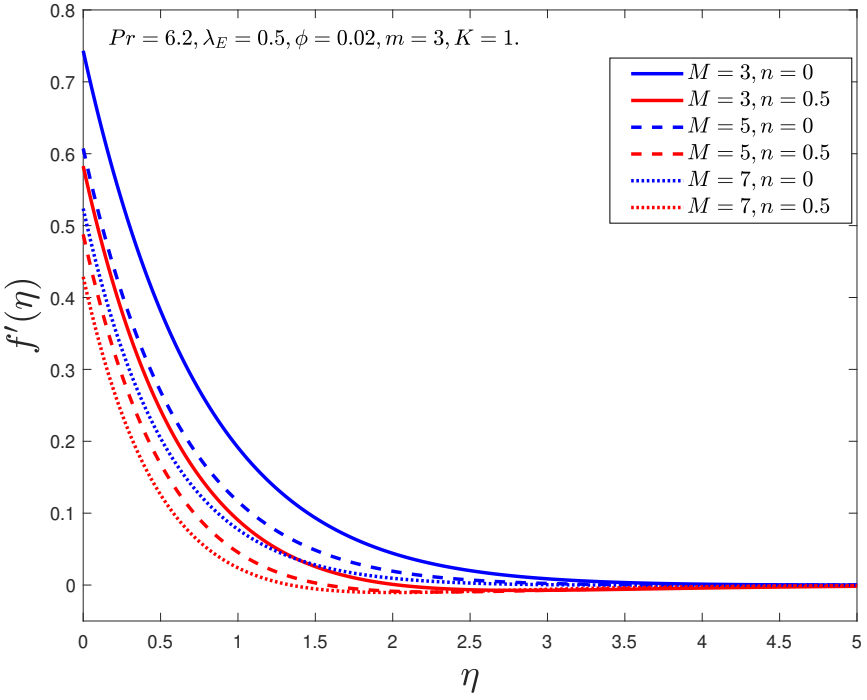

Figure 5.7: Impact on linear velocity for varying magnetic number M.

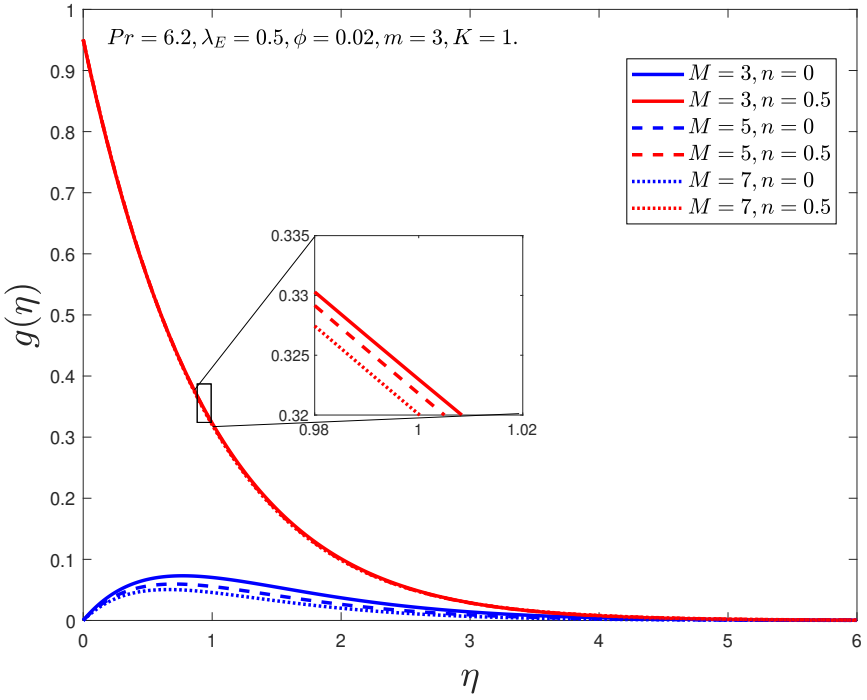

Figure 5.8: impact on temperature for varying magnetic number M.

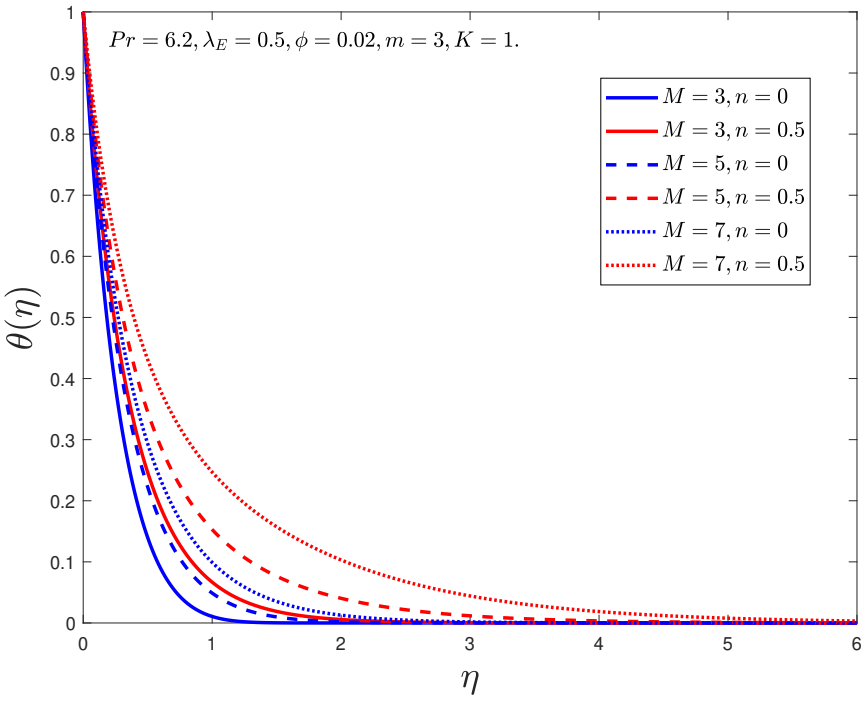

Figure 5.9: impact on temperature for varying magnetic number M.

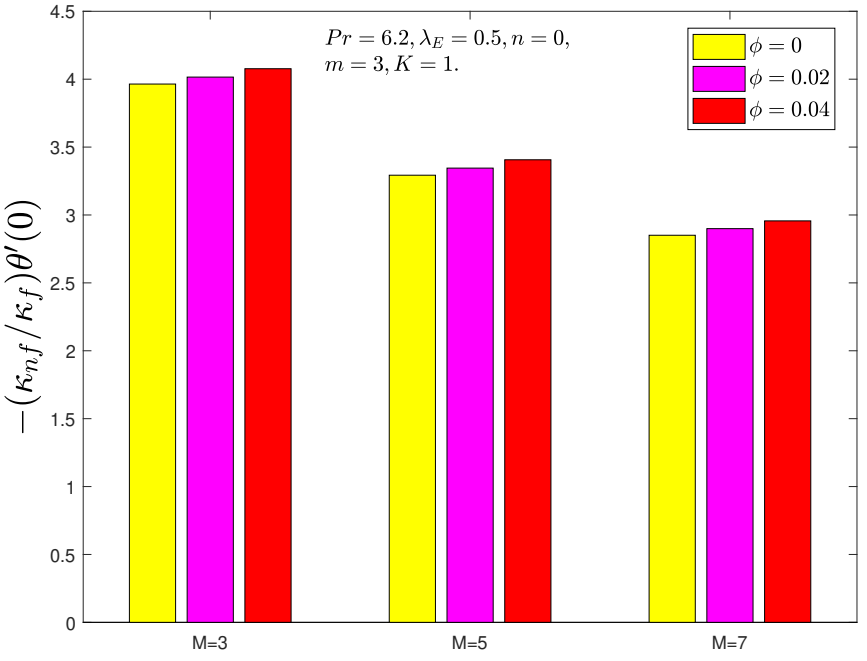

Figure 5.10: Impact on Nusselt number in the presence of microstructures for varying magnetic number M.

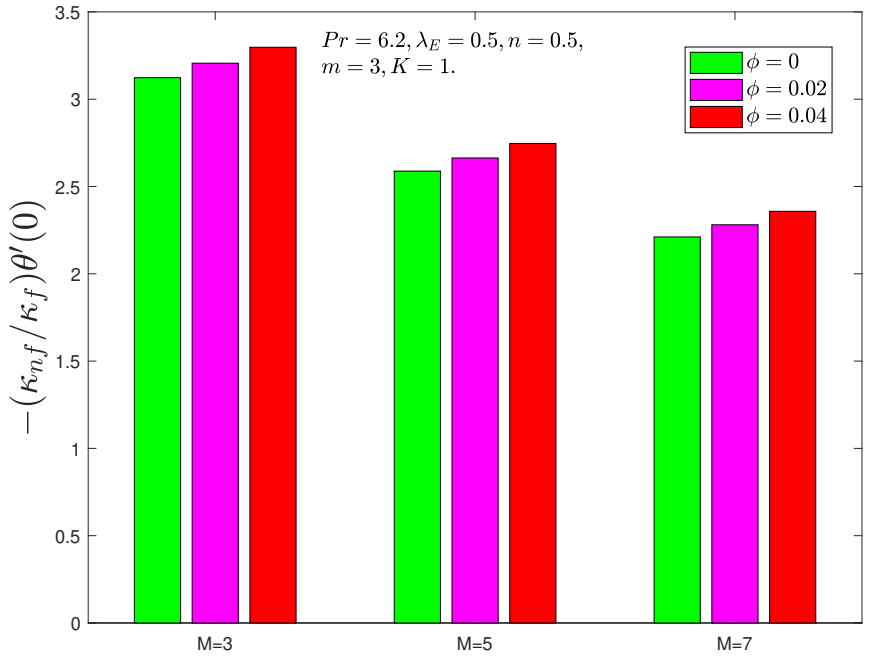

Figure 5.11: Impact on Nusselt Number in the absence of microstructures for varying magnetic number M.

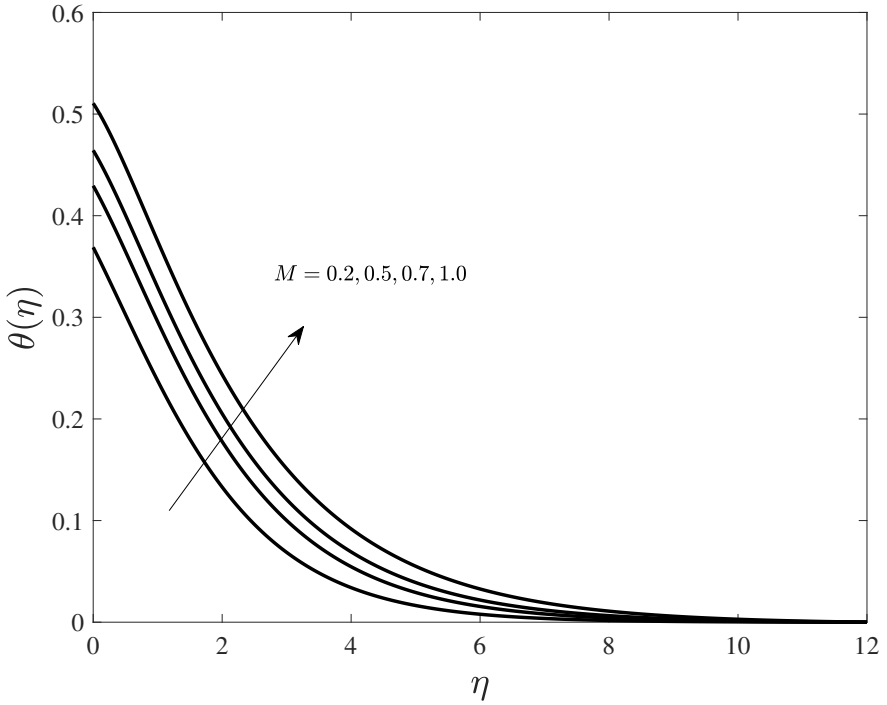

Figure 5.12: Impact on temperature for varying shape factor m.

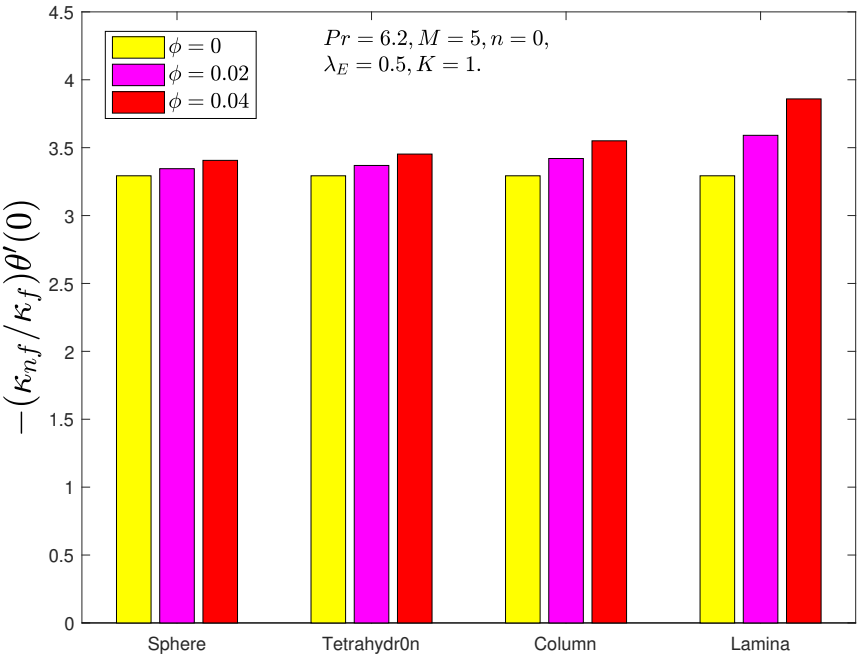

Figure 5.13: Impact on Nusselt number in the absence of microstructures for varying shape factor m.

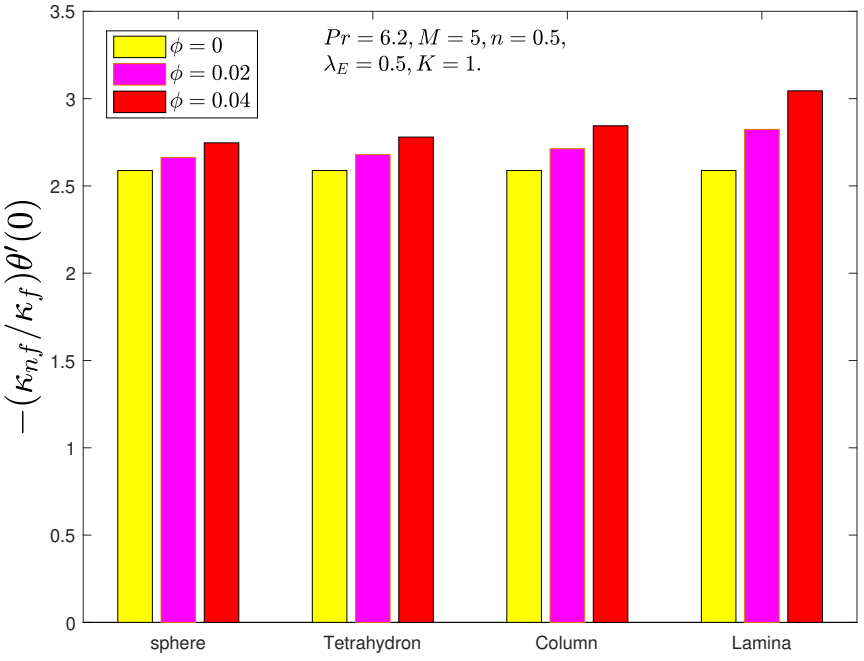

Figure 5.14: Impact on Nusselt number in the presence of microstructures for varying shape factor m.

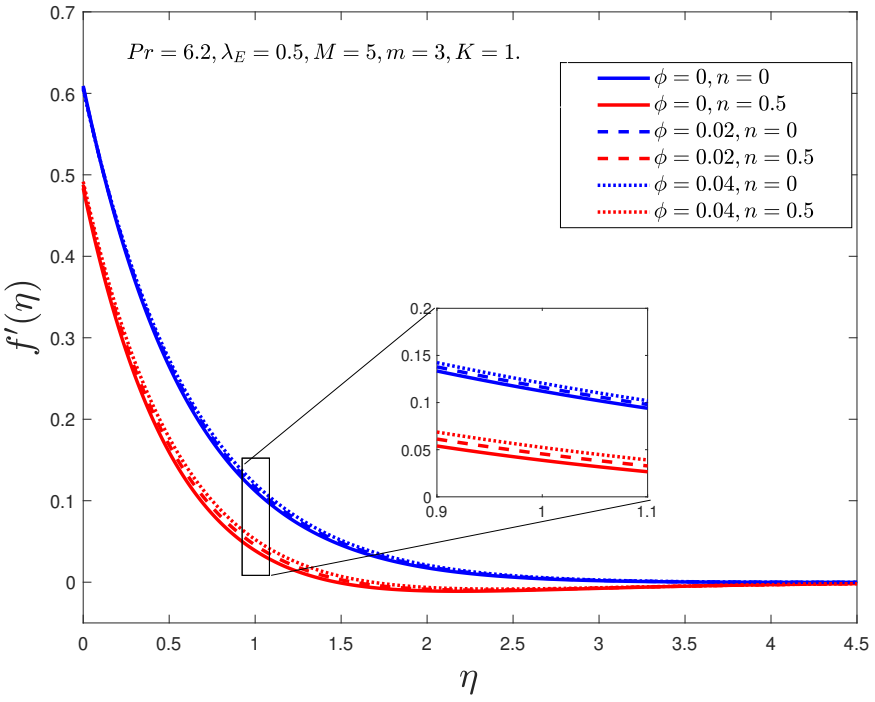

Figure 5.15: Impact on linear velocity for varying nanoparticle volume fraction ϕ.

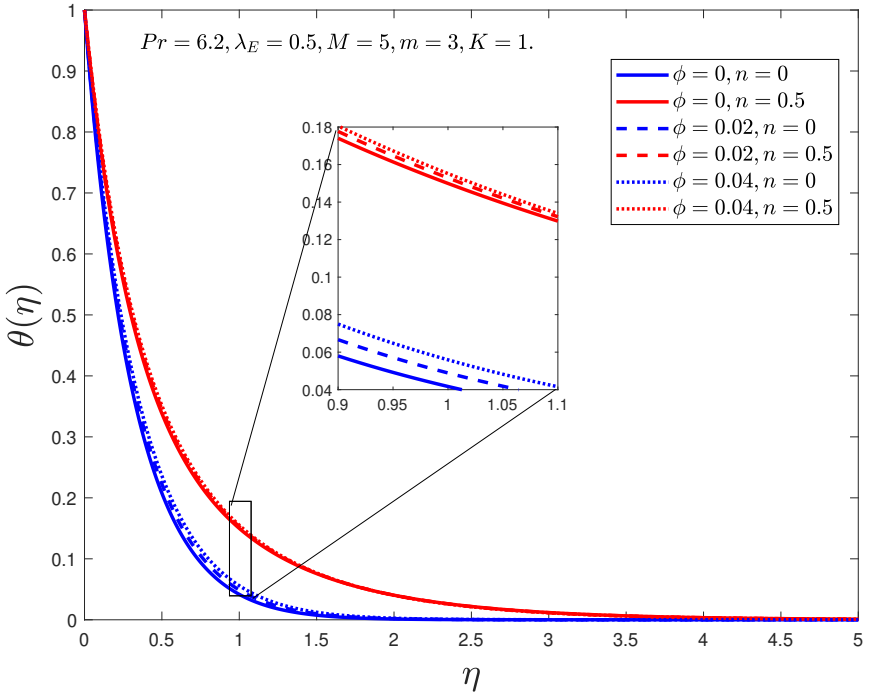

Figure 5.16: impact on temperature for varying nanoparticle volume fraction ϕ.

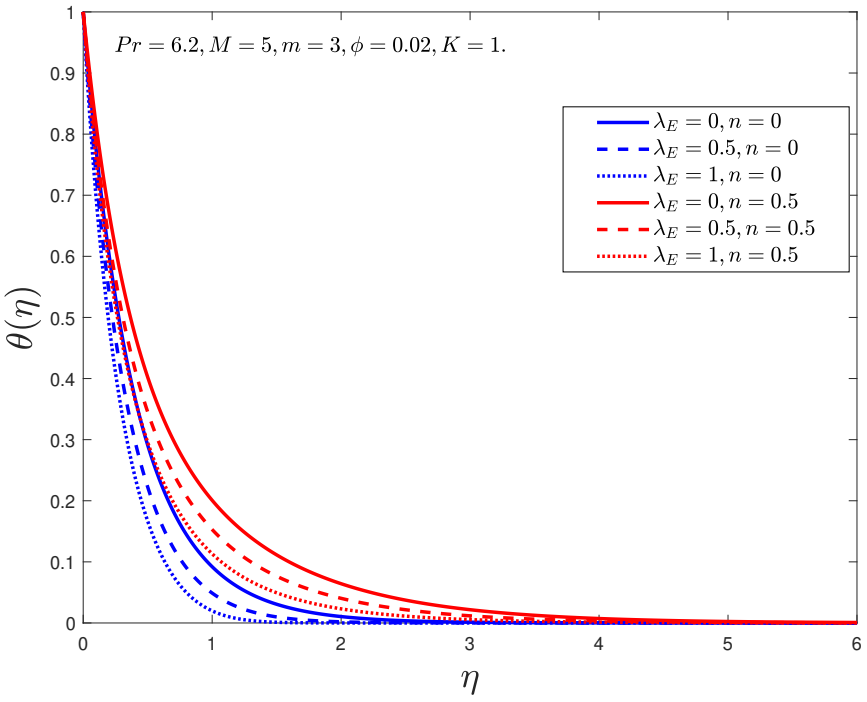

Figure 5.17: impact on temperature for varying λ_E.

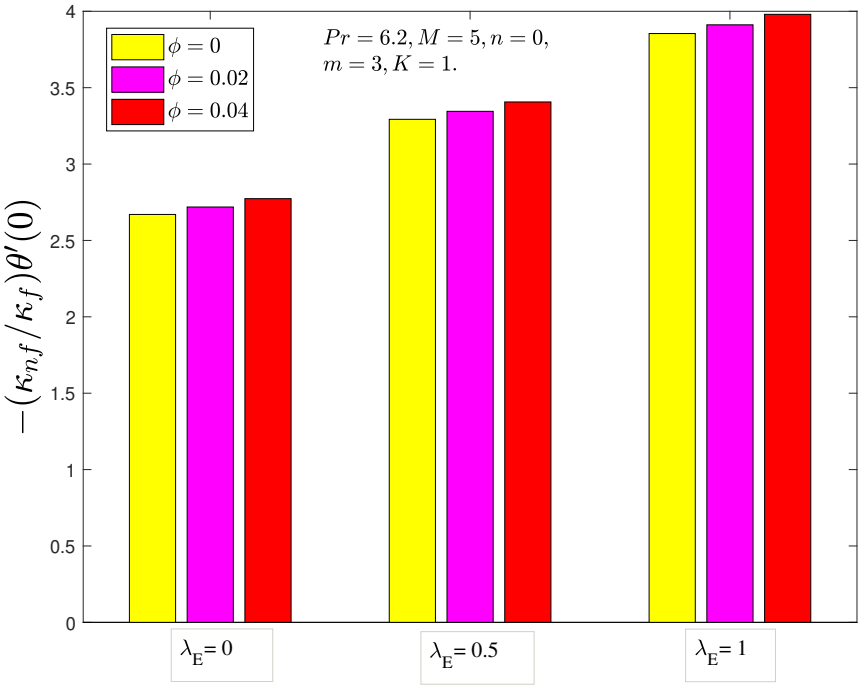

Figure 5.18: impact on Nusselt number in the absence of microstructures for varying λ_E.

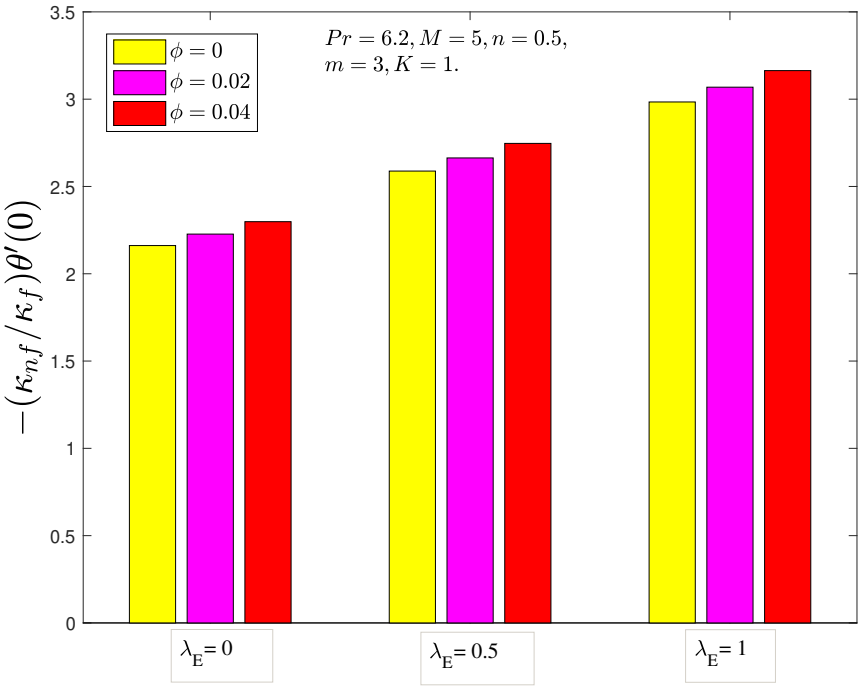

Figure 5.19: impact on Nusselt number in the presence of microstructures for varying λ_E.

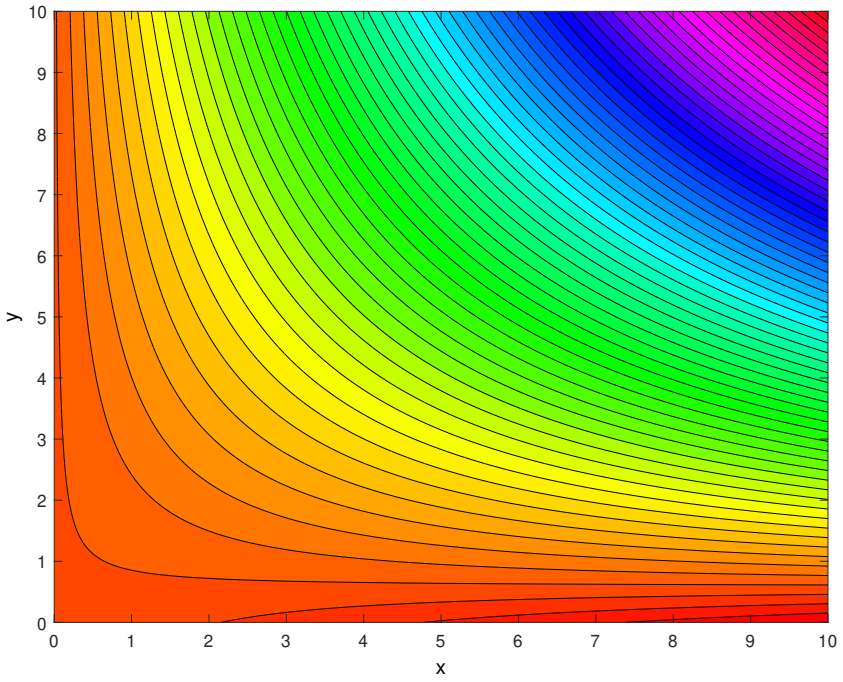

Figure 5.20: Streamlines in the absence of microstructures with $K = 1$, $m = 3$, $\lambda_E = 0.5$ and $M = 5$.

5.5 Chapter Summary

The findings of heat transfer analysis of the problem stated in 5.2 have been summarized as under:

- The increasing values of the material parameter K decrease the linear as well as the spin velocity of the micropolar nanofluid and reduces the heat transfer rate in the micropolar nanofluid.
- Higher magnetic parameter M is proved to be an obstruction to both the linear as well as the angular velocity of the nanofluid thus rising the temperature of the fluid and more heat is found to dissipate, so the heat transfer rate is decreased.
- The temperature in the boundary layer is least for the spherical particles and most for the lamina particles.
- A higher concentration of the nanoparticles augments the linear velocity of the fluid and tends to rise the temperature in the boundary layer and an enhancement in the heat transfer rate.
- Lamina shaped nanoparticle are proved to be the best of all the nanoparticles used in the study for the heat transport in the nanofluid.
- An increase in the thermal time relaxation parameter λ_E decreases the temperature of the nanofluid but increases the heat transfer rate in the nanofluid.

Chapter 6

Jeffery-Hamel Flow and Heat Transport in Non-Newtonian Nanofluid Between Nonparallel Plates

6.1 Introduction

The present chapter focuses on the heat and mass transfer in Jeffery-Hamel flow of a micropolar nanofluid between two converging/diverging plates. Buongiorno nanofluid model is utilized to investigate the heat and mass transfer. The fluid flow has been analyzed by the linear and angular momentum equations of fluid dynamics. Fourier and Fick's laws have been used in the energy and mass conservation equations to discover the heat and mass transfer in the fluid. Magnetic field effects are incorporated in the analysis by applying the magnetic field normal to the flow of the fluid. The Joule heating is assumed to be considerable so its effect is added to the energy equation. The numerical results of the nondimesionalized ODEs are obtained by KBM. A striking feature of the study is the evaluation of the critical Reynolds number Re_c for the diverging channel. The critical Reynolds number is detrimental in identifying the separation flow. The application of the magnetic field and the presence of microstructures impact on the stability on the stability of the flow in the diverging channel.

6.2 Problem Statement and Mathematical Formulation

Consider a two dimensional Jeffery Hamel flow of an electrically conductive, steady, incompressible fluid between two non-parallel walls. The walls make an angle α with the radial axis. The channel is said to be diverging if $\alpha > 0$ and converging if $\alpha < 0$. The flow is assumed to be uni-directional with two dimensions r and Θ. Magnetic field is applied across the walls and it is assumed that the value of magnetic Prandtl number is small so the induced magnetic field effects are ignored. It is assumed that the fluid contains microstructures that influence on the fluid properties. Brownian motion and thermal diffusion effects are significant so Boungiorno nanofluid model has been used in the study. The Joule heating effect is incorporated in the model to observe its impact on the heat transfer rate. Here, $\mathbf{V} = (u(r,\Theta),0,0)$, $\mathbf{B} = (0,r_0,0)$, $\mathbf{N} = (0,0,N(r,\Theta))$, $T = (T(r,\Theta),0,0)$ and $C = (C(r,\Theta),0,0)$. Making use of the assumptions

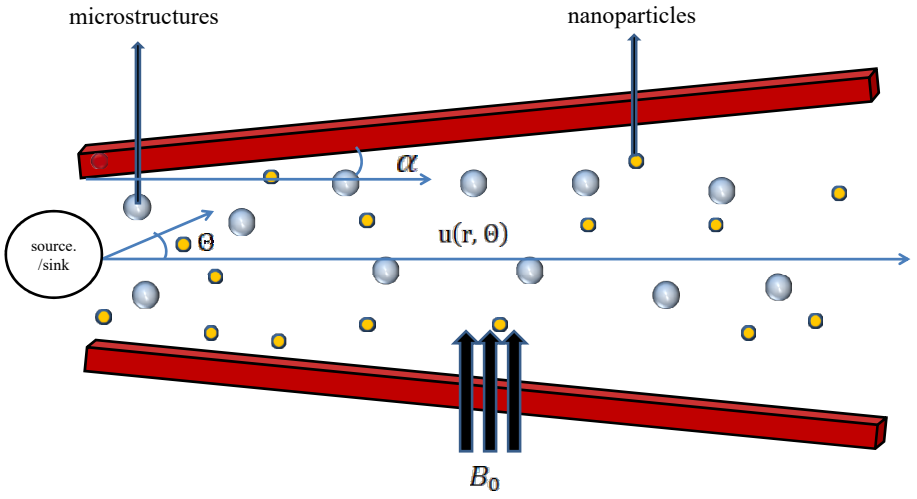

Figure 6.1: Schematic diagram of the flow model

for the present problem, the reduced form of conservation equations for continuity, momentum, angular momentum, energy and concentration is obtained as:

$$\frac{1}{r}\rho\frac{\partial ru}{\partial r} = 0. \tag{6.1}$$

$$\rho u\frac{\partial u}{\partial r}=(\mu+\kappa^*)\left(\frac{\partial^2 u}{\partial r^2}-\frac{u}{r^2}+\frac{1}{r}\frac{\partial u}{\partial r}+\frac{1}{r^2}\frac{\partial^2 u}{\partial\Theta^2}\right)-\frac{\kappa^*}{r}\frac{\partial N}{\partial\Theta}-\frac{\partial p}{\partial r}-\frac{\sigma r_0^2}{\rho_f r^2}u, \tag{6.2}$$

$$0=-\frac{\partial p}{\partial\Theta}+\frac{2(\mu+\kappa^*)}{r}\frac{\partial u}{\partial\Theta}-r\kappa^*\frac{\partial N}{\partial r}-\kappa^* N, \tag{6.3}$$

$$\rho j u\frac{\partial N}{\partial r}=\gamma\left(\frac{\partial^2 N}{\partial r^2}-\frac{N}{r^2}+\frac{1}{r}\frac{\partial N}{\partial r}+\frac{1}{r^2}\frac{\partial^2 N}{\partial\Theta^2}\right)-2\kappa^* N-\frac{\kappa^*}{r}\frac{\partial u}{\partial\Theta}, \tag{6.4}$$

$$\begin{cases} u\frac{\partial T}{\partial r}=\alpha'\left(\frac{\partial^2 T}{\partial r^2}+\frac{1}{r}\frac{\partial T}{\partial r}+\frac{1}{r^2}\frac{\partial^2 T}{\partial\Theta^2}\right)+\frac{\mu+\kappa^*}{\rho C p_f}\left[2\left(\frac{\partial u}{\partial r}\right)^2+2\left(\frac{u}{r}\right)^2+\left(\frac{1}{r}\frac{\partial u}{\partial\Theta}\right)^2\right] \\ +\tau r^2\left[D_B\left(\frac{\partial T}{\partial r}\frac{\partial C}{\partial r}+\frac{1}{r^2}/\frac{\partial C}{\partial\Theta}\frac{\partial T}{\partial\Theta}\right)+\frac{D_T}{T_w}\left(\frac{\partial T}{\partial r}\right)^2+\frac{1}{r^2}\left(\frac{\partial T}{\partial\Theta}\right)^2\right]+\frac{\sigma_{el}r_0^2}{(\rho C_p)_f}u^2, \end{cases} \tag{6.5}$$

Here, $\tau=\dfrac{(\rho C_p)_p}{\rho C_p)_f}$ and $\alpha'=\dfrac{\kappa}{(\rho C_p)_f}$.

$$u\frac{\partial C}{\partial r}=\left[D_B\left(\frac{\partial^2 C}{\partial r^2}+\frac{1}{r}\frac{\partial C}{\partial r}+\frac{1}{r^2}\frac{\partial^2 C}{\partial\Theta^2}\right)+\frac{D_T}{T_w}\left(\frac{\partial^2 T}{\partial r^2}+\frac{1}{r}\frac{\partial T}{\partial r}+\frac{1}{r^2}\frac{\partial^2 T}{\partial\Theta^2}\right)\right], \tag{6.6}$$

Keeping in view of the flow properties, the associated boundary conditions are given as:
At the centerline of the channel:

$$u=Y_{\max},\quad \frac{\partial u}{\partial\Theta}=0,\quad N=0,\quad \frac{\partial T}{\partial\Theta}=0,\quad \frac{\partial C}{\partial\Theta}=0. \tag{6.7}$$

At the walls of the channel:

$$u=0,\quad N=0,\quad T=\frac{T_w}{r^2},\quad C=\frac{C_w}{r^2}. \tag{6.8}$$

The pressure term in Eqs.(6.2) - (6.3) is eliminated by differentiating Eq. (6.2) with respect to "Θ" and Eq. (6.3) with respect to "r" and then comparing the two equations. From the continuity equation (6.1) it is seen that $u(r,\Theta)=F(\Theta)$. The following transformation are introduced to convert the boundary value problem Eqs.(6.1)-(6.8) to nondimensional form:

$$u(r,\Theta)=\frac{f(\Theta)}{r},\ \eta=\frac{\Theta}{\alpha},\ f(\eta)=\frac{f(\Theta)}{Y_{max}},\ N=\frac{g(\eta)Y_{max}}{r^2},\ \theta(\eta)=\frac{r^2T}{T_w},\ \phi(\eta)=\frac{r^2C}{C_w}. \tag{6.9}$$

The nondimensional equations along with the boundary conditions take the form:

$$\begin{cases} (1+K)f'''(\eta)-K\alpha g''(\eta)+4\alpha^2(1+K)f'(\eta)+2K\alpha^3 g(\eta) \\ -Ha^2\alpha^2 f'(\eta)+2\alpha Ref'(\eta)f(\eta)=0, \end{cases} \tag{6.10}$$

$$(1+\frac{K}{2})(3\alpha^2 g(\eta)+g''(\eta))-KB(2g(\eta)+\alpha f'(\eta))+2Re\alpha f(\eta)g(\eta)=0, \tag{6.11}$$

$$\begin{cases} \theta^{''}(\eta) + 4\alpha^2\theta(\eta) + PrRef(\eta)\theta(\eta) + (1+K)PrEc[4\alpha^2 f^2(\eta) + f^{'2}(\eta)] \\ +N_B(4\alpha^2\theta(\eta)\phi(\eta) + \phi^{'}(\eta)\theta^{'}(\eta)) + N_T(4\alpha^2\theta^2(\eta) + \theta^{'2}(\eta)) \\ +Ha^2EcPr\alpha^2 f^2(\eta) = 0, \end{cases} \tag{6.12}$$

$$\phi^{''}(\eta) + ScRe2\alpha^2\phi(\eta)f(\eta) + 4\alpha^2\phi(\eta) + \frac{N_T}{N_B}(4\alpha^2\theta(\eta) + \theta^{''}(\eta)) = 0. \tag{6.13}$$

$$\begin{cases} f(0) = 1, \quad f^{'}(0) = 0, \quad g(0) = 0, \quad \theta^{'}(0) = 0, \quad \phi^{'}(0) = 0, \\ f(1) = 0, \quad g(1) = 0, \quad \theta(1) = 1, \quad \phi(1) = 1. \end{cases} \tag{6.14}$$

Here,

$$Pr = \frac{\nu}{\alpha^{'}}, \quad Re = \frac{\alpha Y_{max}}{\nu} \begin{cases} \alpha > 0, Y_{max} > 0, \text{diverging channel} \\ \alpha < 0, Y_{max} < 0, \text{converging channel} \end{cases}, \quad K = \frac{\kappa^*}{\mu},$$
$$N_B = \frac{\tau D_B C_w}{\alpha^{'}}, M = \sqrt{\frac{\sigma r_0^2}{\mu}}, \quad Ec = \frac{Y_{max}^2}{(C_p)_f T_w}, N_T = \frac{\tau D_T}{\alpha^{'}}, \quad B = \frac{r^2}{j}, \quad Sc = \frac{\nu}{D_B}.$$

The skin friction at the walls of the channel is characterized by the following relation:

$$C_f^* = \frac{(\mu + \kappa^*)}{\rho Y_{max}^2}\frac{1}{r}\frac{\partial u}{\partial \Theta}. \tag{6.15}$$

Heat transfer rate is characterized by the Nusselt number which defined as:

$$Nu^* = -\frac{r}{\kappa T_w}{}_{\zeta-1}t, w\Big|_{\Theta=\alpha}, \tag{6.16}$$

where ${}_{\zeta-1}t, w = -\frac{\kappa}{r}\frac{\partial T}{\partial \Theta}$ is the surface heat flux. The nondimensional forms of Eqs. (6.15)-(6.16) become:

$$C_f = (1+K)f^{'}(1),$$
$$Nu = \frac{1}{r^2\alpha}\theta^{'}(1).$$

6.3 Keller Box Formulation

The present section contains details of the solution procedure of Keller box method explicitly defined for the present problem. The boundary value problem (6.10)-(6.14) is converted to nine

first order ODEs as given in (6.17)-(6.26):

$$f = Y_1,$$
$$Y_1^{'} = Y_2, \tag{6.17}$$
$$Y_2^{'} = Y_3, \tag{6.18}$$
$$g = Y_4,$$
$$Y_4^{'} = Y_5, \tag{6.19}$$
$$\theta = Y_6,$$
$$Y_6^{'} = Y_7, \tag{6.20}$$
$$\phi = Y_8, \tag{6.21}$$
$$Y_8^{'} = Y_9, \tag{6.22}$$

$$\begin{cases} (1+K)Y_3^{'} - K\alpha Y_5^{'} + 4\alpha^2(1+K)Y_2 + 2K\alpha^3 Y_4 \\ -Ha^2\alpha^2 Y_2 + 2\alpha Re Y_2 Y_1 = 0, \end{cases} \tag{6.23}$$

$$(1+\frac{K}{2})(3\alpha^2 Y_4 + Y_5^{'}) - KB(2Y_4 + \alpha Y_2) + 2Re\alpha Y_1 Y_4 = 0, \tag{6.24}$$

$$\begin{cases} Y_7^{'} + 4\alpha^2 Y_6 + PrReY_1Y_6 + PrEc[4\alpha^2 Y_1^2 + Y_2] \\ +N_B(4\alpha^2 Y_6 Y_8 + Y_9 Y_7) + N_T(4\alpha^2 Y_6^2 + Y_7^2) \\ +Ha^2 EcPr\alpha^2 Y_1^2 = 0, \end{cases} \tag{6.25}$$

$$Y_9^{'} + ScRe2\alpha^2 Y_8 Y_1 + 4\alpha^2 Y_8 + \frac{N_T}{N_B}(4\alpha^2 Y_6 + Y_7^{'}) = 0. \tag{6.26}$$

Following section 2.14, the nonlinear system in (6.17)-(6.26) takes the linear discrete form:

$$\frac{(Y_1)_\zeta - (Y_1)_{\zeta-1}}{h} = (Y_2)_{\zeta-\frac{1}{2}}, \tag{6.27}$$
$$\frac{(Y_2)_\zeta - (Y_2)_{\zeta-1}}{h} = (Y_3)_{\zeta-\frac{1}{2}}, \tag{6.28}$$
$$\frac{(Y_4)_\zeta - (Y_4)_{\zeta-1}}{h} = (Y_5)_{\zeta-\frac{1}{2}}, \tag{6.29}$$
$$\frac{(Y_6)_\zeta - (Y_6)_{\zeta-1}}{h} = (Y_7)_{\zeta-\frac{1}{2}}, \tag{6.30}$$
$$\frac{(Y_8)_\zeta - (Y_8)_{\zeta-1}}{h} = (Y_9)_{\zeta-\frac{1}{2}}, \tag{6.31}$$

$$\begin{cases} (1+K)\left(\frac{(Y_3)_\zeta - (Y_3)_{\zeta-1}}{h}\right) - K\alpha\left(\frac{(Y_5)_\zeta - (Y_5)_{\zeta-1}}{h}\right) + 4\alpha^2(1+K)(Y_2)_{\zeta-\frac{1}{2}} \\ +2K\alpha^3(Y_4)_{\zeta-\frac{1}{2}} - Ha^2\alpha^2(Y_2)_{\zeta-\frac{1}{2}} + 2\alpha Re(Y_2)_{\zeta-\frac{1}{2}}(Y_1)_{\zeta-\frac{1}{2}} = 0, \end{cases} \tag{6.32}$$

$$\begin{cases} (1+\frac{K}{2})\left[3\alpha^2(Y_4)_{\zeta-\frac{1}{2}}+\left(\frac{(Y_5)_\zeta-(Y_5)_{\zeta-1}}{h}\right)\right]-KB(2(Y_4)_{\zeta-\frac{1}{2}} \\ +\alpha(Y_2)_{\zeta-\frac{1}{2}})+2Re\alpha(Y_1)_{\zeta-\frac{1}{2}}(Y_4)_{\zeta-\frac{1}{2}}=0, \end{cases} \tag{6.33}$$

$$\begin{cases} \left(\frac{(Y_7)_\zeta-(Y_7)_{\zeta-1}}{h}\right)+4\alpha^2(Y_6)_{\zeta-\frac{1}{2}}+PrRe(Y_1)_{\zeta-\frac{1}{2}}(Y_6)_{\zeta-\frac{1}{2}}+PrEc[4\alpha^2(Y_1)^2_{\zeta-\frac{1}{2}} \\ +(Y_2)_{\zeta-\frac{1}{2}}]+N_B(4\alpha^2(Y_6)_{\zeta-\frac{1}{2}}(Y_8)_{\zeta-\frac{1}{2}}+(Y_9)_{\zeta-\frac{1}{2}}(Y_7)_{\zeta-\frac{1}{2}})+N_T(4\alpha^2(Y_6)_{\zeta-\frac{1}{2}} \\ +(Y_7)_{\zeta-\frac{1}{2}})+Ha^2EcPr\alpha^2(Y_1)^2_{\zeta-\frac{1}{2}}=0, \end{cases} \tag{6.34}$$

$$\begin{cases} \left(\frac{(Y_9)_\zeta-(Y_9)_{\zeta-1}}{h}\right)+ScRe2\alpha^2\left[(Y_8)_{\zeta-\frac{1}{2}}(Y_1)_{\zeta-\frac{1}{2}}+4\alpha^2(Y_8)_{\zeta-\frac{1}{2}}\right] \\ +\frac{N_T}{N_B}\left[4\alpha^2(Y_6)_{\zeta-\frac{1}{2}}+\left(\frac{(Y_7)_\zeta-(Y_7)_{\zeta-1}}{h}\right)\right]=0. \end{cases} \tag{6.35}$$

Linearization of the nonlinear difference equations in (6.27)-(**??**) is carried out using Newton's method defined in section 2.14 as:

$$\frac{\varepsilon(Y_1)_\zeta-\varepsilon(Y_1)_{\zeta-1}}{h}-\frac{\varepsilon(Y_2)_\zeta+\varepsilon(Y_2)_{\zeta-1}}{2}=(r_1)_{\zeta-\frac{1}{2}}, \tag{6.36}$$

$$\frac{\varepsilon(Y_2)_\zeta-\varepsilon(Y_2)_{\zeta-1}}{h}-\frac{\varepsilon(Y_3)_\zeta+\varepsilon(Y_3)_{\zeta-1}}{2}=(r_2)_{\zeta-\frac{1}{2}}, \tag{6.37}$$

$$\frac{\varepsilon(Y_4)_\zeta-\varepsilon(Y_4)_{\zeta-1}}{h}-\frac{\varepsilon(Y_5)_\zeta+\varepsilon(Y_5)_{\zeta-1}}{2}=(r_3)_{\zeta-\frac{1}{2}}, \tag{6.38}$$

$$\frac{\varepsilon(Y_6)_\zeta-\varepsilon(Y_6)_{\zeta-1}}{h}-\frac{\varepsilon(Y_7)_\zeta+\varepsilon(Y_7)_{\zeta-1}}{2}=(r_4)_{\zeta-\frac{1}{2}}, \tag{6.39}$$

$$\frac{\varepsilon(Y_8)_\zeta-\varepsilon(Y_8)_{\zeta-1}}{h}-\frac{\varepsilon(Y_9)_\zeta+\varepsilon(Y_9)_{\zeta-1}}{2}=(r_5)_{\zeta-\frac{1}{2}}, \tag{6.40}$$

$$\begin{cases} (\psi_1)_\zeta j\varepsilon(Y_1)_\zeta+(\psi_2)_\zeta\varepsilon(Y_1)_{\zeta-1}+(\psi_3)_\zeta\varepsilon(Y_2)_\zeta+(\psi_4)_\zeta\varepsilon(Y_2)_{\zeta-1}+(\psi_5)_\zeta\varepsilon(Y_3)_\zeta \\ +(\psi_6)_\zeta\varepsilon(Y_3)_{\zeta-1}+(\psi_7)_\zeta\varepsilon(Y_4)_\zeta+(\psi_8)_\zeta\varepsilon(Y_4)_{\zeta-1}+(\psi_9)_\zeta\varepsilon(Y_5)_\zeta+(\psi_{10})_\zeta\varepsilon(Y_5)_{\zeta-1} \\ +(\psi_{11})_\zeta\varepsilon(Y_6)_\zeta+(\psi_{12})_\zeta\varepsilon(Y_6)_{\zeta-1}+(\psi_{13})_\zeta\varepsilon(Y_7)_\zeta+(\psi_{14})_\zeta\varepsilon(Y_7)_{\zeta-1}+(\psi_{15})_\zeta\varepsilon(Y_8)_\zeta \\ +(\psi_{16})_\zeta\varepsilon(Y_8)_{\zeta-1}+(\psi_{17})_\zeta\varepsilon(Y_9)_\zeta+(\psi_{18})_\zeta\varepsilon(Y_9)_{\zeta-1}=(r_6)_{\zeta-\frac{1}{2}}, \end{cases} \tag{6.41}$$

$$\begin{cases} (\chi_1)_\zeta\varepsilon(Y_1)_\zeta+(\chi_2)_\zeta\varepsilon(Y_1)_{\zeta-1}+(\chi_3)_\zeta\varepsilon(Y_2)_\zeta+(\chi_4)_\zeta\varepsilon(Y_2)_{\zeta-1}+(\chi_5)_\zeta\varepsilon(Y_3)_\zeta \\ +(\chi_6)_\zeta\varepsilon(Y_3)_{\zeta-1}+(\chi_7)_\zeta\varepsilon(Y_4)_\zeta+(\chi_8)_\zeta\varepsilon(Y_4)_{\zeta-1}+(\chi_9)_\zeta\varepsilon(Y_5)_\zeta+(\chi_{10})_\zeta\varepsilon(Y_5)_{\zeta-1} \\ +(\chi_{11})_\zeta\varepsilon(Y_6)_\zeta+(\chi_{12})_\zeta\varepsilon(Y_6)_{\zeta-1}+(\chi_{13})_\zeta\varepsilon(Y_7)_\zeta+(\chi_{14})_\zeta\varepsilon(Y_7)_{\zeta-1}+(\chi_{15})_\zeta\varepsilon(Y_8)_\zeta \\ +(\chi_{16})_\zeta\varepsilon(Y_8)_{\zeta-1}+(\chi_{17})_\zeta\varepsilon(Y_9)_\zeta+(\chi_{18})_\zeta\varepsilon(Y_9)_{\zeta-1}=(r_7)_{\zeta-\frac{1}{2}}. \end{cases} \tag{6.42}$$

$$\begin{cases} (\Omega_1)_\zeta \varepsilon(Y_1)_\zeta + (\Omega_2)_\zeta \varepsilon(Y_1)_{\zeta-1} + (\Omega_3)_\zeta \varepsilon(Y_2)_\zeta + (\Omega_4)_\zeta \varepsilon(Y_2)_{\zeta-1} + (\Omega_5)_\zeta \varepsilon(Y_3)_\zeta \\ +(\Omega_6)_\zeta \varepsilon(Y_3)_{\zeta-1} + (\Omega_7)_\zeta \varepsilon(Y_4)_\zeta + (\Omega_8)_\zeta \varepsilon(Y_4)_{\zeta-1} + (\Omega_9)_\zeta \varepsilon(Y_5)_\zeta + (\Omega_{10})_\zeta \varepsilon(Y_5)_{\zeta-1} \\ +(\Omega_{11})_\zeta \varepsilon(Y_6)_\zeta + (\Omega_{12})_\zeta \varepsilon(Y_6)_{\zeta-1} + (\Omega_{13})_\zeta \varepsilon(Y_7)_\zeta + (\Omega_{14})_\zeta \varepsilon(Y_7)_{\zeta-1} + (\Omega_{15})_\zeta \varepsilon(Y_8)_\zeta \\ +(\Omega_{16})_\zeta \varepsilon(Y_8)_{\zeta-1} + (\Omega_{17})_\zeta \varepsilon(Y_9)_\zeta + (\Omega_{18})_\zeta \varepsilon(Y_9)_{\zeta-1} = (r_8)_{\zeta-\frac{1}{2}}, \end{cases} \tag{6.43}$$

$$\begin{cases} (\zeta_1)_\zeta \varepsilon(Y_1)_\zeta + (\zeta_2)_\zeta \varepsilon(Y_1)_{\zeta-1} + (\zeta_3)_\zeta \varepsilon(Y_2)_\zeta + (\zeta_4)_\zeta \varepsilon(Y_2)_{\zeta-1} + (\zeta_5)_\zeta \varepsilon(Y_3)_\zeta \\ +(\zeta_6)_\zeta \varepsilon(Y_3)_{\zeta-1} + (\zeta_7)_\zeta \varepsilon(Y_4)_\zeta + (\zeta_8)_\zeta \varepsilon(Y_4)_{\zeta-1} + (\zeta_9)_\zeta \varepsilon(Y_5)_\zeta + (\zeta_{10})_\zeta \varepsilon(Y_5)_{\zeta-1} \\ +(\zeta_{11})_\zeta \varepsilon(Y_6)_\zeta + (\zeta_{12})_\zeta \varepsilon(Y_6)_{\zeta-1} + (\zeta_{13})_\zeta \varepsilon(Y_7)_\zeta + (\zeta_{14})_\zeta \varepsilon(Y_7)_{\zeta-1} + (\zeta_{15})_\zeta \varepsilon(Y_8)_\zeta \\ +(\zeta_{16})_\zeta \varepsilon(Y_8)_{\zeta-1} + (\zeta_{17})_\zeta \varepsilon(Y_9)_\zeta + (\zeta_{18})_\zeta \varepsilon(Y_9)_{\zeta-1} = (r_9)_{\zeta-\frac{1}{2}}. \end{cases} \tag{6.44}$$

The above linear equations can be written in matrix form as defined in (2.54)-(2.55).

Making use of the boundary conditions (6.14), we have:

$$\mathrm{x}_1 = \begin{bmatrix} \varepsilon(Y_3)_0 \\ \varepsilon(Y_5)_0 \\ \varepsilon(Y_6)_0 \\ \varepsilon(Y_8)_0 \\ \varepsilon(Y_2)_1 \\ \varepsilon(Y_3)_1 \\ \varepsilon(Y_5)_1 \\ \varepsilon(Y_7)_1 \\ \varepsilon(Y_9)_1 \end{bmatrix}, \quad \mathrm{x}_\zeta = \begin{bmatrix} \varepsilon(Y_1)_{\zeta-1} \\ \varepsilon(Y_4)_{\zeta-1} \\ \varepsilon(Y_6)_{\zeta-1} \\ \varepsilon(Y_8)_{\zeta-1} \\ \varepsilon(Y_2)_\zeta \\ \varepsilon(Y_3)_\zeta \\ \varepsilon(Y_5)_\zeta \\ \varepsilon(Y_7)_\zeta \\ \varepsilon(Y_9)_\zeta \end{bmatrix}, \qquad \zeta = 2, 3, ..., J, \tag{6.45}$$

$$A_1 = \begin{bmatrix} 0 & 0 & 0 & 0 & \frac{-h}{2} & 0 & 0 & 0 & 0 \\ \frac{-h}{2} & 0 & 0 & 0 & 1 & \frac{-h}{2} & 0 & 0 & 0 \\ 0 & -1 & 0 & 0 & 0 & 0 & \frac{-h}{2} & 0 & 0 \\ 0 & 0 & -1 & 0 & 0 & 0 & 0 & \frac{-h}{2} & 0 \\ 0 & 0 & 0 & -1 & 0 & 0 & 0 & 0 & \frac{-h}{2} \\ (\psi_6)_1 & (\psi_{10})_1 & (\psi_{12})_1 & (\psi_{16})_1 & (\psi_3)_1 & (\psi_5)_1 & (\psi_9)_1 & (\psi_{13})_1 & (\psi_{17})_1 \\ (\chi_6)_1 & (\chi_{10})_1 & (\chi_{12})_1 & (\chi_{16})_1 & (\chi_3)_1 & (\chi_5)_1 & (\chi_9)_1 & (\chi_{13})_1 & (\chi_{17})_1 \\ (\Omega_6)_1 & (\Omega_{10})_1 & (\Omega_{12})_1 & (\Omega_{16})_1 & (\Omega_3)_1 & (\Omega_5)_1 & (\Omega_9)_1 & (\Omega_{13})_1 & (\Omega_{17})_1 \\ (\zeta_6)_1 & (\zeta_{10})_1 & (\zeta_{12})_1 & (\zeta_{16})_1 & (\zeta_3)_1 & (\zeta_5)_1 & (\zeta_9)_1 & (\zeta_{13})_1 & (\zeta_{17})_1 \end{bmatrix},$$

$$A_\zeta = \begin{bmatrix} -1 & 0 & 0 & 0 & \frac{-h}{2} & 0 & 0 & 0 & 0 \\ 0 & 0 & 0 & 0 & 1 & \frac{-h}{2} & 0 & 0 & 0 \\ 0 & -1 & 0 & 0 & 0 & 0 & \frac{-h}{2} & 0 & 0 \\ 0 & 0 & -1 & 0 & 0 & 0 & 0 & \frac{-h}{2} & 0 \\ 0 & 0 & 0 & -1 & 0 & 0 & 0 & 0 & \frac{-h}{2} \\ (\psi_2)_\zeta & (\psi_8)_\zeta & (\psi_{12})_\zeta & (\psi_{16})_\zeta & (\psi_3)_\zeta & (\psi_5)_\zeta & (\psi_9)_\zeta & (\psi_{13})_\zeta & (\psi_{17})_\zeta \\ (\chi_2)_\zeta & (\chi_8)_\zeta & (\chi_{12})_\zeta & (\chi_{16})_\zeta & (\chi_3)_\zeta & (\chi_5)_\zeta & (\chi_9)_\zeta & (\chi_{13})_\zeta & (\chi_{17})_\zeta \\ (\Omega_2)_\zeta & (\Omega_8)_\zeta & (\Omega_{12})_\zeta & (\Omega_{16})_\zeta & (\Omega_3)_\zeta & (\Omega_5)_\zeta & (\Omega_9)_\zeta & (\Omega_{13})_\zeta & (\Omega_{17})_\zeta \\ (\zeta_2)_\zeta & (\zeta_8)_\zeta & (\zeta_{12})_\zeta & (\zeta_{16})_\zeta & (\zeta_3)_\zeta & (\zeta_5)_\zeta & (\zeta_9)_\zeta & (\zeta_{13})_\zeta & (\zeta_{17})_\zeta \end{bmatrix}, \qquad \zeta = 2, 3, ..., J,$$

$$r_\zeta = \begin{bmatrix} 0 & 0 & 0 & 0 & \frac{-h}{2} & 0 & 0 & 0 & 0 \\ 0 & 0 & 0 & 0 & -1 & \frac{-h}{2} & 0 & 0 & 0 \\ 0 & 0 & 0 & 0 & 0 & 0 & \frac{-h}{2} & 0 & 0 \\ 0 & 0 & 0 & 0 & 0 & 0 & 0 & \frac{-h}{2} & 0 \\ 0 & 0 & 0 & 0 & 0 & 0 & 0 & 0 & \frac{-h}{2} \\ 0 & 0 & 0 & 0 & (\psi_4)_\zeta & (\psi_6)_\zeta & (\psi_{10})_\zeta & (\psi_{14})_\zeta & (\psi_{18})_\zeta \\ 0 & 0 & 0 & 0 & (\chi_4)_\zeta & (\chi_6)_\zeta & (\chi_{10})_\zeta & (\chi_{14})_\zeta & (\chi_{18})_\zeta \\ 0 & 0 & 0 & 0 & (\Omega_4)_\zeta & (\Omega_6)_\zeta & (\Omega_{10})_\zeta & (\Omega_{14})_\zeta & (\Omega_{18})_\zeta \\ 0 & 0 & 0 & 0 & (\zeta_4)_\zeta & (\zeta_6)_\zeta & (\zeta_{10})_\zeta & (\zeta_{14})_\zeta & (\zeta_{18})_\zeta \end{bmatrix}, \qquad \zeta = 2, 3, ..., J,$$

$$C_\zeta = \begin{bmatrix} 1 & 0 & 0 & 0 & 0 & 0 & 0 & 0 & 0 \\ 0 & 0 & 0 & 0 & 0 & 0 & 0 & 0 & 0 \\ 0 & 1 & 0 & 0 & 0 & 0 & 0 & 0 & 0 \\ 0 & 0 & 1 & 0 & 0 & 0 & 0 & 0 & 0 \\ 0 & 0 & 0 & 1 & 0 & 0 & 0 & 0 & 0 \\ (\psi_1)_\zeta & (\psi_7)_\zeta & (\psi_{11})_\zeta & (\psi_{15})_\zeta & 0 & 0 & 0 & 0 & 0 \\ (\chi_1)_\zeta & (\chi_7)_\zeta & (\chi_{11})_\zeta & (\chi_{15})_\zeta & 0 & 0 & 0 & 0 & 0 \\ (\Omega_1)_\zeta & (\Omega_7)_\zeta & (\Omega_{11})_\zeta & (\Omega_{15})_\zeta & 0 & 0 & 0 & 0 & 0 \\ (\zeta_1)_\zeta & (\zeta_7)_\zeta & (\zeta_{11})_\zeta & (\zeta_{15})_\zeta & 0 & 0 & 0 & 0 & 0 \end{bmatrix}, \qquad \zeta = 1, 2, ..., J.$$

Next, the resulting system is solved by block LU-factorization method. The accuracy of the numerical results are verified by its comparison with the already published results of Turkyilmazoglu [72] in Table 6.1.

6.4 Numerical Results and Discussion

The present section is a discussion on the impact of pertinent parameters on the nanofluid properties like heat transfer, skin friction, velocity profile, angular velocity profile, temperature and

nanoparticle concentration profiles.

The Hartmann number is a measure of the strength of the Lorentz forces acting on the fluid flow. It is observed in Figure 6.2 that the fluid velocity is augmented with an increase in the Hartmann number for both the converging and diverging channel flows. Observing Figure 6.3 the impression comes that the angular velocity of the fluid unlike the linear velocity shows a contrasting behavour. The angular velocity of the nanofluid decreases with a rise in the Hartmann number for both the converging and diverging channel flows. Pondering at this behavior, it seems that the Lorentz forces are diminishing the impact of the microstructures on the flow of the nanofluid which is the cause for an increase in the linear velocity. Figure 6.4 reveals that the temperature profile increases with an increase in the Hartmann number. The reason behind this behavior is the heat dissipation caused in the form of Joule heating which rises the temperature of the nanofluid.

The material parameter K shows the impact of the rotation viscosity on the fluid properties due the presence of the microstructures in the nanofluid. Greater values of K implies an increased number of microstructures and a stronger rotation viscosity. It is observed in Figures 6.5-6.6 that the rising values of the material parameter is increasing the fluid velocity as well as the angular velocity for the diverging case but both the velocities are decreasing for the converging case. This means that the greater rotation viscosity affects positively on both the linear and angular velocities of the fluid in the diverging channel while the opposite in observed in the case of converging channel. Similarly, an increase in temperature is observed in the diverging channel for growing values of the K while a decline in temperature in the case of the converging

		Turkyilmazoglu		Present results	
α	C	$f^{'}(1)$	$-\theta^{'}(1)$	$-f^{'}(1)$	$-\theta^{'}(1)$
-5	0	-2.8339514330	0.0421517243	-2.8339500375	0.0421517198
	1	0.0000000000	0.0464015106	0.0000000000	0.04640151045
	2	3.6697111853	0.0502423154	3.6697112559	0.0502423170
5	0	-1.1093265266	0.0399820121	-1.1093279586	0.0399820131
	1	0.0000000000	0.0464015106	0.0000000000	0.0464015104
	2	-1.0811324373	0.0557422655	-1.0811206439	0.0557422429

Table 6.1: Comparison of the present numerical results with previously published results for $K = B = 0 = N_B = 0 = N_T = Sc = Ha = Ec = 0$ and $Pr = 1$.

channel as evident from Figure 6.7. The increased velocities and temperature of the nanofluid in a diverging channel results in greater skin friction coefficient and heat transfer rate. In case of converging channel, an upsurge is observed in skin friction coefficient but the heat transfer rate declines with rising values of the material parameter K.

An investigation on the impact of the opening angle α on the fluid velocity, angular velocity, temperature and concentration profiles is carried out in Figures 6.8-6.11. It is seen that at greater opening angles, in the case of divergent channel the velocity decreases while it increases in the case of convergent channel (see Figure 6.8). A converse behavior is observed in the case of angular velocity as the fluid velocity grows for divergent channel while it shrinks for the convergent channel flow as evident in Figure 6.9. In Figure 6.10, it is found that the temperature profile increases for both the cases of channel flows. The rise in temperature is more pronouced in the case of convergent channel as compared to the divergent channel. Figure 6.11 shows that the concentration profile declines with inclination in the opening angles for both the channel. A much sharper decline is seen in the case of the divergent channel as compared to the convergent channel.

Figure 6.12 reveals that the higher values of Reynolds number Re causes the velocity profile to decrease in the divergent channel case while the velocity augments in case of the convergent channel. A higher Reynolds number causes the angular velocity to grow for both the cases of convegent and divergent channel flow. Greater Reynolds number happens to decrease in the temperature profile and decreases the heat transfer rate in either of the two cases (see Figure 6.14 and Tables 6.2-6.3). Skin friction coefficient lower with greater Reynolds number in diverging channel flow but increases in the case of high Reynolds number in converging channel flow. The concentration profile shows a decline with an increase in the Reynolds number as it can be seen in Figure 6.15. Eckert number assosiated to energy dissipation increases the temperature profile for both the cases as it is increased (see Figure 6.16). The growing values of Eckert number has a contrasting effect on the concentration as the profile shows an increase in the case of diverging channel but decrease in the case of convergent channel as found in Figure 6.17. Considerable effects of the Brownian motion N_B and thermopherotic N_T on the temperature and concentration profiles are investigated in a divergent channel in Figures 6.18-6.19. Both the profiles and the heat transfer rate at the walls show a decline with an increase in the values of N_B and N_T. In the last, the impact of the Prandtl number Pr is pondered on the temperature and concentration profiles in Figures 6.20-6.21. Increased values of the Prandtl number increases the temperature while the concentration profile shrinks for the case of convergent channel but it grows in the case of divergent channel. Finally, coupling impact of Ha and K on the stability of the flow in the diverging channel are pondered in Figure 6.22 with $\alpha = 10^o$. Looking at the results it is observed that the presence of the microstructures and a strong magnetic field are

instrumental in stabilizing the flow in diverging channel.

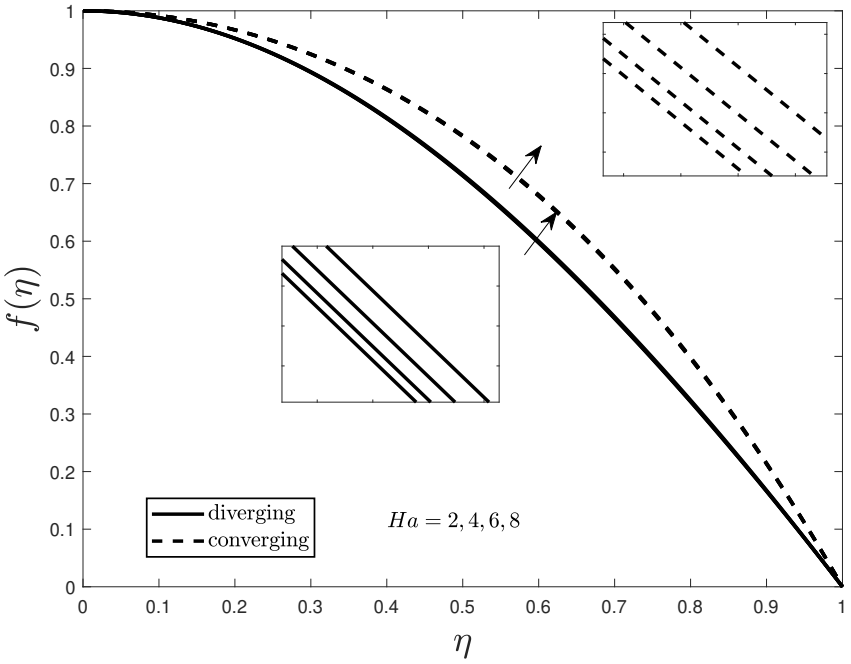

Figure 6.2: Variation in velocity with change in Ha.

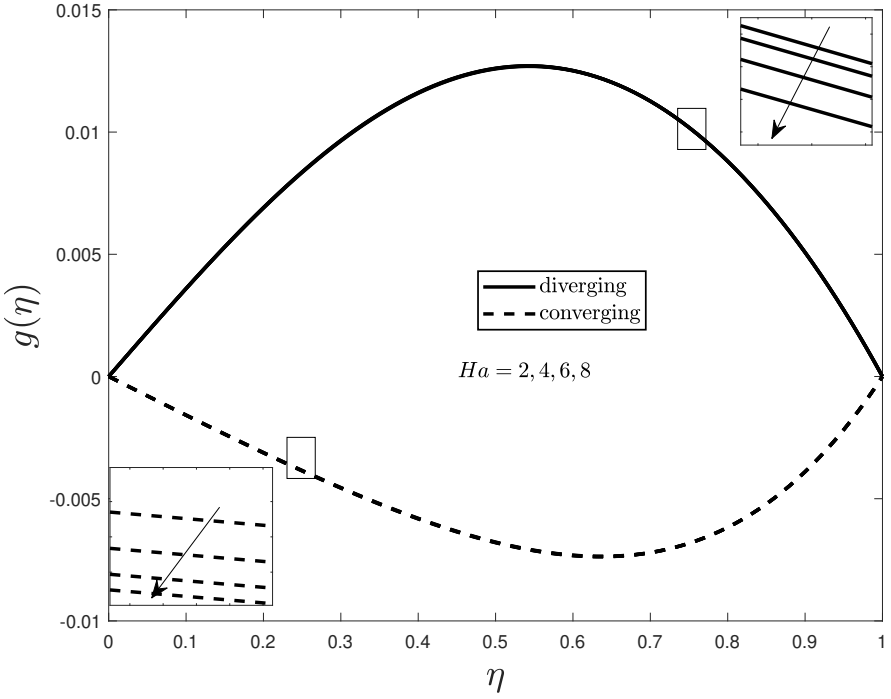

Figure 6.3: Variation in angular velocity with change in Ha.

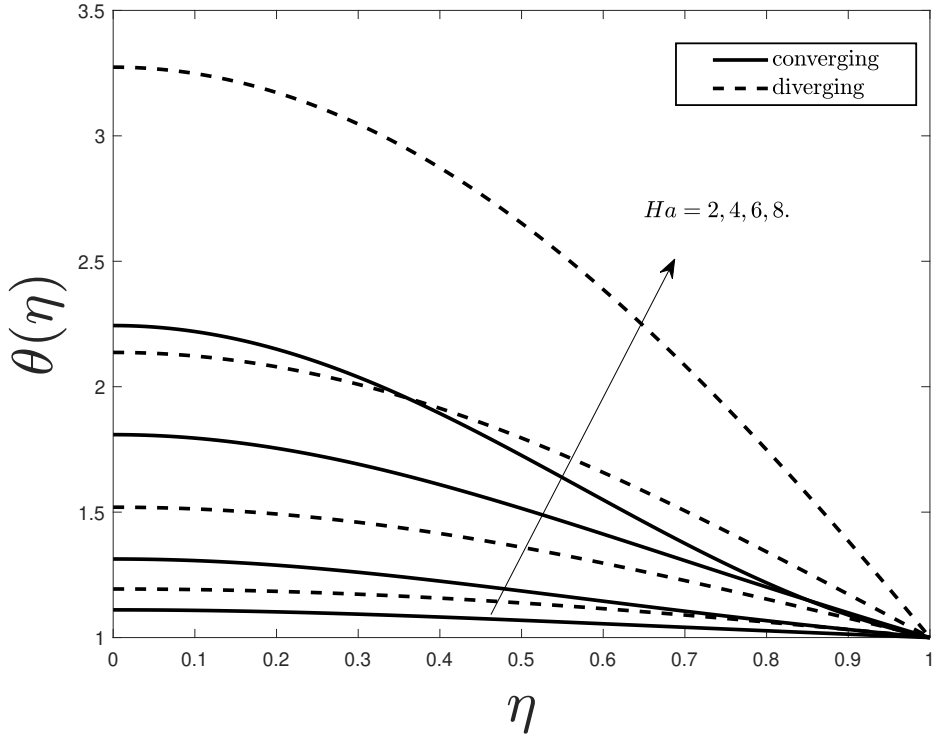

Figure 6.4: Variation in temperature with change in Ha.

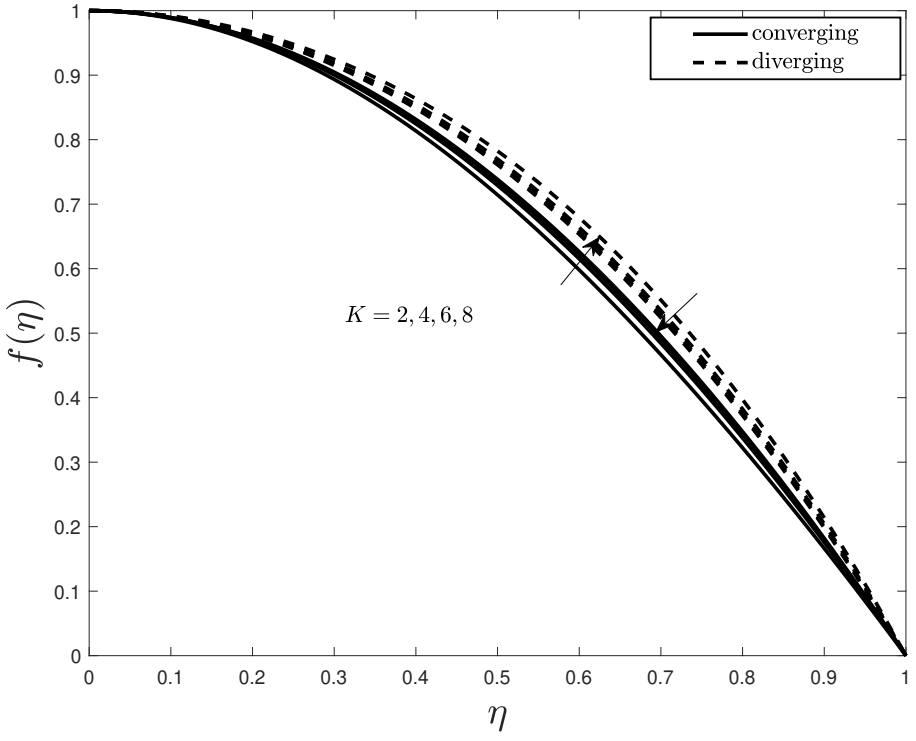

Figure 6.5: Variation in velocity with change in Ha.

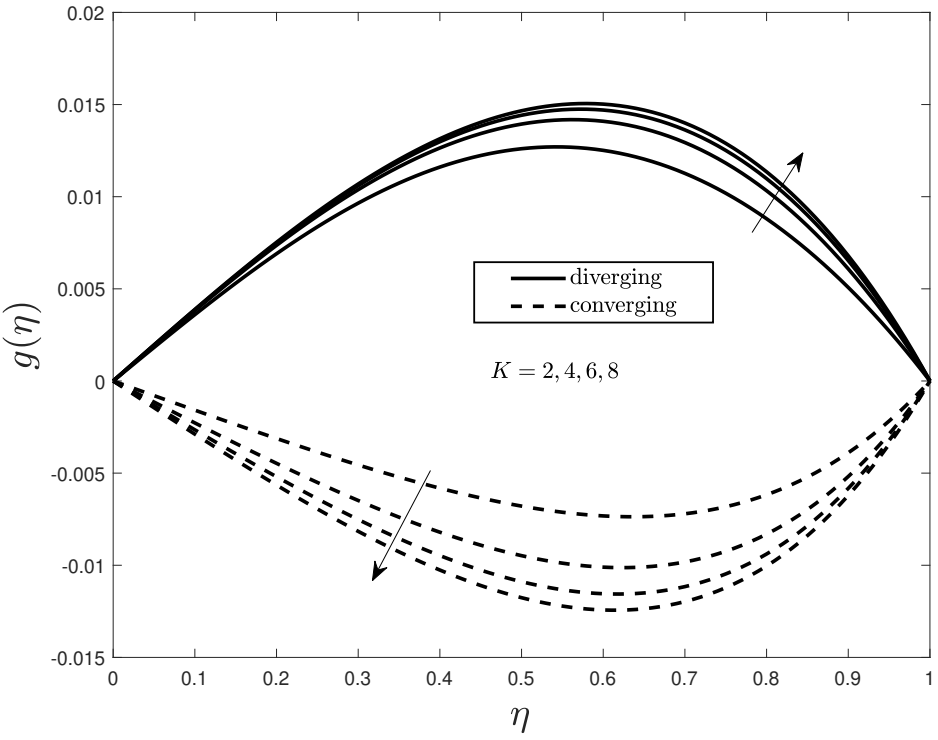

Figure 6.6: Variation in angular velocity with change in K.

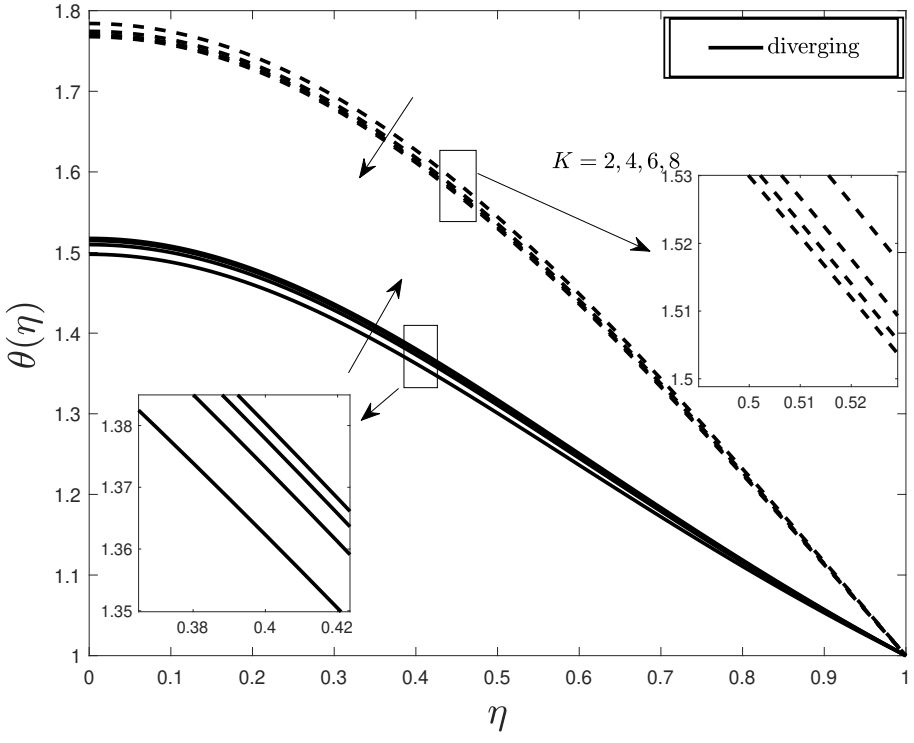

Figure 6.7: Variation in temperature with change in K.

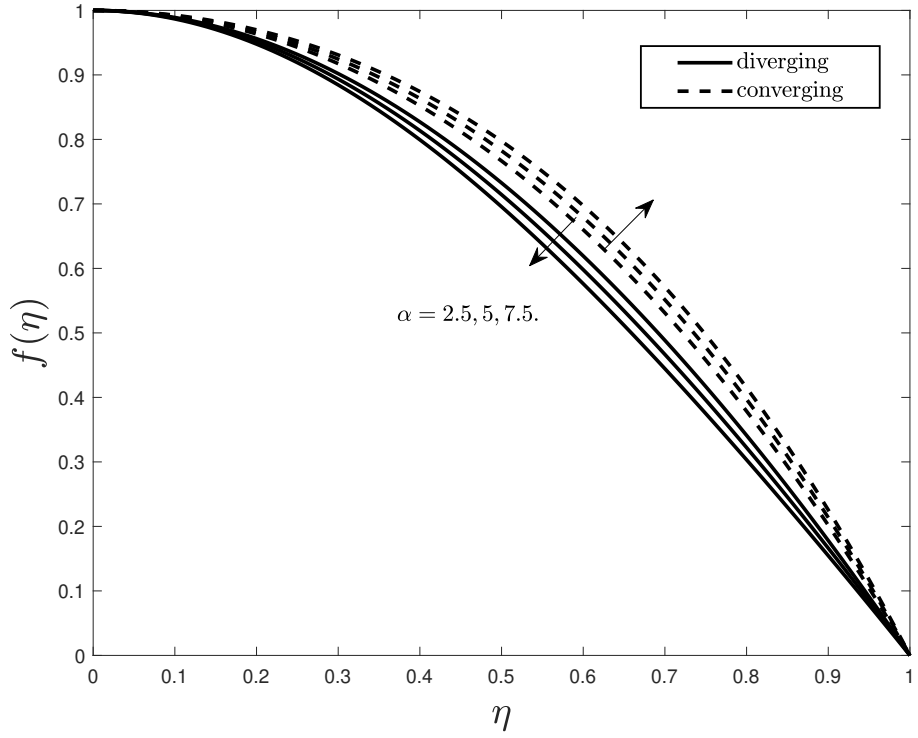

Figure 6.8: Variation in velocity with change in α.

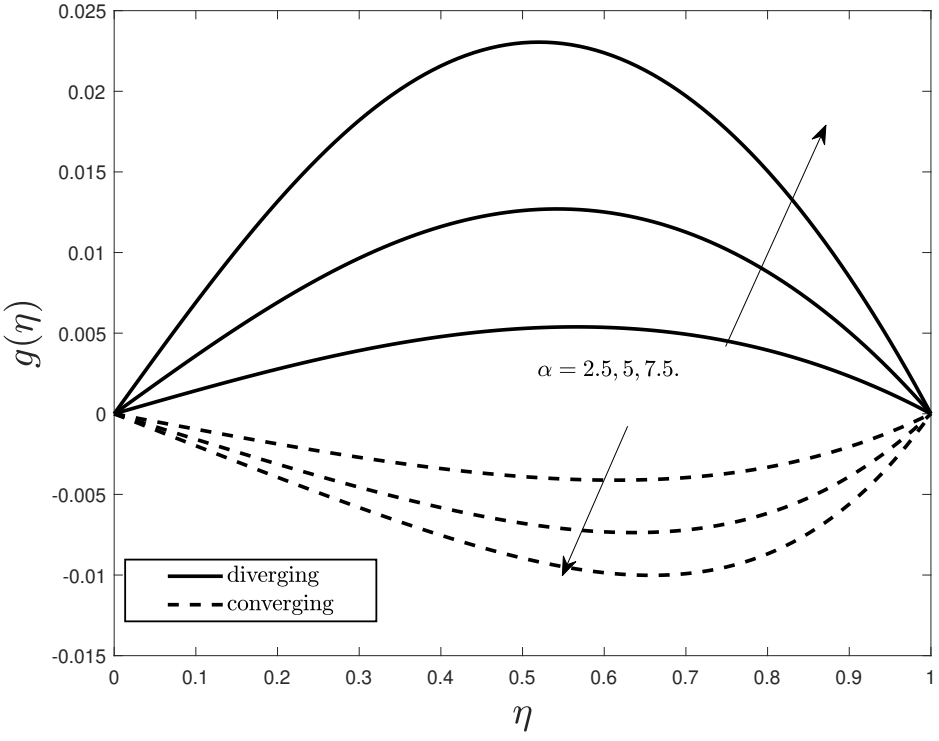

Figure 6.9: Variation in angular velocity with change in α.

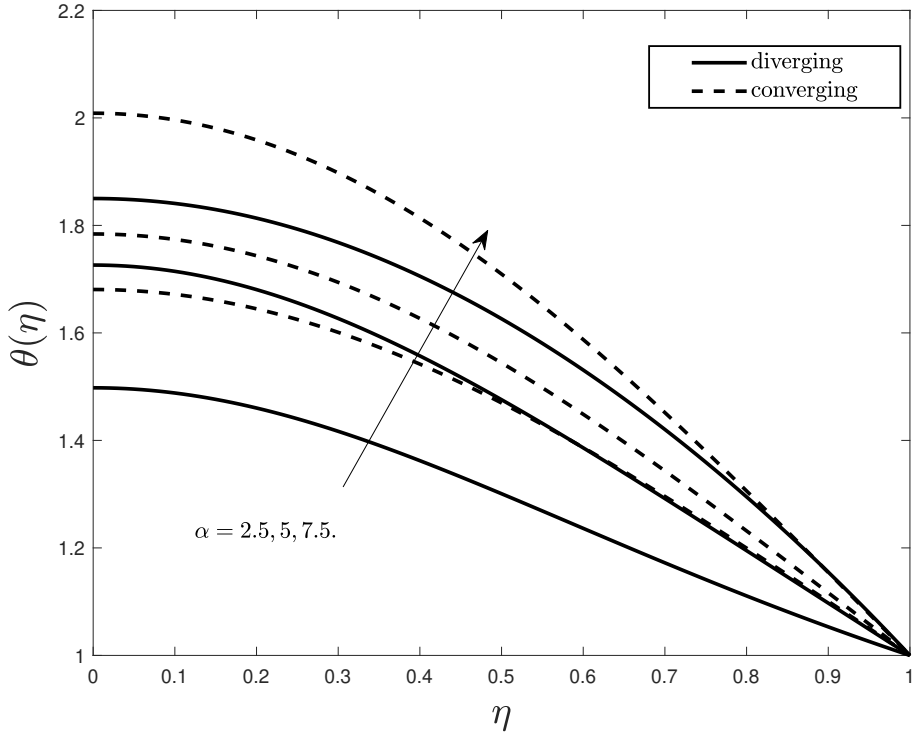

Figure 6.10: Variation in temperature with change in α.

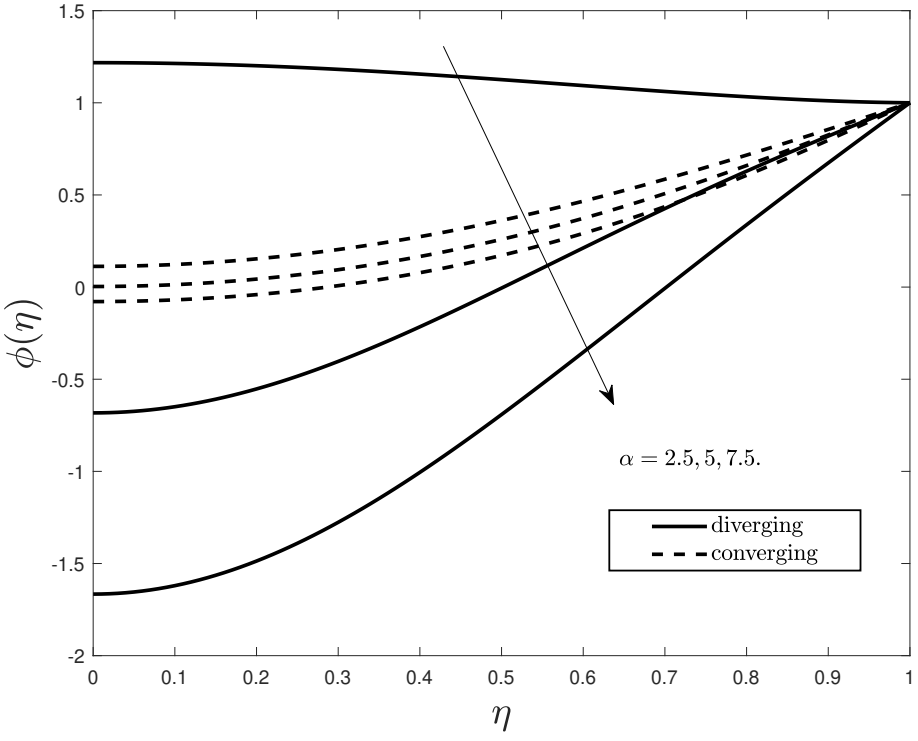

Figure 6.11: Variation in concentration with change in α.

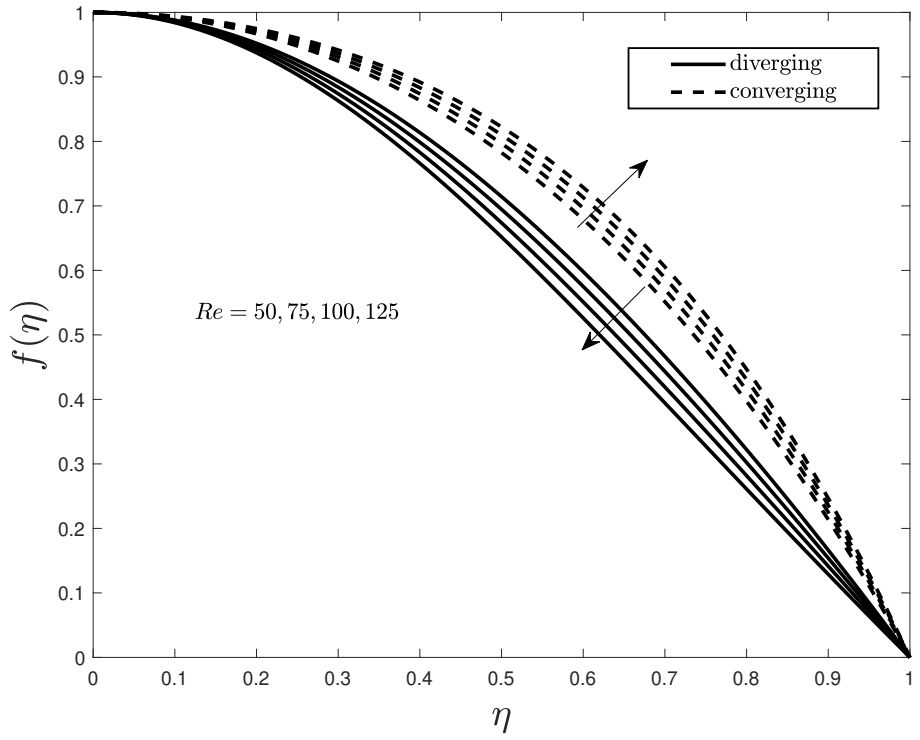

Figure 6.12: Variation in velocity with change in Re.

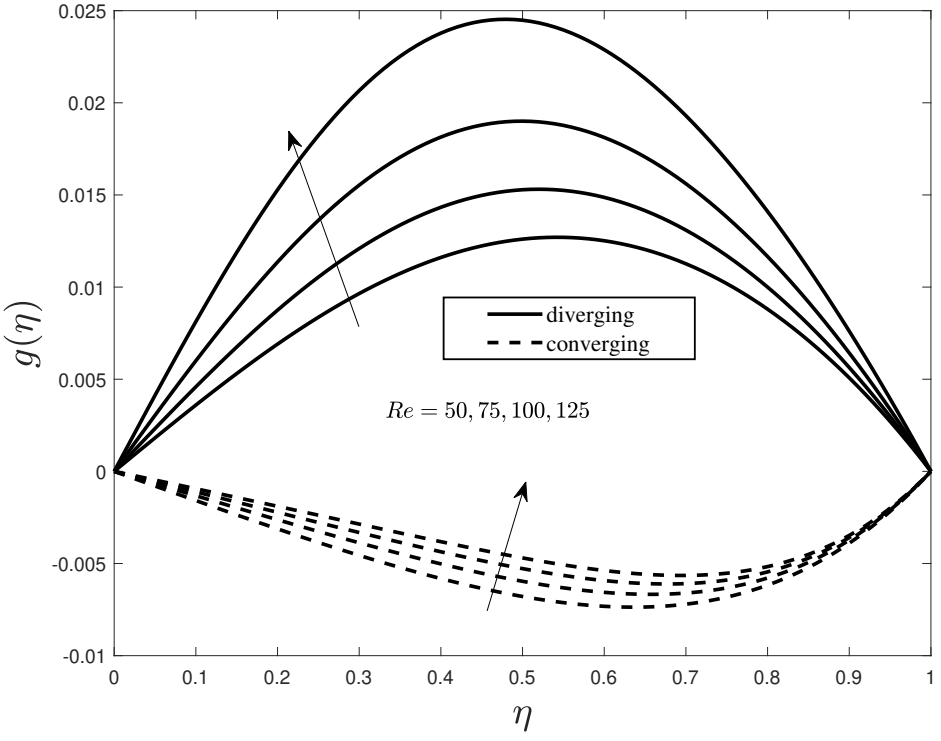

Figure 6.13: Variation in angular velocity with change in Re.

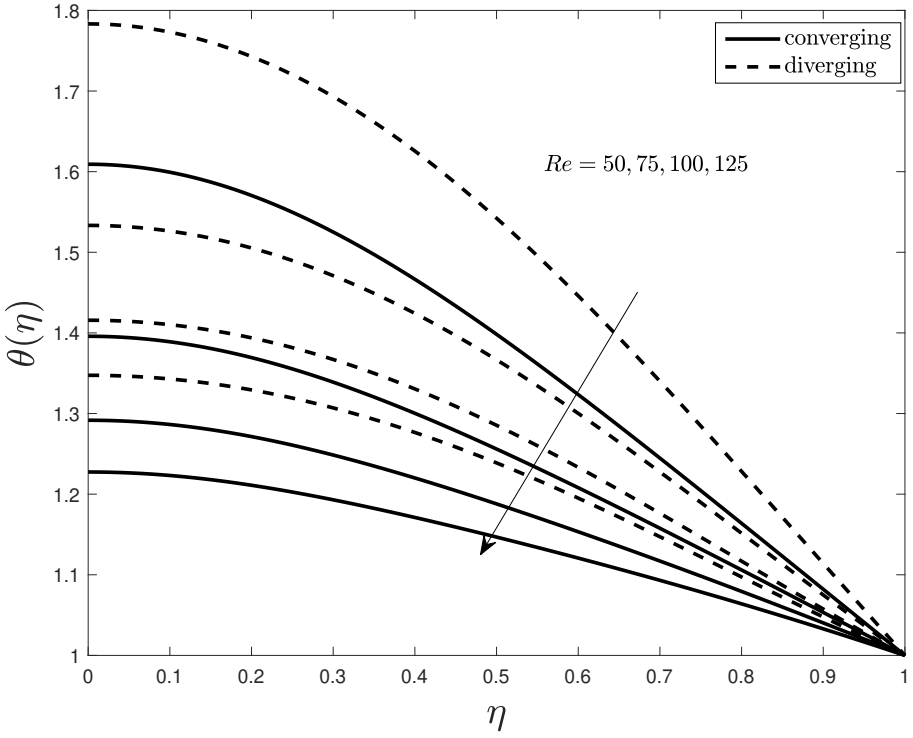

Figure 6.14: Variation in temperature with change in Re.

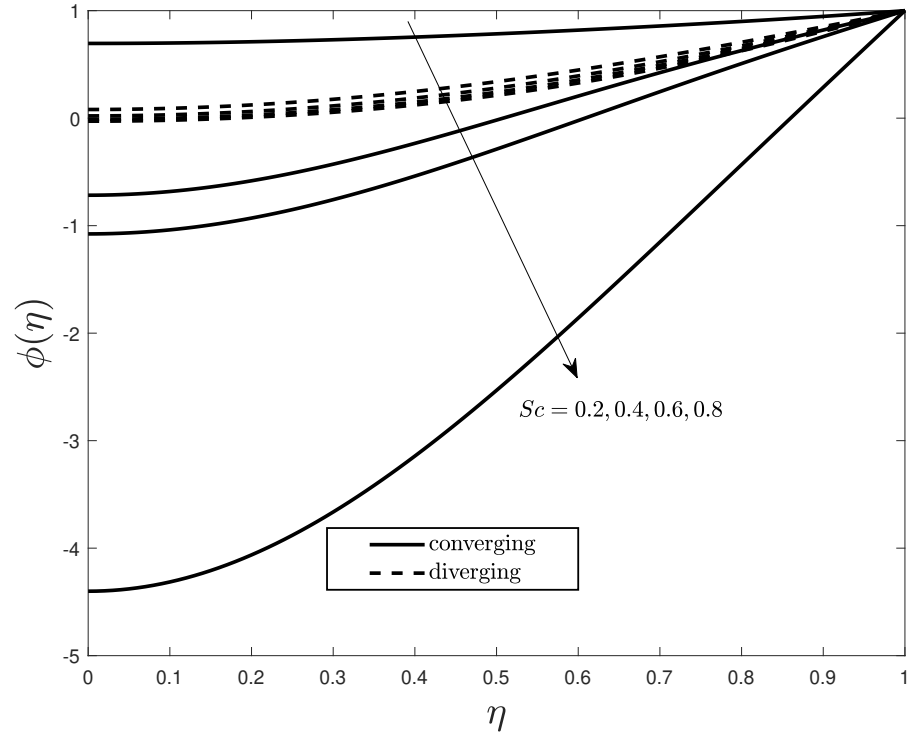

Figure 6.15: Variation in concentration with change in Re.

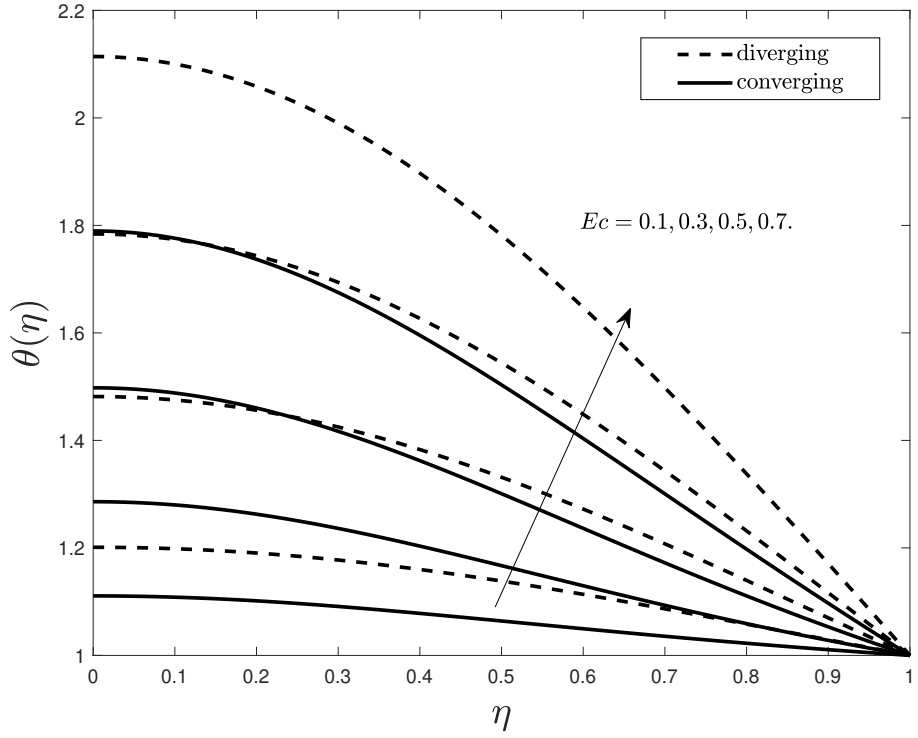

Figure 6.16: Variation in temperature with change in Ec.

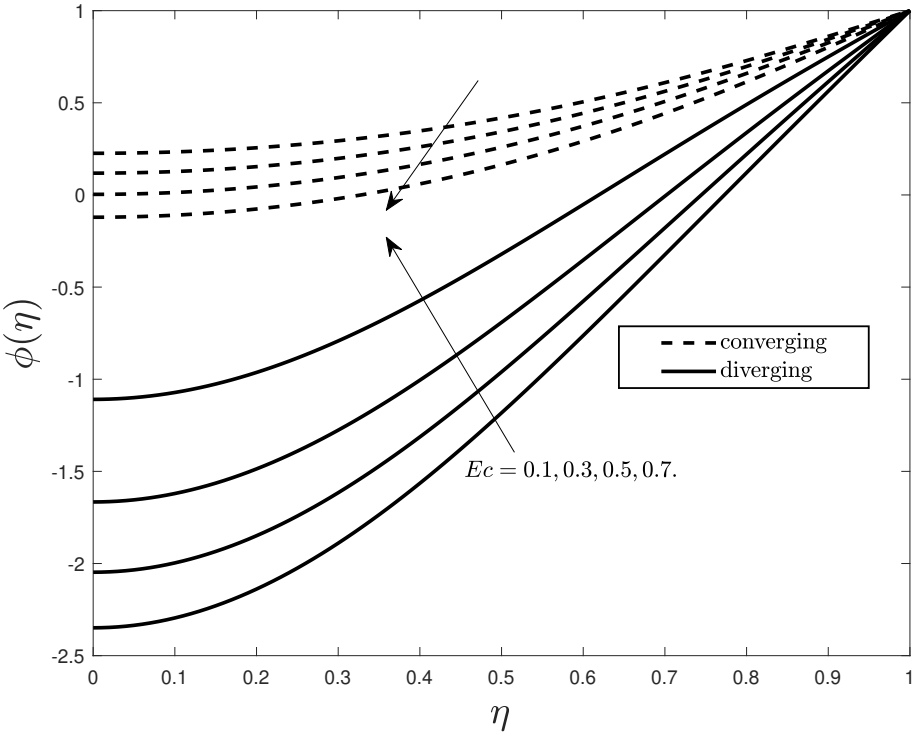

Figure 6.17: Variation in concentration with change in Ec.

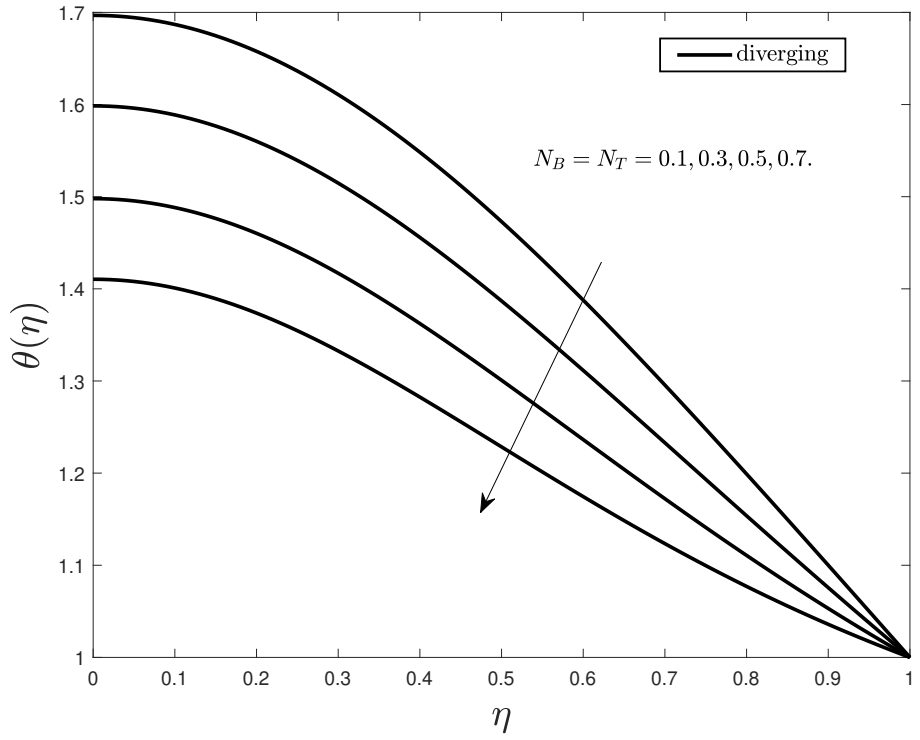

Figure 6.18: Variation in temperature with change in N_B and N_T.

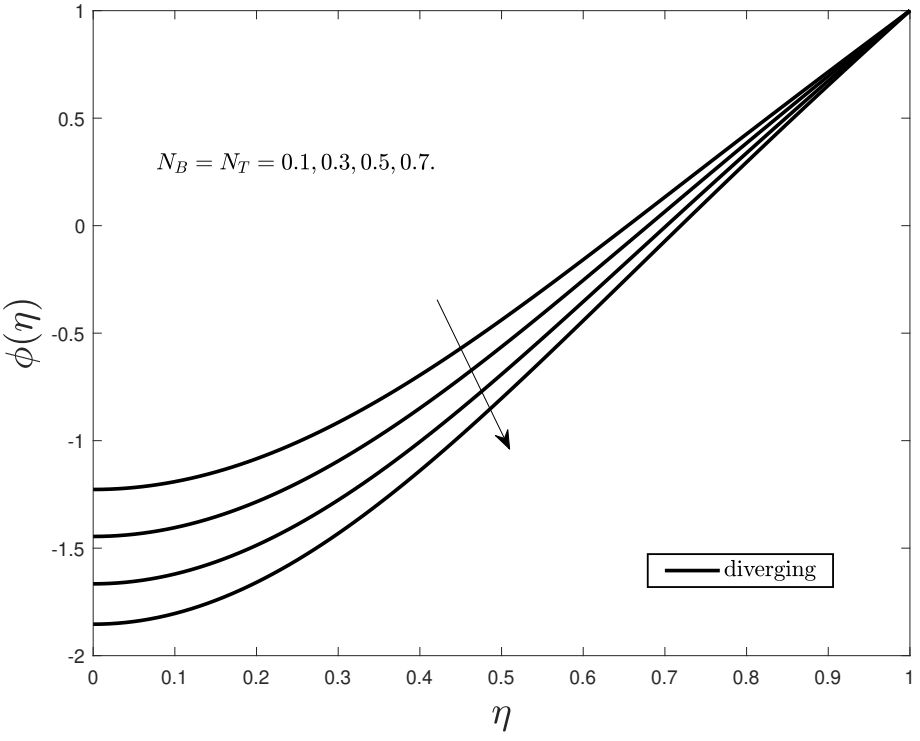

Figure 6.19: Variation in concentration with change in N_B and N_T.

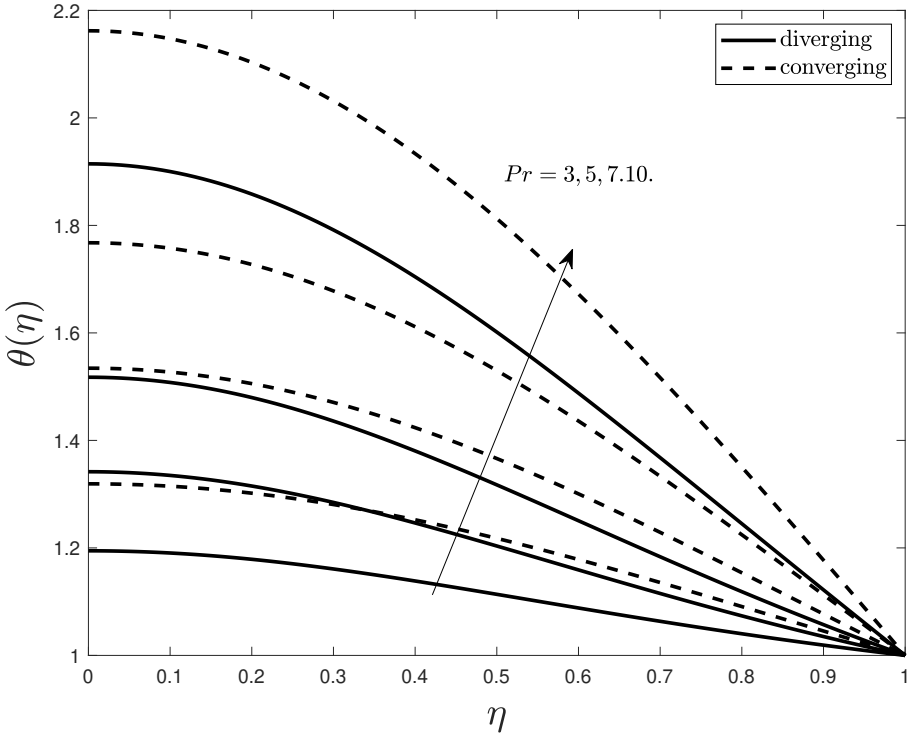

Figure 6.20: Variation in temperature with change in Pr.

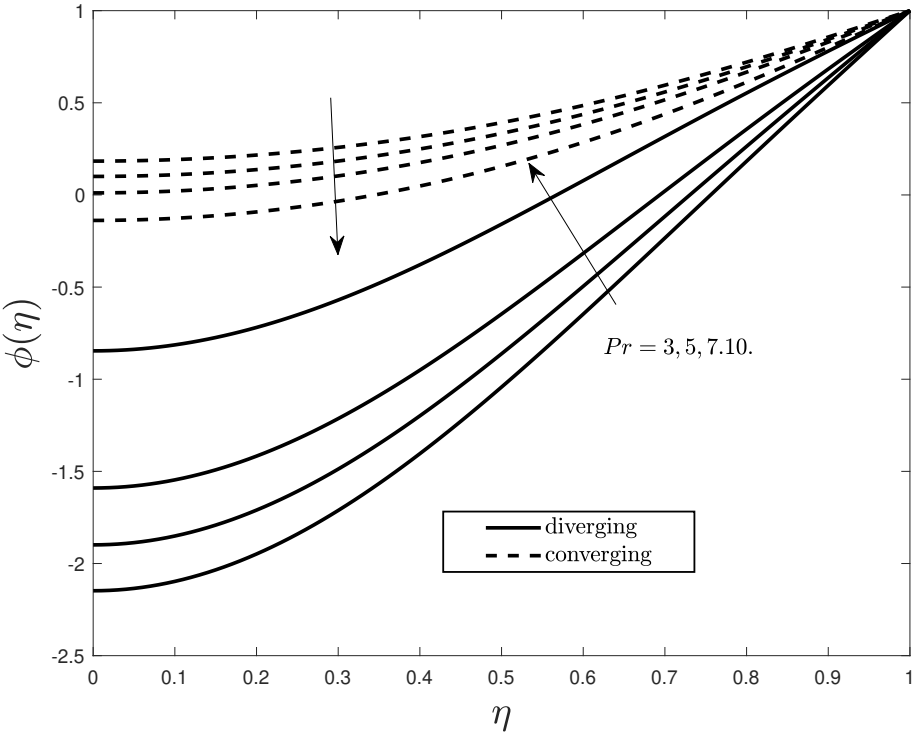

Figure 6.21: Variation in concentration with change in Pr.

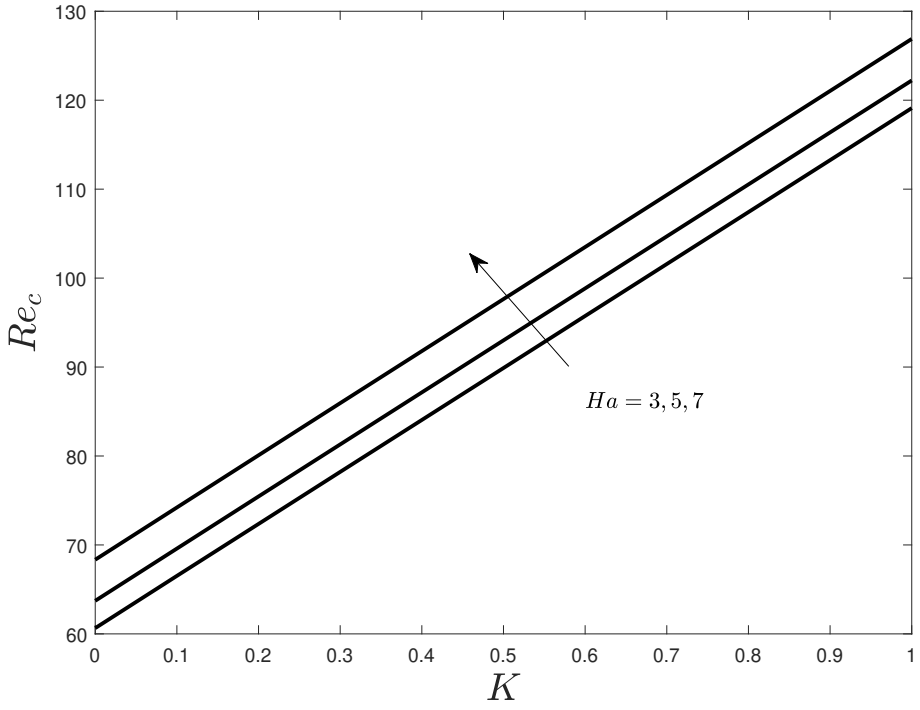

Figure 6.22: Variation in critical Reynolds number with change in K and Ha.

Tables (6.2)-(6.3) provide an insight on the effects of the sundry parameters on the skin friction coefficient and the heat transfer rate at the walls. A positive variation in the Hartmann number causes the skin friction and the heat transfer rates to rise for both the converging and diverging channels walls. Physically, the pressure gradient at the entrance in case of source and at the exit in the case of sink, couples with the Lorentz forces to increase the velocity of the fluid. Accelerated motion tends to increase the heat dissipation inside the channel which in return rise in the temperature in the nanofluid. The accelerated flow is also responsible for an the skin friction coefficient. Positive impact is observed on the Nusselt number as the opening angle α is increased. The skin friction is seen diminishing for the diverging channel at greater angles while it increases for greater α in convergent channel flow.

An increase in the opening angle eases the flow of the fluid in the divergent channel. Deceleration in the flow tends to reduce the frictional effects at the surface. In contrast, in the convergent channel greater values of α means that the channel narrows as a result pressure is generated at the surface, so skin friction tends to increase. The random motion of the nanoparticles is measured by the Brownian diffusion parameter and the impact of the drift velocity is analyzed via thermophoresis parameter. Increase in the Brownian and thermal diffusion of the nanoparticles simultanously tend to decrease the heat transfer rate at the surface in both divergent channel and convergent channels. A high inertial flow tends to stabilize the flow as backflow

is decreased with the rise in Reynolds number Re. This fact results in a decrease in the skin friction coefficient at the surface in case of divergent channel. In the case of convergent channel the accelerated flow increases the skin friction at the surface.

α	N_T	N_B	Pr	Ha	Re	K	$f'(1)$	$\theta'(1)$
5	0.5	0.5	7	5	50	1	3.14147	0.47727
2.5							3.56661	1.60757
7.5							2.72882	0.90969
10							2.33417	1.53381
	0.1	0.1					3.14147	0.97135
	0.3	0.3					3.14147	0.70952
	0.7	0.7					3.14147	0.30966
			3				3.14147	0.15890
			5				3.14147	0.29163
			10				3.14147	1.01454
				2			3.11331	0.12508
				4			3.12941	0.28908
				8			3.19358	0.49002
					75		2.69772	0.41590
					100		2.25612	0.33270
					125		1.82071	0.27534
						2	5.14013	0.50906
						3	7.13812	0.52490
						4	9.13570	0.53437

Table 6.2: Skin friction coefficient and Nusselt number for the diverging channel.

α	N_T	N_B	Pr	Ha	Re	K	$f'(1)$	$\theta'(1)$
-5	0.5	0.5	7	5	50	1	4.87775	1.19859
-2.5							4.43804	1.02380
-7.5							5.31668	1.60856
-10							5.75293	2.78833
	0.1	0.1					4.87775	1.25808
	0.3	0.3					4.87775	1.22827
	0.7	0.7					4.87775	1.16904
			3				4.87775	0.47688
			5				4.87775	0.81285
			10				4.87775	1.90645
				2			4.85283	0.33881
				4			4.89077	1.78266
				8			4.92385	4.10417
					75		5.29185	0.79294
					100		5.69564	0.60779
					125		6.08871	0.50288
						2	6.88009	1.16935
						3	8.87939	1.15444
						4	10.87756	1.14541

Table 6.3: Skin friction coefficient and Nusselt number for the converging channel

6.5 Chapter Summary

The present study is focused at the heat transfer and flow characteristics a Jeffery Hamel micropolar flow of a nanofluid in a converging/diverging channel deemed with transverse magmetic field. The mathematical modeling is carried out via Navier Stokes equations incorporated with Boungiorno nanofluid model. The solution to the nondimensional ODEs is achieved via Keller box method. The results show that:

- The Hartmann number is decreasing the angular velocity of the nanofluids but increasing the linear velocity, temperature, skin friction and the heat transfer rate.
- Material parameter K is effecting positively on the linear velocity and angular momentum while it acts negatively on the heat transfer rate.
- Opening angle α increases the linear velocity in the convergent channel while a converse behavior is observed in the diverging channel case. Angular velocity grows for the diverging and converging channel for greater values of α.
- The present problem has potential applications to the situations where cooling of the system is required.

Chapter 7

Conclusion and Future Work

7.1 Conclusion

This chapter highlights the prominent features of the study carried out in the present dissertation. Numerical procedure was adopted in the study to discuss the thermal transport in nanofluids using the homogeneous single phase model and Boungiorno nanofluid model. The set of equations describing the flow properties were the continuity and momentum equations while to study the heat transfer analysis the energy equation was utilized. In Chapter 4 and Chapter 5, where the homogeneous single phase model was used, base fluids used were water and kerosene oil with the homogeneous dispersion of Al_2O_3 and CNTs as nanoparticles. Buongiorno nanofluid model was utilized in Chapter 3 and Chapter 6. The Casson non-Newtonian nanofluid model and Micropolar nanofluid model were utilized in the modeling. Micropolar nanofluid model required an addition conservation of momentum equation and in Chapter 4, the induced magnetic field effects were observed via Maxwell equations of magnetism. Nanofluid flow was studied in different geometrical situations which often occur in many applications of heat exchange processes. These geometries included the flow over a stretching sheet which is often found in polymer industry and between parallel plates that usually occur in the heat exchangers application.

Heat transfer in the boundary layer and at the surface of the boundary was investigated by the application of boundary layer approximations on the governing equation which converted the PDEs to nondimensional ODEs. Solution procedure of Keller box was adopted to solve the nondimesional ODEs. It was found that the Keller box method was very efficient in finding the solution of linear and nonlinear system of ODEs. The calculation of CPU time required for the

solution of the problems showed that very little computational time was required to obtain a solution accurate up to 10^{-5} decimal places. The coding of the Keller box method for the problems was carried out on Matlab by the author himself in order to adapt to the requirements of the problems. The variation in velocity and thermal boundary layers was observed for variation in the physical parameters appearing in the ODEs via graphical representations. Nusselt number was evaluated at the boundary and examined for heat transfer in the boundary layer flow. The drag force at the surface was investigated by pondering on the numerical values of skin friction coefficient. Some interesting and noteworthy findings are summarized here.

- Velocity profile shows a decline with increase in Hartmann number in all the cases except for the cases in converging/ diverging channel where it is seen to increase in with the increase in Hartmann number.
- Upsurge in velocity slip parameter and Casson parameter also have a negative impact on the linear velocity. Due to greater heat dissipation, the temperature profile increases with the rise in Hartmann number in all cases.
- Greater material parameter has a negative impact on the linear velocity and a positive impact on the angular velocity in the case of porous parallel plates but in converging/ diverging channel case an increase in the material parameter augments the linear as well as angular velocity. Rise in the material parameter increases the induced magnetic field effects.
- Increased volume fraction of nanoparticles results in greater Brownian motion which in returns increases in the linear as well as angular velocity of the nanofluids.
- Induced magnetic field inclines with the inclination in the volume fraction parameter. Temperature profile shows a positive behaviour with the increase in volume fraction concentration.
- Heat transfer rate increase with the increase in volume fraction of nanoparticles while it decreases with the increase in the Hartmann number. MWCNT with kerosene as the base fluid proves to be very effective in increasing the heat transfer rate.
- Increase in the Casson parameter effects negatively on the heat transfer rate. Increase in the material parameter tends to enhance the heat transfer rate in the case of parallel plates and converging/diverging channel but when Marangoni convective flow over a flat plate is considered the converse effect is seen.
- Thermophoresis parameter when increased tends to decrease the heat transfer rate at the boundary surface.

- Greater values of the opening channel reduces both the skin friction as well as Nusselt number at the boundary surface. Thus, a wider channel is useful for decreasing the skin friction but at the same time the heat transfer rate is also affected negatively.
- In the converging/diverging channel problem, skin friction increases when a stronger magnetic field is applied but in case of parallel plates problem, a converse behavior is observed.

7.2 Future Work

The present work can be extended in different direction. Some suggestions are listed here:

- In the present study, single phase nanofluid models are used. The same problems can be explored for two phase nanofluid models.
- The problems can be explored by considering different set of boundary conditions like slip and convective boundary conditions, porous plates can be used, Soret and Dufort effects can be incorporated.
- Different non-Newtonian fluid models like Williamson fluid model, Maxwell fluid model, Jeffery model can be explored.
- In the present study, water and kerosene oil have been used as base fluids. The problems can be pondered using other based fluids like engine oil and engine oil-water base fluid.
- Alumina and CNTs have been utilized for the present study. Other nanoparticles like titanium oxide, ferrous oxides etc can be used to observe there effects on heat transfer rate.

Bibliography

[1] K. V. Wong and L. O. De, "Applications of nanofluids: current and future," *Advances in Mechanical Engineering*, vol. 2, pp. 1–11, 2010.

[2] M. U. Sajid and H. M. Ali, "Recent advances in application of nanofluids in heat transfer devices: A critical review," *Renewable and Sustainable Energy Reviews*, vol. 103, pp. 556–592, 2019.

[3] P. Keblinski, J. A. Eastman, and D. G. Cahill, "Nanofluids for thermal transport," *Materials Today*, vol. 8, no. 6, pp. 36–44, 2005.

[4] S. Kakaç and A. Pramuanjaroenkij, "Single-phase and two-phase treatments of convective heat transfer enhancement with nanofluids–A state-of-the-art review," *International Journal of Thermal Sciences*, vol. 100, pp. 75–97, 2016.

[5] S. U. S. Choi and J. A. Eastman, "Enhancing thermal conductivity of fluids with nanoparticles," Argonne National Lab., IL (United States), Tech. Rep., 1995.

[6] S. M. You, J. H. Kim, and K. H. Kim, "Effect of nanoparticles on critical heat flux of water in pool boiling heat transfer," *Applied Physics Letters*, vol. 83, no. 16, pp. 3374–3376, 2003.

[7] P. Vassallo, R. Kumar, and S. D'Amico, "Pool boiling heat transfer experiments in silica-water nanofluids," *International Journal of Heat and Mass Transfer*, vol. 47, no. 2, pp. 407–411, 2004.

[8] G. M. Moldoveanu, G. Huminic, A. A. Minea, and A. Huminic, "Experimental study on thermal conductivity of stabilized Al_2O_3 and SiO_2 nanofluids and their hybrid," *International Journal of Heat and Mass Transfer*, vol. 127, pp. 450–457, 2018.

[9] R. Loni, E. A. Asli-Ardeh, B. Ghobadian, K. A. B., and E. Bellos, "Thermal performance comparison between Al_2O_3/oil and SiO_2/oil nanofluids in cylindrical cavity receiver based on experimental study," *Renewable Energy*, vol. 129, pp. 652–665, 2018.

[10] A. A. Minea and P. Estellé, "Numerical study on CNT nanofluids behavior in laminar pipe flow," *Journal of Molecular Liquids*, vol. 271, pp. 281–289, 2018.

[11] M. Sheikholeslami, S. A. Shehzad, Z. Li, and A. Shafee, "Numerical modeling for alumina nanofluid magnetohydrodynamic convective heat transfer in a permeable medium using Darcy law," *International Journal of Heat and Mass Transfer*, vol. 127, pp. 614–622, 2018.

[12] M. Bilal, S. Hussain, and M. Sagheer, "Boundary layer flow of magneto-micropolar nanofluid flow with hall and ion-slip effects using variable thermal diffusivity," *Bulletin of the Polish Academy of Sciences Technical Sciences*, vol. 65, no. 3, pp. 383–390, 2017.

[13] K. Mehmood, S. Hussain, and M. Sagheer, "Mixed convection in alumina-water nanofluid filled lid-driven square cavity with an isothermally heated square blockage inside with magnetic field effect: Introduction," *International Journal of Heat and Mass Transfer*, vol. 109, pp. 397–409, 2017.

[14] S. Hussain, S. E. Ahmed, and T. Akbar, "Entropy generation analysis in MHD mixed convection of hybrid nanofluid in an open cavity with a horizontal channel containing an adiabatic obstacle," *International Journal of Heat and Mass Transfer*, vol. 114, pp. 1054–1066, 2017.

[15] I. A. Brownlee, C. J. Seal, M. Wilcox, P. W. Dettmar, and J. P. Pearson, "Applications of alginates in food," pp. 211–228, 2009.

[16] H. H. Tønnesen and J. Karlsen, "Alginate in drug delivery systems," *Drug Development and Industrial Pharmacy*, vol. 28, no. 6, pp. 621–630, 2002.

[17] L. Wang, F. Zhu, and D. Lu, "Rheological properties of sodium alginate and xanthan pastes on cotton with reactive dye in screen printing," *Textile Research Journal*, vol. 83, no. 17, pp. 1873–1884, 2013.

[18] S. Thakur, B. Sharma, A. Verma, J. Chaudhary, S. Tamulevicius, and V. K. Thakur, "Recent progress in sodium alginate based sustainable hydrogels for environmental applications," *Journal of Cleaner Production*, vol. 198, pp. 143–159, 2018.

[19] E. V. Gonçalves and S. C. Lannes, "Chocolate rheology," *Food Science and Technology*, vol. 30, no. 4, pp. 845–851, 2010.

[20] H. A. Barnes, J. F. Hutton, and K. Walters, *An introduction to rheology*. Elsevier, 1989.

[21] Z. Wang and S. Tang, "Casson rheological model in drilling fluid mechanics," in *International Petroleum Exhibition and Technical Symposium*. Society of Petroleum Engineers, 1982.

[22] G. Lukaszewicz, *Micropolar fluids: theory and applications*. Springer Science & Business Media, 1999.

[23] A. C. Eringen, "Theory of micropolar fluids," *Journal of Mathematics and Mechanics*, vol. 0, pp. 1–18, 1966.

[24] R. K. Tiwari and M. K. Das, "Heat transfer augmentation in a two-sided lid-driven differentially heated square cavity utilizing nanofluids," *International Journal of Heat and Mass Transfer*, vol. 50, no. 10, pp. 2002—2018, 2017.

[25] M. Z. Swalmeh, H. T. Alkasasbeh, A. Hussanan, and M. Mamat, "Heat transfer flow of Cu-water and Al_2O_3 – water micropolar nanofluids about a solid sphere in the presence of natural convection using Keller-box method," *Results in Physics*, vol. 9, pp. 717–724, 2018.

[26] T. Cebeci and P. Bradshaw, *Physical and computational aspects of convective heat transfer*. Springer Science & Business Media, 2012.

[27] M. Izadi, S. A. M. Mehryan, and M. A. Sheremet, "Natural convection of CuO-water micropolar nanofluids inside a porous enclosure using local thermal non-equilibrium condition," *Journal of the Taiwan Institute of Chemical Engineers*, vol. 88, pp. 89–103, 2018.

[28] N. Crainic, A. T. Marques, D. Bica, L. Vekas, P. J. Novoa, and C. P. De, "The use of the nanomagnetic fluids and the magnetic field to enhance the production of composite by RTM–MNF," *Molecular Crystals and Liquid Crystals*, vol. 418, no. 1, pp. 29–40, 2004.

[29] H. Hong, B. Wright, J. Wensel, S. Jin, X. R. Ye, and W. Roy, "Enhanced thermal conductivity by the magnetic field in heat transfer nanofluids containing carbon nanotube," *Synthetic Metals*, vol. 157, no. 10-12, pp. 437–440, 2007.

[30] J. Wensel, B. Wright, D. Thomas, W. Douglas, B. Mannhalter, W. Cross, H. Hong, J. Kellar, P. Smith, and W. Roy, "Enhanced thermal conductivity by aggregation in heat transfer nanofluids containing metal oxide nanoparticles and carbon nanotubes," *Applied Physics Letters*, vol. 92, no. 2, pp. 023 110–1–023 110–3, 2008.

[31] H. Hong, X. Luan, M. Horton, C. Li, and G. P. Peterson, "Alignment of carbon nanotubes comprising magnetically sensitive metal oxides in heat transfer nanofluids," *Thermochimica Acta*, vol. 525, no. 1-2, pp. 87–92, 2011.

[32] P. Shima, J. Philip, and B. Raj, "Magnetically controllable nanofluid with tunable thermal conductivity and viscosity," *Applied Physics Letters*, vol. 95, no. 13, pp. 133 112–1–133 112–3, 2009.

[33] Z. Haddad, H. F. Oztop, E. Abu-Nada, and A. Mataoui, "A review on natural convective heat transfer of nanofluids," *Renewable and Sustainable Energy Reviews*, vol. 16, no. 7, pp. 5363–5378, 2012.

[34] N. Putra, W. Roetzel, and S. K. Das, "Natural convection of nano-fluids," *Heat and Mass Transfer*, vol. 39, no. 8-9, pp. 775–784, 2003.

[35] L. Benos and I. E. Sarris, "Analytical study of the magnetohydrodynamic natural convection of a nanofluid filled horizontal shallow cavity with internal heat generation," *International Journal of Heat and Mass Transfer*, vol. 130, pp. 862–873, 2019.

[36] H. Sithole, H. Mondal, and P. Sibanda, "Entropy generation in a second grade magneto-hydrodynamic nanofluid flow over a convectively heated stretching sheet with nonlinear thermal radiation and viscous dissipation," *Results in Physics*, vol. 9, pp. 1077–1085, 2018.

[37] H. Hashemi, Z. Namazian, S. M. H. Zadeh, and S. A. M. Mehryan, "MHD natural convection of a micropolar nanofluid flowing inside a radiative porous medium under LTNE condition with an elliptical heat source," *Journal of Molecular Liquids*, vol. 271, pp. 914–925, 2018.

[38] Y. Mehmood, M. Sagheer, S. Hussain, and M. Bilal, "MHD stagnation point flow and heat transfer in viscoelastic fluid with Cattaneo–Christov heat flux model," *Neural Computing and Applications*, vol. 1, pp. 1–8, 2017.

[39] K. Mehmood, S. Hussain, and M. Sagheer, "Mixed convection flow with non-uniform heat source/sink in a doubly stratified magnetonanofluid," *AIP Advances*, vol. 6, no. 6, pp. 065 126–1–065 126–23, 2016.

[40] Sarveshanand and A. K. Singh, "Magnetohydrodynamic free convection between vertical parallel porous plates in the presence of induced magnetic field," *SpringerPlus*, vol. 4, pp. 333–346, 2015.

[41] C. H. Chun, "A micro-gravity simulation of the Marangoni convection," *Acta Astronautica*, vol. 5, no. 9, pp. 681–686, 1978.

[42] Y. Lin and L. Zheng, "Marangoni boundary layer flow and heat transfer of copper-water nanofluid over a porous medium disk," *AIP Advances*, vol. 5, no. 10, p. 107225, 2015.

[43] B. Mahanthesh and B. J. Gireesha, "Thermal Marangoni convection in two-phase flow of dusty Casson fluid," *Results in Physics*, vol. 8, pp. 537–544, 2018.

[44] S. Mukhopadhyay, "Casson fluid flow and heat transfer over a nonlinearly stretching surface," *Chinese Physics B*, vol. 22, no. 7, pp. 074 701–1–074 701–5, 2013.

[45] K. Rehman, N. Saba, M. Y. Malik, and I. Zehra, "Nanoparticles individualities in both Newtonian and Casson fluid models by way of stratified media: a numerical analysis," *The European Physical Journal E*, vol. 41, no. 3, pp. 37–47, 2018.

[46] T. Papanastasiou, G. Georgiou, and A. N. Alexandrou, *Viscous fluid flow.* CRC press, 1999.

[47] C. I. Christov, "On frame indifferent formulation of the maxwell–cattaneo model of finite-speed heat conduction," *Mechanics Research Communications*, vol. 36, no. 4, pp. 481–486, 2009.

[48] F. P. Incropera, A. S. Lavine, T. L. Bergman, and D. P. DeWitt, *Fundamentals of Heat and Mass Transfer.* Wiley, 2007.

[49] R. J. Moreau, *Magnetohydrodynamics.* Springer Science & Business Media, 2013.

[50] M. R. Safaei, A. Jahanbin, A. Kianifar, S. Gharehkhani, A. S. Kherbeet, M. Goodarzi, and M. Dahari, "Mathematical modeling for nanofluids simulation: A review of the latest works," in *Modeling and Simulation in Engineering Sciences.* IntechOpen, 2016.

[51] R. L. Hamilton and O. K. Crosser, "Thermal conductivity of heterogeneous two-component systems," *Industrial & Engineering Chemistry Fundamentals*, vol. 1, no. 3, pp. 187–191, 1962.

[52] J. Buongiorno, "Convective transport in nanofluids," *ASME Journal of Heat Transfer*, vol. 128, pp. 240–250, 2006.

[53] H. Schlichting and K. Gersten, *Boundary-layer theory.* Springer, 2016.

[54] L. C. Woods, *The thermodynamics of fluid systems.* Oxford University Press, 1975.

[55] O. Mahian, L. Kolsi, M. Amani, P. Estellé, G. Ahmadi, C. Kleinstreuer, J. S. Marshall, M. Siavashi, R. A. Taylor, H. Niazmand, S. Wongwisescn, T. Hayat, A. Kolanjiyil, A. Kasaeianq, and I. Pop, "Recent advances in modeling and simulation of nanofluid flows-part I: Fundamental and theory," *Physics Reports*, vol. 790, pp. 1–48, 2018.

[56] A. Kamran, S. Hussain, M. Sagheer, and N. Akmal, "A numerical study of magnetohydrodynamics flow in Casson nanofluid combined with Joule heating and slip boundary conditions," *Results in Physics*, vol. 7, pp. 3037–3048, 2017.

[57] M. H. Abolbashari, F. N. Freidoonimehr, and M. M. Rashidi, "Analytical modeling of entropy generation for Casson nano-fluid flow induced by a stretching surface," *Advance Powder Technology*, vol. 26, pp. 542–552, 2015.

[58] J. Qing, M. M. Bhatti, M. A. Abbas, M. M. Rashidi, and M. E. Ali, "Entropy generation on MHD Casson nanofluid flow over a porous stretching/shrinking surface," *Entropy*, vol. 18, pp. 123–137, 2016.

[59] J. San, W. Worek, and Z. Lavan, "Entropy generation in combined heat and mass transfer," *International Journal of Heat and Mass Transfer*, vol. 30, pp. 1359–1369, 1987.

[60] S. J. Liao, "An optimal homotopy-analysis approach for strongly nonlinear differential equations," *Communication in Nonlinear Sciences and Numerical Simulation*, vol. 30, pp. 2003–2016, 2010.

[61] C. Y. Wang, "Free convection on a vertical stretching surface," *ZAMM-Journal of Applied Mathematics and Mechanics*, vol. 69, pp. 418–420, 1989.

[62] R. R. Gorla and I. Sidawi, "Free convection on a vertical stretching surface with suction and blowing," *Applied Scientific Research*, vol. 52, pp. 247–257, 1994.

[63] W. A. Khan and I. Pop, "Boundary-layer flow of a nanofluid past a stretching sheet," *International Journal of Heat and Mass Transfer*, vol. 53, pp. 2477–2483, 2010.

[64] O. D. Makinde and A. Aziz, "Boundary layer flow of a nanofluid past a stretching sheet with a convective boundary condition," *International Journal of Thermal Sciences*, vol. 50, pp. 1326–1332, 2011.

[65] M. Sheikholeslami and H. B. Rokni, "Nanofluid two phase model analysis in existence of induced magnetic field," *International Journal of Heat and Mass Transfer*, vol. 107, pp. 288–299, 2017.

[66] O. Abdulaziz and I. Hashim, "Fully developed free convection heat and mass transfer of a micropolar fluid between porous vertical plates," *Numerical Heat Transfer, Part A: Applications*, vol. 55, no. 3, pp. 270–288, 2009.

[67] Sarveshanand and A. K. Singh, "Magnetohydrodynamic free convection between vertical parallel porous plates in the presence of induced magnetic field," *SpringerPlus*, vol. 4, no. 1, pp. 333–346, 2015.

[68] W. A. Khan, Z. H. Khan, and M. Rahi, "Fluid flow and heat transfer of carbon nanotubes along a flat plate with Navier slip boundary," *Applied Nanoscience*, vol. 4, no. 5, pp. 633–641, 2014.

[69] M. Sheikholeslami and D. D. Ganji, "Influence of magnetic field on CuO-H_2O nanofluid flow considering Marangoni boundary layer," *International Journal of Hydrogen Energy*, vol. 42, no. 5, pp. 2748–2755, 2017.

[70] X. Xu and S. Chen, "Cattaneo–Christov heat flux model for heat transfer of Marangoni boundary layer flow in a copper–water nanofluid," *Heat Transfer—-Asian Research*, pp. 1–13, 2017.

[71] N. M. Ariffin, N. M. Arifin, and N. Bachok, in *AIP Conf Proc*, vol. 1795, no. 1. AIP Publishing, (2017), p. 020011.

[72] M. Turkyilmazoglu, "Extending the traditional Jeffery-Hamel flow to stretchable convergent/divergent channels," *Computers & Fluids*, vol. 100, pp. 196–203, 2014.